SOLUTE PARTITIONING INTO MODEL BIOLOGICAL MEMBRANES

STUDIED WITH TIME-RESOLVED EMISSION SPECTROSCOPY AND CALORIMETRY

by

Katelyn Marie Duncan

A dissertation submitted in partial fulfillment
of the requirements for the degree

of

Doctor of Philosophy

in

Chemistry

MONTANA STATE UNIVERSITY
Bozeman, Montana

May 2022

DEDICATION

This dissertation is dedicated to my wonderful family and fiancé for their love and support. Mom and Dad, thank you for always pushing me to be my best and teaching me that anything is possible with hard work and faith. Brady, thank you for the laughs, the support, and all the talks when things got tough. JD, thank you for the love, support, and helping me through the tough times.

ACKNOWLEDGEMENTS

First and foremost, I would like to thank my advisor, Dr. Rob Walker. Thank you for helping me overcome the large learning curve and for all your guidance throughout the way. I would also like to thank my committee members: Dr. Erik Grumstrup, Dr. Nick Stadie, Dr. Mary Cloninger, and Dr. Stephanie Ewing, all of whom provided valuable input and guidance. I would also like to thank Dr. Doreen Brown for all her help and support throughout the last five years.

An extended thank you to the Walker Research Group, both past and present. With a special thank you to Dr. Christine Gobrogge for the several hours she spent mentoring and instructing me. Thank you to Nida Shaikh for being a great friend and roommate, it has been awesome working through this adventure with you. Marshall, Josh, Tanner and all the Walker group members, thank you for all the coffee runs and fun conversations.

I would like to thank the NSF EPSCoR for their funding of my studies. With a special thank you to all those involved in the EPSCoR team who challenged me to think outside my discipline. I really enjoyed the opportunity to work with everyone and experience some outstanding research through cross-discipline collaboration.

I am, and always will be, forever grateful to my family, fiancé, and friends for their never-ending support and encouragement. For the countless conversations, phone calls, and coffee runs that fueled my graduate career and especially this body of work. Thank you all and making these last five years something I've truly enjoyed.

TABLE OF CONTENTS

TABLE OF CONTENTS CONTINUED

TABLE OF CONTENTS CONTINUED

TABLE OF CONTENTS CONTINUED

LIST OF TABLES

Table Page

LIST OF TABLES CONTINUED

LIST OF FIGURES

Figure Page

LIST OF FIGURES CONTINUED

Figure Page

LIST OF FIGURES CONTINUED

Figure Page

LIST OF FIGURES CONTINUED

Figure Page

ABSTRACT

Bioaccumulation and bioconcentration are terms used to quantify the concentration of the solute in an organism with respect to the source of exposure. Empirical values are commonly used to predict a solutes tendency for bioconcentration. While they are useful zeroth order indicators, empirical values lack the chemical specificity required to fully understand the exact solute-solute and solute-lipid chemical interactions that occur when a solute is introduced to a biological membrane. The work described here uses fluorescence spectroscopy and thermoanalytical techniques to quantify solute partitioning into model biological membranes. The model membranes used in this study are lipid bilayer vesicles that are analyzed as a function of temperature from the rigid gel-phase through the transition temperature and into the fluid liquid-crystalline phase. Studies described in this work seek to create a quantitative, mechanistic description of solute behavior in heterogeneous chemical environments.

Each body of work either altered the solute used for partitioning or altered the membrane to add chemical complexity. The first body of work describes a proof-of-concept study analyzing the change in partitioning behavior from small structural changes in the solute. This study found that small changes to the solute affects membrane permeability in a way that is not accounted for in empirical models. The subsequent study sought to understand how the addition of amino acids to the membrane changes partitioning tendencies. Further analysis was done to study the partitioning behavior of amino acid L-Phenylalanine. Studies showed L-Phenylalanine integrates into the membrane and experiences a conformationally restricted environment. Additional studies were done on a pharmaceutical candidate and found membrane permeability does not correlate with drug activity. The drug was predicted to interact with the target-protein directly. Furthermore, analysis on the herbicide Dicamba has shown some indication of membrane interaction; however, more studies are required to fully understand the partitioning behavior.

CHAPTER ONE

INTRODUCTION

Motivation

Due to growing concerns about public health and ecosystem vitality, the environmental fate of synthetic organic solutes is attracting attention from public engineers, health care workers, and scientists. Of particular interest is how chemicals used for agriculture persist in watersheds, soils, and biological membranes.[1-5] Bioaccumulation and bioconcentration describes the absorption of the solute within an organism with respect to the source of exposure.[6-7] Prolonged exposure to contaminants can cause harmful ecological effects that necessitate costly remediation.[2, 4] This behavior is particularly relevant for an agriculturally intensive state like Montana where organic solutes are commonly used to manage crop production. Furthermore, some synthetic organic solutes have a tendency to appear even where not intended resulting in expensive law remediation and reclassification of crops.[8-9] Despite bioaccumulation and bioconcentrations detrimental effects, surprisingly little is known about the mechanisms responsible for solute partitioning into biological membranes and even less about the chemistry these solutes undergo once localized in the heterogenous environment found within lipid bilayers. The research described in this dissertation carefully analyzes the partitioning behavior of synthetic organic solutes to understand the specific chemical interactions that occur when an organic solute interacts with model biological membranes.

Solute uptake into a biological organism is often reported using either bioaccumulation or bioconcentration factors, with the difference being in the source of solute exposure.[7] Bioaccumulation is defined as an organism's uptake of a solute from any environmental source, including dietary uptake, inhalation, metabolic transformation, dilution through organism growth, and excretion.[7] Bioaccumulation is often characterized by the bioaccumulation factor (BAF) which reports the ratio of the solute concentration in the organism (C_B) relative to the sum of the solute concentrations in sediment (C_S), water (C_W), and food (C_F) (Equation 1.1).

$$\mathrm{BAF} = \frac{C_B}{C_S + C_W + C_F} \tag{1.1}$$

The bioconcentration factor (BCF) is the most common measure of solute partitioning and refers to the solute absorption through respiratory and dermal surfaces alone. Diet is not included. The BCF is defined as the ratio of the concentration of the solute within the organism to the concentration of the solute in the water (Equation 1.2).[7, 10]

$$\mathrm{BCF} = \frac{C_B}{C_W} \tag{1.2}$$

The BCF and BAF are commonly found in literature to describe a solute's absorption into the environment. The biomagnification factor (BMF) is a food chain description where the concentration of the compound is only studied in respect to its food source (Equation 1.3).[7]

$$\mathrm{BMF} = \frac{C_B}{C_F} \tag{1.3}$$

The BAF and BCF are commonly used to describe a solute's persistence in the environment; however, they can be difficult to measure directly. One empirical tool often used to predict a solute's tendency to bioconcentrate in membranes is the partitioning

coefficient (log P) which is the log of the concentration of the solute between an organic phase (1-octanol) and an aqueous phase (water) (Equation 1.4).[7, 11-12]

$$\log P = \log\left(\frac{[solute]_{octanol}}{[solute]_{water}}\right) \quad (1.4)$$

A synthetic organic pollutant is deemed hazardous to the environment depending on their characterization of toxicity, persistence, and ability to transport across distances, as well as their potential for bioaccumulation.[13] One of the main identifying tests is done with the Log P scale. If the partitioning coefficient is greater than 5, the solute is deemed unusable for the agricultural, applications.[14]

The log P scale has a long, distinguished history and was first developed to better understand the intermolecular forces between synthetic organics and biomacromolecules.[14] Prior to the 1970's, scientists and pharmacologists used the log P scale as the primary standard to predict narcotic uptake and drug activity in order to screen solute bioavailability.[15-16] Subsequently, high-throughput screening (HTS) techniques have been developed, allowing solutes to be targeted and selected based on the log P values of analogs. HTS provided the ability to screen several compounds quickly; however, the resulting solute libraries required additional filtering to assess chemical functionality. Thus, HTS techniques started to shift the balance from simple solute solubility considerations to a more molecular perspective based on chemical functionality to account for solute-solute and solute-target interactions.[14-15, 17-20]

In the l990s, Lipinski *et. al*. proposed a set of criteria for evaluating solute affinity for absorption, distribution, metabolism, and excretion (ADME) that is now referred to as the Lipinski Rule of Five (Ro5).[17-18] The Ro5 considers certain molecular properties

intended to capture solutes that display effective ADME behavior. Solutes likely to bioconcentrate will have 1) molecular weight less than 500 g/mol; 2) a calculated log P greater than 0 but less than 5.0; 3) 5 or fewer H-bond donors; and 4) fewer than 10 H-bond acceptors.[15, 18] Solutes with some and/or all of these properties, including candidate pharmaceuticals, are predicted to have the right balance of hydrophilic and hydrophobic properties allowing for solubility in the bloodstream and the ability to partition into the organic interior of membranes. Interestingly, three of the four criteria of the Ro5 depend simply on solute structure (molecular weight, hydrogen bond acceptors, and hydrogen bond donors). Only the log P criterion requires experimental measurement; however, log P can also be calculated using computational tools that combine the additive partitioning characteristics of a solute's individual functional groups.[14, 21-22, 11, 23]

While log P is a useful zeroth order indicator of membrane affinity, it a simple solubility description and fails to describe the specific solute-solute and solute-lipid chemical interactions that occur. Work described in the following chapters represents a step forward from HTS techniques to a more quantitative and chemically specific description of solute partitioning. In effort to understand the specific chemical interactions that occur when a solute is introduced to a biological membrane, fluorescence spectroscopy in combination with thermoanalytical techniques were employed to answer specifically:

1. Does the solute partition into the biological membrane?
2. If so, w*here* does the solute partition within the membrane?
3. *How much* of the solute resides *within* that local solvation environment?

4. Does the solute alter membrane properties?

Each chapter in this body of work was analyzed different classes of solutes in an effort to create a quantitative and mechanistic understanding of solute partitioning into model biological membranes. The proposed questions studied model solutes, pharmaceuticals, and herbicides and their partitioning tendencies into pure lipid bilayer vesicles used as model biological membranes. This work was originally proposed for just pharmaceuticals and herbicide analysis; however, an unexpected outcome of this work was the analysis of biorelevant solutes. Specifically, the addition of amino acids to the lipid bilayer vesicle in effort to create a more realistic model of real biological membranes.

Adding Membrane Complexity

The investigation of the interactions between amino acids and biological membranes were motivated by the fact that real biological membranes consist of more than simply phospholipid bilayers. The fluid mosaic model describes real biological membranes to contain protein, cholesterol, and carbohydrates.[24] More sophisticated models of biological membranes include the lipid raft hypothesis describing the transient interaction between the lipids, proteins, and cholesterol and the complex nature involved in the organization, assembly, and regulation of all components.[25] In effort to create a more accurate description of real biological membranes, amino acids were added to the phosphocholine bilayers used in this work. Specifically, aromatic amino acids were integrated into lipid bilayers.

The first amino acid chosen was L-Phenylalanine (L-Phe, Phe). L-Phe has a hydrophilic log P value of -1.4 in its neutral, uncharged form. The pKa values for Phe are

1.83 and 9.13 and studies described here are in a pH 7 buffer solution making the molecule zwitterionic with a net charge of zero in this work.[26] The local charges on the Phe molecule changes the log P value to 0.12 indicating a more even distribution between the organic and aqueous phase. Phe is one of three naturally fluorescent aromatic amino acids. However, upon excitation, Phe will transfer its energy to Tyrosine (Tyr) then to Tryptophan (Trp) which is speculated to occur through electronic energy transfer.[26-27] Phe, in its neutral, uncharged form, has an oscillator strength of 0.0005 and a quantum yield of 0.024 in aqueous solutions making it difficult to study and not commonly reported in literature.[28-30] The small fluorescence quantum yield is predicted to be a protection from undesired photoreactions resulting in ultrafast internal conversion of the molecule and higher photostability.[30]

The fluorescence behavior and membrane affinity of aromatic amino acids have been studied extensively since it was discovered in 1956 that proteins fluoresce.[28] The majority of the research has been devoted to Tyr and Trp fluorescence due to the larger contribution to protein fluorescence and higher quantum yields of 0.14 and 0.13, respectively.[28] The fluorescence behavior of the amino acids are reported to change have a strong dependence on their local environment resulting in a change in the fluorescence decay times and corresponding quantum yields.[31] Local charges and structure of the of the amino acid has proven to play a large role in membrane permeability with uncharged molecules predicted to have a higher membrane affinity than charged molecules.[32] Additionally, at low temperatures the permeability of amino acids to the membrane is low and increases as temperature increases.[32] The amino acids that do permeate into the

bilayer at low temperatures are predicted to permeate through membrane transient defects. These defects are small cavities in the membrane surface that allow small ions to pass without overcoming a large energy barrier.[32]

Computational studies have analyzed amino acid membrane affinity by calculating the free energy required to partition into the membrane.[33-35] As expected, bulkier amino acids, such as Trp, require a higher energy to permeate into the bilayer in comparison to Phe and Tyr. Hydrophobicity also plays a large role in the partitioning behavior and the cost to solvate in the nonpolar region of the lipid bilayer.[34, 36] While extremely useful, these studies used molecular dynamic simulations and fluorescent probes to understand amino acid membrane affinity and not through direct analysis. One large benefit to the studies described herein is the ability to analyze the solute *directly* without the need for fluorescent probes. The major requirement for a solute to be a candidate for this work is the need to be naturally fluorescent.

Experimental Methods.

Experimental Considerations

Time-resolved fluorescence spectroscopy was used to measure the fluorescence lifetimes of the solute in various solvation environments as well as integrated into lipid bilayer vesicles. The phosphatidylcholine lipid bilayer vesicles used in this study create a unique heterogenous chemical environment across ~4 nm. To fully understand the partitioning behavior of these solutes in a lipid bilayer vesicle, the photophysical behavior of the solute was first characterized in various bulk solvents that model the unique potential local solvation environment: acetonitrile was chosen to model the polar

aprotic headgroup, methanol to model the polar protic headgroup in the event water integrates into the bilayer, and cyclohexane to model the nonpolar tails. An important point to note is that the lipid bilayer headgroup is intrinsically polar aprotic with hydrogen-bond accepting capabilities but no hydrogen-bond donating properties. Therefore, if the polar headgroup region is displaying a polar protic environment, the headgroup region has become hydrated.

The lipid bilayer vesicles used in this work were made in a pH 7 buffer solution. Either potassium buffered phosphate (PBS) or carbonate buffer was used models the solute not interacting with the bilayer at all. The use of two different buffer solutions was a result of PBS buffer fluorescing at ~260 nm (with a 1.5 ns lifetime) and carbonate buffer was confirmed to not fluoresce at ultraviolet wavelengths. For all lipid vesicle systems excited in the visible wavelength region, PBS buffer was used and did not influence the fluorescence behavior of the solute. For all systems excited in the UV-wavelength region, carbonate buffer was used and did affect the fluorescence behavior of the solute. All lipid bilayer vesicles were made with lipid concentrations of 1.5 mM and were filtered to 200 nm using Avanti Lipids Mini-Extruder (Alabaster, AL) to create large unilamellar vesicles (LUVs).

The structure of most lipid bilayer membranes is temperature dependent and frequently includes a uniquely defining transition temperature ($T_{gel\text{-}lc}$). Below the $T_{gel\text{-}lc}$ the membrane is in a rigid, structured gel phase and as temperatures increase, the membrane enters into a fluid, disordered liquid-crystalline phase. Slightly before the $T_{gel\text{-}lc}$, the membrane experiences a pre-transition or ripple phase where water begins to

intercalate into the polar headgroup region. Studies described in this dissertation were performed as a function of temperature to understand how solutes partitioning depended on membrane phase and to evaluate the reversibility of partitioning.

Steady-State Fluorescence Spectroscopy

The steady-state excitation and emission behavior of each solute in all bulk solvents were characterized using a Horiba Fluorolog-3 (Irvine, CA). To study each solute's interactions in each of the local solvation environments of a lipid bilayer, a wavelength that overlapped the solutes excitation spectra in all bulk solvents were chosen for both excitation and emission in a lipid vesicle solution. This was done in effort to probe all potential local solvation environments. No difference in steady-state excitation or emission spectra was found by exciting at each solvent's specific excitation and emission peak or the chosen wavelength that overlaps all solvation environments.

Time-Correlated Single Photon Counting (TCSPC) Spectroscopy

The TCSPC assembly was built around a Ti:sapphire oscillator (Coherent Chameleon, 80 MHz, 85 fs pulse length, 680-1040 nm wavelength range, Santa Clara, CA) coupled with an APE autotracker harmonic generator (Berlin, Germany). The harmonic generator was used to frequency double (second harmonic generation) and triple (third harmonic generation) the fundamental wavelength. For second harmonic generation and third harmonic generation, a Conoptics Model 350-10 modulator, and a Conoptics Model 350-80 modulator (Danbury, CT), respectively, was used to reduce the repetition rate to 4 MHz. Picoquant PicoHarp 300 and FluoTime 200 software were used for data collection. Samples were equilibrated at the reported temperature for 5 minutes

using a Quantum Northwest TC125 control (Seattle, WA). A long pass filter was placed after the sample and before the detector to cut any fundamental excitation wavelength. The filter was chosen at an intermediate wavelength between excitation and emission wavelengths to reduce scattering from the sample and set-up. For experiments with vesicle containing solutions, the excitation wavelength chosen was one that overlapped all four bulk solvents in steady-state spectra.

All time-resolved emission data in vesicle containing solutions were fit independently and all determined lifetimes and amplitudes were chosen using fitting parameters that are adjusted to minimize residuals and optimize χ^2. The resulting lifetimes were then compared to lifetimes determined in the same bulk solvents mentioned above. A linear combination of lifetimes determined in bulk solvents was created and used to determine local solvation environments of solute in lipid bilayer. The fluorescence decay and amplitude expression are shown in Equation 1.5 where τ_i and A_i are the lifetime and amplitude of the i^{th} component, respectively.

$$I(t) = \int_0^t IRF\,(t') \sum_{i=1}^{n} A_i e^{-\frac{t-t'}{\tau_i}}\, dt' \qquad (1.5)$$

Each equation was fit independently, without any constraints, for the lifetimes and amplitudes with a typical χ^2 between 0.9 – 1.1 when accounting for at most, four lifetimes. Typical uncertainties in lifetimes and amplitudes were 0.2 ns and 0.04, respectively. Reported data represent an average of 3-5 experiments with independently prepared, equivalent samples. Lifetime uncertainties are reported as ± 0.2 ns due to TCSPC instrument response function (IRF); however, lifetimes reported herein are an average of all 3-5 trials with a single standard deviation reported for the average of those

trials. This technique was done at each temperature independently and only corresponding temperatures were compared and averaged.

Differential Scanning Calorimetry (DSC)

A TA Instruments DSC2500 (New Castle, DE) was used for calorimetry experiments. Vesicle solutions were made at 20 mM concentrations. To make the vesicles, the lipids were first dissolved in chloroform in a round bottom flask and the solvent was subsequently evaporated via rotary evaporation. The resulting thin-lipid film on the round-bottom flask was rehydrated with a pure buffer solution or solute-buffer solution. The rehydrated vesicles were then sonicated at ~10 °C above the lipid gel-liquid crystalline transition temperature ($T_{gel\text{-}lc}$) for 30 minutes. The solution was not filtered to a specific size to select vesicles and was left to sit in fridge overnight. For experiments, Tzero pans and Tzero hermetic lids from TA Instruments were used. Temperature runs were equilibrated 15 °C below the lipids $T_{gel\text{-}lc}$ and ran 1 °C/min to 15 °C above lipids $T_{gel\text{-}lc}$. Temperature sensitivity of DSC2500 is ± 0.025 °C. Data were analyzed using TA Instruments TRIOS software.

Thesis Outline

Research discussed in this work was all done in effort to understand the specific *chemical* interactions that occur when a solute is introduced to a model biological membrane. The first part of this work (Chapter 2) was a proof-of-concept study to understand how membrane affinity is altered by small structural changes to a solute in a way that is not predicted by traditional empirical tools like log P. Taking advantage of

these first discoveries, subsequent studies changed the solute in question (Chapters 4, 5, and 6) or the membrane (Chapter 3 and 4). Chapter 4 was the study of the partitioning behavior of one of the amino acids alone which is an expansion on both categories, changing the solute being analyzed as well as being done to study how the alterations affect the membrane. Chapters 2 and 3 consist of journal articles published in 2020 and 2021, respectively. Chapter 4 is a prepared manuscript that has been recently submitted to a journal and Chapter 5 is in preparation for submission. Due to their publication in literature, information in the introduction, materials, and methods sections of these chapters may be redundant. Chapter 6 consists of preliminary work from an on-going experiment of an herbicide commonly found in Montana waterways and displaying interesting photophysical behaviors.

Chapter 2. Coumarin partitioning in Model Biological Membranes: Limitations of Log P as a Predictor

This study analyzed three structurally identical coumarin derivatives differing only by a methyl group on the 7-amine. The tertiary-amine, Coumarin 152 (C152: log P = 2.7), showed full partitioning behavior with ~20% in the nonpolar tails, ~40% in the polar aprotic headgroup, and ~40% residing in buffer solution. As the lipid transitioned into the liquid-crystalline phase of the membrane, the polar lifetime switched from a polar aprotic limit to a polar protic limit. This indicated water accompanied C152 into the polar headgroup and the concentration of C152 in the headgroup increased up to 90%. The primary amine, Coumarin 151 (C151: log P = 1.6) showed no affinity for the lipid bilayer despite a log P value indicating it should. Throughout the entire temperature ramp and bilayer phase transition, the lifetime remained that of C151 remaining in bulk buffer. The

secondary amine, Coumarin 151.5 (C151.5: log P = 1.9) was synthesized for this study with the help of Dr. Matt Cook and Dr. Aoife Casey. C151.5 showed intermediate partitioning behavior with the appearance of a second lifetime, that of C151.5 in acetonitrile, indicating C151.5 partitioned into the polar aprotic headgroup. As temperature increased and the bilayer transitioned into the liquid-crystalline phase, C151.5 showed a slight tendency to exsolvate from the bilayer and back into buffer solution. This study proved that small structural changes to the solute dramatically alter the solutes membrane affinity, regardless of their log P values indicate. This work displayed the need for additional factors, more than solubility affinities, when predicting partitioning behavior. All supplemental information for this chapter can be found in Appendix A and is referenced as such within the chapter. This manuscript was published in the Journal of Physical Chemistry B in 2020 and slightly modified for this body of work.

Chapter 3. Amino Acids Change Solute Affinity for Lipid Bilayers

In effort to create a more realistic, and therefore more accurate, description of lipid bilayer membranes, amino acids were integrated into the system and their effect on solute partitioning was measured. Separately, L-Phenylalanine and N-Acetyl-Tryptophan, were added to the lipid bilayer and the change in partitioning behavior for C151 and C152 were quantified. The addition of L-Phenylalanine did not change C151 affinity for the lipid bilayer vesicle and C151 remained in buffer solution. This indicated L-Phenylalanine only influences the solutes partitioning behavior if the solute has an affinity to partition initially. Alternatively, the addition of L-Phenylalanine did impact the

partitioning behavior of C152. In the gel phase of the bilayer, there was an increase in concentration of C152 in the nonpolar tails and in buffer solution. In the polar headgroup, there was a decrease in C152 concentration. This indicated that while the membrane was in the gel-phase, L-Phenylalanine integrated into the polar headgroup and drove more of the already existing C152 further into the bilayer and blocked C152 from entering the polar headgroup. However, when the membrane transitioned into the liquid-crystalline phase, L-Phenylalanine did not have a large effect on C152 partitioning behavior.

N-Acetyl-Tryptophan had an extremely different effect on C151 and C152 partitioning behavior. For C151, there was the appearance of a second lifetime that occurred with the addition of N-Acetyl-Tryptophan to the vesicle containing solution. This result is different than what was seen in the absence of an amino acid or with L-Phenylalanine. The second lifetime did not match anything found in bulk solvents and is predicted to be a C151/N-Acetyl-Tryptophan/lipid complex. This complex is predicted to create an alternate binding site for C151 to interact. This complex is also predicted to occur with C152; however, is less evident as C152 shows strong partitioning behavior initially.

This study was done in effort to expand on pure lipid bilayer vesicles by the addition of biorelevant molecules creating a more accurate representation of real biological membranes. Results showed amino acids dramatically change partitioning behavior of the solute if the solute has a tendency to partition initially. The partitioning behavior observed also alters depending on the amino acid involved. The supplemental

work for this chapter can be found in Appendix B and is indicated as such within the chapter. This work was published in the Biophysical Journal in 2021.

Chapter 4. Quantitative Membrane Partitioning Studies of L-Phenylalanine

Motivated by the work in Chapter 3, this study was done in effort to confirm hypothesis formed that L-Phenylalanine integrates into the polar headgroup of the bilayer and disrupts cohesive lipid chain-chain forces. The results showed ~70% of L-Phenylalanine resided in aqueous buffer and ~30% is a lifetime that does not match anything found in bulk solvents. This lifetime is predicted to be a conformationally restricted rotamer induced by integration into the lipid bilayer. This second lifetime matches a lifetime reported in literature of single L-Phenylalanine molecule in a 29-mer peptide. The appearance of this second lifetime only occurs in the liquid-crystalline phase of the bilayer as water is integrated within the bilayer. This integration of water into the headgroup is critical to the observation of L-Phenylalanine. A switch from a polar aprotic to polar protic local solvation environment results in a 5.5-fold increase the quantum yield. To understand generalizability of the appearance of a second lifetime at/around the $T_{gel\text{-}lc}$, the same experiments were run with three other different lipid systems. For DSPC and DMPC, the second lifetime appeared at/around the lipids $T_{gel\text{-}lc.}$ Interestingly, the smallest lipid used, DLPC with a $T_{gel\text{-}lc}$ of -1.2 °C, displayed no evidence of a second lifetime despite being almost entirely in the liquid-crystalline phase of the bilayer throughout the sampled temperature range. This lack of a second rotamer lifetime either below our detection limits, or potentially a result of a switch in non-radiative decay pathways due to the low temperature of the experimental procedure. This switch alters

the photophysical properties of the solute and therefore is not evident with our current system. This body of work confirmed the hypothesis that L-Phenylalanine integrates into the bilayer as hypothesized in Chapter 3. All supplemental data for this body of work can be found in Appendix C and is indicated as such within the chapter. This work has been prepared for submission to the Journal of American Chemical Society for publication.

Chapter 5. Testing Membrane Affinity of Thienopyrimidine Drug Candidates with Time-Resolved Fluorescence Emission

This work was done in collaboration with Dr. Mary Cloninger and Sarah Hopfner. This work analyzed three Thieno[3,2-d]pyrimidin-4-amine derivates synthesized by Sarah Hopfner. Each compound varied by the functional group in the 4' position: a hydrogen, a methyl-group, and *tert*-butyl group for compounds **1**, **2**, and **3**, respectively. The fluorescence properties of all three compounds displayed extremely short fluorescence lifetimes. Compound 2 displayed the most promising behavior for membrane interactions with two lifetimes that corresponded to that of the compound in bulk buffer and two unique lifetimes, one sub-nanosecond lifetime and one long lifetime. The extremely short lifetime is predicted to be compound **2** in a conformationally restricted environment induced by the lipid bilayer creating an efficient non-radiative decay pathway. The long lifetime is predicted to be an alternate non-radiative decay pathway that is stabilized by the lipid bilayer. This work concluded that while predictions are speculative, each of these synthesized compounds are predicted to operate through direct protein-target interaction and not binding induced by membrane proximity. This work was recently submitted to Journal of Molecular Pharmaceuticals and slightly modified for this body of work.

Chapter 6. Quantitative Membrane Partitioning of Dicamba

This chapter contains the preliminary work studying Dicamba, an herbicide commonly found in Montana waterways. Dicamba has shown unique photophysical behavior with a dual excitation and dual emission peak that changes depending on experimental procedures. Dicamba is predicted to undergo photodegradation with prolonged exposure to light. The quantification of the exact degradation product is currently being worked on in collaboration with Dr. Sharon Neufeldt and graduate student Grace Ibsen. Once the degradation products are known, the partitioning behavior of the herbicide can be better understood. However, preliminary partitioning results have shown a strong concentration dependence as well as a change in photophysical behavior in a lipid vesicle solution. This chapter describes the current work and the direction of future studies.

Chapter 7. Conclusion and Future Directions.

This chapter contains all general closing conclusions for this body of work as a whole. Included within are the potential future directions that I think are interesting projects building off of discoveries described in the chapters below.

CHAPTER TWO

COUMARIN PARTITIONING IN MODEL BIOLOGICAL MEMBRANES: LIMITATIONS OF LOG P AS A PREDICTOR

Contribution of Authors and Co-Authors

Manuscript in Chapter 2

Author: Katelyn M. Duncan

Contributions: Collected and analyzed all data, generated figures, and wrote manuscript in preparation for publication.

Co-Author: Aoife Casey

Contributions: Synthesized and purified Coumarin 151.5 for analysis using time-resolved and steady-state fluorescence spectroscopy.

Co-Author: Christine A. Gobrogge

Contributions: Advised on data collection.

Co-Author: Rhys C. Trousdale

Contributions: Assisted in collection of steady-state fluorescence spectra of all solutes in each of the bulk solvents.

Co-Author: Stefan M. Piontek

Contributions: Created original synthesis for Coumarin 151.5.

Co-Author: Matthew J. Cook

Contributions: Advised in preparation of Coumarin 151.5 synthesis and purification.

Co-Author: William H. Steel

Contributions: Assisted

Co-Author: Robert A. Walker

Contributions: Contributed important insight into performing experiments and interpreting results. Edited and assisted in the preparation of the manuscript.

Manuscript Information

Katelyn M. Duncan, Aifoe Casey, Christine A. Gobrogge, Rhys C. Trousdale, Stefan M. Piontek, Matthew J. Cook, William H. Steel, and Robert A. Walker.

The Journal of Physical Chemistry B

Status of Manuscript:

____ Prepared for submission to a peer-reviewed journal

____ Officially submitted to a peer-reviewed journal

____ Accepted by a peer-reviewed journal

__x_ Published in a peer-reviewed journal

Published by the Journal of Physical Chemistry B

In Volume 124, Issue 38, 8299-8308 (2020)

DOI 10.1021/acs.jpcb.0c06109

COUMARIN PARTITIONING IN MODEL BIOLOGICAL MEMBRANES: LIMITATIONS OF LOG P AS A PREDICTOR

Katelyn M. Duncan[†], Aoife Casey[†], Christine A. Gobrogge[†], Rhys C. Trousdale[†], Stefan M. Piontek[†], Matthew J. Cook[†], William H. Steel[‡], and Robert A. Walker[†§]*

[†]Department of Chemistry and Biochemistry, Montana State University, Bozeman, Montana 59717, United States.
[‡]Department of Chemistry, York College of Pennsylvania, York, Pennsylvania 17403, United States
[§]Montana Materials Science Program, Montana State University, Bozeman, Montana 59717, United States

Abstract

Time-resolved fluorescence measurements were used to quantify partitioning of three different 7-amino coumarin derivatives into DPPC vesicle bilayers as a function of temperature. The coumarin derivatives were structurally equivalent except for the degree of substitution at the 7-amine position. Calculated log P (octanol: water partitioning) coefficients, a common indicator that correlates with bioconcentration, predict that the primary amine (coumarin 151 or C151) would experience a ~40-fold partition enrichment in polar organic environments (log P_{C151} = 1.6) while the tertiary amine's (coumarin 152 or C152) concentration should be >500 times enhanced (log P_{C152} = 2.7). Both values predict that partitioning into lipid membranes is energetically favorable. Time-resolved emission spectra from C151 in solutions containing DPPC vesicles showed that within detection limits, the solute remained in the aqueous buffer regardless of temperature and vesicle bilayer phase. C152 displayed a sharp uptake into DPPC bilayers as the temperature approached DPPC's gel-liquid crystalline transition temperature, consistent

with previously reported results (*J. Phys. Chem. B.* **121** 4061-4070 (2017)). The secondary amine, synthesized specifically for these studies and dubbed C151.5 with a measured log P value of 1.9, partitioned into the bilayer's polar head group with no pronounced temperature dependence. These experiments illustrate the limitations of using a gross descriptor of preferential solvation to describe solute partitioning into complex, heterogeneous systems having nanometer-scale dimensions. From a broader perspective, results presented in this work illustrate the need for more chemically informed tools for predicting a solutes tendency for *where* and *how much* it will bioconcentrate within a biological membrane.

Introduction

Solute affinity for biological membranes is an extensively studied topic, given the importance of membrane partitioning in pharmaceutical applications and environmental toxicology.[15-17, 20, 37-38] The ability for solutes to partition into nonpolar phases underpins the general phenomenon of bioaccumulation as the basis for regulatory limits, used to identify harmful levels of pollutants in natural and municipal water systems.[7, 39-41] While certain methods can be used to identify solutes that are likely to partition more readily into membranes, most bioaccumulation predictors are based either upon empirical results or models that simply use properties such as functional group additivity and overall solute polarity.[39, 42] Missing are considerations of how subtle structural changes can affect a solute's affinity for one solvation environment over another.[19]

The experiments described in this work examine how small changes in solute structure affect a solute's tendency to partition into model biological membranes.

Moreover, our results also identify *where* in the membrane solutes accumulate. This work extends the scope of previous studies that quantified the partitioning a 7-aminocoumarin, Coumarin 152 (or C152, 7-dimethylamino-4-(trifluoromethyl)chromen-2-one) into lipid vesicle bilayers.[43-46] Specifically, results presented below illustrate how small changes in solute structure can induce large changes in solute partitioning into biological membranes . Furthermore, the small differences in molecular architecture can create a large difference in the partitioning behavior which is not captured using a log P model. The three solutes used in this study are all 7-amino-4-(trifluoromethyl)chromen-2-one Coumarin derivatives, and they vary solely in their substitution at the 7-amino position. C152 is a tertiary amine that can only accept hydrogen bonds, whereas Coumarin 151 (C151: 7-amino-4-(trifluoromethyl)chromen-2-one) is a primary amine capable of both accepting and donating hydrogen bonds. Both are commercially available. The corresponding secondary amine is not commercially available and was synthesized for these studies. For convenience, this solute was dubbed Coumarin "151.5" (C151.5: 7-methylamino-4-(trifluoromethyl)chromen-2-one). In the studies described below, the Coumarin derivatives are identified collectively as "C15X" (Figure 2.1).

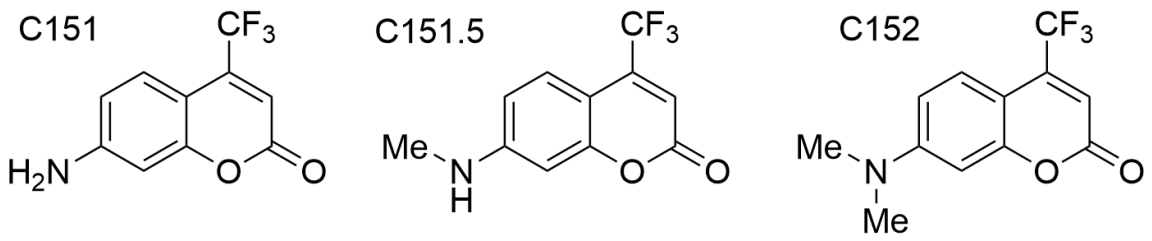

Figure 2.1. Coumarin derivative structures from left to right: C151, C151.5, C152.

Log P coefficients for C151, C151.5, and C152 were calculated using ChemDraw Prime 19.0. These coefficients scale with increasing hydrophobic content - 1.6 (C151),

1.9 (C151.5), and 2.7 (C152) - but all three values meet the Lipinski Ro5 log P criterion. It is worth noting the variability in log P values depends on how they're calculated and/or measured.[47-48] The molecular weight and hydrogen bonding opportunities also fall within acceptable Ro5 limits, implying that each solute should show strong affinity for biological membranes in comparison to water. Previous studies have reported that C152 partitions primarily into the polar glycerol-backbone region of phosphatidylcholine (PC) bilayers, and that the partitioning behavior is strongly temperature dependent.[43-46]

The model biological membranes used are lipid vesicles comprised of 1,2-dipalmitoyl-sn-glycero-3-phosphocholine (DPPC) lipid vesicles. DPPC bilayers create diverse solvation environments across a distance of ~4 nm consisting of (1) a nonpolar, hydrophobic region formed by DPPC's saturated, acyl tails; (2) a polar region arising from the lipids' ester groups and glycero-backbones; and (3) a zwitterionic phosphate head group (Figure 2.2). One-point worth noting is that the environment created by DPPC's glycerol-backbone segment is polar but does not contain any explicit hydrogen bond donating groups.

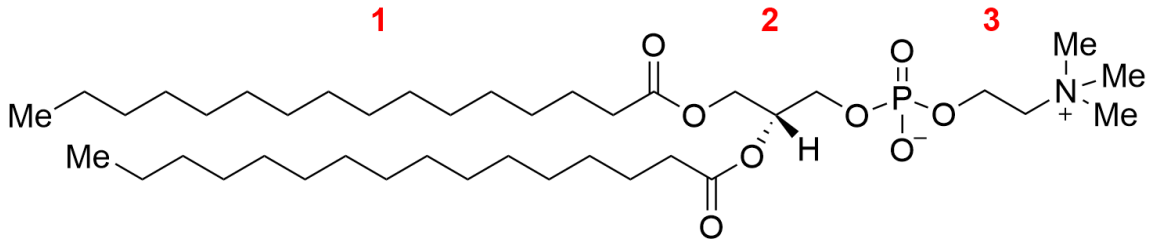

Figure 2.2. Chemical structure of 1,2-dipalmitoyl-sn-glycero-3-phosphocholine (DPPC) lipid. Number assignments correlate to various parts of lipid with the (1) hydrophobic hydrocarbon tail, (2) polar glycerol-backbone, and (3) the zwitterionic phosphate head group.

Results presented here show that at ambient temperatures, approximately 60% of C152 partitions into the bilayer, with two-thirds of the partitioned solute molecules localized in the aprotic polar headgroup region and one-third solvated by the lipids' nonpolar acyl chains. Similarly, ~60% of C151.5 partitions into the lipid bilayer with all of the partitioned solutes localized near the lipids' polar headgroups. Contrary to predictions from the log P model, C151 shows no measurable partitioning into the lipid bilayer and remains solely in the aqueous buffer at all temperatures. Temperature dependent changes in solute emission lifetimes suggest that the increase in C152 partitioning as the membrane passes through its gel-liquid crystalline transition is accompanied by water also moving into the bilayer's polar headgroup region. C151.5, however, shows no corresponding evidence of associating with the hydration of the bilayer at any temperature. Collectively, these results illustrate the limitations of using macroscopic descriptors to infer mechanistic details involving solute partitioning into biological membranes.

Experimental Methods

Materials

Solvents were purchased from Sigma-Aldrich and used as received. Millipore water (18.2 MΩ) was used to make a phosphate-buffered saline. 1,2-Dipalmitoyl-*sn*-glycero-3-phsophocholine (16:0 DPPC) was purchased from Avanti Polar Lipids. Laser grade C151 and C152 were purchased from Exciton and used as received. C151.5 was synthesized according to the procedure shown in Scheme 2.1 with modification to

Reference [49]. A more detailed description of the synthesis can be found in the Appendix A (Figure A-2.1). All bulk solvent solutions were made at 6 µM concentrations with 1.5 mM DPPC vesicles used for fluorescence experiments and 20 mM DPPC vesicles made for thermoanalytical experiments.

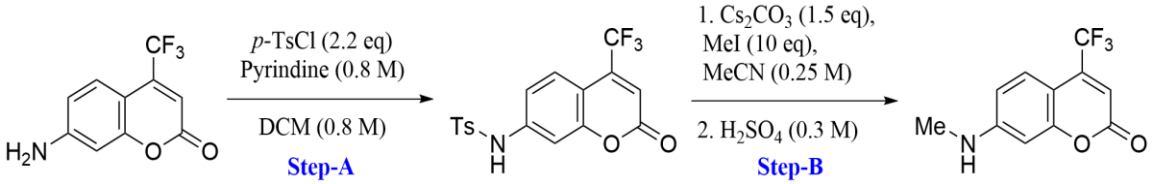

Scheme 2.1. Synthesis of C151.5.

Lipid Bilayer Vesicle Preparation

Lipid bilayer vesicles were prepared by dissolving DPPC in chloroform. The solvent was then removed via rotary evaporation. The resulting thin lipid film was subsequently rehydrated using a 6 µM coumarin and 10 mM phosphate-buffered saline (PBS, pH = 7) to form a lipid vesicle solution. The solution was sonicated for 30 minutes at ~50 °C. The solution was heated (50 °C) and passed through an Avanti Mini Extruder 10 times with a membrane pore size of 200 nm.[43-46]

Time-Correlated Single-Photon Counting (TCSPC)

Fluorescence lifetimes were measured using a Ti:sapphire oscillator (Coherent Chameleon, 80 MHz, 85 fs pulse duration, 680-1040 nm wavelength range) coupled with an APE autotracker capable of frequency doubling the fundamental to select solute-specific excitation wavelengths. A Conoptics model 350-10 modulator was used to reduce the repetition rate to 4 MHz. Picoquant PicoHarp 300 and FluoTime 200 software

were used for data collection. Samples were equilibrated at reported temperatures for 5 minutes using a Quantum Northwest TC125 control. A neutral density filter (80% transmission >455 nm) was placed after the sample to reduce scattering from the vesicles. Photon emission was collected at wavelengths specific to each solute in bulk solvent as well as a wavelength that overlapped all emission spectra in bulk solvents. Excitation wavelength chosen were unique to each solute in bulk solvent as well as one that overlapped all the bulk solvents in the excitation spectra which was then used to excite the solute in vesicle solution. The difference in excitation and emission wavelengths between the bulk solvent wavelengths used for C15X in vesicle solution did not change fluorescence lifetimes of that system. Additional details about this assembly can be found in References.[43, 45-46, 50-51]

Time-resolved emission data from vesicle-containing solutions are fit with a linear combination of independent lifetimes and amplitudes using fitting parameters for that are adjusted to minimize residuals and optimize χ^2. The resulting fluorescence lifetimes are then compared to lifetimes of the solute in different solvents chosen to mimic local solvation environments within the lipid bilayer. The fluorescence decay and amplitude expression is shown in Eq. 2.4, where A_i and τ_i are the amplitude and lifetime of the i^{th} component, respectively.[52]

$$I(t) = \int_0^t IRF\,(t') \sum_{i=1}^{n} A_i e^{-\frac{t-t'}{\tau_i}}\, dt' \qquad (2.4)$$

Each trace was fit independently, without any constraints, for the lifetimes or amplitudes. The typical χ^2 were from 0.9-1.10 when accounting for at most three lifetimes. Typically, uncertainties in lifetimes and amplitudes were 0.2 ns and 0.04, respectively. Reported

data represent the averaged results from at least 4 and sometimes as many as 6 experiments with independently prepared, equivalent samples. There is an intrinsic uncertainty in the lifetimes reported of ± 0.2 ns due to the TCSPC instrument response function; however, the data and error bars presented in this work are 4-6 trials averaged together with a standard deviation reported for the average of those trials. The average lifetimes and amplitudes and their respective standard deviations are reported for each specific temperature and only compared to their respective temperatures.

Results

Using the methods described above, we have examined how the molecular structure of C15X affects partitioning into model biological membranes. Prior to analyzing solute partitioning into DPPC bilayers, we measured time-resolved emission data from the C15X solutes in various solvation environments, modeled with bulk solvents. The bulk solvents were chosen to mimic specific solvation environments created within lipid bilayers: data from C15X in PBS buffer was used to identify the response from solutes that remained in bulk solution; acetonitrile approximated the polar aprotic head group region created by DPPC's ester groups; methanol was chosen to characterize solute behavior in polar, *protic* environments; and the nonpolar membrane interior was approximated with cyclohexane. Excitation and emission wavelengths and fluorescence lifetimes of C151, C151.5, and C152 are reported in Table 2.1. Time-resolved emission traces from all three solutes in bulk solvents are shown in Figure 2.3. Steady-state spectra for C15X in the bulk solvents are shown in Appendix A (Figures A-

2.4 – A-2.6). For the commercially available C151 and C152, data in Table 2.1 agree with previously reported findings in the literature. [51, 53, 54]

Table 2.1. Fluorescence properties of C151, C151.5, and C152. Fluorescence excitation and emission spectra for all three solutes in bulk solvents are shown in Appendix A (Figures A-2.4 – A-2.6). How the quantum yields, and radiative rates were calculated can be seen in Appendix A.

Solvent	**C151**				
	λ_{exc} (nm)	λ_{em} (nm)	τ_f (ns)[a]	φ_f[b]	k_f[b] (10^7 s^{-1})
PBS Buffer	336	490	4.51	0.01[c]	11.8
Methanol	379	479	5.26	0.37[d]	11.11
Acetonitrile	367	459	5.24	0.57[d]	6.97
Cyclohexane	348	397	1.21(0.65) 3.27(0.35)	0.28[d]	23.37
Solvent	**C151.5**				
	λ_{exc} (nm)	λ_{em} (nm)	τ_f (ns)[a]	φ_f[c]	k_f[c] (10^7 s^{-1})
PBS Buffer	389	514	3.47	0.31	8.9
Methanol	388	503	4.5	0.76	16.9
Acetonitrile	381	488	5.49	0.28	5.1
Cyclohexane	356	436	4.03	0.45	11.2
Solvent	**C152**				
	λ_{exc} (nm)	λ_{em} (nm)	τ_f (ns)[a]	φ_f[d]	k_f[d] (10^7 s^{-1})
PBS Buffer	400	520	0.62(0.92) 4.15(0.08)	0.05	8.1
Methanol	396	509	1.03	0.09	8.3
Acetonitrile	392	494	2.07	0.22	9.8
Cyclohexane	373	426	4.39	0.97	25.1

[a]Lifetimes are ± 0.2-0.3 ns. Numbers in parentheses next to lifetimes are amplitudes of that lifetime.
[b]Quantum yields (ϕ_r) and radiative rates (k_r) reported by Pal *et. al.* and Gobrogge *et. al.*[43-46, 53]
[c]Quantum yields (ϕ_r) and radiative rates (k_r) measured in this work.
[d]Quantum yields (ϕ_r) and radiative rates (k_r) reported by Pal et al. [54]

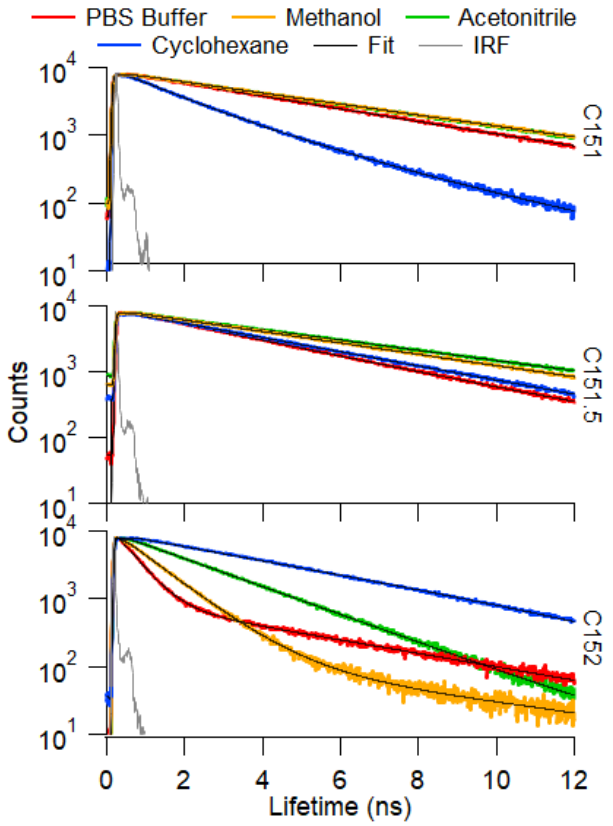

Figure 2.3. TCSPC spectra of 6 µM coumarins in bulk solvents taken at 10 °C. Top panel shows data for C151; the middle panel shows data for C151.5 and the bottom panel shows data for C152. Results from fitting these emission traces to Equation 2.4 are reported in Table 2.1. Grey trace is instrument response function (IRF).

Both C151 and C152 show strong solvatochromic responses in their steady state emission spectra consistent with an excited state having charge transfer character (see Appendix A, Figures A-2.4 – A-2.6). Where C151 and C152 differ, however, is in their respective time-dependent emission properties in bulk solvents. In polar solvents, C151's time-resolved emission is characterized by a single exponential decay having relatively long lifetimes that depend on proticity. In PBS buffer, C151's emission lifetime is 4.51 ns; in both methanol and acetonitrile, the emission lifetime lengthens to 5.25 ns. In a nonpolar solvent (cyclohexane), the dominant contribution to a biexponential decay is

considerably shorter (1.21 ns). C151's solvent-dependent emission behavior has been attributed photoisomerization where excited state C151 can form a planar intramolecular charge transfer (ICT) state that is stabilized in polar media.[53,54,51] In contrast to C151, C152 is believed to form a nonradiative, twisted intramolecular charge transfer (TICT) state in polar, protic environments with a correspondingly short, sub-ns emission lifetime.[53-55] In nonpolar solvents that do not enable the nonradiative decay pathway, C152's lifetime lengthens to 4.39 ns. Solute emission lifetimes are largely independent of temperature over the 10 - 70 ˚C window used in this work, with lifetimes changing by ≤ 0.4 ns between the two extremes.

C151.5's photophysical properties are being reported for the first time, we note that C151.5's steady state emission redshifts almost 80 nm as solvent polarity changes from a nonpolar limit (cyclohexane) to an aqueous environment (Appendix A, Figures A-2.4 – A-2.6). This large bathochromic shift implies that C151.5's first excited state – like those of C151 and C152 – also has a degree of charge transfer character. From the perspective of using C151.5 as an intermediate for testing membrane partitioning and the accuracy of log P as a partitioning predictor, C151.5's time dependent emission behavior shows measurable differences between C151.5 in the different bulk solvents with ~0.5 ns differences between the PBS buffer (3.47 ns), cyclohexane (4.03 ns), methanol (4.50 ns) and acetonitrile (5.49 ns).

Using ChemDraw Prime 19.0, we calculated log P values for C151 (1.6), C151.5 (1.9), and C152 (2.7). ChemDraw Prime uses a summation of the lipophilicity of each of the molecule's functional groups to calculate the log P value. We note again that all

C15X solutes meet the Lipinski Ro5 criteria and should be suitable candidates for bioconcentration in lipid membranes with C152 (log P = 2.7) having the highest affinity and C151 (log P = 1.6) the lowest. The log P value predicts that C151.5 (log P = 1.9) should behave more like C151 than C152.

Figure 2.4 shows the temperature dependent time-resolved emission from all three C15X solutes in solutions containing DPPC vesicles. As noted in the Experimental section, each decay was fit using Equation 2.4 and the resulting lifetime and amplitude data are reported in Table 2.2. For all emission traces, the minimum number of lifetimes were included that could adequately describe the data as determined from the resulting residuals and χ^2 values. Data for selected temperatures are reported in Table 2.2 and Figure 2.5 summarizes the lifetime results for all three solutes in DPPC vesicle solutions measured as a function of temperature. A full collection of lifetimes and amplitudes is provided in Appendix A (Table A-2.1). An important point to note is that no effort is made to constrain the C15X calculated lifetimes in vesicle solutions to those measured in the bulk solvents. Rather, C15X lifetimes in vesicle solutions were first calculated and then compared to bulk solvent lifetimes to determine the nature of the local solvation environment the solutes experiences and if/when they were absorbed by the bilayer. Furthermore, even though data shown in Figure 2.4 were acquired using single excitation and emission wavelengths, these wavelengths were chosen so that they overlapped with excitation and emission spectra of the C15X solutes in all 4 model solvents. Control experiments demonstrated that in the model solvents, emission lifetimes did not change

from those reported in Table 2.1 (acquired at different wavelengths) and those measured with the common excitation wavelength. (Data not shown.)

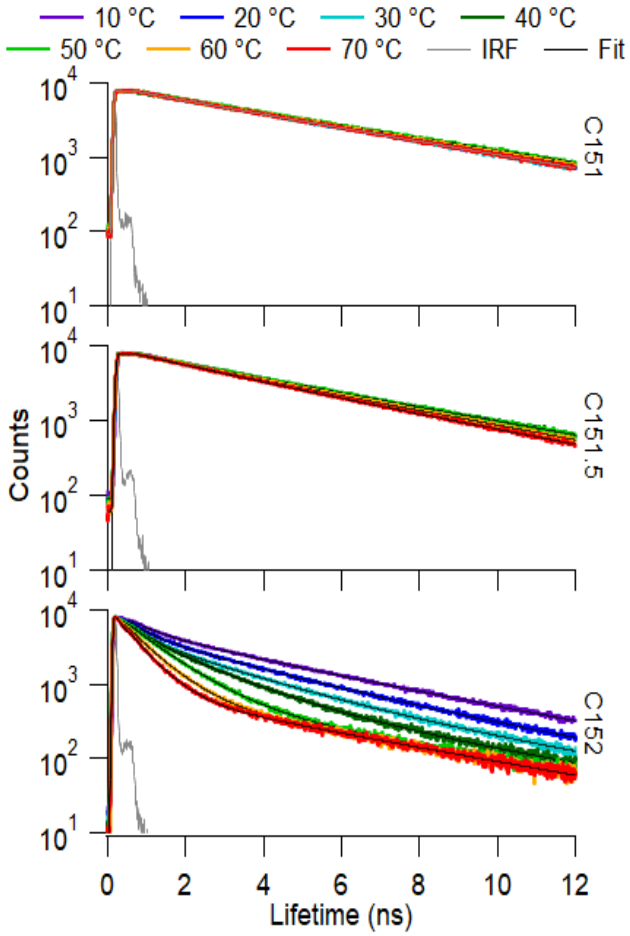

Figure 2.4. TCSPC spectra of Coumarins in DPPC as a function of temperature. Top panel shows data for C151; the middle panel shows data for C151.5 and the bottom panel shows data for C152. Results from fitting these emission traces to Equation 2.4 are reported in Table 2.2.

Table 2.2. Selected fluorescence lifetimes (in ns) and amplitudes (in parentheses) of Coumarins in DPPC at a temperature ramp from 10, 30, 50, and 70 °C and back down to 10 °C. Amplitudes have been corrected for their respective radiative rates (See text). Uncertainties in lifetimes are ± 0.2 ns; uncertainties in amplitudes are ± 0.04.

temp. (°C)	**C151**	**C151.5**		**C152**		
	buffer τ_1	buffer τ_1 (A_1)	polar τ_2 (A_2)	buffer τ_1 (A_1)	polar τ_2 (A_2)	nonpolar τ_3 (A_3)
10	4.62	3.37 (0.34)	5.73 (0.66)	0.62 (0.43)	2.27 (0.39)	4.55 (0.18)
30	4.52	3.22 (0.48)	6.09 (0.52)	0.45 (0.47)	1.99 (0.49)	4.56 (0.04)
50	4.81	3.48 (0.29)	5.59 (0.71)	0.35 (0.10)	1.03 (0.88)	4.61 (0.02)
70	4.52	3.19 (0.54)	6.03 (0.46)	0.32 (0.20)	0.65 (0.78)	4.25 (0.02)
50	4.69	3.36 (0.29)	5.74 (0.71)	0.39 (0.11)	1.03 (0.87)	4.73 (0.02)
30	4.57	3.18 (0.39)	6.16 (0.61)	0.43 (0.42)	1.88 (0.53)	4.41 (0.05)
10	4.70	3.09 (0.30)	6.15 (0.70)	0.65 (0.43)	2.34 (0.38)	4.56 (0.19)

Several observations about the data in Figure 2.4 and Table 2.2 stand out. First, fluorescence emission trends of C15X differ significantly as a function of temperature. While emission lifetime from C151 does not change as the vesicle solution temperature is cycled from 10˚C to 70˚C and back down, C152 emission changes markedly. C151.5 time-resolved emission lifetimes show small but measurable changes as a function of temperature. C151 emission can be fit with a single lifetime of ~4.6 ns, a result that is indistinguishable from C151 emission in pure PBS buffer. On this basis, we conclude that C151 does not partition into the DPPC vesicle bilayers, despite its favorable structural properties and log P value.

Fitting C152's time-resolved emission requires a minimum of three exponential decays: a long decay corresponding to a fluorescence lifetime ≥ 4 ns, a short, sub-ns lifetime, and an intermediate lifetime that changes reversibly from 2.2 ns at 10˚C to 0.6 ns at 70˚C. Similar to C152's 4.4 ns lifetime in cyclohexane, the longer lifetime is assigned to C152 in the nonpolar environment created by DPPC's acyl chains. These

results match previously reported findings.[43-46] The short lifetime matches C152's behavior in PBS buffer. The intermediate lifetime changes from a polar aprotic limit (2.2 ns) to a polar protic limit (≤ 1ns) as the solution passes through its gel-liquid crystalline transition temperature ($T_{gel\text{-}lc}$) at 41 °C. This behavior has been observed previously and has been interpreted as evidence of water intercalation into the polar region of the lipid bilayer as the bilayer melts.[43] The relevance of this shift in fluorescence lifetime corresponding to the lipids phase transition for solute partitioning is discussed in more detail below.

C151.5's time-resolved emission is characterized by two fluorescent lifetimes: a short lifetime of ~3.3 ns that is assigned to C151.5 in the PBS buffer and a longer lifetime of 5.9 ns that is longer than emission in any bulk solvent, but most closely matches C151.5 emission in a polar, aprotic environment (5.5 ns). The population of C151.5 responsible for this long-lived emission is assigned to C151.5 that has partitioned into the lipid bilayer's polar headgroup and glycerol-backbone regions. Unlike C152, this long C151.5 lifetime does not show evidence of transitioning to a value consistent with polar, protic solvation as the bilayer passes through $T_{gel\text{-}lc}$. As discussed below, we believe these observations provide important details about the mechanisms responsible for C152 and C151.5 partitioning into DPPC membranes.

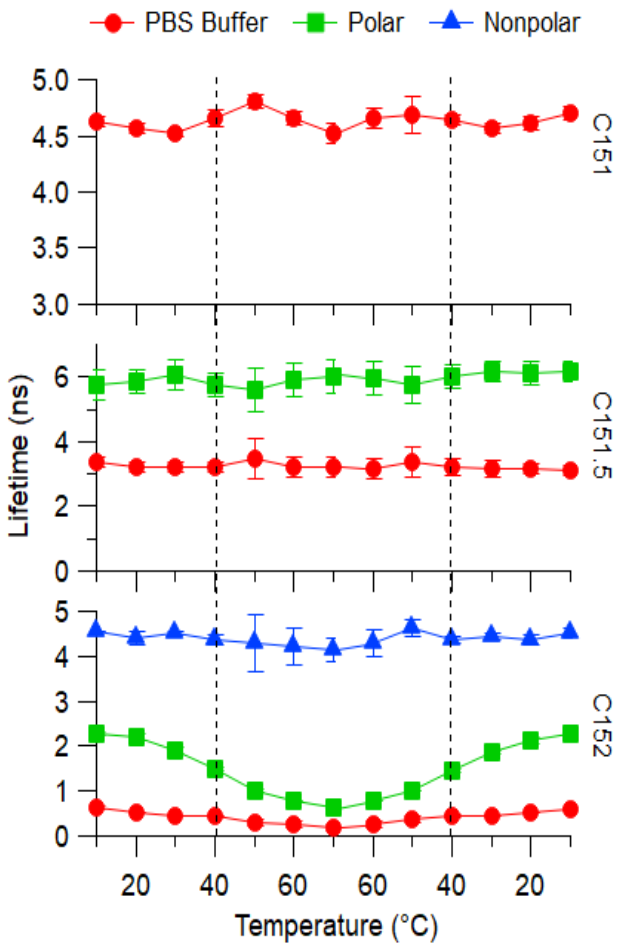

Figure 2.5. Fluorescence lifetimes of C15X in DPPC with three potential partitioning environments: PBS buffer (τ_1, red circles), polar head group (τ_2, green squares), and nonpolar tails (τ_3, blue triangles). The dashed lines represent DPPC transition temperature from gel to liquid-crystalline state at 41 °C. Error bars on each point reflect the one standard deviation uncertainty of several (4-6) measurements averaged together. In some cases, the uncertainty is smaller than the symbols used to represent the data.

Data in Figure 2.4 can be used to determine quantitative populations of solutes partitioning into DPPC membranes after the amplitudes have been corrected for their respective radiative rates.[44] To do this, we used radiative rates for C152 in the bulk solvents that most closely approximated the corresponding lifetimes were used (Amplitude data in Table 2.2 are radiative rate corrected and correspond to solute

population within the membrane). C151's radiative rate in water has been reported previously and was confirmed in our own laboratory. C151.5's quantum yields and radiative rates in various solvents are reported here for the first time. Radiative rate corrected amplitudes from the time-resolved emission data in Figure 2.4 are shown in Figure 2.6.

While C152 and C151.5 show changes to their respective fluorescence decay's as a function of temperature, C151 shows no change in its fluorescence lifetimes and is assumed to remain completely in aqueous solution. As reported previously, C152 shows strong uptake by the bilayer in the vicinity of the gel-liquid crystalline transition temperature (41˚C) with up to 90% of the available solutes molecules absorbed into the bilayer.[44] Based on lifetime amplitudes, above the $T_{gel\text{-}lc}$, C152 exsolvates out of the aqueous buffer and the nonpolar region of the bilayer into the polar headgroup where 88% of C152 is localized. This behavior is reversible as temperature is cycled above and below the $T_{gel\text{-}lc}$.

Despite having structural similarities and a similar log P value to C151, C151.5 shows behavior more similar to that of C152. Specifically, the biexponential decay of C151.5 in DPPC implies that C151.5 has some affinity for the DPPC membrane and the radiative-rate adjusted amplitudes show that up to 70% of the C151.5 is solvated in a polar, aprotic environment near the transition temperature. Above the transition temperature, partitioning appears to be enthalpically unfavorable as further increases in temperature drive a small amount of exsolvation from the bilayer back into aqueous solution. However, C151.5 does not show the same dramatic uptake by the DPPC bilayer

in the vicinity of the transition temperature, nor does C151.5 ever show any affinity for the nonpolar lipid bilayer interior. C151.5's amplitudes suggest more nuanced partitioning behavior below the transition temperature (with evidence for small amounts of exsolvation below 41˚C) but interpreting these observations would require additional experiments with finer temperature resolution between 10 and 40˚C.

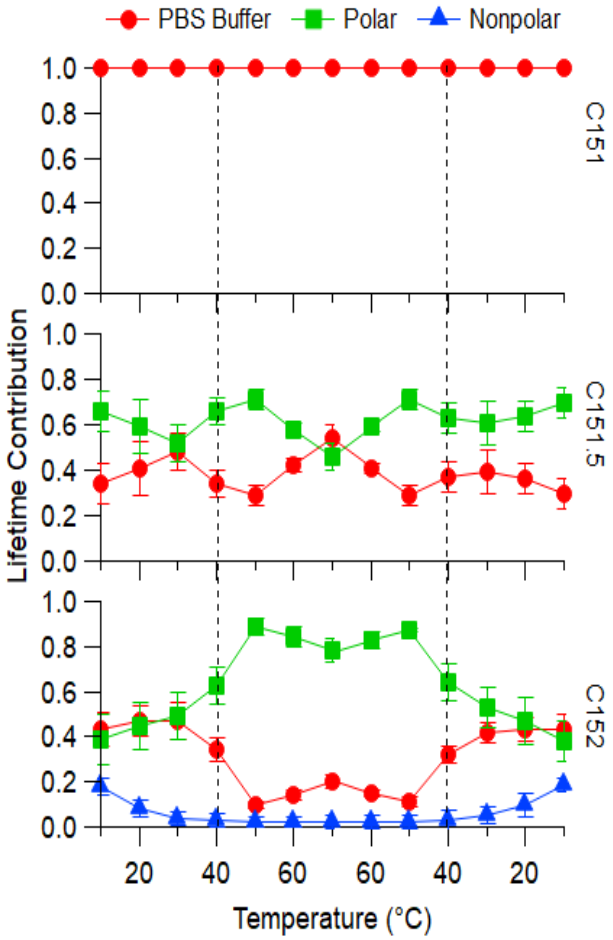

Figure 2.6. Radiative rate corrected fluorescence contribution of C15X in DPPC with three potential contribution environments: PBS Buffer (τ_1, red circles), polar head group (τ_2, green squares), and nonpolar tails (τ_3, blue triangles). The dashed lines represent DPPC transition temperature from gel to liquid crystalline state at 41 °C. Error bars on each point reflect uncertainty of several measurements averaged together.

Given the markedly different affinities C15X solutes appear to have for DPPC bilayers, we performed differential scanning calorimetry (DSC) measurements determine if solute partitioning affected the gel-liquid crystalline melting temperature of pure DPPC bilayers. DSC traces shown in Figure 2.7 illustrate that DPPC's $T_{gel\text{-}lc}$ remains unchanged by partitioning of coumarin solutes, even C152. This result is surprising given the strong uptake of C152 into the bilayer near the transition temperature. DSC traces of DPPC vesicle containing solutions with C151.5 also show no difference from data acquired with pure DPPC vesicle solutions.

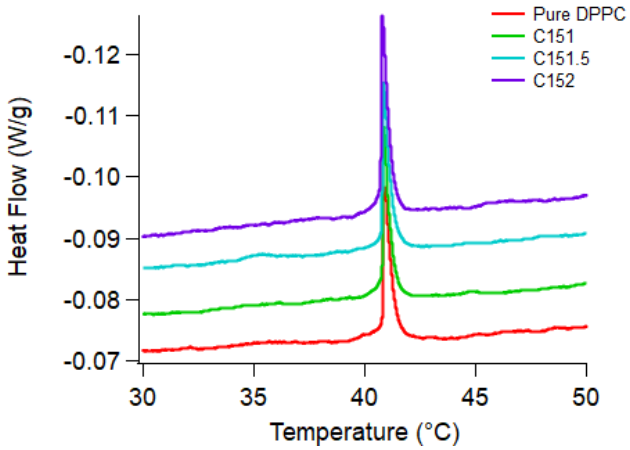

Figure 2.7. DSC spectra of pure DPPC vesicle solutions and DPPC vesicle solutions containing 6 μM C151, C151.5 or C152. All transitions are endothermic and offset for ease of viewing.

Discussion

Given the findings shown in Figures 2.5-2.6 and reported in Table 2.2, two phenomena require explanation:

- Differences in C15X uptake by the lipid bilayer as a function of solute identity and temperature

- The role of water in C15X/DPPC bilayers solvation

The discussion below considers each phenomenon, focusing on changes in DPPC vesicle bilayer structure as it melts and the non-covalent associations that are involved as well as the membrane hydration as a function of bilayer phase.

Differences in C15X Uptake

Solute transfer between two adjacent (liquid) phases is often analyzed in the context of a Flory-Huggins model that considers the volume changes required for a solute to migrate from one medium into the other (Equation 2.5).[56-57]

$$\Delta(\Delta G)_{FH} = -RTln\left(\frac{[x]_{org}}{[x]_{aq}}\right) - RT\left(\frac{V_x}{V_{aq}} - \frac{V_x}{V_{org}}\right) \quad (2.5)$$

Here, $\Delta(\Delta G)_{FH}$ is a Flory–Huggins based description of the solvation energy change when a solute migrates between phases, $[x]_i$ is the concentration of the solute in the organic and aqueous phases, and V_i are the molar volumes of the solute, water, and organic medium. Given that $V_{C152} > V_{C151.5} > V_{C151}$ and that $V_{aq} < V_{org}$ (where V_{org} for DPPC will correspond that part of the organic structure that must be rearranged to accommodate an incoming solute), Eq. 2.5 predicts that C152 partitioning into the bilayer should make the largest favorable (= negative) contribution to the system's overall free energy. This same size-only consideration predicts that C151 partitioning will have the smallest impact on $\Delta(\Delta G)_{FH}$. C151.5's contribution to $\Delta(\Delta G)_{FH}$ will be intermediate between the C152 and C151. Qualitatively this description captures differences in C15X partitioning at temperatures above $T_{gel\text{-}lc}$.

This Flory-Huggins description, however, cannot account for all of the observed partitioning behaviors. At the lowest temperatures sampled in this work (10˚C), ~20% more C151.5, compared to C152, partitions into the bilayer (Table 2.2). The amount of C151.5 in the bilayer changes little as a function of temperature, varying between ~70% (50˚C) and ~50% (70˚C). Across most of the temperature range sampled, the amount of C151.5 in the bilayer fluctuates between ~55 and 60%. In contrast, C152 partitioning shows a strong temperature dependence with ~90% of the available solute taken up by the membrane at 50˚C and ~55% at 10˚C.

Previous descriptions, of C152 partitioning into DPPC lipid bilayers have included a van't Hoff analysis and noted that C152 partitioning showed several temperature discontinuities.[43] Above $T_{gel\text{-}lc}$, C152 partitioning was exothermic ($\Delta H_{partitioning}$ = -48 kJ/mole) and entropically unfavorable ($\Delta S_{partitioning}$= -133 J/mole-K). At temperatures well below the melting transition, C152 partitioning was weakly exothermic ($\Delta H_{partitioning}$ = -8 kJ/mole) and again, entropically unfavorable ($\Delta S_{partitioning}$= -26 J/mole-K). Between 30 and 40˚C, however, C152 partitioning became endothermic ($\Delta H_{partitioning}$ = +85 kJ/mole) and entropically favorable ($\Delta S_{partitioning}$= 278 J/mole-K).[43] These quantitative enthalpic and entropic changes between 30 and 40˚C coincide with the temperature window where DPPC bilayers exist in a metastable 'ripple' phase characterized by domains of a splayed gel phase and a crystalline, interdigitated gel phase separated by regions of disordered lipids.[58]

A similar van't Hoff analysis has been performed with the C151.5 partitioning data (Appendix A, Figure A-2.8. Data for C152 are included for comparative purposes in

Figure A-2.9). In the pre-transition temperatures (T_{pre}), below $T_{gel\text{-}lc}$, the thermodynamic quantities associated with C151.5 partitioning show striking differences from those of C152. Specifically, from the lowest temperature sampled in this work (10˚C) to 40˚C, C151.5 partitioning shows virtually no thermal dependence. ($\Delta H_{partitioning}$ = -2.5 ± 2 kJ/mole; $\Delta S_{partitioning}$ = -3.2 J/mole-K). Above the transition temperature, C151.5 partitioning shows a similar dependence to C152, but with slightly attenuated enthalpic and entropic contributions. ($\Delta H_{partitioning}$ = -48 kJ/mole; $\Delta S_{partitioning}$ = -142 J/mole-K). Results from the van't Hoff analyses for both solutes are reported in Table 2.3.

Table 2.3. Results from a van't Hoff analysis of C151.5's temperature dependent partitioning behavior. (See Appendix A, Figure A-2.8). Uncertainties in reported enthalpies are ≤ 4 kJ/mole, and uncertainties in reported entropies are ≤ 10 J/mole-K. Values reported for C152 are included for comparative purposes and were taken from Reference 21 (See Appendix A, Figure A-2.9). Note that the signs of ΔH and ΔS assume that $C15X_{aq}$ is the 'reactant' and $C15X_{membrane}$ is the 'product'.

		C151.5	C152
ΔH (kJ/mole)	**$T < T_{pre}$**	-2.5	-8
	$T_{pre} \leq T \leq T_{gel\text{-}lc}$		85
	$T > T_{gel\text{-}lc}$	-48	-48
ΔS (J/mole-K)	**$T < T_{pre}$**	-3.2	-26
	$T_{pre} \leq T \leq T_{gel\text{-}lc}$		278
	$T > T_{gel\text{-}lc}$	-142	-133

These differences between C151.5 and C152, especially below $T_{gel\text{-}lc}$, are striking and suggest that their partitioning behaviors are driven by fundamentally different mechanisms. C151.5 partitioning is largely insensitive to bilayer phase and system temperature, whereas bilayer disorder significantly enhances C152 partitioning. Again, we note that C151 shows no measurable tendency to associate with the bilayer at any

temperature. The sole structural differences between the three solutes occur at the 7-amine position. All three solutes can accept hydrogen bonds through the amine's lone pair (as well as each solute's ester group), but C152 cannot donate hydrogen bonds, whereas C151 and C151.5 can donate 2 and 1 hydrogen bonds, respectively.

In light of the C15X behaviors shown in Figure 2.6 and Table 2.3, we propose that C151's ability to form strong hydrogen bonds with the aqueous buffer prevents it from partitioning into the bilayer, despite a favorable log P value of 1.6. Below $T_{gel\text{-}lc}$ and in the T_{pre}, DPPC vesicles are irregularly shaped and adopt 'crumpled' structures with complex, irregularly shaped topological defects.[59] Similarities in the C151.5 and C152 behavior at lower temperatures imply that non-covalent association is driving both species to partition into the bilayer – presumably through defects in the well-ordered, frozen bilayer membrane structure – with those solutes in the polar headgroup region being solvated in an aprotic environment. Compared to C151.5, a larger fraction of the more hydrophobic C152 partitions into the hydrophobic region created by the acyl chains. As the membrane begins to melt (at the pre-transition), the disordered region(s) of the bilayer can accommodate more C152, albeit at an enthalpic cost of +85 kJ/mole. Driving this partitioning, however, is an accompanying increase in system entropy that results from removing the hydrophobic solute from its aqueous solvation cavity. From a molecular perspective, C152 partitioning can be enhanced by the large lateral density fluctuations reduction that accompany formation of DPPC's disordered phase.[60-61] Data reported in Table 2.3 show clearly that C151.5 is not sensitive to bilayer structure below $T_{gel\text{-}lc}$. Above $T_{gel\text{-}lc}$ both C152 and C151.5 show similar partitioning behaviors with

solute exsolvation from the bilayer being driven by a large, exothermic contribution. The negative change in partitioning entropy above $T_{gel\text{-}lc}$ for both solutes is interpreted as a loss of entropy in the buffer as the solvent needs to accommodate the relatively hydrophobic solutes.

Water's Role in Solute Partitioning

The second observation from the C15X partitioning data requiring discussion is apparent in Figure 2.5: C152's polar headgroup solvation lifetime shortens from 2.3 ns at low temperatures to ≤ 1.0 ns at higher temperatures. This change implies that C152 solvation in the polar headgroup region changes from a polar, aprotic environment to a polar, protic environment as the DPPC bilayer melts. In contrast, C151.5's polar headgroup solvation lifetime remains relatively constant at 5.9 ± 0.2 ns across the entire temperature range sampled. As noted in the results section, this value most closely matches C151.5 solvated in a polar, aprotic environment (τ = 5.5 ns in acetonitrile) and is far from the C151.5 emission lifetime in polar, protic media (τ = 4.5 ns in methanol; 3.5 ns in aqueous buffer).

Studies have shown that water content in a lipid bilayer increases when the bilayer transitions from its gel to liquid crystalline state.[62-65] As a DPPC bilayer passes from its well-ordered gel state to disordered liquid crystalline, the membrane swells and the average area per lipid molecule increases from 57 $Å^2$/lipid to 65 $Å^2$/lipid.[66-68] Pandey *et. al*. used classical molecular dynamics simulations to predict that in the expanded state, the choline's cationic $N(CH_3)_3^+$ group folds towards the membrane, bringing with it noncovalently bound water molecules.[69] This same study predicted that above the

transition temperature, water molecules could be found throughout the nonpolar tails albeit with decreasing concentration. Similarly, Alarcon, *et al.* calculated that the amount of water in the bilayer doubled as the bilayer passed from its gel to liquid crystalline state.[62] This prediction from classical MD simulations was verified by Umakoshi and co-workers who used time-resolved emission spectra from the probe Laurdan to create 'water maps' and estimate water population per lipid.[65] Water in the bilayer tends to be organized in string or branched structures having lower H-bond coordination with only a small population of isolated monomers.[62]

We propose that C152 solvation in DPPC bilayers is sensitive to bilayer hydration, while C151.5 solvation in the bilayer is not. From this difference, we infer that C152 solvated in the polar headgroup region is not as strongly associated through non-covalent interactions with the polar headgroup as is C151.5. If this supposition is true, C152 will be able to utilize the increased water concentration in the bilayer that accompanies melting to accept a hydrogen bond through C152's amine lone pair. In contrast, if C151.5's noncovalent interactions in the polar headgroup region – most notably hydrogen bonds to either the choline or ester groups – are suitably strong *and* prevent partitioned solutes from interacting with water molecules already in the (gel-phase) bilayer, then we surmise C151.5 will be insensitive to the influx of additional water following melting. While this interpretation is admittedly speculative and does not explicitly consider the specific contributions from water entering the bilayer, it does raise interesting questions about the role water plays in facilitating bioconcentration and intramembrane chemistry.

Conclusion

Understanding a solute's tendency for bioconcentration is a topic of interest as it could lead to adverse ecological or physiological effects and require a costly remediation in the future. This work examined how three closely related 7-aminocoumarin solutes partitioned into DPPC lipid bilayers as a function of temperature. All three solutes have log P values that predict strong membrane affinity, however each solute exhibited distinctively different partitioning behavior. C151 with a log P value of 1.6 and showed no partitioning into the DPPC bilayer regardless of temperature and lipid bilayer phase. C151.5 has a log P value of 1.9 partitioned only into the bilayer's polar head group region and the amount of C151.5 that partitioned into the bilayer varied only slightly with temperature and lipid bilayer phase. C152 partitioning showed a strong temperature dependence with ~90% of the available solute being absorbed into the bilayer near the DPPC transition temperature, qualitatively consistent with a log P value of 2.5.

These differences illustrate clearly that membrane partitioning and the tendency of a solute to bioconcentrate depends on more than simply differential solubilities between aqueous and polar organic (e.g. 1-octanol) phases. In predicting bioconcentration, additional factors must be considered, including specific solvation forces such as solute-hydrogen bonding. The data suggest differences in partitioning mechanisms that provide clear benchmarks for further experimental and computational studies.

CHAPTER THREE

AMINO ACIDS CHANGE SOLUTE AFFINITY FOR LIPID BILAYERS

Contribution of Authors and Co-Authors

Manuscript in Chapter 3

Author: Katelyn M. Duncan

Contributions: Collected and analyzed all data, generated figures, and wrote manuscript in preparation for publication.

Co-Author: William H. Steel

Contributions: Assisted with data accumulation. Assisted with editing of manuscript.

Co-Author: Robert A. Walker

Contributions: Contributed important insight into performing experiments and interpreting results. Edited and assisted in the preparation of the manuscript.

Manuscript Information

Katelyn M. Duncan, William H. Steel, and Robert A. Walker.

Biophysical Journal

Status of Manuscript:

____ Prepared for submission to a peer-reviewed journal

____ Officially submitted to a peer-reviewed journal

____ Accepted by a peer-reviewed journal

__x_ Published in a peer-reviewed journal

Published by the Biophysical Journal

In Volume 120, Issue 17, 3676-3687 (2021)

DOI 10.1016/j.bpj.2021.07.021

AMINO ACIDS CHANGE SOLUTE AFFINTY FOR LIPID BILAYERS

Katelyn M. Duncan[a], *William H. Steel*[b], *and Robert A. Walker*[a,c,]*

[a]Department of Chemistry and Biochemistry, Montana State University, Bozeman, Montana 59717, United States.
[b]Department of Chemistry, York College of Pennsylvania, York, Pennsylvania 17403, United States
[c]Montana Materials Science Program, Montana State University, Bozeman, Montana 59717, United States

Abstract

Time resolved fluorescence and differential scanning calorimetry were used to examine how two amino acids, L-Phenylalanine (L-PA) and N-Acetyl-DL-tryptophan (NAT), affect the temperature-dependent membrane affinity of two structurally similar coumarin solutes for DPPC vesicles. The 7-aminocoumarin solutes, Coumarin 151 (C151) and Coumarin 152 (C152), differ in their substitution at amine position – C151 is a primary amine and C152 is a tertiary amine – and both solutes show different tendencies to associate with lipid bilayers consistent with differences in their respective log P values. Adding L-PA to the DPPC vesicle solution did not change C151's propensity to remain freely solvated in aqueous solution, but C152 showed a greater tendency to partition into the hydrophobic bilayer interior at temperatures below DPPC's gel-liquid crystalline transition temperature ($T_{gel\text{-}lc}$). This finding is consistent with L-PA's ability to enhance membrane permeability by disrupting chain-chain interactions. Adding NAT to DPPC vesicle-containing solutions changed C151 and C152 affinity for the DPPC membranes in unexpected ways. DSC data show that NAT interacts strongly with the lipid bilayer, lowering $T_{gel\text{-}lc}$ by up to 2˚C at concentrations of 10 mM. These

effects disappear when either C151 or C152 is added to solution at concentrations below 10 μM, and T_{gel-lc} returns to a value consistent with unperturbed DPPC bilayers. Together with DSC results, fluorescence data imply that NAT promotes coumarin adsorption to the vesicle bilayer surface. NAT's effects diminish above T_{gel-lc} and imply that unlike L-PA, NAT does not penetrate into the bilayer but instead remains adsorbed to the bilayer's exterior. Taken in their entirety, these discoveries suggest that amino acids - and by inference, polypeptides and proteins - change solute affinity for lipid bilayers with specific effects that depend on individualized amino acid/lipid bilayer interactions.

Introduction

Synthetic organic solutes have long been the subject of partitioning studies that seek to assess properties such as bioavailability, toxicity, and environmental persistence [70-73]. The most commonly cited measure of partitioning behavior is the log P (or log $K_{o/w}$) partitioning coefficient that describes solute affinity for an organic environment (1-octanol) relative to an aqueous environment. Despite being developed in the late 19th century as a predictor of anaesthetic efficacy [74-75], log P continues to be used as a model describing solute accumulation in biological membranes [14] and serves one of five criteria in the Lipinski Rule of 5 framework that guides pharmaceutical development [15, 18].

While log P remains a valuable predictive tool, more chemically informed models describing solute affinity for membranes continue to be developed. To account for charged solutes with various pKa's, the log D scale was created and accounted for pH dependent changes in solute charge [48, 76-77]. The liposome-water coefficient (log $K_{lip/w}$)

was developed to provide more accurate description of a solute's membrane affinity by adding liposomes to an aqueous phase [78-79]. The log $K_{lip/w}$ shares a parabolic relationship with the log P for lower molecular weight solutes, but this relationship breaks down for larger molecules due to higher energies required to displace solutes within the membrane structure [71, 78]. Other studies have also shown that solute accumulation in membranes varies between lipid types, meaning that these equilibrium coefficients fail to capture 'real' partitioning tendencies because biological cells contain a host of environments, including those created by storage lipids (fatty lipids) and the heterogeneous membrane bilayer [80]. When anticipating solute accumulation in adipose tissue (composed primarily of storage lipids), olive oil is often used as a replacement for the octanol phase in the determination of the log P (now log $K_{olive\ oil/water}$) for storage lipids [80].

While these modifications to log P are useful and provide a more realistic perspective into membrane partitioning tendencies, they are still limited in their capabilities. Common shortcomings include a limited ability to function correctly for larger solutes and an oversimplification of lipid membrane heterogeneity [17, 70]. In summary, log P and its derivatives are useful tools; however, they are unable to account for specific solute-solute and solute-membrane interactions that underlie all partitioning behaviors. In an effort to add complexity and improve the accuracy and predictive power of $K_{lip/w}$, a number of studies have created lipid vesicles containing additional components such as cholesterol [81], surfactants [82], and proteins [83].

Recent work in our own laboratory demonstrated that time resolved fluorescence spectroscopy can determine the extent of solute accumulation in simple lipid vesicle

bilayers and, more importantly, identify how solutes distribute themselves across the bilayer. Specifically, solutes having fluorescence lifetimes sensitive to local solvation environments can effectively report on whether solutes sample conditions attributed to either an aqueous buffer, a hydrophobic alkane-like environment, or surroundings that can be approximated as polar organic solvents. These studies illustrated how solute partitioning depends on bilayer phase [84] and composition [45] and also demonstrated that partitioning ratios could be quantified [46].

Our previous work in this area examined the temperature dependence of solute partitioning into single or dual-component phospholipid bilayers. Understanding how the presence of additional biologically relevant species affects membrane properties is necessary for developing accurate descriptions of how solute affinity for lipid bilayers changes. The studies described below examine solute affinity for lipid bilayers in the presence of two amino acids, L-phenylalanine (L-PA) and N-acetyl-tryptophan (NAT). Several reports have suggested that amino acids alter solute binding to lipid membranes and change membrane permeability to organic solutes [35, 85-89]. Complementing the body of experimental work have been computational studies that examined how amino acids and peptides associate with lipid membranes, the free energy changes involved with such associations, and the impact of peptide association on bilayer properties [33-34, 90]. Experimental findings particularly relevant to the studies described below reported that L-PA increased lipid bilayer permeability at L-PA concentrations of 5 mM and 20 mM [91]. This study proposed that the increase in permeability was due to phenylalanine aggregates forming within the membrane. Other studies by Nandi *et. al.*, compared the

effects of D-Phenylalanine to L-Phenylalanine on lipid bilayer vesicles and how the different enantiomers interact with the lipid membrane, concluding that a L-Phenylalanine increases the lipid membrane fluidity and membrane permeability more than D-Phenylalanine [92]. Additionally, Kanwa *et. al.*, reported that amino acid formal charge affects how effectively the amino acid is accommodated into lipid membranes [93]. Specifically, cationic amino acids fluidize the membrane while anionic amino acids dehydrate the membrane. Given that these studies demonstrate that amino acids affect membrane permeability, we hypothesize that partitioning behavior and solute distributions in the lipid bilayers' varied solvation environments will also change.

Materials and Methods

Chemicals

Structures of all 5 chemicals used in these experiments – C151, C152, L-PA, NAT, and 1,2-dipalmitoyl-*sn*-glycero-3-phosphocholine (DPPC) – are shown in Figure 3.1.

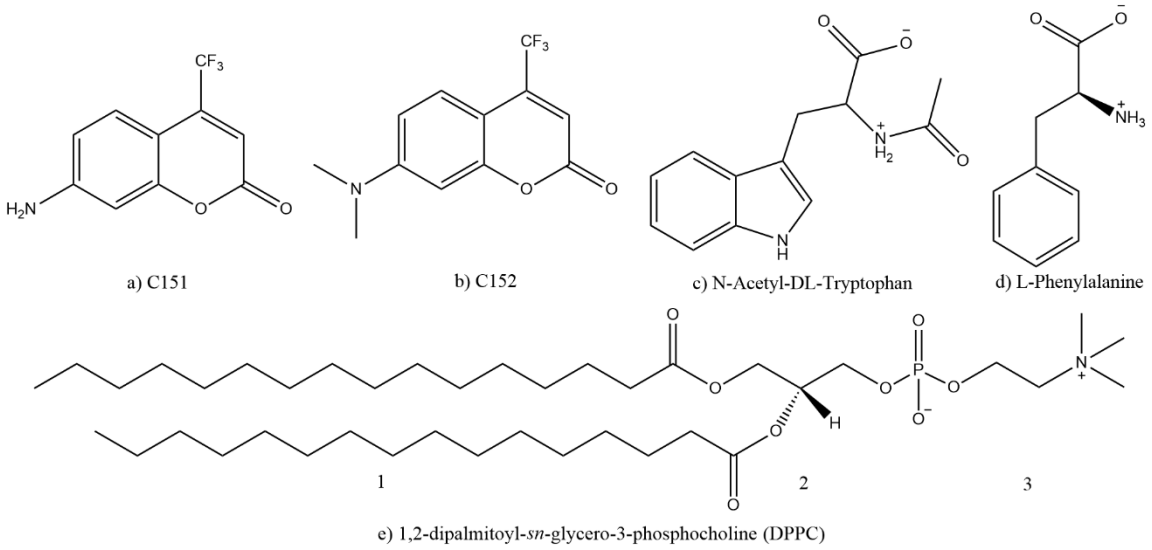

Figure 3.1. Chemical Structures of a) Coumarin 151 (C151), b) Coumarin 152 (C152), c) N-Acetyl-DL-Tryptophan (NAT), and d) L-Phenylalanine (L-PA), e) and 1,2-dipalmitoyl-sn-glycero-3-phosphocholine (DPPC) lipid. Number assignments refer to various environments created by lipid with the (1) nonpolar, hydrophobic hydrocarbon tail, (2) the polar glycerol-backbone and ester groups, and (3) the polar zwitterionic phosphate headgroup. The COOH pKa values for NAT and L-PA are 3.6 and 2.2 respectively (ChemDraw Prime 19.0) giving local charges on structures at a pH of 7 used for these experiments.

Laser Grade C151 and C152 were purchased from Exciton; L-PA and NAT were purchased from Sigma Aldrich and Alfa Aesar, respectively; and DPPC was purchased from Avanti Polar Lipids. All chemicals were used as received. Solutions were made in using Millipore water (18.2 MΩ) buffered to a pH of 7.0 with a PBS buffer (ionic strength = 10 mM). C151 and C152 concentrations in all solutions were kept constant at

6 μM. L-PA and NAT concentrations were kept constant at 10 mM. Control experiments were performed with 20 mM PBS buffer solutions without amino acids to test whether a simple change in ionic strength might change C15X affinity for membranes. These experiments with higher PBS concentrations resulted in findings equivalent to those performed in a 10 mM PBS buffer (Reference 20), demonstrating that over this limited concentration range, solute affinity for DPPC bilayers is not sensitive to ionic strength. (Data not shown).

C151 and C152 have been extensively studied and have well characterized photophysical properties [43-46, 51, 53-55, 84]. In its neutral form, L-PA has a log P of -1.4 indicating it should remain in the aqueous environment. The pKa_1 of the COOH group of L-PA is 2.2, and the pKb_2 for the $R\text{-}NH_3^+$ 9.9 (calculated by ChemDraw Prime 19.0); this combination results in a zwitterionic form in the PBS pH 7 buffer used in these experiments. As a zwitterion L-PA has a (calculated) log P of 0.12, implying a greater tendency to partition into the DPPC bilayer than in its neutral form. The other amino acid used in this study is NAT. In its neutral form NAT has a log P value of 1.1, indicating its affinity for the organic medium; however, under experimental conditions (pH = 7.0) NAT is also zwitterionic and its log P value diminishes to 0.34.

Lipid Bilayer Preparation

Lipid bilayer vesicles were prepared by dissolving DPPC in chloroform. The solvent was then removed via rotary evaporation. The resulting thin lipid film was subsequently rehydrated using a 6 μM coumarin and 10 mM amino acid solution in 10 mM phosphate-buffered saline (PBS, pH=7) to form a lipid vesicle solution. The solution was sonicated

for 30 minutes at ~50 °C. The solution temperature was then maintained at 50 °C as the solution was passed through an Avanti Mini Extruder 10 times with a membrane pore size of 200 nm [43-46]. Fluorescence experiments were made with 1.5 mM DPPC vesicles solutions and DSC experiments used 20 mM DPPC vesicles solutions.

Differential Scanning Calorimetry (DSC)

Differential scanning calorimetry (DSC) measurements were done using a TA Instruments Discovery Q2000 DSC. Vesicle solutions were made using the method described above with concentrations of 20 mM DPPC vesicles and rehydrated with 10 mM PBS buffer (pH =7), for pure DPPC vesicles. For C15X-AA doped DPPC vesicles, a 6 μM Coumarin solution with 10 mM amino acid solution in a 10 mM PBS buffer was used to rehydrate vesicles. The vesicles made for DSC experiments were not filtered to size select vesicles. For experiments, Tzero pans and Tzero hermetic lids (TA Instruments) were used and equilibrated at 20 °C and heated 1 °C/min to 55 °C to capture the gel-liquid crystalline transition temperature ($T_{gel\text{-}lc}$).

Time-Correlated Single-Photon Counting (TCSPC)

Fluorescence lifetimes were measured following coumarin excitation by a Ti:sapphire oscillator (Coherent Chameleon, 80 MHz, 85 fs pulse duration, 680-1040 nm wavelength range) coupled with an APE autotracker harmonic generator used to frequency double the fundamental wavelength. A Conoptics model 350-10 modulator was used to reduce the repetition rate to 4 MHz. Picoquant PicoHarp 300 and FluoTime 200 software were used for data collection. Samples were equilibrated at reported temperatures for 5 minutes using a Quantum Northwest TC125 temperature controller, longer equilibration times led

to no discernable change in emission traces. Excitation wavelengths were unique to each solute in individual bulk solvents. For experiments carried out with vesicle containing solutions, excitation wavelengths were chosen that overlapped coumarin absorption in all bulk solvents. Adding amino acids did not change the C15X steady state excitation/emission spectra in the different bulk solvents. Changes to C15X emission lifetimes, when they were observed, were modest and discussed in the relevant sections below. Additional details about experimental procedures and assemblies can be found in References [43-46, 50-51, 84].

Time-resolved emission data from vesicle-containing solutions are fit with a linear combination of independent lifetimes and amplitudes using fitting parameters that are adjusted to minimize residuals and optimize χ^2. The resulting lifetimes are then compared to solute lifetimes in different bulk solvents that were chosen to mimic local solvation environments within the lipid bilayer. The fluorescence decay and amplitude expression is shown in Eq. 3.1, where A_i and τ_i are the amplitude and lifetime of the i^{th} component, respectively [52].

$$I(t) = \int_0^t IRF\,(t') \sum_{i=1}^{n} A_i e^{\frac{-t-t'}{\tau_i}}\, dt' \qquad (3.1)$$

Each equation was fit independently, without any constraints, for the lifetimes and amplitudes with a typical χ^2 between 0.90-1.10 when accounting for at most three lifetimes. Typically, uncertainties in lifetimes and amplitudes were 0.2 ns and 0.04, respectively. Reported data represent the averaged results from at least 4-5 experiments with independently prepared, equivalent samples. Lifetime uncertainties are reported as ± 0.2 ns due to the TCSPC instrument response function; however, the error bars presented

in this work are the result of 4-5 trials averaged together with deviations reported for an average of those trials. The average lifetimes and amplitudes and their respective standard deviations are reported for each specific temperature.

Results and Discussion

L-Phenylalanine Results & Discussion

Structural changes in the lipid bilayer can be inferred from changes in $T_{gel\text{-}lc}$ as a function of L-PA concentration. L-PA's reported ability to increase bilayer permeability [91] implies weaker intermolecular forces between the bilayer's acyl chains, a hypothesis borne out by the small but measurable shift in $T_{gel\text{-}lc}$ from 41.0˚C to 40.5˚C (Figure 3.2). The effect of L-PA concentration on the DPPC $T_{gel\text{-}lc}$ is shown found in Figure B-3.1 of Appendix B. The DSC endothermic peak remains at 40.5 °C as the concentration of L-PA increases. Adding C151 to the phenylalanine-containing vesicle solution does not further alter $T_{gel\text{-}lc}$, but the addition of C152 to the solution results in significant changes the DSC behavior. Specifically, the endotherm peak diminishes in intensity and broadens considerably. Such behavior indicates synergistic effects where the two solutes – L-PA and C152 – disrupt cohesive forces between the DPPC acyl chains [94].

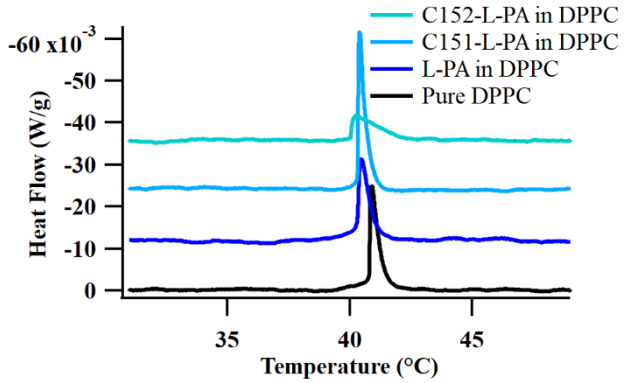

Figure 3.2. DSC trace of pure DPPC, 10 mM L-PA in DPPC, and C151 with 10 mM L-PA in DPPC, and C152 with 10 mM L-PA in DPPC. Each trace is endothermic and offset for ease of viewing.

If C152 partitioning into the DPPC bilayer is enhanced by L-PA as implied by the DSC results, the next question to resolve is where within the bilayer does C152 accumulate? C152's log P value of 2.2 predicts that partitioning into membranes should be favored. Previous work used C152's time-dependent fluorescence emission to assess its local solvation environment in lipid bilayers based on its behavior in bulk solvation environments [43, 84]. In polar protic environments, C152 is believed to form a twisted intramolecular charge transfer (TICT) state and has a correspondingly short (≤ 1 ns) lifetime [53]. In polar aprotic environments, this lifetime lengthens to ~2 ns and in nonpolar, alkane environments, C152 emission is dominated by a relatively long ~4 ns lifetime. In all organic solvents, C152 fluorescence decay is well described by single exponential kinetics. In aqueous solution, C152 emission is dominated by a short (sub-ns) component with a longer lifetime (~3.6 ns) contributing to < 20% of the decay trace intensity. C151's time resolved emission behavior is also well characterized by a 4.51 ns lifetime in PBS buffer; a 5.25 ns lifetime in both methanol and acetonitrile; and

biexponential decay with shorter lifetimes (1.21 ns (65%) and 3.27 ns (35%)) in alkanes [84].

Given findings from the DSC experiments, we assumed that adding L-PA to vesicle containing solutions did not change C151 partitioning into DPPC bilayers but did change C152's partitioning behavior. The assumption regarding C151 behavior was borne out by time resolved fluorescence measurements described below. To assess C152 partitioning into DPPC bilayers infiltrated with L-PA, we first measured the time resolved emission from C152 in methanol, acetonitrile and cyclohexane. These solvents were chosen to represent the different solvation environments C152 might encounter across the DPPC bilayer. All solvents contained 10 mM L-PA, although the L-PA concentration in cyclohexane was likely smaller due to solubility constraints. Data from these studies are reported in Table 3.1 for C152 (and C151) in solutions of cyclohexane (nonpolar), acetonitrile (polar aprotic), methanol (polar protic) and the pH 7 PBS buffer. Bulk solvent fluorescence decay traces can be found in Appendix B (Figure B-3.2). In the event of a biexponential fluorescence decay resulting in two lifetimes, the lifetime with the highest amplitude was used as representative for that environment. Including minority lifetimes (and amplitudes) for a given solvent did not improve fitting accuracy by statistically significant amounts. The fluorescence lifetimes of C151 and C152 with L-PA in each of the bulk solvents were taken as a function of temperature and decreased by less than 0.3 ns in all solvents as temperature increased from 10˚C to 60˚C (Appendix B Table B-3.1 and B-3.2, respectively). In every instance the lifetimes were virtually unchanged from those of the C15X solutes alone in the respective solvents. L-PA does, however,

appear to change the relative amplitudes in cases where fluorescence emission is biexponential, particularly for C151 in cyclohexane.

Table 3.1. Fluorescence lifetimes (in ns) of C151-L-PA and C152-L-PA in bulk solvents. The numbers reported in parenthesis are the respective amplitudes of the reported lifetimes. The fluorescence lifetimes reported were measured at 10 °C.

Solvent	**C151-L-PA** τ_f (ns)	**C152-L-PA** τ_f (ns)
PBS Buffer	4.58	0.60 (0.81) 3.77 (0.19)
Methanol	5.24	1.04
Acetonitrile	5.37	2.16
Cyclohexane	1.12 (0.24) 3.80 (0.76)	3.98

To examine how L-PA affects C151 and C152 partitioning into DPPC lipid bilayers, both solutes were introduced (separately) to DPPC vesicle solutions containing 10 mM L-PA, and each coumarin's time-resolved emission was measured as a function of temperature over a range from 10 °C to 60 °C. To determine whether effects were reversible, spectra were collected as the temperature was increased and then decreased. As mentioned in the Experimental section, each emission trace was fit independently with a minimum number of lifetimes leading to a χ^2 between 0.9-1.1. The fluorescence lifetimes of C15X-L-PA in DPPC lipid bilayers at each temperature were then compared to the lifetimes found in bulk solvents to infer the local solvation environment surrounding the solute. Each respective amplitude was radiative rate corrected using the fluorescence quantum yield of pure C15X in the respective environment. The results of C15X-L-PA in DPPC lipid vesicles can be seen in Figure 3.3 with the results of the fitting seen in Table 3.2.

Table 3.2. Fluorescence lifetimes (in ns) of C15X-L-PA in DPPC respective amplitudes (in parentheses) from 10 °C to 60 °C and back. Amplitudes have been corrected for their respective radiative rates. Lifetime uncertainties are ± 0.2 ns; amplitude uncertainties are ± 0.04.

	C151-L-PA	**C152-L-PA**		
temp. (°C)	buffer τ_1	buffer τ_1 (A_1)	polar τ_2 (A_2)	nonpolar τ_3 (A_3)
10	4.90	0.55 (0.54)	1.44 (0.20)	4.21 (0.26)
20	4.87	0.43 (0.51)	1.45 (0.30)	4.10 (0.19)
30	4.81	0.35 (0.50)	1.41 (0.37)	4.10 (0.13)
36	4.85	0.32 (0.42)	1.35 (0.48)	4.34 (0.10)
42	4.97	0.29 (0.29)	1.28 (0.64)	4.56 (0.07)
50	5.02	0.18 (0.17)	0.98 (0.78)	5.10 (0.05)
60	4.90	0.17 (0.21)	0.77 (0.74)	5.02 (0.05)
50	5.04	0.17 (0.17)	0.97 (0.78)	5.01 (0.05)
42	5.07	0.26 (0.24)	1.25 (0.69)	4.40 (0.07)
36	4.89	0.31 (0.40)	1.32 (0.50)	4.25 (0.10)
30	4.87	0.34 (0.44)	1.41 (0.44)	4.14 (0.12)
20	4.85	0.41 (0.47)	1.53 (0.35)	4.16 (0.18)
10	4.90	0.53 (0.51)	1.45 (0.23)	4.27 (0.26)

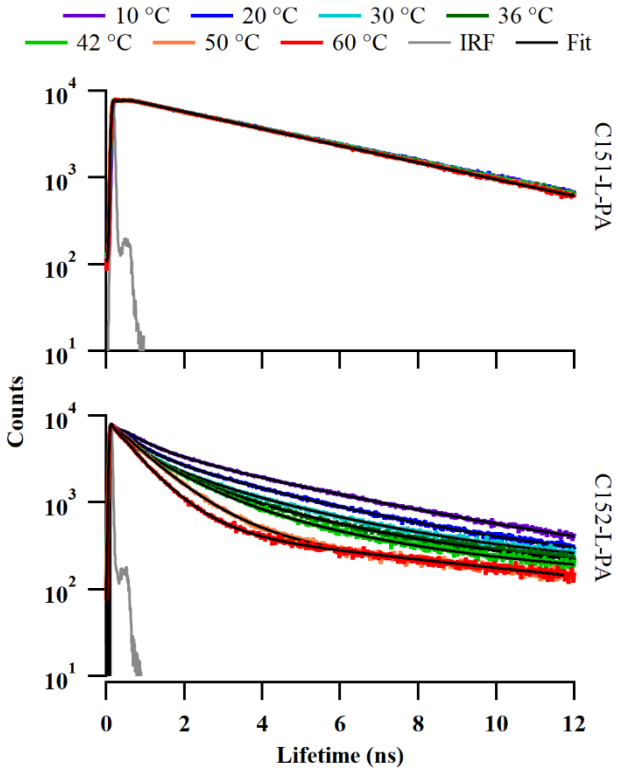

Figure 3.3. TCSPC spectra of C151-L-PA in DPPC (top) and C152-LP In DPPC (bottom) as a function of temperature. Each trace was fit using Equation 3.1 and are reported in Table 3.2.

Figure 3.3 and Table 3.2 show that C151 fluorescence decay traces in L-PA/DPPC solutions can be fit to a single lifetime that matches that of C151-L-PA in PBS buffer. This result demonstrates that C151/L-PA does not partition into the lipid vesicles, similar to this solute's behavior in the absence of L-PA [84]. This finding also reinforces conclusions from DSC experiments showing that adding C151 to a L-PA/DPPC solution did not further change the bilayer's gel-liquid crystalline transition.

C152 lifetimes identified for L-PA/DPPC solutions are very similar to those measured for C152 in DPPC solutions in the absence of L-PA. The emission decay data in Figure 3.3 are best fit to three, unique lifetimes. The short, sub-ns lifetime corresponds

to C152-L-PA in PBS buffer, indicating some C152 remains in the aqueous solution and does not associate with the DPPC vesicles. The intermediate lifetime at temperatures below T_{gel-lc} falls between the polar aprotic (2.16 ns in acetonitrile) and polar protic (1.04 ns in methanol) limits but clearly indicates a C152 population sampling a local environment having an appreciable static dielectric constant. Above T_{gel-lc}, this intermediate lifetime closely matches C152's lifetime in methanol indicating a polar protic solvation environment. While we cannot definitively assign C152's intermediate lifetime at low temperatures to specific solvation forces, above T_{gel-lc} C152 in the polar headgroup region behaves as if it is associating solvating water molecules in the glycero-backbone region of the DPPC bilayer. This phenomenon has been reported before and is attributed to bilayer hydration above T_{gel-lc} [43, 84]. Lastly, the long lifetime most closely matches that of C152-L-PA in cyclohexane, implying a portion of the C152 solute molecules are fully solvated within the acyl chain region of the lipid bilayer. Data reported in Table 3.2 are illustrated in Figure 3.4.

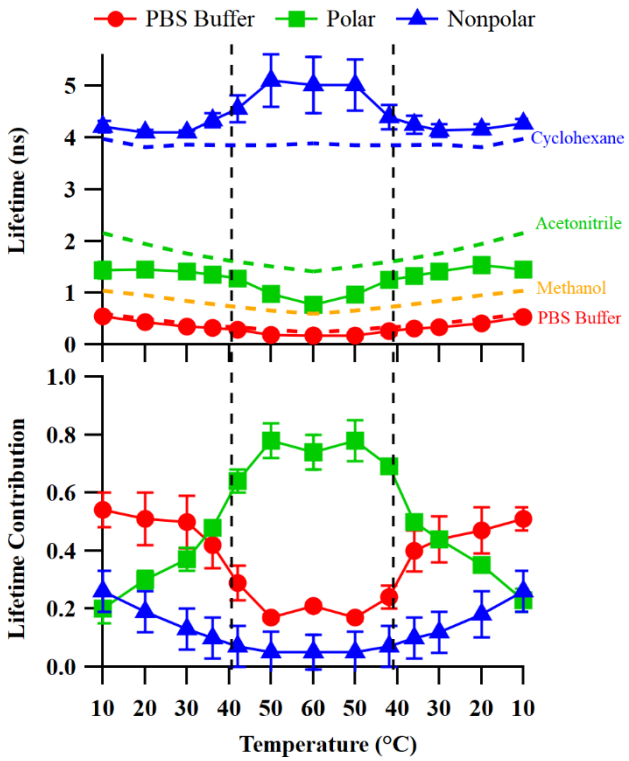

Figure 3.4. C152 fluorescence lifetimes (top) in L-PA/DPPC solutions and the respective radiative rate corrected lifetime contributions (bottom). The three lifetimes are assigned to C152 in PBS Buffer (τ_1, red circles), DPPC's polar head group region (τ_2, green squares), and DPPC's nonpolar interior (τ_3, blue triangles). The dashed lines indicate the $T_{gel\text{-}lc}$ of DPPC bilayer at ~41.5 °C. Each point is an average of 5 independent trials and the respective error bars on each point indicate an uncertainty of one standard deviation based on the results from those 5 trials. In some instances, the uncertainty is smaller than the marker used to represent that data point.

While the lifetimes for C152 partitioning into DPPC bilayers are very similar, regardless of whether or not L-PA is present, the contributions of these lifetimes to the C152 emission traces are measurably different between the two systems. In the absence of L-PA and at the lowest temperature sampled (10˚C), the distribution of C152 between aqueous:polar:interior environments is approximately 0.40:0.40:0.20, where polar refers to the polar, glycero-backbone region of the bilayer and interior refers to the nonpolar acyl chain region of the bilayer. When L-PA is present, this aqueous:polar:interior

balance changes to 0.55:0.20:0.25. In other words, adding L-PA depletes C152 in the polar headgroup region pushing more C152 back into aqueous buffer and some into the bilayer's hydrophobic interior. If the bilayer is infiltrated by L-PA and L-PA not only disrupts chain-chain interactions but is better solvated than C152 in the polar headgroup region, then L-PA would afford C152 easier access to the membrane's low polarity region for the hydrophobic C152. Furthermore, L-PA might also occupy 'sites' in the polar headgroup region that are then no longer able to accommodate C152 thereby increasing C152's concentration in aqueous solution. This latter assertion is speculative but does raise questions about bioconcentration mechanisms and the nature of solute solvation in biological membranes.

At the highest temperatures sampled, 50˚C and 60˚C, the fraction of C152 in the polar headgroup region reaches ~75-80% with the polar region showing strong evidence of hydration above $T_{gel\text{-}lc}$. At these elevated temperatures, the C152 fraction in the nonpolar region falls to almost zero and the C152 fraction in aqueous solution drops to ~20%. This gradual increase of C152 in the bilayer's polar headgroup region stands in contrast with the more abrupt uptake of C152 shown by DPPC bilayers *in the absence* of L-PA [84]. The data in Figure 3.4 are consistent with the DSC results that show how L-PA and C152 synergistically suppress and broaden the DPPC bilayer's $T_{gel\text{-}lc}$. The fact that L-PA affects C152 partitioning but has no affect on C151 affinity for DPPC bilayers implies that this amino acid will only influence partitioning for those solutes that already have a tendency to accumulate in bilayers. As will be noted below, these observations have direct consequences for predicting *how* L-PA associates with DPPC bilayers.

N-Acetyl-DL-Tryptophan Results & Discussion

Given how L-PA affects C152 partitioning into membranes, we sought to determine if these findings were general for amino acids. In that context, we employed the same techniques to determine how N-Acetyl-DL-Tryptophan (NAT) influences C151 and C152 partitioning into DPPC lipid bilayers containing 10 mM NAT.

NAT's effects on DPPC's properties are evident in concentration dependent DSC experiments. Figure 3.5 reports DSC endotherms of DPPC vesicle solutions over a range of NAT concentrations. At concentrations above 6 mM, NAT causes DPPC's $T_{gel\text{-}lc}$ to shift to lower temperatures and develop an additional low temperature shoulder. These effects are much more pronounced than any observed with L-PA, indicating that NAT associates more strongly with the DPPC bilayer.

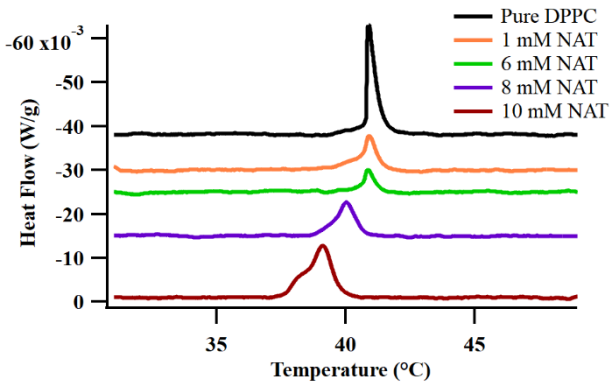

Figure 3.5. DSC spectra of 20 mM DPPC vesicles rehydrated with pure PBS buffer as well as 1, 6, 8, and 10 mM NAT in PBS buffer. Each trace is endothermic and offset for ease of viewing.

The DSC data show that at low NAT concentrations, $T_{gel\text{-}lc}$ of the NAT/DPPC systems remains virtually unchanged from that of pure DPPC. As NAT concentration increases from 6 to 10 mM, the primary feature in the isotherm

shifts from 41˚C to 39˚C, a change much larger than the -0.5˚C shift induced by 10 mM L-PA. In addition to the shift to lower temperatures, NAT induces a low temperature shoulder to the endotherm, suggesting that a second mechanism may also be affecting the gel-liquid crystalline lipid bilayer phase transition. Earlier work studying saccharide adsorption to lipid films attributed a *high* temperature shoulder to dehydration of the lipid bilayer headgroups, allowing stronger Coulomb interactions to further stabilize the bilayer's gel phase [95-96]. A *low temperature* shoulder may signify disruption of acyl chain interactions. Alternatively, this observation may also hint at more direct NAT-choline headgroup interactions that weakens Coulomb attractions between headgroups in a way that also disrupts the gel-liquid crystalline phase transition [97].

Similar to the L-PA/DPPC experiments, pH 7 PBS buffer solutions containing 6 μM coumarin and 10 mM NAT were used to rehydrate 20 mM DPPC vesicles that were then analyzed using DSC (Figure 3.6). As noted in Figure 3.5, NAT by itself at concentrations ≥ 6 mM significantly perturbs $T_{gel\text{-}lc}$. However, in NAT-DPPC solutions, both coumarins cause $T_{gel\text{-}lc}$ to shift back to *higher* temperatures (40.4 °C). The DSC endotherm peak also sharpens and intensifies for C151-NAT-DPPC and C152-NAT-DPPC solutions, implying that the coumarin solutes, despite their 1000-fold smaller concentration (6 μM C15X vs. 10 mM NAT) offset the disruptive effect(s) that NAT has on the DPPC bilayer cohesion (Figure 3.6).

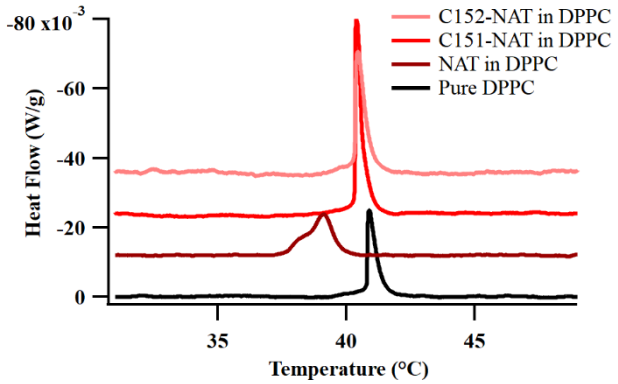

Figure 3.6. DSC spectra of 20 mM DPPC vesicles rehydrated with pure PBS buffer, 10 mM NAT in PBS buffer, and 6 µM C151 and C152 with 10 mM NAT in PBS buffer. Each trace is endothermic and offset for ease of viewing.

Time resolved emission data provide insight into the unusual and surprising DSC results. Table 3.3 reports the fluorescence lifetimes of C151 and C152 in the model solvents containing NAT and the respective decay traces of C15X-NAT in each of the model solvents can be found in Figure B-3.3 of Appendix B. The lifetimes of C151-NAT and C152-NAT in each bulk solvent were also measured as a function of temperature and these data can be found in Tables B-3.3 and B-3.4, respectively, of Appendix B. The lifetimes of C15X-NAT as a function of temperature changed little with the exception of C151-NAT in cyclohexane. In that system, C151's emission lifetime increased from 4.20 ns (in the NAT containing solutions) to 4.83 ns (in the solutions without NAT).

Table 3.3. Fluorescence lifetimes (in ns) of C151-NAT and C152-NAT in bulk solvents. The numbers reported in parenthesis are the respective amplitudes of the reported lifetimes. The fluorescence lifetimes reported were measured at 10 °C

Solvent	**C151-NAT** τ_f (ns)	**C152-NAT** τ_f (ns)
PBS Buffer	4.04	0.58 (0.77) 3.36 (0.23)
Methanol	4.36	1.08
Acetonitrile	4.24	1.98
Cyclohexane	4.20 (0.79) 0.78 (0.21)	3.70

NAT changed C151 lifetimes measurably in the different solvents implying specific C151-NAT interactions. In particular, C151's PBS buffer lifetime shortens from 4.51 to 4.04 ns, and the decay lifetimes in both methanol and acetonitrile shorten by ~1 ns (from ~5.3 to ~4.3 ns). In cyclohexane, C151 continues to show biexponential decay but the amplitudes switch. In the absence of NAT, C151 emission in cyclohexane is dominated by the shorter lifetime (τ_1 = 1.21 ns, A_1 = 0.65; τ_2 = 3.27 ns, A_2 = 0.35). In a cyclohexane solution that contains NAT, the *longer* lifetime component (τ_1 = 4.20 ns) dominates (A_1 = 0.79) over the shorter component (τ_2 = 0.78 ns, A_2 = 0.21). In contrast to C151 behavior in NAT-free solvents, the results in Table 3.3 indicate significant solute-solute interactions. In particular, these results imply that in nonpolar solvents, NAT stabilizes C151's planar charge transfer excited state. In contrast to C151, C152's emission behavior in bulk solvents containing 10 mM NAT differ little from behavior in the solvents by themselves implying much weaker solute-solute interactions.

After characterizing the time-resolved emission of C15X-NAT in the model solvents (Appendix B, Figure B-3.3 and Tables B-3.3 – B-3.4), a PBS buffered solution of 6 μM C15X and 10 mM NAT was used to prepare DPPC vesicles. These systems were studied as a function of temperature using time resolved fluorescence (Figure 3.7). The resulting decay traces were fit using Equation 3.1. Once determined, the lifetimes of C151 and C152 in the NAT/DPPC solutions, were compared to the lifetimes of C15X-NAT in bulk solvents to determine each solute's solvation environments. Amplitudes were radiative rate corrected using the radiative rates of pure C15X in each bulk solvent. Results of this analysis of C15X in NAT/DPPC solutions are summarized in Table 3.4.

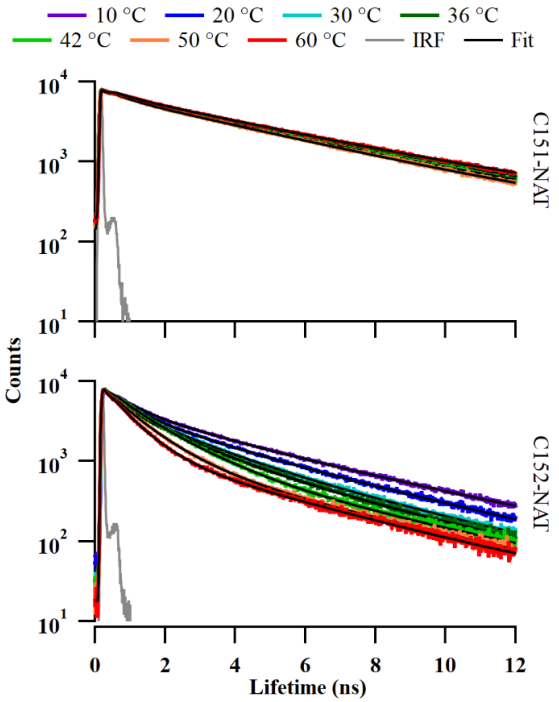

Figure 3.7. TCSPC spectra of C151-NAT in DPPC (top) and C152-NAT in DPPC (bottom) as a function of temperature. Each trace was fit using Equation 3.1 and are reported in Table 3.4.

Table 3.4. Fluorescence lifetimes (in ns) of C15X-NAT in DPPC respective amplitudes (in parenthesis) from 10 °C to 60 °C and back down to 10 °C. Amplitudes have been corrected for their respective radiative rates. Lifetime uncertainties are ± 0.2 ns; amplitude uncertainties are ±0.04.

	C151-NAT		**C152-NAT**		
temp. (°C)	buffer τ_1 (A_1)	complex τ_2 (A_2)	buffer τ_1 (A_1)	polar τ_2 (A_2)	nonpolar τ_3 (A_3)
10	4.12 (0.89)	0.63 (0.11)	0.52 (0.63)	1.63 (0.22)	4.16 (0.15)
20	3.98 (0.90)	0.66 (0.10)	0.43 (0.60)	1.42 (0.28)	3.90 (0.12)
30	3.87 (0.89)	0.72 (0.11)	0.39 (0.57)	1.51 (0.35)	3.69 (0.08)
36	3.84 (0.88)	0.77 (0.12)	0.36 (0.53)	1.42 (0.40)	3.62 (0.07)
42	4.06 (0.85)	0.70 (0.15)	0.34 (0.22)	1.27 (0.74)	3.72 (0.04)
50	3.90 (0.86)	0.78 (0.14)	0.23 (0.21)	0.98 (0.75)	3.86 (0.04)
60	3.66 (0.87)	0.73 (0.13)	0.21 (0.23)	0.76 (0.73)	3.48 (0.04)
50	3.86 (0.86)	0.70 (0.14)	0.23 (0.21)	0.97 (0.75)	3.58 (0.04)
42	4.07 (0.85)	0.75 (0.15)	0.29 (0.21)	1.22 (0.75)	3.75 (0.05)
36	3.82 (0.88)	0.76 (0.12)	0.34 (0.52)	1.38 (0.41)	3.67 (0.08)
30	3.88 (0.89)	0.77 (0.11)	0.38 (0.54)	1.47 (0.37)	3.75 (0.09)
20	4.02 (0.88)	0.72 (0.12)	0.41 (0.55)	1.45 (0.32)	3.88 (0.13)
10	4.14 (0.88)	0.65 (0.12)	0.45 (0.52)	1.41 (0.31)	4.14 (0.17)

The first observation that stands out is that C151 emission in NAT/DPPC solutions requires *two* emission lifetimes, not a single lifetime as was the case for C151 in DPPC and L-PA/DPPC solution (and in the buffer solution by itself). Specifically, C151 emission in the NAT/DPPC solutions contains a measurable (~15%) contribution from a short lived, ~0.70 ns component. This lifetime is absent in C151/NAT solutions in any bulk solvent. C151's photophysical behavior attributes short lifetimes to its inability to form a stable, planar intramolecular charge transfer (ICT) state [54]. ICT formation is favored in polar solvents – both protic and aprotic – and diminished in nonpolar solvents where excited state C151 is believed to retain sp^3 hybridization about the amine. The short lifetime observed in the C151/NAT/DPPC systems implies that a subset of the solvated C151 samples a local environment where it is conformationally restricted and photoexcitation does not lead to ICT formation. Similar behavior has been reported for C151 adsorbed to silica-methanol interfaces where hydrogen bonding between adsorbed C151 and silica's surface silanol groups coupled with surface induced changes in solvent organization introduce a short emission lifetime (~1.2 ns) to what should otherwise be a single exponential decay with a lifetime of ~5.3 ns [51].

Two other observations from the C15X/NAT/DPPC systems stand out. First, in addition to the short C151 lifetime noted above, the decay spectra of C152/NAT/DPPC show evidence of three unique lifetimes that are temperature dependent: a short (~0.4 ns) lifetime corresponding to that of C152-NAT solvated in the PBS buffer; an intermediate (1.6 ns) lifetime below $T_{gel\text{-}lc}$ that is similar to C152-NAT in acetonitrile; and a long (4 ns) lifetime that corresponds to that of the C152-NAT pairing solvated in cyclohexane.

All three lifetimes grow shorter at higher temperatures, and above $T_{gel\text{-}lc}$ the intermediate lifetime changes from a polar aprotic to a polar protic limit. Figure 3.8 summarizes these two observations by plotting the temperature-dependent lifetimes of C15X-NAT in DPPC vesicles; overlaid on these data are dashed lines to indicate the dominant lifetimes of C152 in the four bulk model solvents containing 10 mM NAT. The respective lifetime contributions for the lifetimes found in Figure 3.9 and Table 3.4.

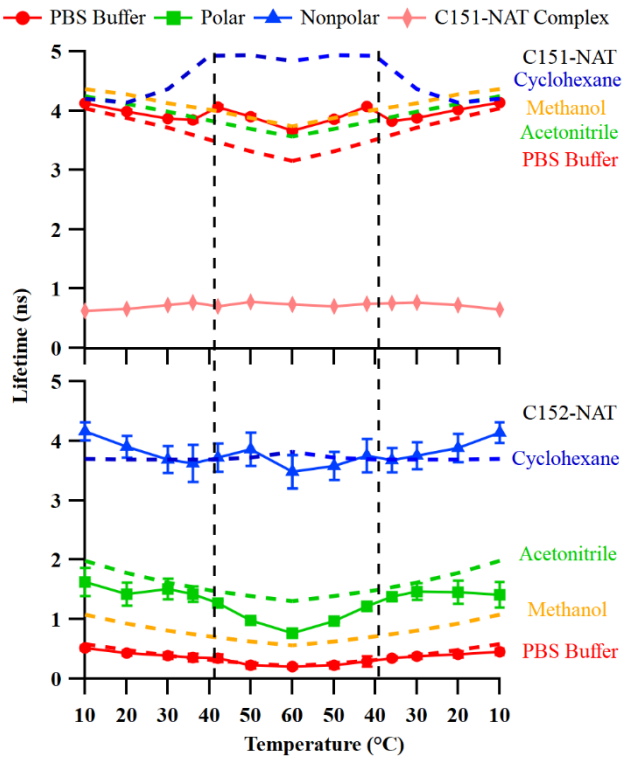

Figure 3.8. Fluorescence lifetimes of C151-NAT (top) in DPPC and C152-NAT in DPPC (bottom). The three lifetimes in the C152 traces are assigned to C152 in the PBS Buffer (τ_1, red circles), polar head group region (τ_2, green squares), and nonpolar bilayer interior (τ_3, blue triangles). The horizontal dashed lines represent the dominant lifetime of C15X-NAT in bulk solvents for comparison. The vertical dashed lines note $T_{gel\text{-}lc}$ of DPPC bilayer at ~41.5 °C. Each point is an average of 4 trials and the respective error bars on each point indicate one standard deviation of uncertainty from the 4 trials. In some cases, the uncertainty is smaller than the marker used to represent that data point.

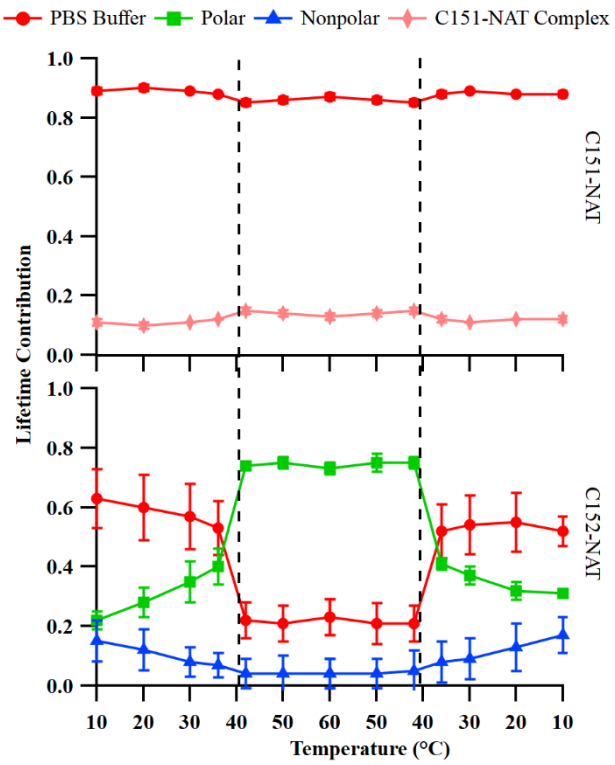

Figure 3.9. Radiative rate corrected lifetime contributions of C15X-NAT in DPPC. The lifetime contributions seen here correlate with the lifetimes reported in Figure 3.8 with C151 sampling two distinct environments and C152 sampling three environments in the DPPC/NAT solutions. For C151, the short lifetime contributions (pink diamonds) cannot be represented by C151 behavior in any bulk solvent (containing NAT) (Table 3.3). For C152, the three environments are assigned to C152 in the PBS buffer (τ_1, red circles), the polar headgroup region (τ_2, green squares), and the nonpolar bilayer interior (τ_3, blue triangles). The dashed lines indicate the $T_{gel\text{-}lc}$ at ~41.5 °C. Each point is an average of 4 trials and the error bars on each point are one standard deviation of the 4 trials.

The lifetime contributions determined for the C151 in NAT/DPPC system change very little as a function of temperature. In contrast, C152's behavior shows a strong temperature dependence with a large increase in the intermediate lifetime's contribution, assigned to C152 solvated in the polar backbone region, in the vicinity of DPPC's $T_{gel\text{-}lc}$. Similar behavior has been observed previously and was assigned to C152 moving into the polar part of a lipid bilayer as the bilayer melted and was able to accommodate more solutes in its interior [43, 46, 84].

Given these findings, three unexpected behaviors must be addressed:

1. The effects of C151 and C152 on DPPC's phase transition in the presence of NAT.
2. The origin of C151's second emission decay lifetime in NAT/DPPC solutions.
3. C152's abrupt uptake into DPPC bilayers in the vicinity of $T_{gel\text{-}lc}$ when NAT is present in contrast to the more gradual temperature dependent partitioning behavior observed in L-PA/DPPC solutions.

Each issue is addressed below and, together, these explanations lead to a description of NAT associating strongly with DPPC's charged headgroups in a way that affects bilayer properties and solute (C151 and C152) accumulation mechanisms.

1. The Effect of C15X on DPPC's Phase Transition in the Presence of NAT

The DSC results in Figure 3.5 show a clear trend in DPPC's $T_{gel\text{-}lc}$ as a function of NAT concentration: as NAT concentration rises, $T_{gel\text{-}lc}$ shifts to lower temperatures and develops an even lower temperature shoulder. With 10 mM NAT in solution, DPPC's main transition temperature is 2.5˚C lower than in the PBS buffer alone. Figure 3.6 shows that with 6 μM coumarin also in the NAT-DPPC solution, $T_{gel\text{-}lc}$ is virtually indistinguishable from solutions containing pure DPPC vesicles (40.4˚C (Coumarin/NAT/DPPC) vs. 40.5˚C (DPPC)). This behavior contrasts with that of L-PA where a 10 mM L-PA concentration leads to a very modest but reproducible -0.5˚C shift in $T_{gel\text{-}lc}$. Both L-PA and NAT are zwitterionic with a net charge of zero; however, NAT is slightly more hydrophobic (log P = 0.34 vs 0.12 for L-PA) and has more hydrogen

bonding opportunities. Whereas L-PA is predicted to migrate into the bilayer, possibly aggregating in the hydrophobic interior [91], we propose that NAT associates primarily with DPPC's charged headgroups.

DSC and time-resolved emission data also show that C151 does not associate with DPPC bilayers in the absence of NAT (nor with DPPC bilayers in the presence of L-PA). In order for the DSC endotherm in a NAT/DPPC (10 mM) solution to 'snap back' to its original temperature and shape with the addition of C151 (and C152), we propose that membrane destabilization by NAT results from a weakening of headgroup-headgroup interactions through direct, Coulomb interactions between the zwitterionic NAT and the zwitterionic DPPC head group. However, we maintain that these NAT adsorbates remain on the *surface* of the bilayer (perhaps with the aromatic rings penetrating into the glycero backbone region) and afford opportunities for either the C151 or C152 to hydrogen bond directly with this surface complex, weakening the NAT/DPPC association enough for the bilayer to recover its original phase stability. If C151 (or C152)/NAT association were strong enough for the complex to dissociate from the membrane surface, we would expect the >1000:1 NAT:C15X ratio to result in no change in DPPC's DSC behavior relative to solutions containing only 10 mM NAT and the DPPC vesicles. Furthermore, if the NAT partitioned into the bilayer interior as is presumed to be the case for L-PA, we would not expect C151 to associate with the membrane at all and $T_{gel\text{-}lc}$ would remain unchanged from the C151-free NAT/DPPC solutions.

2. C151's Second Lifetime in NAT/DPPC Solutions.

Fitting C151 time-resolved fluorescence emission in NAT/DPPC solutions requires two lifetimes, one long (τ_1 ~ 4.0 ns) assigned to C151 remaining in PBS buffer and one short (τ_2 ~ 0.7 ns) that does not correspond to C151 in any of the bulk solvents containing NAT. The relative contributions from these two lifetimes (~85% for τ_1 and 15% for τ_2) change little over the temperature range sampled. The shorter lifetime is consistent with C151 solvated in nonpolar solvents or in confinement where a long-lived ICT state cannot be stabilized [51, 54]. The insensitivity of τ_2 (and A_2) to membrane phase implies that these short-lived C151 species are not affected by the bilayer's backbone and acyl chain organization. This observed behavior *is* consistent with independent C151-NAT-choline headgroup complexes that remain intact from 10˚C to 60˚C.

3. An Abrupt Uptake of C152 Into the Bilayer in the Vicinity of the $T_{gel\text{-}lc.}$

Comparing the lower panels of Figures 3.4 and 3.9 is instructive. Both show the temperature-dependent changes in amplitude associated with C152 solvated in DPPC's polar headgroup region. The lifetimes of these amplitudes change from a value close to the polar aprotic limit at lower temperatures to a polar protic limit at temperatures above $T_{gel\text{-}lc}$ implying that above the transition temperature, C152 in the headgroup region can accept hydrogen bonds from putative H_2O that has hydrated the membrane. In both L-PA/DPPC and NAT/DPPC solutions, C152 shows a greater affinity for the polar region of the membrane than the surrounding aqueous solution. However, in the L-PA/DPPC solutions, C152 concentration increases almost monotonically as the solution passes

through $T_{gel\text{-}lc}$ (Figure 3.4) whereas in NAT/DPPC solutions, C152 concentration increases abruptly near $T_{gel\text{-}lc}$.

As noted earlier, results from the L-PA/DPPC solution can be explained by a mechanism where L-PA penetrates into the lipid bilayer, disrupting chain-chain interactions and enabling C152 accumulation. As the temperature rises, this disruption becomes more pronounced and allows increasing amounts of C152 to be absorbed by the bilayer (both from the hydrophobic part of the bilayer *and* from the bulk buffer). This result is consistent with the DSC data that show $T_{gel\text{-}lc}$ becoming broader and less pronounced when L-PA and C152 are both present in a DPPC vesicle solution (Figure 3.2).

In the case of NAT/DPPC, however, C152 accumulation into the bilayer changes little below $T_{gel\text{-}lc}$ and then rises abruptly at temperatures above $T_{gel\text{-}lc}$. DSC data show that $T_{gel\text{-}lc}$ in this system is sharp and narrow. If the NAT had penetrated into the DPPC bilayer, we would expect that the bilayer would accommodate increasing amounts of C152 as the temperature rose and that the C152 in the bilayer would sample a lifetime similar to that in L-PA/DPPC systems. The data in Figures 3.8 and 3.9 do not support this picture. Instead, C152's behavior can be understood and reconciled with items 1 and 2 above *if* NAT is bound to the DPPC headgroups and effectively blocks C152 partitioning into the bilayer. Only after the bilayer melts and the vesicle expands does C152 have the access to begin accumulating in the membrane's polar backbone region. Compared to the 33% increase of C152 into the DPPC backbone region when L-PA is present and the bilayer melts (A_2 changing from 0.48 to 0.64), bilayer melting in the presence of NAT

increases A_2 by 75% (A_2 changing from 0.40 to 0.70). This difference in % increase further emphasizes the different effects that different amino acids have on solute accumulation in biological membranes.

Conclusions

Results presented in this work examined how two amino acids, L-phenylalanine (L-PA) and N-acetyl-DL-tryptophan (NAT) affect partitioning of two coumarin solutes, Coumarin 151 (C151) and Coumarin 152 (C152), into DPPC vesicle bilayers. These studies were motivated by earlier work that illustrated how amino acids affected bilayer structure and permeability. Results from differential scanning calorimetry (DSC) and time resolved fluorescence emission showed that L-PA increases the amount of C152 in the nonpolar region of the DPPC bilayer at lower temperatures but decreases the amount of C152 in the polar backbone region. L-PA did not affect C151's behavior, with virtually all C151 remaining in the aqueous buffer unaffected by the vesicle bilayers. These results implied that L-PA integrated into the bilayer and disrupting cohesive chain-chain interactions and also possibly becoming solvated in the glycero-backbone region. In contrast, the DSC results together with time resolved fluorescence emission suggested a different mechanism describing NAT-DPPC interactions. Specifically, changes to DPPC's gel-liquid crystalline transition temperature ($T_{gel\text{-}lc}$) as a function of NAT concentration and the presence of a coumarin solute imply that NAT interacts directly with the charged DPPC headgroup – presumably through Coulomb interactions – and this NAT-DPPC binding induced site-specific adsorption of coumarin solutes from solution to the bilayer surface. These NAT/ DPPC complexes introduced a new emission lifetime

for C151 implying C151 association with the (modified) membrane surfaces. This association also drew C152 to the DPPC bilayer surface but inhibited C152 partitioning *into* the bilayer relative to L-PA/ DPPC systems at temperatures below $T_{gel\text{-}lc}$. Once the bilayer melts, NAT had no discernible effect on C152 partitioning relative to C152 partitioning into NAT-free DPPC vesicle bilayers.

These descriptions of how different amino acids control solute partitioning into lipid bilayers are admittedly speculative and will likely evolve with improved experiments and more sophisticated modeling. Nevertheless, findings from these combined thermal and time resolved emission studies necessitate different mechanisms describing how amino acids affect membrane properties. Discoveries described above will provide grist for the mill for continued studies of heterogeneous chemistry in complex biological systems.

CHAPTER FOUR

QUANTITATIVE MEMBRANE PARTITIONING STUDIES OF L-PHENYLALANINE

Contribution of Authors and Co-Authors

Manuscript in Chapter 3

Author: Katelyn M. Duncan

Contributions: Collected and analyzed all data, generated figures, and wrote manuscript in preparation for publication.

Co-Author: Cristina Gonzales

Contributions: Assisted with data accumulation.

Co-Author: William H. Steel

Contributions: Assisted with data accumulation. Assisted with editing of manuscript.

Co-Author: Robert A. Walker

Contributions: Contributed important insight into performing experiments and interpreting results. Edited and assisted in the preparation of the manuscript.

Manuscript Information

Katelyn M. Duncan, Cristina Gonzales, William H. Steel, and Robert A. Walker.

Journal of

Status of Manuscript:

__x_ Prepared for submission to a peer-reviewed journal

____ Officially submitted to a peer-reviewed journal

____ Accepted by a peer-reviewed journal

____ Published in a peer-reviewed journal

QUANTITATIVE MEMBRANE PARTITIONING STUDIES OF L-PHENYLALANINE

Katelyn M. Duncan[†], *Cristina Gonzales*[|], *William H. Steel*[‡], *and Robert A. Walker*[*†§]

[†]Department of Chemistry and Biochemistry, Montana State University, Bozeman, Montana 59717, United States.
[|]Department of Chemistry, Reed College, Portland, Oregon 97202, United States
[‡]Department of Chemistry, York College of Pennsylvania, York, Pennsylvania 17403, United States
[§]Montana Materials Science Program, Montana State University, Bozeman, Montana 59717, United States

Abstract

Time-resolved fluorescence spectroscopy in combination with differential scanning calorimetry (DSC) was used to study the chemical interactions that occur when L-Phenylalanine is introduced to a phosphatidylcholine vesicle bilayer. L-Phenylalanine (L-Phe), along with tyrosine (Tyr) and tryptophan (Trp), comprise the three naturally fluorescent aromatic amino acids and is the least studied of the three due to its low fluorescence quantum yield. Studies reported in this work address open questions about L-Phe's affinity for lipid vesicle bilayers, the effects of L-Phe partitioning on bilayer properties, L-Phe's solvation within a lipid bilayer, and the amount of L-Phe that partitions into lipid bilayers from bulk aqueous solution. DSC data show that L-Phe reduces the amount of heat necessary to melt saturated phosphatidylcholine bilayers from their gel to liquid crystalline state but does not change the transition temperature ($T_{gel\text{-}lc}$). This result implies that L-Phe weakens lipid monomer interactions within the bilayer without completely disrupting the cohesive forces responsible for keeping acyl chains rigid and highly ordered below $T_{gel\text{-}lc}$. Time resolved emission shows only a single L-Phe

lifetime at low temperatures corresponding to L-Phe remaining solvated in an aqueous buffer. At temperatures close to $T_{gel\text{-}lc}$, however, a second, shorter lifetime appears that is assigned to L-Phe already embedded within the membrane that becomes hydrated as water starts to permeate the lipid bilayer. This new lifetime is attributed to a conformationally restricted rotamer in the bilayer's polar headgroup region and accounts for up to 30% of the emission amplitude. Results reported for dipalmitoylphosphatidylcholine (DPPC, 2 saturated C_{16} acyl chains) lipid vesicles prove to be general with similar effects observed for dimyristoylphosphatidylcholine (DMPC, C_{14} chains) and distearoylphosphatidylcholine (DSPC, C_{18} chains). Taken together, these results create a complete and compelling picture of how L-Phe associates with model biological membranes. Furthermore, this approach to examining amino acid partitioning into membranes and the resulting solvation forces points to new strategies for studying the structure and chemistry of membrane soluble peptides and selected membrane proteins.

Introduction

Bioconcentration affects membrane function, permeability and, ultimately, membrane viability.[6, 71] Furthermore, bioconcentration is a foundational concern when considering whether an organic solute such as an herbicide or a pharmaceutical will accumulate in biological membranes. As a measure of a solute's tendency to accumulate in biomembranes from the surrounding aqueous environment, bioconcentration is a metric considered by the FDA and EPA when developing exposure estimates and persistence times of synthetic organic solutes used in pharmaceuticals and agriculture.[98-

[99] Historically, a solutes tendency to partition is empirically predicted by the partitioning coefficient (logP) which calculates a solutes solubility preference for an organic phase in comparison to an aqueous phase.[14] LogP has long historical relevance and is still being used today in agriculture and pharmaceuticals.[18, 100] While logP is a useful, zeroth order predictor, it is still a solubility argument and therefore does not account for the chemical complexity found within biological membranes. Understanding specific chemical interactions that occur is important as actual partitioning behavior depends on much more than molecular solubility parameters.

Often, biological membranes are simplified and portrayed as pure lipid bilayer vesicles. Real biological membranes are quite complex in nature as they include proteins, carbohydrates, and cholesterol within the bilayer as depicted in the fluid mosaic model.[101-102] Proteins are very prominent in the fluid-mosaic model and are responsible for diverse functions within the membrane. In order to build complexity into model lipid bilayers, species such as amino acids and cholesterol are frequently included in lipid vesicle bilayer formulations. A recent study by Perkins *et. al.* found that Phenylalanine (L-Phe, Phe) increases membrane permeability.[91] Using cryo-TEM, the authors proposed that Phe aggregated to form fibrils that reduced membrane rigidity making it more permeable. Motivated by this study, recent work in our lab studied the effects that the isomer L-Phe has on coumarin partitioning in lipid bilayer vesicles.[103] Results showed that L-Phe increased *relative* solute partitioning into the lipid bilayer's nonpolar region but blocked a large amount of solute from partitioning while the lipid was in the rigid and structured gel phase.[103]

L-Phe has been studied extensively over the years. The calculated logP value for L-Phe is -1.4 in the uncharged, neutral phase indicating the a solubility preference for the aqueous environment rather than the organic phase or partitioning into the membrane.[14, 87, 103] However, at a biologically relevant pH (~7.4), L-Phe is zwitterionic in a pH 7 solution and its logP value rises to 0.12 making L-Phe just as likely to partition into a polar organic phase as remain in an aqueous phase.[103] Initial literature reports predicted that only the neutral phase of L-Phe permeates into the membrane and comprises only a small fraction of the total amount of L-Phe in solution.[104-105] However, more recent studies determined L-Phe permeates deeper into the membrane in the zwitterionic form allowing the solutes to be more dynamic as they interact with the lipid.[106] The zwitterionic L-Phe intercalates into the polar headgroup of the lipid, primarily through membrane deformities when the membrane is in its frozen gel phase.[87-88, 104-106] Computational studies show that L-Phe's aromatic ring increases the solute's tendency to enter into the lipid bilayer displacing the water that is in the polar headgroup creating a polar aprotic environment.[87] L-Phe then arranges itself with its aromatic ring aligning normal to the nonpolar acyl chains.[33-34, 89, 107]

Discoveries from these reports have implications that extend beyond simple, fundamental descriptions of solute behavior in heterogeneous environments. Phenylketonuria is a genetic disorder that arises when high concentrations of Phe cannot be processed correctly within the human body.[108] In effort to understand this disorder, model membranes were used to study how phenylalanine interacts with biological membranes.[91-92] One study analyzed Oleic acid vesicles and a fluorescent probe to

analyze Phe's effect son the vesicle and found Phe reduces vesicle rigidity and changes membrane hydration.[109] Another study analyzed L-Phe's effects on the lipid monolayer and discovered L-Phe integrates into the film and affects surface tension, phase morphology and ordering of the lipid film.[106]

L-Phe is one of three aromatic amino acids that are naturally fluorescent and contribute to protein fluorescence. L-Phe is the least fluorescent of the three of aromatic amino acids with a quantum yield of 0.023 in an aqueous solution where the quantum yields for Tyrosine (Tyr) and Tryptophan (Trp) are 0.14 and 0.13, respectively.[26, 28, 110-111] Interestingly, L-Phe does not directly contribute to a protein's fluorescence emission as it efficiently transfers its energy to Tyr then to Trp. Because of this lack of direct contribution to protein fluorescence and low quantum yields, the excited state photochemistry of L-Phe has not been studied as thoroughly as for Tyr and Trp.[26, 30, 112-115] In the early 1970's, Mittal *et. al.* predicted that L-Phe photodissociates and forms benzyl radicals through a long-lived excited state and analyzed in more detail over the years.[110-111, 116-117] These benzyl radicals that form have long lived excited states in polar media and have a long phosphorescence lifetime at 385 nm with a lifetime of 5.5 s.[111] The molecular behavior of L-Phe has been studied with differing functional groups in effort to understand how each addition affects its fluorescence behavior.[118-119] The cyclization of L-Phe increased fluorescence lifetimes and quantum yields and pH decreased the fluorescence lifetimes and quantum yields.[118-119] Phenylalanine's behavior in a short peptide was characterized when phenylalanine and serine were analyzed as

monomers in the gas phase and then again in its excited state as the two monomers formed a dimer and relaxed to form a short chain dipeptide.[114]

In most of the studies described above, L-Phe and other amino acids have been analyzed indirectly either by using a fluorescent probe or computational studies to study the amino acid partitioning into membranes. These surrogate studies were simpler to carry out relative to direct measurements due to L-Phe's intrinsically low fluorescence yields. Findings reported below measure L-Phe's partitioning behavior *directly* using time-resolved fluorescence spectroscopy in four different lipid bilayer systems. Using time-resolved and steady-state fluorescence spectroscopy, we seek to understand the chemical interactions that occur when L-Phe is introduced to a model biological membrane. Specifically, these studies identify *where* within the membrane does L-Phe integrate; *how much* L-Phe partitions within the heterogeneous membrane environment; and the effects L-Phe has on the lipid bilayer itself. This work is done in effort to directly analyze the partitioning behavior of L-Phe as well as characterize the photophysical behavior of L-Phe in various solvation environments.

Experimental Methods

Materials

Solvents used were purchased from Sigma-Aldrich and used as received. Millipore water (18.2 MΩ) was used to make carbonate buffer to a pH of 7.0 with an ionic strength of 10 mM. 1,2-dilauroyl-sn-glycero-3-phosphocholine (12:0 DLPC), 1,2-dimyristoyl-sn-glycero-3-phosphocholine (14:0 DMPC), 1,2-Dipalmitoyl-*sn*-glycero-3-phsophocholine (16:0 DPPC), and 1,2-distearoyl-sn-glycero-3-phosphocholine (18:0

DSPC) was purchased from Avanti Polar Lipids (Alabaster, AL). Structures of all molecules can be found in Appendix C (Figure C-4.1). L-Phenylalanine (L-Phe) was purchased from Alfa Aesar and used as received. All bulk solvent solutions were made at 10 mM concentration with 1.5 mM lipid vesicles for fluorescence experiments and 20 mM lipid vesicles for thermoanalytical techniques.

Lipid Bilayer Vesicle Preparation

Lipid bilayer vesicles were prepared by dissolving the lipid in chloroform and subsequently removing via rotary evaporation. The resulting thin lipid film was then rehydrated using a 10 mM L-Phe in 10 mM carbonate buffer (pH = 7) to form a lipid vesicle solution. The solution was sonicated for 30 minutes at 10 °C higher than the lipids' gel-liquid crystalline transition temperature ($T_{gel\text{-}lc}$). The solution then passed through a PTFE syringe filter (450 nm) to remove giant unilamellar vesicles. The solution was subsequently heated to 10 °C higher than the lipids $T_{gel\text{-}lc}$ and passed through an Avanti Mini Extruder 11 times with a membrane pore size of 200 nm.

Differential Scanning Calorimetry (DSC)

Differential scanning calorimetry (DSC) measurements were done using a TA instruments Discovery DSC 2500. Vesicle solutions were made using the method described above with the lipid vesicles at a concentration of 20 mM and rehydrated with a 10 mM carbonate buffer, for pure lipid vesicles. For L-Phe doped lipid vesicles, the lipid vesicles solution was rehydrated with a 10 mM L-Phe in 10 mM carbonate buffer solution. The vesicles for DSC experiments were not filtered to any specific vesicle size. For experiments, Tzero pans and Tzero hermetic lids (TA instruments) were used,

temperature scans began at 15 °C below the $T_{gel\text{-}lc}$ and heated 1°C/min to 15 °C above the $T_{gel\text{-}lc}$ to capture the full gel-liquid crystalline transition temperature ($T_{gel\text{-}lc}$).

Time-Correlated Single-Photon Counting (TCSPC)

Fluorescence experiments were measured following L-Phenylalanine excitation by a Ti:sapphaire oscillator (Coherent Chameleon, 80 MHz, 85 fs pulse duration, 680-1040 nm wavelength range) coupled with an APE autotracker harmonic generator used to frequency triple the fundamental wavelength. A Conoptics model 350-80 modulator was used to reduce the repetition rate to 4 MHz. Picoquant PicoHarp 300 and FluoTime 200 software were used for data collection. Samples were equilibrated at the reported temperatures for 5 minutes using a Quantum Northwest TC125 control (Seattle, WA). A long pass filter (90% transmission >280 nm) was placed after the sample to reduce scattering from the vesicles. Photon emission was collected at 290 nm, a wavelength that overlapped all emission spectra in bulk solvents. Excitation wavelength chosen was 260 nm for all solutes, a wavelength that overlapped all solutes in each of the bulk solvents.

Time-resolved emission data from vesicle-containing solutions were fit with a linear combination of independent lifetimes and amplitudes using fitting parameters that are adjusted to minimize residuals and optimize χ^2. The resulting fluorescence lifetimes were then compared to the lifetimes of the solute in different solvents chosen to mimic local solvation environments within the lipid bilayer. The fluorescence decay and amplitude expression are shown in Eq. 4.1, where A_i and τ_i are the amplitude and the lifetime of the i^{th} component, respectively.

$$I(t) = \int_0^t IRF\,(t') \sum_{i=1}^{n} A_i e^{-\frac{t-t'}{\tau_i}}\, dt' \qquad (4.1)$$

Each trace was fit independently, without any constraints, for the lifetimes or amplitudes. The typical χ^2 were from 0.9-1.1 when accounting for at most three lifetimes. Typically, uncertainties in lifetimes and amplitudes were 0.2 ns and 0.04, respectively. There is an inherent uncertainty in the lifetimes reported of ± 0.2 ns due to the detection limit of the instrument; however, the data and error bars presented in this work are 3 independently prepared, equivalent trials averaged together with a single population standard deviation of those trials. The average lifetime and amplitudes and their respective standard deviations are reported for each specific temperature and only compared to their respective temperature.

Results

TCSPC in combination with DSC was used to quantify L-Phe interactions with DPPC lipid bilayers. These studies focused on several specific questions: (1) does L-Phe associate with lipid bilayers? (2) If so, how much L-Phe can a bilayer accommodate? And (3) what local solvation forces does L-Phe experience within the bilayer? Results shown below strongly suggest that L-Phe partitions into the DPPC bilayers but remains spectroscopically 'invisible' until water begins to percolate into the membrane. Furthermore, the L-Phe that does partition into the membrane does so in a way that does little to disrupt the cohesive interactions between lipids. The $T_{gel\text{-}lc}$ phase transition for DPPC remains unchanged for L-Phe concentrations up to 10 mM.[103] Taken together with the TCSPC data also imply that photoexcited L-Phe embedded within the DPPC bilayer undergoes an intramolecular charge transfer reaction but only when water is present in

the bilayer. Furthermore, these findings are general for other saturated phosphatidylcholine lipids.

Analyzing L-Phenylalanine's effect on DPPC lipid vesicles

To understand how, or even if, L-Phe interacts with DPPC bilayers, differential scanning calorimetry (DSC) was employed to understand the effect L-Phe has on bilayer properties. Two separate lipid vesicles solutions at a 20 mM concentration were hydrated with a 10 mM bulk carbonate buffer solution with and without the presence of the L-Phe. Previous work has shown that small solutes associating with lipid bilayers can disrupt monomer-monomer interactions leading to a decrease in the bilayer gel to the liquid-crystalline phase transition temperature ($T_{gel\text{-}lc}$). [94, 120] Alternatively, some studies have reported that strong solute-headgroup association can dehydrate the membrane's outer layer, enhancing monomer-monomer interactions and *increasing* $T_{gel\text{-}lc}$.[97, 121]

The DSC traces of DPPC lipid vesicles with and without L-Phe show that the $T_{gel\text{-}lc}$ remained unchanged from the addition of the amino acid to the vesicle system (Figure 4.1). However, the addition of L-Phe to the lipid bilayer vesicle resulted in a decrease in the heat flow required to drive the gel phase into the liquid-crystalline phase transition with a slight, asymmetric widening of the peak base to lower temperatures. From this result, we infer that any L-Phe that does partition into the bilayer has minimal

effect on the cohesive chain-chain interactions, although any effect that L-Phe does induce is weakly disruptive given the subtle low-temperature tailing.

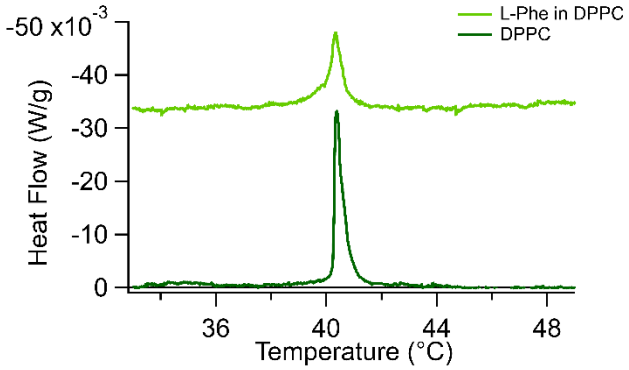

Figure 4.1. DSC spectra of pure DPPC vesicle solutions and DPPC vesicle solutions containing 10 mM L-Phe. The two endotherms are offset for the ease of viewing.

To evaluate the partitioning mechanisms of L-Phe, we first analyzed the L-Phe's fluorescence behavior in bulk solvents chosen to model the various local solvation environments of a lipid bilayer vesicle: acetonitrile for the polar aprotic headgroup, methanol for a polar protic headgroup, and cyclohexane to model the nonpolar tails. This approach has been used previously to identify changes in solvation opportunities within the membrane interior as the membrane melts.[43, 103, 122] One important consideration is that the region created by the lipid glycero-backbones is polar and intrinsically aprotic. Only when water begins hydrating this region is there any opportunity for hydrogen bond formation. Water is expected to percolate into the membrane as the membrane adopts its 'ripple phase' or, equivalently, in the vicinity of its gel-liquid crystalline pre-transition.[123] DPPC's ripple phase occurs at 35 °C.[124-125]

The lipid bilayer vesicles used in this study are prepared in a 10 mM carbonate buffer (pH =7). Consequently, similarities in L-Phe emission lifetimes in the pure buffer

and in DPPC lipid vesicle solutions are attributed to L-Phe solutes that do not associate with the bilayer. The lifetimes of L-Phe in bulk solvents and DPPC lipid vesicle solutions are determined independently. After L-Phe's lifetimes are determined in DPPC vesicle solutions, results are compared to L-Phe behavior in the bulk solvents to assign L-Phe's local solvation environment within the lipid bilayer vesicle. The fluorescence properties of L-Phe in each of the bulk solvents are reported in Table 4.1.

The first observation from Table 4.1 is the quantum yield of L-Phe is extremely poor in aqueous solvents at 0.023. In comparison, the quantum yields of Tyr and Trp in an aqueous solvent are 0.14 and 0.13, respectively.[26, 28, 110-111] The second observation is the quantum yield of L-Phe changes depending on the solvation environment with the largest quantum yield of 0.033 measured in a polar protic solvent, methanol. L-Phe's quantum yield decreases 5-fold to 0.006 in a polar aprotic environment (acetonitrile). A description of how the values reported for each quantum yield in Table 4.1 were calculated can be found in Appendix C. The quantum yield (φ_f) and radiative rate (k_f) for carbonate buffer and methanol were calculated as a function of temperature with the full list found in Appendix C (Table C-4.1) with only values calculated at 20 °C reported in Table 4.1. The quantum yield of L-Phe in carbonate buffer as a function of temperature was quantitatively calculated, reproducible, and closely matches those reported in literature of L-Phe in an aqueous solution.[126] The quantum yield and radiative rate of L-Phe in acetonitrile was only calculated at 20 °C due to poor solubility and low absorbance and emission intensities.

Table 4.1. Fluorescence properties of L-Phe in each of the bulk solvents at 20 °C. The steady-state spectra for L-Phe in each of the bulk solvents can be found in Appendix C (Figures C-4.1).

solvent	λ_{ex} (nm)	λ_{em} (nm)	τ_f (ns)	φ_f	k_f (10^6 s^{-1})
Carbonate Buffer	264	287	6.42	0.023[a]	3.52
Methanol	265	290	6.74	0.033	4.89
Acetonitrile	262	299	3.22	0.006	1.72
Cyclohexane	262	301	1.01 (0.85), 4.51 (0.15)		

[a] Quantum yield were calculated in this study but consistent with literature.[126]

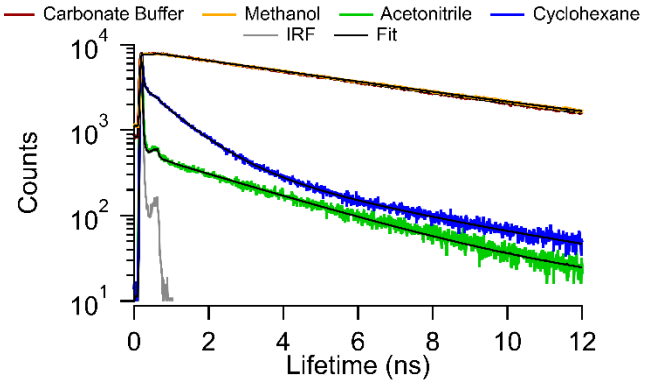

Figure 4.2. TCSPC spectra of L-Phe in each of the bulk solvents taken at 20 °C. Results from fitting these emission traces to Equation 4.1 are reported in Table 4.1. Gray trace is instrument response function (IRF).

The time-resolved fluorescence behavior of L-Phe in all bulk solvents are shown in Figure 4.2 with the corresponding fluorescence lifetimes reported in Table 4.1. The fluorescence emission of cyclohexane was best fit to two fluorescence decays with the 1.01 ns lifetime as the marker for a nonpolar environment due to the higher amplitude of 85%. The time-resolved fluorescence behaviors of L-Phe in bulk carbonate buffer and methanol were measured, separately, as a function of temperature and results are reported in Appendix C (Table C-4.1 and Figure C-4.3 – C-4.4, respectively). The resulting L-Phe lifetimes in carbonate buffer matched those found in literature except for the appearance

of a second lifetime at 60 and 70 °C not previously reported.[126] The significance of this second lifetime will be discussed below.

The time-resolved fluorescence behavior of L-Phe in a carbonate buffer solution containing DPPC lipid vesicles was characterized as a function of temperature through the $T_{gel\text{-}lc}$ of DPPC (41 °C) up to 70 °C and back. The resulting fluorescence decays are shown in Figure 4.3 with the corresponding calculated lifetimes and amplitudes reported in Table 4.2. For each temperature, the lifetimes were calculated with the minimum number of lifetimes required for a χ^2 between 0.9 – 1.1. The resulting lifetimes for each temperature were compared to lifetimes found in bulk solvents to correlate local solvation environments experienced by L-Phe within the DPPC lipid bilayer. Each amplitude was radiative rate corrected using the fluorescence quantum yield of L-Phe in carbonate buffer and methanol at each corresponding temperature. The explanation for why methanol was chosen to radiative rate correct the amplitude of the second fluorescence lifetime can be found in Appendix C.

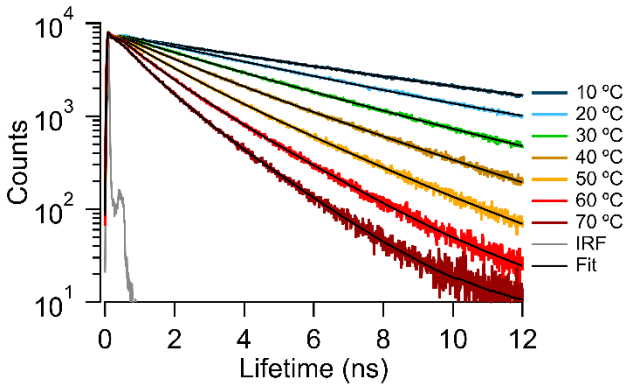

Figure 4.3. TCSPC spectra of L-Phe in DPPC vesicles as a function of temperature. Results from fitting these emission traces to Equation 4.1 are reported in Table 4.2.

Table 4.2. Fluorescence lifetimes (in ns) and amplitudes (in parentheses) of L-Phe in DPPC vesicles at a temperature ramp from 10 to 70 °C in and back down to 10 °C in 10 °C increments. The second lifetime at higher temperatures, labeled K_{rot}, is assigned to an L-Phe rotamer state that is described in the Discussion section. Amplitudes have been corrected for their respective radiative rates. Uncertainties in lifetimes are ± 0.2 ns; uncertainties in amplitudes are ± 0.04.

temp. (°C)	buffer τ_1 (A_1)	K_{rot} τ_2 (A_2)
10	6.59	
20	4.92	
30	4.19 (0.85)	1.85 (0.15)
40	3.33 (0.74)	1.68 (0.26)
50	2.54 (0.74)	1.28 (0.26)
60	1.96 (0.73)	0.94 (0.27)
70	1.55 (0.71)	0.71 (0.29)
60	1.97 (0.73)	0.95 (0.27)
50	2.51 (0.75)	1.25 (0.25)
40	3.25 (0.77)	1.61 (0.23)
30	4.25 (0.83)	1.89 (0.17)
20	4.98 (0.97)	1.16 (0.03)
10	6.53	

Lifetimes reported in Table 4.2 show a single lifetime for fluorescence decay at both 10 and 20 °C. This relatively long lifetime corresponds to L-Phe in bulk carbonate buffer. Once the temperature was raised to 30 °C, however, the decay trace could only be fit to two lifetimes with the first lifetime corresponding to L-Phe in bulk carbonate buffer and accounting for 85% of the overall fluorescence decay, and a second lifetime (1.8 ns, 15%) that does not match any result found in bulk solvents but *does* correspond to L-Phe in a polypeptide that is assigned to a different L-Phe rotamer state.[127] This temperature is approximately where the ripple phase (35 °C) occurs for DPPC lipid bilayers. As temperature increases the 2nd lifetime decreases (to 0.7 ns) and the amplitude increases 30%. These results are quantitatively reversible. Given this lifetime's clear correlation with L-Phe in vesicle containing solutions, we assign this lifetime to a new radiative decay pathway for L-Phe associated with the lipid bilayer. While the origin of this new

pathway is not immediately apparent, we propose that it results from L-Phe in the bilayer and any rotational isomerization is restricted resulting in a shorter fluorescence lifetime (K_{rot}) that only becomes optically visible when water begins to associate with the lipid bilayer. The basis for this assignment is presented in discussion section below.

Data reported in Table 4.3 are summarized in Figure 4.4 where changes in the lifetimes and amplitudes are shown as a function of temperature. Also shown is the dashed line corresponding to L-Phe's lifetime in bulk carbonate buffer and two vertical dashed lines that denote DPPC's $T_{gel\text{-}lc}$. Note that the x-axis reporting temperature starts at 10 °C, rises to 70 °C at the axis midpoint and returns to 10 °C. The symmetry shown by all traces at ~70 °C demonstrates reversibility of the observed effects.

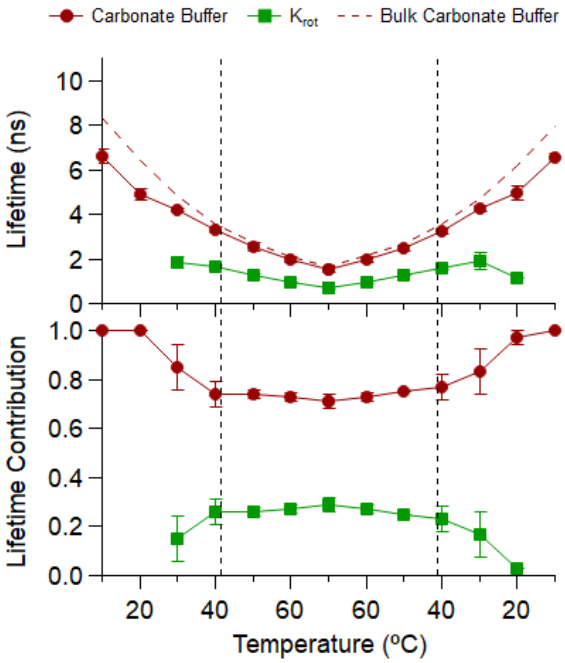

Figure 4.4. Fluorescence lifetimes (top) and respective radiative rate corrected lifetime contribution (bottom) of L-Phe in DPPC lipid vesicles. The major lifetime is assigned to a L-Phe in carbonate buffer (τ_1, burgundy circles), and a restriction of L-Phe rotamer in the DPPC polar headgroup region (τ_2, green squares). The dashed lines indicate the $T_{gel\text{-}lc}$ of the DPPC lipid bilayer at ~41.5 °C. Each point is an average of 3 independent trials and the respective error bars are one standard deviation based on the results of those 3 trials. In some instances, the uncertainty is smaller than the marker used to represent that data point.

Given that the 2nd shorter lifetime was attributed to L-Phe associated with the DPPC bilayer that becomes hydrated as the system approaches $T_{gel\text{-}lc}$, additional experiments were carried out to test whether or not this phenomenon was general. These subsequent studies used three other lipid bilayer systems: DSPC (18:0, $T_{gel\text{-}lc}$ = 53.5 °C), DMPC (14:0, $T_{gel\text{-}lc}$ = 22.5 °C), and DLPC (12:0, $T_{gel\text{-}lc}$ = -1.2 °C). All three lipids are phosphatidylcholine (PC) lipids and contain the same headgroup with the only difference being in the length of the saturated acyl chains and corresponding phase transition temperatures.

Generalization of the partitioning behavior of L-Phe

The effect L-Phe has on the $T_{gel\text{-}lc}$ was analyzed using DSC with 20 mM lipid vesicles rehydrated in pure carbonate buffer solutions as well as with 10 mM L-Phe/vesicle carbonate buffer solutions. Figure 4.5 shows the DSC traces of DSPC, DMPC, and DLPC in carbonate buffer both with and without L-Phe. The same behavior found in DPPC lipid vesicles is consistent with DSPC, DMPC, and DLPC lipid vesicles. Namely, there was no change in the $T_{gel\text{-}lc}$ but there was a decrease in peak intensity. For DSPC and DMPC vesicles, the same peak broadening as in DPPC vesicles was observed. Interestingly, as the lipid hydrocarbon chain lengthened, the effect of L-Phe on the transition increased. When evaluating the asymmetric broadening in the DSC data with the addition of L-Phe, DSPC showed the most apparent effects and DLPC showed no evidence of asymmetric peak broadening. The low temperature peak widening in DSPC and DMPC indicate L-Phe is interacting with the membrane in a way that does not change membrane properties but decreases the heat flow required to induce the transition.

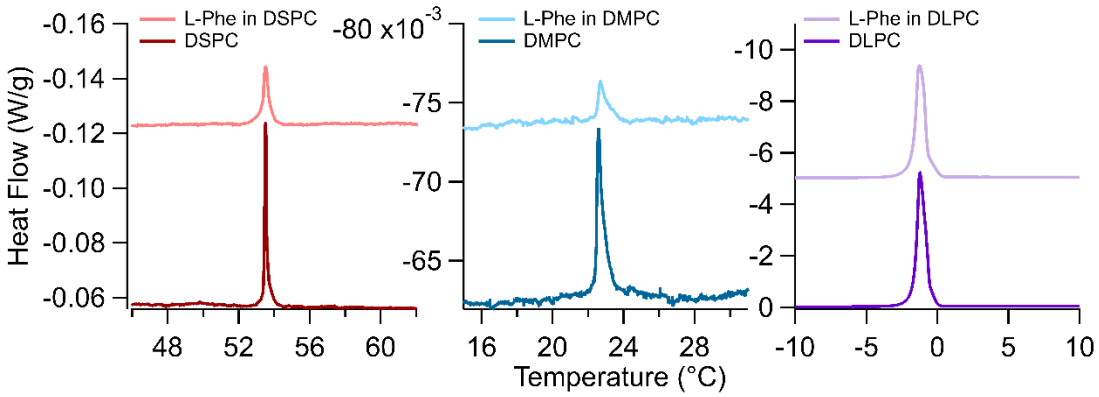

Figure 4.5. DSC spectra of DSPC (left, red), DMPC (middle, blue), and DLPC (right, purple) vesicle containing solutions rehydrated with carbonate buffer and 10 mM L-Phe in carbonate buffer. All transitions are endothermic and offset for the ease of viewing.

In a manner similar to studies performed with L-Phe in DPPC vesicle solutions, time-resolved fluorescence behaviors of L-Phe in DSPC, DMPC, and DLPC vesicle solutions were measured as a function of temperature (Figure 4.6). The temperature regions sampled were adjusted for each lipid vesicle system to capture any behavioral changes with respect to each bilayer's $T_{gel\text{-}lc}$. The data shown in Figure 4.6 were analyzed in the same way as the L-Phe/DPPC system.

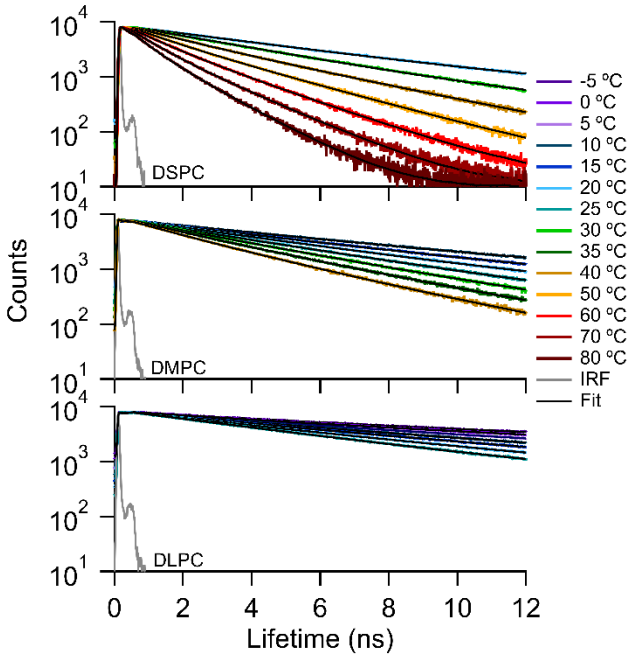

Figure 4.6. TCSPC spectra of L-Phe in DSPC (top), DMPC (middle), and DLPC (bottom) lipid vesicles as a function of temperature. Results from fitting these emission traces to Equation 4.1 are reported in Table 4.3.

Table 4.3. Fluorescence lifetimes (in ns) and amplitudes (in parentheses) of L-Phe in DSPC, DMPC, and DLPC lipid vesicles at a temperature ramp corresponding to each lipid's $T_{gel\text{-}lc}$ to fully encompass the behavior of L-Phe in the gel phase and the liquid crystalline phase (see text). Amplitudes have been corrected for their respective radiative rates. Uncertainties in lifetimes are ± 0.2 ns; uncertainties in amplitudes are ± 0.04.

DSPC			**DMPC**			**DLPC**	
temp. (°C)	buffer τ_1 (A_1)	K_{rot} τ_2 (A_2)	temp. (°C)	buffer τ_1 (A_1)	K_{rot} τ_2 (A_2)	temp. (°C)	buffer τ_1 (A_1)
20	5.18		10	6.46		-5	9.82
30	3.85		15	5.64		0	8.83
40	3.43 (0.80)	1.61 (0.20)	20	4.86		5	7.94
50	2.63 (0.78)	1.27 (0.22)	25	4.58 (0.91)	1.70 (0.09)	10	7.22
60	2.04 (0.76)	0.96 (0.24)	30	4.11 (0.85)	1.84 (0.15)	15	6.39
70	1.62 (0.73)	0.72 (0.27)	35	3.46 (0.85)	1.53 (0.15)	20	5.65
80	1.30 (0.69)	0.55 (0.31)	40	3.23 (0.75)	1.66 (0.25)	25	4.96
70	1.62 (0.73)	0.73 (0.27)	35	3.52 (0.82)	1.65 (0.18)	20	5.61
60	2.02 (0.77)	0.91 (0.23)	30	4.02 (0.89)	1.73 (0.11)	15	6.31
50	2.61 (0.79)	1.24 (0.21)	25	4.63 (0.90)	1.72 (0.10)	10	7.07
40	3.29 (0.84)	1.43 (0.16)	20	4.87		5	7.84
30	3.83		15	5.67		0	8.75
20	5.16		10	6.58		-5	9.42

Table 4.3 shows that L-Phe fluorescence in all lipid vesicle solutions is described by a single lifetime at low temperatures. For L-Phe in DSPC and DMPC, the appearance of a second lifetime occurs in the vicinity of the $T_{gel\text{-}lc}$ and, like DPPC, the second lifetime does not match behavior observed in bulk solvents. In DLPC, L-Phe fluorescence is characterized by a single lifetime corresponding to L-Phe fluorescence in bulk carbonate buffer. From these data, we conclude that L-Phe does not partition into DLPC vesicles. The second general observation is that L-Phe in DSPC and DMPC vesicles behaves similarly to L-Phe in DPPC vesicles. A more detailed assessment is provided below.

Starting with DSPC (18:0, $T_{gel\text{-}lc}$ = 53.5 °C), time-resolved emission was measured every 10 °C between 20 °C to 80 °C. Results reported in Table 4.3 display a major lifetime that corresponds to L-Phe in a bulk carbonate buffer solution. For the DSPC vesicle system, the appearance of a second lifetime does not appear until 40 °C,

slightly below the ripple phase of pure DSPC lipid vesicles (~45 °C).[125] The reversibility of L-Phe in DSPC displays the same behavior as seen in DPPC system (Figure 4.7).

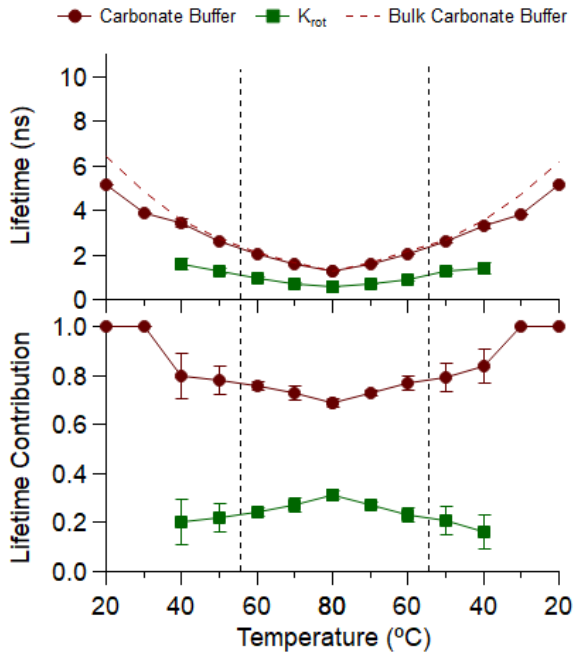

Figure 4.7. Fluorescence lifetimes (top) and respective radiative rate corrected lifetime contribution (bottom) of L-Phe in a DSPC lipid vesicle solution. The major lifetime is assigned to a L-Phe in carbonate buffer (τ_1, maroon circles), and a second lifetime assigned to L-Phe in the membrane appears at 40˚C (τ_2, dark green squares). The dashed lines indicate the $T_{gel\text{-}lc}$ of the DSPC lipid bilayer at ~53.5 °C. Each point is an average of 3 independent trials and the respective error bars are one standard deviation based on the results of those 3 trials. In some instances, the uncertainty is smaller than the marker used to represent that data point.

Results are not quite so definitive for L-Phe in DMPC vesicle containing solutions. Results in Table 4.3 are shown in Figure 4.8 and depict the same long lifetime corresponding to L-Phe in in bulk carbonate buffer. However, the appearance of the second lifetime does not occur until 25 °C or at approximately the same temperature as the DMPC $T_{gel\text{-}lc}$ (22.5°C). This is behavior differs from observations made in DPPC and

DSPC lipid vesicle solutions where the second lifetime appeared ~10-12 °C before the $T_{gel\text{-}lc}$.

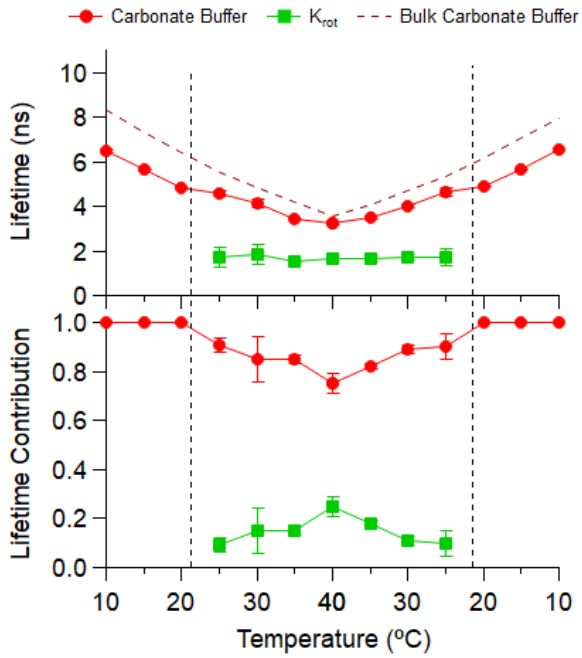

Figure 4.8. Fluorescence lifetimes (top) and respective radiative rate corrected lifetime contribution (bottom) of L-Phe in a DMPC lipid vesicle solution. The major lifetime is assigned to a L-Phe in carbonate buffer (τ_1, red circles), and a second lifetime assigned to L-Phe in the membrane appears at 25 ˚C (τ_2, light green squares). The dashed lines indicate the Tgel-lc of the DMPC lipid bilayer at 22.5 °C. Each point is an average of 3 independent trials and the respective error bars are one standard deviation based on the results of those 3 trials. In some instances, the uncertainty is smaller than the marker used to represent that data point.

Lastly, DLPC with a pair of C_{12} acyl chains and a $T_{gel\text{-}lc}$ = -1.2 °C shows L-Phe emission with only a single lifetime that is assigned to L-Phe in buffer. From these findings, we conclude that L-Phe does not associate in any measurable way with DLPC lipid bilayers. The reasons for this pattern of L-Phe association with lipid bilayers – noticeably with DSPC and DPPC, modestly with DMPC, and not at all with DLPC – is discussed below.

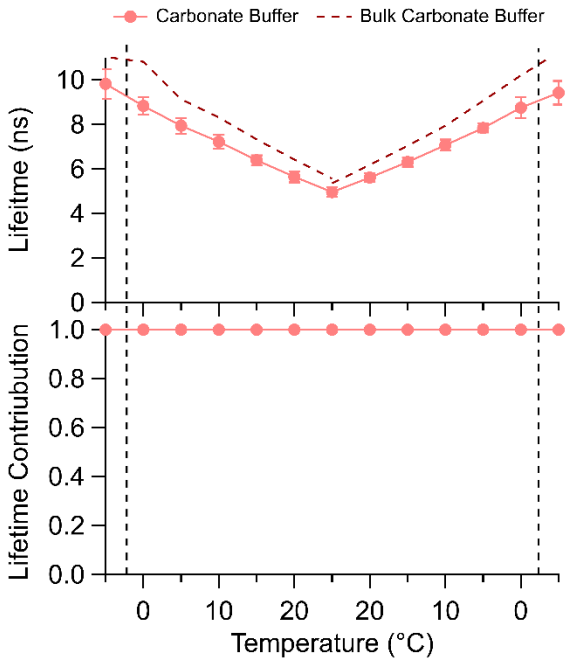

Figure 4.9. Fluorescence lifetimes (top) and respective radiative rate corrected lifetime contribution (bottom) of L-Phe in a DLPC lipid vesicle solution. The single lifetime is assigned to a L-Phe in carbonate buffer (τ_1, pink circles). The dashed lines indicate the $T_{gel\text{-}lc}$ of the DLPC lipid bilayer at -1.2 °C. Each point is an average of 3 independent trials and the respective error bars are one standard deviation based on the results of those 3 trials. In some instances, the uncertainty is smaller than the marker used to represent that data point.

Discussion

The partitioning behavior of L-Phe in model biological membranes was characterized using time-resolved fluorescence spectroscopy in combination with differential scanning calorimetry. From results reported above, three discoveries stand out and require discussion:

- DSC data show that L-Phe does not alter bilayer $T_{gel\text{-}lc}$ but does decrease the energy required to melt the bilayer from its gel-phase to liquid-crystalline phase. This finding applies to DSPC, DPPC and DMPC but *not* to DLPC.

- In the vicinity of $T_{gel\text{-}lc}$, L-Phe time-resolved emission in vesicle solutions begins showing a second, faster emission lifetime (< 2 ns) in addition to a longer lifetime assigned to L-Phe in bulk carbonate buffer. The shorter L-Phe lifetime is readily apparent in DSPC, DPPC, and DMPC vesicle solutions but *not* in DLPC vesicle solutions. A short lifetime for L-Phe matching those observed in the vesicle solutions *does* appear in bulk carbonate buffer at temperatures above 60 °C and this correlation forms the basis of our assignment of this lifetime to a rotamer of L-Phe.
- The 2nd, shorter lifetime can comprise up to 30% of the amplitude in the emission decay. In DSPC and DPPC vesicle solutions, this shorter lifetime decreases from ~1.8 ns at temperatures just below the $T_{gel\text{-}lc}$ to < 1 ns at 70 °C. Whereas in DMPC vesicles, the lifetime stays almost constant at ~1.6 ns. Furthermore, in DSPC, DPPC and DMPC vesicle solutions the amplitude of the short lifetime contribution rises with temperature.

The discussion below considers each issue individually to fully analyze the behavior of L-Phe in a lipid bilayer vesicle.

The L-Phe that integrates into the
bilayer does not disrupt bilayer properties

The DSC traces in Figures 4.1 and 4.5 display the $T_{gel\text{-}lc}$ phase transition behavior for each lipid system studied with and without L-Phe in solution. Two observations stand out. First, L-Phe does not affect the transition temperature for any of the lipid bilayers. The peak in the different endotherms remain at 53.5 °C, 40.4 °C, 22.5 °C and -1.2 °C for

DSPC, DPPC, DMPC and DLPC, respectively, regardless of whether or not L-Phe is present. Given that bilayer melting is controlled by van der Waals forces between acyl chains *and* Coulomb forces between the charged choline headgroups,[94,128] the DSC findings support a L-Phe-bilayer interaction mechanism where the L-Phe integrates into the bilayer's 'near-surface' polar interior created by the lipid glycero-backbones in a manner that does not interfere intermolecular interactions responsible for the transition itself but reduces cooperativity within the bilayer.[129]

The second observation is that L-Phe *does* change quantitative details related to $T_{gel\text{-}lc}$. For DSPC, DPPC and DMPC, the presence of L-Phe significantly reduces the amount of heat needed to drive the gel-liquid crystalline transition to completion. The differences in enthalpy of transition (ΔH) between the solutions containing pure vesicles and vesicle solutions with L-Phe are 144, 179, and 122 J/mol for DSPC, DPPC, and DMPC, respectively. Furthermore, the DPPC and DSPC endotherms show very subtle tailing to lower temperatures, suggesting that any L-Phe within the bilayer does weaken slightly the cohesive interactions between chains and/or headgroups. We expect that L-Phe, with its polar functional groups, relatively low logP, and partial zwitterionic character is more likely to have stronger attraction to the choline headgroups than the hydrophobic interior. This question of where solutes incorporated into the bilayer accumulate and the consequences for bilayer stability becomes an interesting one for all-atom molecular dynamics simulations to tackle now that experimental data can serve as benchmarks.[130] Also telling is that L-Phe does not appear to affect the gel-liquid crystalline transition temperature in DLPC vesicles. This observation is consistent with

those from independent TCSPC that show no detectable affinity between L-Phe and DLPC bilayers.

Assigning the 2nd lifetime

To demonstrate the universal behavior of L-Phe in each lipid bilayer vesicle system, Figure 4.10 shows all fluorescence lifetimes of L-Phe in DSPC, DPPC, DMPC, DLPC, and bulk carbonate buffer across the entire temperature range sampled. Also included on Figure 4.10 are L-Phe lifetimes in bulk carbonate buffer including the second, shorter lifetime that appears only at elevated temperatures (labeled as CB τ_2).

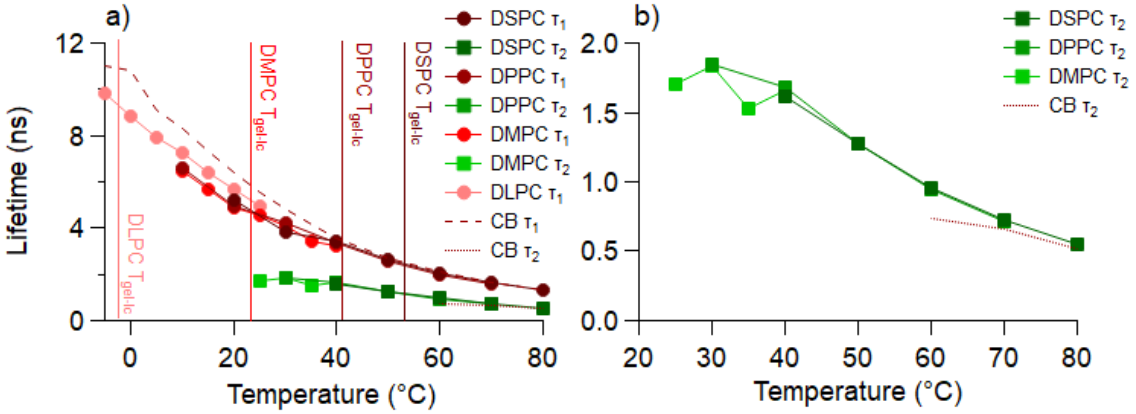

Figure 4.10. Fluorescence lifetimes of L-Phe in bulk carbonate buffer, DSPC, DPPC, DMPC, and DLPC lipid vesicles. Left panel (a) overlays all major lifetimes assigned to a L-Phe in carbonate buffer (τ_1: DSPC, maroon circles; DPPC, burgundy circles; DMPC, red circles, and DLPC, pink circles), and the and a second lifetime assigned to L-Phe in the membrane appears (τ_2: DSPC, dark green squares; DPPC, green squares; and DMPC, light green squares). Dashed traces indicate L-Phe in bulk carbonate buffer (CB) with long dashes indicating first fluorescence lifetime and short dashes indicating second fluorescence lifetime. Solid vertical lines indicate each lipid's $T_{gel\text{-}lc}$ and which are color coded using same scheme as color assignments for lifetime attributed to carbonate buffer and labeled as such within figure. Right panel (b) is expanded view of 2nd lifetime alone attributed L-Phe rotamer (K_{rot}) in the polar headgroup region of L-Phe in DMPC, DPPC, and DSPC, and bulk carbonate buffer (CB). Each point is an average of 3 independent trials of each respective system.

In each vesicle-containing solution, the dominant contribution to the emission decay trace matches L-Phe emission in bulk carbonate buffer. This agreement enables us to assign the major lifetime of L-Phe in vesicle containing solutions to solutes that do not associate with the lipid vesicles. In the DSPC, DPPC and DMPC vesicle solutions, the second, shorter lifetime appears at temperatures close to each lipid's respective $T_{gel\text{-}lc}$. Interestingly, the time resolved emission of L-Phe in bulk carbonate buffer also has a short lifetime that appears at temperatures ≥ 60 °C. This shorter lifetime does not coincide with emission behavior in any bulk organic solvents, although it does match

closely the 1.7 ns lifetime assigned to L-Phe in the EGFRtm peptide as reported by Duneau, *et al.*[127]

Multiple studies have either inferred or predicted that the hydrophobic L-Phe should insert into the lipid bilayer membrane through membrane surface defects.[34, 87-89, 104-105] In its gel phase, the lipid bilayer is very rigid and will limit the intramolecular conformational freedom of embedded L-Phe. The benzyl-group of L-Phe is believed to extend into the nonpolar tails and L-Phe's zwitterionic carboxylic acid and amino groups are directed towards the lipid's glycero-backbone and headgroup.[87, 89] Olsztynska *et. al.* reported the appearance of a second, shorter L-Phe emission lifetime (2.6 ns) and proposed that this behavior resulted either from protonation of the carboxylic acid or the formation of aggregates that enabled a faster radiative decay pathway.[131] Supporting this finding are reports of excimer excitation of 100 mM L-Phe evidenced by an emission peak at 320 nm that disappears with decreasing concentration.[126]

Findings presented in this work do not support the proposal that the short lifetime reflects L-Phe aggregation. First, in all three lipid systems where L-Phe shows membrane affinity, the short lifetime amplitude *increases* with increasing temperature. If the short emission lifetime observed in these systems were due to noncovalently bound aggregates, we would expect aggregation to play *less* of a role at higher temperatures, not more. Second, emission spectra of L-Phe in carbonate buffer (Appendix C Figure C-4.2) show no evidence of excimer formation at the concentrations used in the vesicle solution experiments. Additionally, a 4-fold concentration decrease of L-Phe (2.5 mM) in DPPC vesicles showed no change in partitioning behavior from that of 10 mM L-Phe in DPPC

lipid vesicles (Appendix C Figures C-4.5 – C-4.6 and Table C-4.2). The possibility that aggregation and excimer formation controls L-Phe photophysical behavior at high concentrations as reported by Leroy and Laustrait cannot be discounted, but these effects are unlikely to be present at the 10 mM L-Phe solutions employed in this work.[29]

An alternative hypothesis explaining the short L-Phe lifetime was proposed by Duneau, *et al.*, and attributed emission from L-Phe in two different peptides to L-Phe rotamer states at room temperature.[127] In the 29-mer peptide ErbB-2*tm, the single L-Phe residue shows three different emission lifetimes, two of which are sub-ns and a longer, 2.2 ns lifetime. The longer lifetime was assigned to different rotamer states that interconvert on timescales slower than the measured emission lifetimes. L-Phe emission from a second peptide, EGFRtm, is characterized by a single, 1.70 ns lifetime that matches the lifetime observed for L-Phe in the lipid vesicle solutions.[127] The authors proposed that the single lifetime either reflects different rotamers that interconvert rapidly on the timescale of the experiment or L-Phe in a single rotamer state, before concluding that the first explanation, that of rapidly interconverting rotamers, is more consistent with their findings.[127] Similarly, a study done by Rzeska *et. al.* analyzed analogues of L-Phe and determined that all possible rotamer conformations result in a similar fluorescence lifetime and are indistinguishable from one another.[118-119]

In contrast to Duneau, *et. al*, we believe that the short lifetime emission we observe is due to a single rotamer. An alternate study by Cavanaugh *et. al.* studied the temperature variations of chemical shifts and coupling of L-Phe rotational isomerization.[132] The authors reported that temperature played a large role in

intramolecular and intermolecular parameters of L-Phe and changed depending on the local environment.[132] Through NMR analysis, this study had two conclusions: either the rotamer energies are temperature dependent and gain stability as temperature increases, or the results require a deviation from the original proposed rotamer structures to understand experimental data.[132] Our findings support the conclusion that a single rotamer structure is stabilized at higher temperatures long enough for a radiative decay pathway to contribute to the overall fluorescence behavior. This stabilization effect of high temperatures is evident in the appearance of a second fluorescence lifetime in bulk carbonate buffer starting at 60 °C.

We propose that L-Phe in the bilayer experiences a conformationally restricted environment that forces L-Phe to adopt conformations that do not fluoresce. As the membrane begins to become more fluid, L-Phe can adopt a rotamer state that *does* decay radiatively. We expect that this emissive state is stabilized by water as water will begin to percolate into the lipid bilayer's polar glycero-backbone region as the system temperature approaches $T_{gel\text{-}lc}$.[133-134] The second lifetime found in bulk carbonate buffer at 60 °C is thought to be the same rotamer conformation that becomes accessible in bulk solution at higher temperatures.

To determine what role the water protons play in assisting rotamer formation, the fluorescence lifetimes of L-Phe in a deuterated water (D_2O) carbonate buffer solution were measured as a function of temperature (Appendix C Table C-4.3). L-Phe in D_2O carbonate buffer displays a decrease in the fluorescence lifetimes (τ_f at 10 °C = 10.81 ns) at low temperatures in comparison to H_2O carbonate buffer (τ_f at 10 °C = 8.00 ns).

Similarly, the appearance of a second lifetime (0.88 ns, 11%) at 60 °C also occurs in D_2O carbonate buffer. However, the amplitude of the second, short lifetime is significantly different from 60 – 80 °C. Namely, the second lifetime displays a sharp increase in amplitude of 57% (80 °C) in D_2O carbonate buffer in comparison to 20% (80 °C) in H_2O carbonate buffer. In D_2O, the hydrogen-bonding capabilities are much stronger than that of H_2O and, therefore, inducing a more stable rotamer lifetime at high temperatures as evidenced by the increase in amplitudes.

Local solvation environment dependence
of the 2nd lifetime of L-Phe in lipid vesicles

The results described above depict a strong dependence on bilayer phase with the appearance of the second lifetime. For the DSPC and DPPC lipid vesicles, the appearance of the second lifetime occurred ~10-15 °C before the transition temperature of the lipid bilayer. Uniquely, the second lifetime of L-Phe in DMPC lipid vesicles does not appear until after the $T_{gel\text{-}lc}$ of the lipid bilayer. Whereas in DLPC lipid vesicles, there is no second lifetime across the entire temperature range. We speculate this second lifetime, that is evidence of a confined L-Phe rotamer, becomes 'optically visible' only when water is present.

L-Phe in the polar headgroup of the lipid bilayer in its gel phase is subject to a polar, aprotic solvation environment. Our studies of L-Phe in bulk acetonitrile show that in such an environment, fluorescence is weak with the quantum yield of less than 0.01 (in acetonitrile, L-Phe's quantum yield is 0.006 (Table 4.1)). However, as temperature increases and water percolates into the polar headgroup, hydrogen bonding opportunities become available and L-Phe can sample a polar, protic solvation environment where its

quantum yield 5.5-fold larger (0.033 in methanol) than in polar aprotic environments. Based on the results described above, we expect that L-Phe in a tightly packed, polar aprotic environment of a lipid bilayer is optically invisible. Bilayer hydration near the gel-liquid crystalline transition temperature allows L-Phe to become optically active and contribute to the overall fluorescence decay. This result explains why the second lifetime appears at different temperatures for each of the different lipid vesicle systems and in the vicinity of the $T_{gel\text{-}lc}$. For DSPC and DPPC, the second lifetime appears ~10-15 °C before the $T_{gel\text{-}lc}$ and for DMPC, the lifetime appears shortly after the $T_{gel\text{-}lc}$.

Before the lipids fully transition from the gel-phase into the liquid-crystalline phase, a pre-transition phase occurs right before the $T_{gel\text{-}lc}$ (also known as the ripple phase) where water begins to percolate into the lipid bilayer vesicle.[123, 125] This ripple phase occurs at 16.5 °C, 35 °C, and 46.7 °C for DMPC, DPPC, and DSPC, respectively.[124-125] Shinoda *et. al.* studied transition temperatures through MD simulations and found the insertion of ethanol in the bilayer creates a defect where water can permeate into the bilayer before the ripple phase and affects larger lipids more significantly.[135] Therefore, the L-Phe that is in the membrane is speculated to create a pathway for water to enter the bilayer at an earlier temperature than that of the reported ripple phase. This early onset of the ripple phase is thought to be the reasoning for the appearance of the second lifetime of L-Phe in DSPC and DPPC vesicles before the reported temperature of the ripple phase in pure vesicles.

Despite the early permeation of water into the membrane, the gel-phase of the membrane is still relatively rigid and the solutes within the bilayer are expected to have

little conformational freedom. As water begins to permeate into the membrane, the bilayer expands by ~25% for DPPC vesicles[136] and transitions into the liquid-crystalline phase of the bilayer where the local solvation environment is polar protic, and solutes have more conformational freedom. As seen in Figures 4.4, 4.7, and 4.8, the concentration of L-Phe in the bilayer increases in concentrations up to 30% at high temperatures. The increase in concentration of the rotamer state implies one of two things: (1) more L-Phe is entering the bilayer as the bilayer expands and experiences this rotamer state. Or (2), as the bilayer expands and water increases concentration within the bilayer, more of the L-Phe that is already in the bilayer becomes optically visible. The increase in the second lifetime contribution is predicted to occur by scenario (2) as the free L-Phe in bulk solvent would not experience conformational restriction as the vesicles increase in size. Therefore, the L-Phe that is already in the bilayer is speculated to become more optically visible as the lipid bilayer expands and its concentration of water increases.

There is still a remaining question of the second lifetime *after* the $T_{gel\text{-}lc}$ of DMPC lipid vesicles and the absence of a second lifetime in DLPC lipid vesicles. Literature has reported large temperature dependence on the fluorescence lifetimes of L-Phe in an aqueous solvent attributed to a switch in the non-radiative decay pathways as a function of temperature. Leroy *et. al.* reported that at higher temperatures (>0 °C), internal conversion is the main non-radiative decay pathway of L-Phe in aqueous solvents.[126] However, at low temperatures (<0 °C), the main non-radiative decay pathway begins to transition from internal conversion to intersystem crossing.[126] If this switch from an

internal conversion to intersystem crossing non-radiative decay pathway begins to happen not exactly at 0 °C and at slightly higher temperatures (0-20 °C), this would explain the lack of an appearance of a second lifetime in DLPC vesicles and why, in DMPC vesicles, the second lifetime does not appear until after the $T_{gel\text{-}lc}$ at 25 °C.

Conclusion

Studies reported in this work used time-resolved fluorescence spectroscopy in combination with differential scanning calorimetry to understand the partitioning behavior of L-Phe into a model biological membrane. Results showed that L-Phe integrates into the bilayer through membrane deformities and does not significantly impact the $T_{gel\text{-}lc}$. However, the decrease in heat flow and asymmetric peak base widening is evidence of interactions between L-Phe and the lipid bilayer. The L-Phe that integrates into the bilayer remains largely in carbonate buffer. Evidence of a conformational rotamer fluorescence lifetime of 1.8 ns is seen in DSPC, DPPC, and DMPC lipid vesicles that only becomes optically visible when water integrates into the bilayer. The switch in the local solvation environment from a polar aprotic to a polar protic environment increases the quantum yield by a factor of 5.5 from 0.006 to 0.033, respectively. The L-Phe rotamer lifetime increases in concentrations of up to 30% at high temperatures and is predicted to be L-Phe in the bilayer that becomes more optically visible as the bilayer expands as water percolates within. The absence of a rotamer lifetime for DLPC is predicted to be due to a switch in non-radiative decay pathways.

Quantifying the partitioning behavior of L-Phe in a model biological membrane was done to understand the specific *chemical* interactions that occur when a biorelevant

solute partitions into the bilayer. Time-resolved fluorescence spectroscopy determined L-Phe does integrate into the polar headgroup of the lipid membrane in concentrations of up to 30%. The local solvation forces between L-Phe and the lipid itself creates a conformationally restricted environment disallowing L-Phe to radiative decay. As the bilayer expands and water permeates into the bilayer, the conformationally restricted rotamer becomes optically visible as a 1.8 ns lifetime that is stabilized by the polar protic environment. The photophysical behavior of L-Phe was characterized in this study and, some of which, has not been previously reported to the authors knowledge. The authors hope the work reported here sparks further studies into the specifics of the rotamer conformation and potential charge transfer character behavior of L-Phe. The work described here paves the way for future studies of other aromatic amino acids and small peptide chains to quantify the specific chemical interactions that occur when introduced to a lipid bilayer vesicle.

CHAPTER FIVE

TESTING MEMBRANE AFFINITY OF THIENOPYRIMIDINE DRUG CANDIDATES WITH TIME-RESOLVED FLUORESCENCE EMISSION

Contribution of Authors and Co-Authors

Manuscript in Chapter 3

Author: Sarah M. Hopfner

Contributions: Collected and analyzed all drug-activity data, generated figures, and wrote manuscript in preparation for publication. Co-first author with Katelyn Duncan.

Author: Katelyn M. Duncan

Contributions: Collected and analyzed all time-resolved data, generated figures, and wrote manuscript in preparation for publication. Co-first author with Sarah Hopfner.

Co-Author: Rhys C. Trousdale

Contributions: Assisted with time-resolved data accumulation.

Co-Author: Mary J. Cloninger

Contributions: Contributed important insight into performing experiments and interpreting results. Edited and assisted in the preparation of the manuscript.

Co-Author: Robert A. Walker

Contributions: Contributed important insight into performing experiments and interpreting results. Edited and assisted in the preparation of the manuscript.

Manuscript Information

Sarah M. Hopfner, Katelyn M. Duncan, Rhys C. Trousdale, Mary J. Cloninger, and Robert A. Walker.

Journal of

Status of Manuscript:

__x__ Prepared for submission to a peer-reviewed journal

____ Officially submitted to a peer-reviewed journal

____ Accepted by a peer-reviewed journal

____ Published in a peer-reviewed journal

TESTING MEMBRANE AFFINITY OF THIENOPYRIMIDINE DRUG CANDIDATES WITH TIME-RESOLVED FLUORESCENCE EMISSION

Sarah M. Hopfner[‡1], *Katelyn M. Duncan*[‡1], *Rhys C. Trousdale*[1], *Mary J. Cloninger*[1], *Robert A. Walker*[1,2]

[1]Department of Chemistry and Biochemistry, Montana State University, 103 Chemistry and Biochemistry Building, Bozeman, Montana 59717, United States
[2]Montana Materials Science Program, Montana State University, Bozeman, Montana, 59717, United States
[‡]Both authors contributed equally to this study

Abstract

Time resolved fluorescence emission spectroscopy was used to study the affinity of structurally related thienopyrimidines for model biological membranes. The thienopyrimidines were chosen due to their potential to block activity in cytochrome-*bd* oxidase, an important protein in *Mycobacterium tuberculosis*. Experiments tested the hypothesis that a large lipophilic log *P* value and a high IC_{50} activity should correlate with bioaccumulation within a lipid vesicle bilayer. Experiments reported herein did not confirm the hypothesis. The thieno[3,2-*d*]pyrimidin-4-amines bearing aryl methyl and *tert*-butyl substituents exhibited evidence of a non-radiative decay pathway induced by association with the model biological membrane with the methyl substituted species having the strongest membrane affinity. The methyl-substituted thienopyrimidine also displayed a conformationally restricted local solvation environment despite having an intermediate log *P* value and IC_{50} value. These results strongly suggest that targeted protein specificity by these drug candidates is primarily responsible for the observed

differences in IC_{50} values across the series of compounds rather than membrane accumulation.

Introduction

Drug design involves the multiparameter optimization of many physiochemical properties for each therapeutic molecule.[137] For example, compounds having poor bioavailability or off-target toxicity will not move forward in development. One way to enhance the efficacy of a therapeutic is to design it in such a way so that its local concentration in or near its intended target is higher than in the general periplasm. Therefore, knowing the affinity of a drug compound for biological membranes is an important structural consideration.[138-140] A common prediction tool for partitioning behavior is the partitioning coefficient (log *P*), a tool that has been employed since the late 1800's and is still widely used today in drug development.[1, 141-145] Log *P* is a helpful, zeroth order measure of solute affinity for biological membranes, but the log *P* scale is also based on a simple equilibrium constant description and fails to account for the specific *chemical* interactions that occur when a solute is introduced to a biological membrane. In effort to identify the specific chemical interactions that occur when a solute associates with a biological membrane, time-resolved fluorescence spectroscopy can be a valuable tool for quantifying relative populations and specific interaction mechanisms.

Experiments described in this study use time correlated single photon counting (TCSPC) spectroscopy to measure the lifetimes of different thienopyrimidine solutes in solutions containing vesicles composed of 1,2-dipalmitoyl-*sn*-glycero-3-phosphocholine (16:0 DPPC). This family of solutes are promising drugs to combat *Mycobacterium*

tuberculosis (Mtb). While there are many ways of disabling *Mycobacterium tuberculosis* (Mtb), whether through interruption of cell wall synthesis[146] or inhibition of DNA replication,[147] one of the most promising methods of sterilizing Mtb is through cessation of energy metabolism.[148] Mtb is an obligate aerobe, meaning that it requires oxygen in order to grow. Under low oxygen conditions Mtb persists in a non-replicating state[149, 150] and requires oxidative phosphorylation to make ATP.[148, 151] There are two terminal oxidases in this pathway; cytochrome *bcc:aa*$_3$ (cyt-*bcc:aa*$_3$) and cytochrome *bd* (cyt-*bd*). Cyt-*bcc:aa*$_3$ functions as the main oxidase, and cyt-*bd* is upregulated only when cyt-*bcc:aa*$_3$ is inactivated.[152] Thus, Cyt-*bd* protects Mtb against oxidative stress and, more importantly, against chemotherapies.[153]

The thienopyrimidine scaffold is of interest to medicinal chemists, and thienopyrimidine derivatives have been studied for use as anti-bacterial agents[154] including those that target Mtb.[155-157] Various thienopyrimidine derivatives have also shown promising activity against cancer,[158-161] autoimmune diseases,[162] and malaria.[163] Because of their noteworthy biological activity, assessing the membrane partitioning properties of the thienopyrimidine derivatives is an important consideration when developing mechanisms to describe thienopyrimidine activity. We hypothesized that partitioning into a biological membrane will correlate with anti-Mtb activity; thienopyrimidine derivatives that partition into the DPPC membrane should exhibit better IC_{50} values for a transmembrane target protein such as the respiratory oxidase cytochrome *bd* (cyt-*bd*) in *Mycobacterium tuberculosis* (vide infra). To test this

hypothesis, our studies focused on three specific thienopyrimidine solutes having different log *P* values *and* very different IC_{50} values (Figure 5.1).

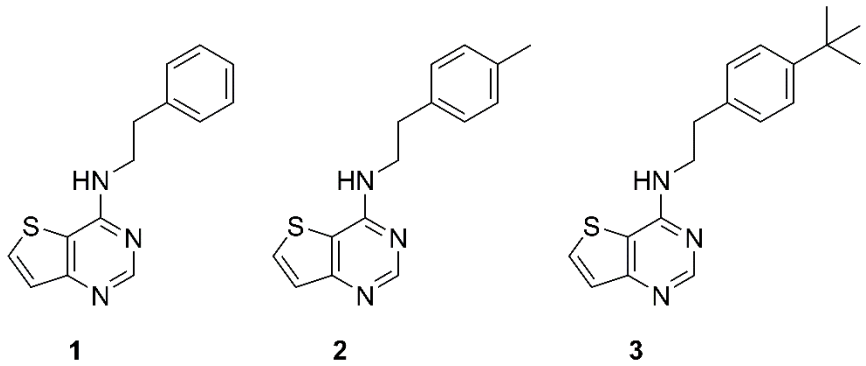

Figure 5.1. Thieno[3,2-*d*]pyrimidin-4-amines 1–3.

All three compounds share a phenethylamine attached to the same thieno[3,2-*d*]pyrimidine heterocyclic ring. These three solutes are distinguished by the substitution in the 4' position of the aryl ring. Compound **1** is the most hydrophilic, having a log *P* value of 4.0. Compound **3** with its *tert*-butyl group is the most hydrophobic solute and has a log *P* value of 5.9. With its methyl group at the para position, Compound **2** is intermediate in its hydrophobicity and log *P* value (4.5). Of these three solutes, Compound **3** is predicted to be the most promising candidate for further development as an anti-TB agent with an IC_{50} of 9 μM against N0145-Mtb in the presence of Q203.[164] Compounds **1** and **2** have weaker activity against N0145-Mtb (IC_{50} values of 52 and 37 μM, respectively when Q203 was added).

Compounds that simultaneously inhibit cyt-*bcc:aa*$_3$ and cyt-*bd* have proven lethal to replicating and non-replicating Mtb.[165] For this reason, the IC_{50} values of compounds **1**–**3** were studied previously with coadministration of the cyt-*bcc:aa*$_3$ inhibitor Q203. Although the structure of cytochromes *bd* have been reported in *Escherichia coli* (*E.*

coli),[166-167] *Geobacillus thermodenitrificans* (*G. th*),[168] and *Mycobacterium smegmatis (M. smegmatis)*,[169] significant structural differences between the cytochromes *bd* of these three organisms were noted, indicating that the existing structures cannot serve as useful comparisons for cyt-*bd* in Mtb.[169] Compounds that effectively inhibit cyt-*bd* activity have the potential to dramatically improve the destruction of Mtb, making the recently reported structure of cyt-*bd* in Mtb[170] a spectacular benefit to the design of drugs to inhibit cyt-*bd*.[166-167] Since the structures of cyt-*bd* are unknown in other prokaryotes, having additional methods of predicting potency is important for the development of antimicrobial agents.

Experiments were carried out with several structurally related compounds to assess whether the calculated log *P* values tracked with measured membrane affinity. DPPC vesicle bilayers were chosen because DPPC is often the dominant lipid in eukaryotic cell membranes. Real biological membranes are, of course, more complex than a single component lipid bilayer systems as biological membranes also contain proteins, carbohydrates, and cholesterol as described by the fluid mosaic model.[24, 171] Nevertheless, single-component lipid vesicle bilayers have proven useful in determining the physiological partitioning tendencies of aspirin,[172] methotrexate,[173] and doxorubicin.[174] Furthermore, as one criterion in the Lipinski Rule of 5 guidelines used to assess whether or not a given pharmaceutical is a candidate for further development, a solute's log *P* value is assumed to be an important indicator of whether or not it will bioaccumulate.[175-176] Recent reports suggest that adding heterogeneity to lipid membranes

(in the form of other constituents) can change quantitative (but not qualitative) solute partitioning behavior.[177]

For those solutes that fluoresce, TCSPC has proven an invaluable tool for identifying solute partitioning tendencies. Reported studies have found that small structural changes to the solute alter partitioning behavior drastically.[178-181] In addition, chemical complexity in the form of other biologically relevant, available solutes change a solute's partitioning tendencies and local solvation environment. In the studies discussed below, a suite of independent methods was used to assess the properties and structures of thienopyrimidines in aqueous buffer and the tendencies of these structurally related solutes to accumulate in DPPC membranes. TCSPC data provide important evidence not only of membrane association, but also *where* in the membrane the solutes partition.

While only weakly fluorescent, the thienopyrimidine compounds (Figure 5.1) *do* have measurable time dependent fluorescence that depends on the local solvation environment. This fluorescence behavior allows us to employ TCSPC for analysis of each compound's partitioning behavior in 1,2-dipalmitoyl-*sn*-glycero-3-phosphocholine (DPPC) vesicles. The data show that despite having only an intermediate IC_{50} value, Compound **2** showed the strongest affinity for DPPC bilayers. Specifically, Compound **2** displayed a conformationally restricted local solvation environment and evidence of membrane assisted aggregation predicted to be due to association with the DPPC charged headgroup in concentrations of 40% and 4%, respectively. In contrast, neither Compound **1** nor Compound **3** showed any detected membrane affinity. Taken together, these findings imply that the efficacy of this next generation of anti-TB drugs likely operate

through direct association with the cytochrome *bd* oxidase protein in the cell membrane, rather than through enrichment in/near the membrane followed by less specific binding.

Materials & Methods

Synthesis Materials

ACS grade sodium hydroxide (97%), ACS plus grade hydrochloric acid (37%), ACS grade potassium hydrogen phthalate (99% purity) were purchased from Sigma-Aldrich Chemical Co. (Milwaukee, WI). All working solutions for pKa determination were prepared with degassed Aquafina water. The titrant solution of NaOH was prepared at 0.01 M and standardized with potassium hydrogen phthalate. The exact concentration was determined to be 0.009 ± 0.001 M. This solution was stored in a capped plastic bottle. The standardized NaOH solution was then used to standardize the hydrochloric acid solution. The hydrochloric acid solution was found to be 0.014 ± 0.0005 M. The PASCO Scientific pH probe was connected to a Model 270 Denver Instrument pH meter. The pH meter was calibrated with standard buffers at pH 4.01 ± 0.01 (0.05 M potassium biphthalate), pH 6.86 ± 0.01 (0.05 M potassium phosphate monobasic – sodium hydroxide), pH 10.01 ± 0.02 (0.05 M potassium carbonate – potassium borate – potassium hydroxide) Buffers were purchased from Fisher Scientific, Pittsburgh, PA.

Synthesis

The thieno[3,2-*d*]pyrimidin-4-amines were prepared as reported previously.[157]

1D Selective Gradient Nuclear Overhauser Effect (NOE) spectra were recorded at 300 K on a Bruker 600 MHz Avance III NMR Spectrometer using standard acquisition parameters: spectral width 12,019 Hz, acquisition time 2.73 seconds, pulse width 8 μs,

relaxation delay 2 s, mixing time 0.3 seconds, number of scans 128. Peaks were selected for excitation in each experiment.

Sample Preparation for pKa Measurements

Compounds were dissolved in 2 mL of DMSO, diluted with water, sonicated, heated, and allowed to stir for 1 week. The solution was continuously mixed with a magnetic stirrer. Titrations were performed in triplicate at ambient temperature (20 °C). A Hamilton syringe was used to incrementally add sodium hydroxide or hydrochloric acid, and the solution was equilibrated to reach a stable pH reading prior to the next acid or base addition. After each experiment, the pH probe was thoroughly washed with Aquafina water and recalibrated.

Time-Resolved Fluorescence Measurement Materials

Solvents were purchased from Sigma-Aldrich and used as received. Millipore water (18.2 MΩ) was used to make 10 mM carbonate buffer (pH = 7). 1,2-Dipalmitoyl-*sn*-glycero-3-phosphocholine (16:0 DPPC) was purchased from Avanti Polar Lipids (Alabaster, AL). All bulk solvent solutions were made at a 45 μM concentration and lipid vesicles used for fluorescence experiments were made at 1.5 mM concentration.

Lipid Bilayer Vesicle Preparation

Lipid vesicles were prepared by dissolving DPPC in chloroform and subsequently removed via rotary evaporation, resulting in a thin lipid film. The resulting lipid film was rehydrated with 45 μM solution of **1**, **2**, or **3** in 10 mM carbonate buffer to form a lipid vesicle solution. The solution was sonicated for 30 minutes at ~50 °C. The solution was then passed through a PTFE syringe filter (450 nm) to remove giant

unilamellar vesicles. The solution was then subsequently heated to 50 °C and passed through an Avanti Mini Extruder 11 times with a membrane pore size of 200 nm.

Time-Correlated Single-Photon Counting (TCSPC)

Fluorescence lifetimes were measured using a Ti:sapphire oscillator (Coherent Chameleon, 80 MHz, 85 fs pulse duration, 680-1040 nm wavelength range) coupled with an APE autotracker capable of frequency tripling the fundamental to select solute specific excitation wavelengths. A Conoptics model 350-80 modulator was used to reduce the repetition rate to 4 MHz. Picoquant PicoHarp 300 and FluoTime 200 software were used for data collection. Samples were equilibrated at reported temperatures for 5 minutes using a Quantum Northwest TC125 control (Seattle, WA). A long pass filter (90% transmission >300 nm) was placed after the sample to reduce scattering from the vesicles. Photon emission was collected at 370 nm, a wavelength that overlapped all solutes in each of the bulk solvents. Excitation wavelength was 260 nm for all solutes, a wavelength that overlapped all solutes in each of the bulk solvents.

Time-resolved emission data were collected for each compound in bulk solvents chosen to mimic the unique environments a solute could solvate within lipid bilayer vesicle: carbonate buffer to model the compound not integrating into the lipid bilayer, acetonitrile to model the polar aprotic headgroup, and methanol to model the polar protic headgroup when water has integrated into the membrane. Such an approach has been used previously to approximate small molecule partitioning into lipid bilayer membranes.[182-183] The fluorescence behavior of each compound was measured in cyclohexane used to model the nonpolar tails, however, were excluded from this work

due to low solubility. Next, the fluorescence behavior was analyzed in vesicle-containing solutions. The corresponding lifetimes and amplitude parameters were independently calculated and adjusted to optimize χ^2. When possible, a linear combination of lifetimes found in the bulk solvents (mentioned above) was created to assign local solvation environments of the compound in a lipid bilayer vesicle. The fluorescence decay and amplitude expressions are shown in Eq. 5.1 where A_i and τ_i are the amplitude and lifetime of the i^{th} component, respectively, and IRF is the instrument response function allowing for reconvolution of the histogram.

$$I(t) = \int_0^t IRF\ (t') \sum_{i=1}^{n} A_i e^{-\frac{t-t'}{\tau_i}}\ dt' \qquad (5.1)$$

Each trace was fit independently, without any constraints, for the lifetimes or amplitudes with a typical χ^2 between 0.9 and 1.1 when accounting for, at most, four lifetimes. Reported data represent averaged lifetimes from three experiments with independently prepared, equivalent samples. Lifetime uncertainties are reported as ± 0.2 ns because and typical uncertainties in amplitudes are ±0.03. Error bars presented in this work are a result of 3 trials averaged together with a single standard deviation reported for the 3 averaged trials. The averaged lifetimes and amplitudes are reported for each temperature.

Results

As noted above, thienopyrimidines have been studied for a variety of biological applications. One particularly compelling application is their development as anti-*Mycobacterium tuberculosis* (Mtb) compounds. Previously, Moraski and co-workers

have reported that thieno[3,2-*d*]pyrimidin-4-amines **1**–**3** (shown in Figure 5.1) have encouraging activity against *Mycobacterium bovis* BCG, *Mycobacterium tuberculosis* H37Rv, and *Mycobacterium tuberculosis* clinical isolate N0145.[157] As summarized in Table 5.1, the phenethyl analog **1** was found to have weak potency when co-administered with Q203. Additional experiments demonstrated that Mtb requires oxidative phosphorylation for growth.[148, 151] Mtb has two terminal oxidases within the oxidative phosphorylation pathway, cytochrome *bcc:aa*$_3$ (cyt-*bcc:aa*$_3$) serving as the main aerobic oxidase and cyt-*bd* helping in a less-efficient, redundant manner. Q203 binds to the cytochrome *b* subunit on cyt-*bcc:aa*$_3$, deactivating its function.[164] When this occurs, cyt-*bd* activity is upregulated[152] and sustains ATP production sufficiently for Mtb to survive in a non-replicating state.[150, 184] In this way, Mtb is shielded from complete shutdown of the oxidative phosphorylation pathway from cyt-*bcc:aa*$_3$ inhibitors such as Q203. We have shown that inhibition of both cyt-*bcc:aa*$_3$ and cyt-*bd* is bactericidal against Mtb.[165] The 4-methylphenethyl analog **2** had better potency than **1**, and the most potent derivative was found to be the 4-*tert*-butylphenethyl analog **3** (in the presence of Q203; none of the described compounds displayed significant activity in the absence of Q203). Interestingly, compound **3** showed the greatest potency against all three bacterial strains (BCG, H37Rv, and N0145) and has the highest log *P* value. The partitioning coefficients for **1**–**3** all indicate a strong preference for solubility in the organic phase and, by inference, a strong tendency to partition into membranes.

Table 5.1. Partition coefficients of **1**–**3** and activity against *Mycobacterium bovis* BCG, *Mycobacterium tuberculosis* H37Rv, and *Mycobacterium tuberculosis* clinical isolate N0145.[157]

Compound	Log *P*	BCG IC_{50} (μM) (+Q203)[a]	H37Rv IC_{50} (μM) (+Q203)[a]	N0145 IC_{50} (μM) (+Q203)[a]
1	4.0	43 ± 9	>100	52 ± 4
2	4.5	40 ± 11	108 ± 8	37 ± 10
3	5.9	6 ± 1	19 ± 9	9 ± 2

[a]Table 5.1. In vitro activity of thieno[3,2-*d*]pyrimidin-4-amines against three Mycobacterial strains (*M. bovis* BCG, *M. tuberculosis* H37Rv, *M. tuberculosis* clinical isolate N0145) – previously reported values.[157]

In this work, we examine how each thieno[3,2-*d*]pyrimidin-4-amine compound interacts with a lipid bilayer vesicle using time-resolved fluorescence spectroscopy. Prior to the solutes being introduced to lipid vesicle-containing solutions, the compounds were first modeled in bulk solvents. The bulk solvents were chosen to mimic the various solvation environments of a lipid bilayer vesicle: acetonitrile for the polar aprotic headgroup region, cyclohexane for the nonpolar tails, and methanol for a polar protic headgroup region that has water percolated into the membrane. Due to the low solubility limit of these compounds in cyclohexane, the behavior of compounds **1**–**3** in a nonpolar environment is omitted from this work. The vesicles in this study are prepared in a 10 mM carbonate buffer (pH 7) and therefore represent the solute remaining in aqueous solution and not integrating with the bilayer. The steady-state excitation and emission peak wavelengths as well as the fluorescence lifetimes of compounds **1**, **2**, and **3** in carbonate buffer, methanol, and acetonitrile are shown in Table 5.2 and Figures 5.2 – 5.3, respectively.

Table 5.2. Fluorescence properties of **1**–**3** in each of the bulk solvents. Uncertainties in reported lifetimes are ± 0.2 ns. Numbers in parentheses next to lifetimes are amplitudes of that lifetime. In the case of a biexponential fluorescence decay, the lifetime with the largest amplitude will be used as an indicator for that local solvation environment.

Solvent	Compound 1			Compound 2			Compound 3		
	λ_{exc} (nm)	λ_{em} (nm)	τ_f (ns)	λ_{exc} (nm)	λ_{em} (nm)	τ_f (ns)	λ_{exc} (nm)	λ_{em} (nm)	τ_f (ns)
Carbonate Buffer	246/298	360	0.27 (0.97), 1.45 (0.03)	270	395	0.29 (0.69), 1.48 (0.31)	253/298	360	0.28 (0.94), 1.44 (0.06)
Methanol	245/295	350	0.22	245/295	350	0.22 (0.99), 1.60 (0.01)	270	350	0.21 (0.97), 0.54 (0.03)
Acetonitrile	245/295	350	0.18	245/295	350	0.18 (0.98), 2.05 (0.02)	245/290	350	0.18 (0.99), 2.00 (0.01)

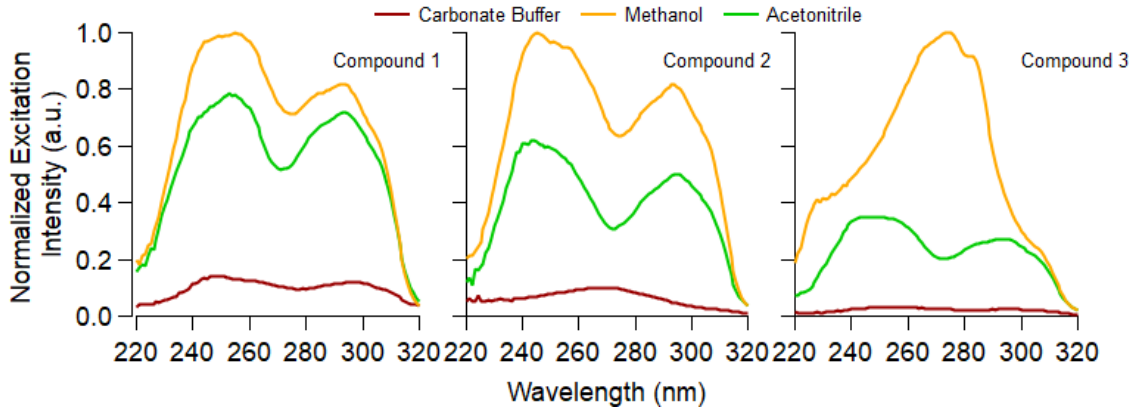

Figure 5.2. Excitation spectra of Compounds **1**, **2**, and **3** in each of the bulk solvents.

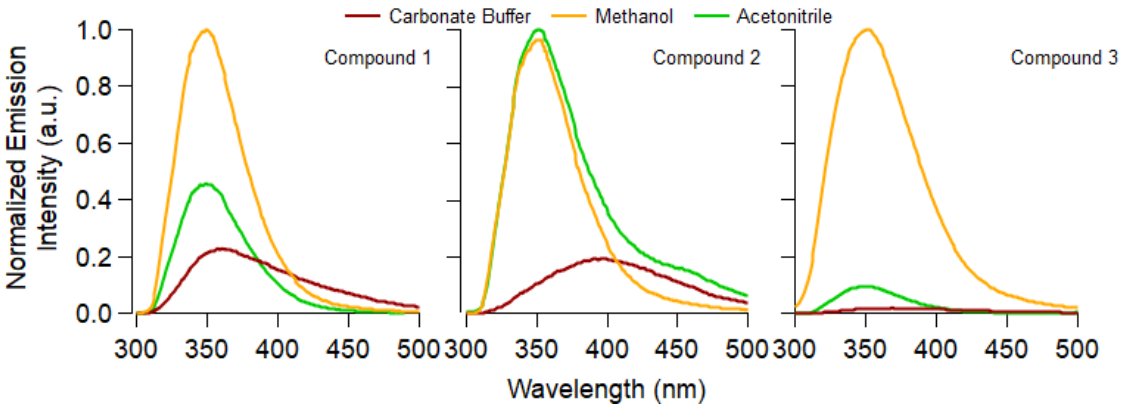

Figure 5.3. Emission spectra of Compounds **1**, **2**, and **3** in each of the bulk solvents.

Excitation and emission wavelengths for **1**–**3** was selected based on each solute's steady state excitation and fluorescence emission spectrum. These data were used to

determine the excitation and emission wavelengths used in the TCSPC experiments. While all three solutes were weakly solvatochromic, the excitation and emission wavelengths used in TCSPC measurements were chosen to access all relevant solvation environments. All time-resolved fluorescence spectra were excited at 260 nm and emission was collected at 370 nm. The time-resolved fluorescence decay of **1**–**3** in bulk solvents is shown in Figure 5.4.

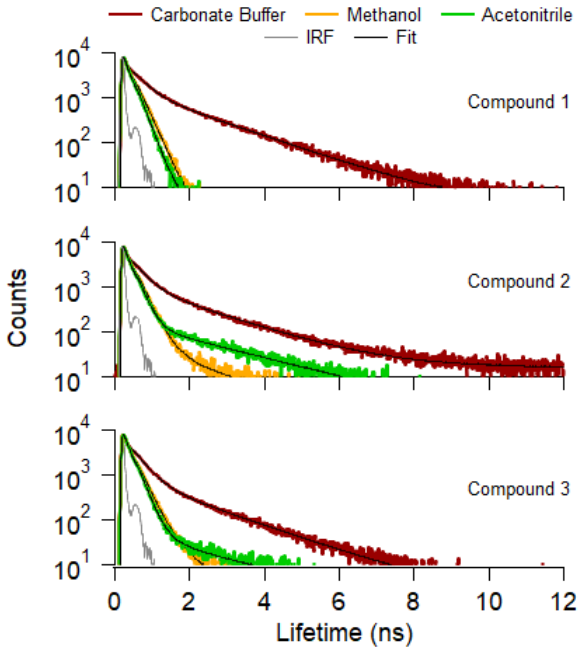

Figure 5.4. TCSPC spectra of 45 µM solutions of 1, 2, or 3 in each of the bulk solvents at 20 °C. Results from fitting these emission traces to Eq. 5.1 are reported in Table 5.2. Gray trace is instrument response function (IRF).

The lifetimes of each compound differ very little between each of the bulk solvents, with the major lifetime being 0.18 – 0.29 ns (Table 5.2). Compound **1** only displays a dual lifetime in carbonate buffer, while **2** and **3** display dual lifetimes in all three solvents, albeit with one of those lifetimes typically having very small amplitudes.

For amplitudes ≤ 3%, the lifetime is not considered significant and is reported solely for fitting purposes.

Once the fluorescence behavior of each compound was characterized, each compound, separately, was introduced to a solution of lipid bilayer vesicles and was analyzed as a function of temperature in 10 °C increments from 10 °C to 70 °C and then back to 10 °C (Figure 5.5). The variable temperature protocol was used to analyze the effect of the compounds on the vesicle as it transitions from the gel phase through the transition temperature into the liquid crystalline phase ($T_{gel\text{-}lc}$: 41 °C) and to evaluate each compound's membrane affinity as a function of membrane phase. Each trace was fit using Eq. 5.1. Lifetimes and corresponding amplitudes are reported in Table 5.3.

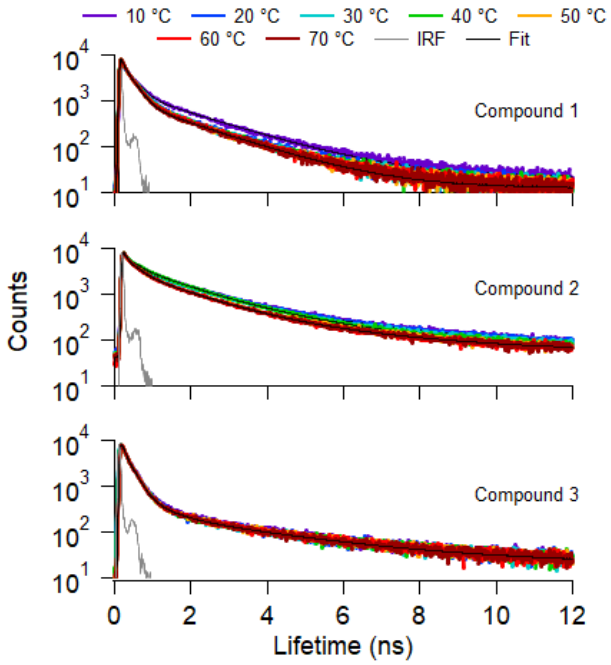

Figure 5.5. TCSPC spectra of 45 µM solutions of 1, 2, or 3 in a DPPC lipid vesicle solution as a function of temperature. Top panel: 1; middle panel: 2; bottom panel: 3. Results from fitting these emission traces to Eq. 5.1 are reported in Table 5.3. Gray trace is instrument response function (IRF).

Table 5.3. Fluorescence lifetimes (in ns) and amplitudes (in parentheses) for **1**–**3** in solutions of DPPC vesicles obtained between 10 and 70 °C and back down to 10 °C in 10 °C increments. Uncertainties in lifetimes are ± 0.2 ns; uncertainties in amplitudes are ± 0.03.

	Compound 1		**Compound 2**				**Compound 3**		
temp. (°C)	buffer τ_1 (A_1)	buffer τ_2 (A_2)	buffer τ_1 (A_1)	buffer τ_2 (A_2)	new K_{nr} τ_3 (A_3)	conf. restricted τ_4 (A_4)	buffer τ_1 (A_1)	buffer τ_2 (A_2)	new K_{nr} τ_3 (A_3)
10	0.25 (0.89)	1.71 (0.11)	0.31 (0.38)	1.40 (0.19)	3.89 (0.04)	0.06 (0.39)	0.19 (0.93)	0.84 (0.05)	3.60 (0.02)
20	0.26 (0.91)	1.70 (0.09)	0.29 (0.39)	1.36 (0.19)	3.98 (0.04)	0.05 (0.37)	0.19 (0.93)	0.78 (0.05)	3.42 (0.02)
30	0.23 (0.92)	1.69 (0.08)	0.28 (0.44)	1.35 (0.21)	3.94 (0.04)	0.05 (0.32)	0.18 (0.92)	0.70 (0.06)	3.22 (0.02)
40	0.25 (0.92)	1.67 (0.08)	0.28 (0.46)	1.01 (0.22)	3.57 (0.03)	0.07 (0.29)	0.18 (0.92)	0.74 (0.06)	3.26 (0.02)
50	0.23 (0.92)	1.63 (0.08)	0.25 (0.48)	1.37 (0.19)	4.22 (0.03)	0.08 (0.30)	0.17 (0.93)	0.80 (0.05)	3.49 (0.02)
60	0.23 (0.93)	1.62 (0.07)	0.23 (0.52)	1.27 (0.19)	3.59 (0.03)	0.14 (0.26)	0.17 (0.90)	0.71 (0.08)	3.15 (0.02)
70	0.22 (0.93)	1.61 (0.07)	0.24 (0.54)	1.39 (0.22)	5.05 (0.02)	0.10 (0.22)	0.17 (0.91)	0.68 (0.08)	3.03 (0.02)
60	0.23 (0.93)	1.62 (0.07)	0.24 (0.51)	1.37 (0.22)	4.58 (0.02)	0.09 (0.25)	0.17 (0.90)	0.74 (0.08)	3.17 (0.02)
50	0.23 (0.92)	1.64 (0.08)	0.24 (0.41)	1.30 (0.20)	3.96 (0.03)	0.09 (0.36)	0.17 (0.91)	0.81 (0.07)	3.23 (0.03)
40	0.24 (0.92)	1.65 (0.08)	0.25 (0.50)	1.29 (0.22)	3.59 (0.04)	0.06 (0.24)	0.18 (0.90)	0.80 (0.07)	3.19 (0.03)
30	0.25 (0.90)	1.67 (0.10)	0.27 (0.42)	1.30 (0.26)	3.36 (0.05)	0.07 (0.28)	0.18 (0.87)	0.79 (0.09)	3.06 (0.04)
20	0.25 (0.89)	1.70 (0.11)	0.28 (0.36)	1.31 (0.25)	3.63 (0.05)	0.07 (0.33)	0.18 (0.85)	0.79 (0.11)	3.10 (0.05)
10	0.25 (0.89)	1.70 (0.11)	0.31 (0.34)	1.36 (0.23)	3.58 (0.06)	0.09 (0.37)	0.18 (0.85)	0.90 (0.10)	3.22 (0.05)

Figures 5.6 and 5.7 provide a visual representation of the lifetimes and lifetime contributions listed in Table 5.3 as a function of temperature and bilayer phase. Compound **2** was best fit to 4 lifetimes (at 20˚C) with τ_1 (0.30 ns) and τ_2 (1.40 ns) matching **2's** behavior in carbonate buffer. The third long lifetime (τ_3: ~3.90 ns) does not match any behavior observed in bulk solvents and indicates a new radiative decay pathway (new K_{rad}). An origin of this new emission is proposed in the Discussion section below. The fourth lifetime is extremely short (τ_4: 0.06 ns). We propose that this lifetime originates from compound **2** in a conformationally restricted environment where it interacts with the bilayer below the $T_{gel\text{-}lc}$. The basis for this assignment is also considered in the Discussion section. Compound **3** was best fit to 3 lifetimes with τ_1 and τ_2 that match **3** in bulk carbonate buffer, and a long (~3.60 ns) lifetime that again does not match

any observed behavior in bulk solvents. The low amplitude of the fluorescence decay for the third lifetime suggests that **3** remains largely in the carbonate buffer rather than partitioning into the vesicle. This result stands in contrast to the anticipated behavior based on the large log *P* value for **3**. As seen in Figures 5.6 and 5.7, solute fluorescence shows no strong dependence on temperature or bilayer phase for any of the compounds in a lipid vesicle solution. There is a slight variation at higher temperatures above the $T_{gel\text{-}lc}$ for **2** (τ_3: 5.05 ns); however, the amplitude for the third lifetime approaches zero (2%) at these elevated temperatures and therefore is present strictly for fitting purposes. An important point to note is that the number of lifetimes chosen to fit a fluorescence decay is based on the χ^2 parameter for a value between 0.9-1.1 using the lowest number of exponentials required to do so. These fits are carried out independent of any results measured for the bulk solvents.

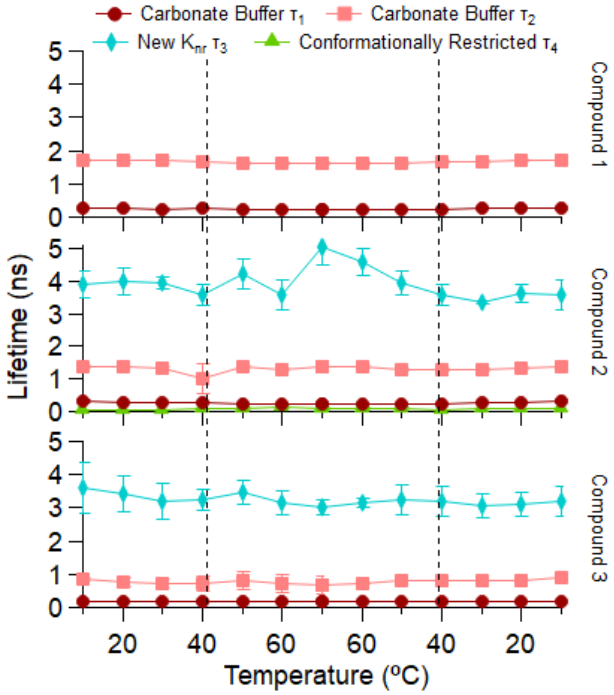

Figure 5.6. Fluorescence lifetimes of each compound in solutions of DPPC vesicles as a function of temperature: carbonate buffer (τ_1, burgundy circles; τ_2, pink squares), possible new non-radiative decay (K_{nr}) pathway (τ_3, teal diamonds), conformationally restricted environment (τ_4, green triangles). Dashed lines show the temperature (41 °C) at which the vesicle transitions between the gel phase and the liquid-crystalline phase. Note that the x-axis follows an experiment as the temperature is raised (to 70˚C) and then lowered (to 10˚C). Error bars on each point reflect one standard deviation of uncertainty from 3 measurements averaged together. In some cases, the uncertainty is smaller than the symbols used to represent the data.

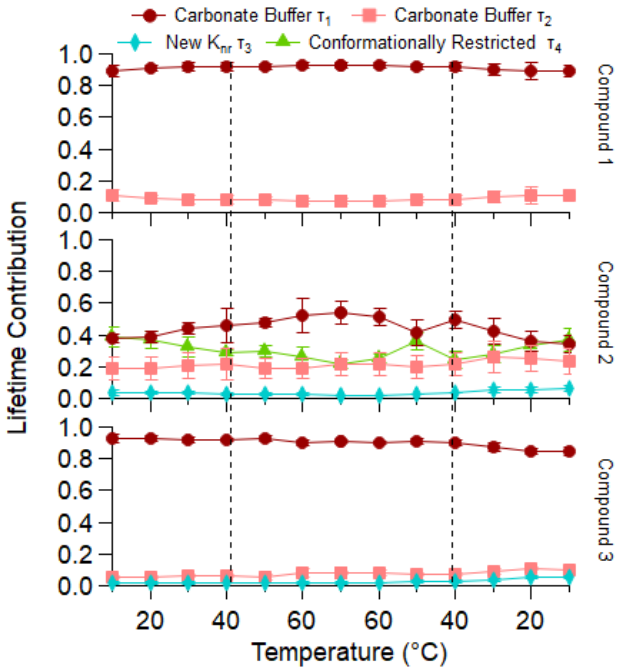

Figure 5.7. Lifetime contributions of **1**–**3** in solutions of DPPC vesicles as a function of temperature: carbonate buffer (τ_1, burgundy circles; τ_2, pink squares), possible new non-radiative decay (K_{nr}) pathway (τ_3, teal diamonds), conformationally restricted environment (τ_4, green triangles), Dashed lines show the temperature (41 °C) at which the vesicle transitions between the gel phase and the liquid-crystalline phase. Note that the x-axis follows an experiment as the temperature is raised (to 70˚C) and then lowered (to 10˚C). Error bars on each point reflect one standard deviation of uncertainty from 3 measurements averaged together. In some cases, the uncertainty is smaller than the symbols used to represent the data.

Compound **2** with a log *P* value of 4.5 displayed the largest change in fluorescence lifetime in the presence of DPPC vesicles, although the nature of this interaction is mysterious given that neither the long new lifetime (τ_3: ~3.90 ns) nor extremely short new lifetime (τ_4: 0.06 ns) matches results from the bulk solvent experiments. To understand these lifetimes and assign significance to the third and fourth lifetime, **2** was frozen in carbonate buffer to observe its fluorescence behavior in a conformationally restricted environment (Figure 5.8 and Table 5.4). A similar analysis

has been carried out recently to simulate the effects of conformational restriction in confining environments.[55]

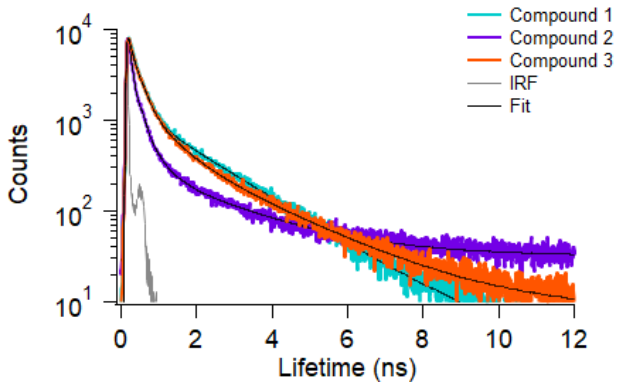

Figure 5.8. TCSPC spectra of 45 µM solutions of **1**, **2**, or **3** in a frozen carbonate buffer. Results from fitting these emission traces to Eq. 5.1 are reported in Table 5.4. Gray trace is instrument response function (IRF).

Table 5.4. Fluorescence lifetimes (in ns) and amplitudes (in parentheses) of **1**–**3** in frozen carbonate buffer solutions. Uncertainties in lifetimes are ± 0.2 ns; uncertainties in amplitudes are ± 0.03.

Compound	τ_1 (A_1)	τ_2 (A_2)	τ_3 (A_3)
1	0.21 (0.89)	1.68 (0.11)	
2	0.10 (0.88)	0.37 (0.10)	2.23 (0.02)
3	0.18 (0.82)	0.66 (0.12)	2.18 (0.05)

The results found in Table 5.4 from fitting the fluorescence decays in Figure 5.8 display a short lifetime that accounts for the majority of the fluorescence decay for all three compounds. This short lifetime also matches closely with the dominant lifetime for compounds **1, 2,** and **3** in bulk aqueous buffer. Compound **1** emission decay also displays the second lifetime generally associated with solvation in the carbonate buffer (1.68 ns, 0.11). From this result, we conclude that the frozen aqueous matrix does not force compound **1** to experience solvation forces that are any different than the liquid carbonate

buffer. Compounds **2** and **3** each show a second lifetime on the order of 0.6 ns with small but measurable amplitudes (~0.1). The long, 2.2 ns lifetimes in the **2** and **3** emission traces are longer than long aqueous lifetime (1.5 ns) lifetime and relatively close to the long, small amplitude lifetimes shown by **2** and **3** in polar, aprotic solvents like acetonitrile.

Discussion

The studies described above were motivated by the hypothesis that membrane affinity and resulting bioconcentration could be causing differences in efficacy, as characterized by the differences in IC_{50} values for **1**–**3**. While our findings do not support the original hypothesis, they do highlight some very unusual photophysical behavior of this class of compounds. Differences in membrane affinity inferred from the TCSPC measurements also strongly suggest that simple log *P* considerations are not sufficient to predict anti-Mtb activity for this family of compounds. Compounds **1**-**3** are neutral at physiological pH (pKa measurements are found in the Supporting Information of the manuscript, Figures S1 – S18, respectively)[185], which suggest alternative mechanisms – specifically direct compound-protein binding – are responsible for deactivating these bacteria. The balance of this section will consider several surprising discoveries made about how compounds **1**–**3** behave in bulk buffer and in the presence of simple lipid vesicle membranes. These discoveries include: 1) preferential association of compound **2** with membranes relative to compounds **1** and **3**; 2) the origin of the very short lifetime of **2** in vesicle solutions; and 3) the origin of the long (≥ 3 ns) lifetime in solutions containing DPPC vesicles shown by compounds **2** and **3**.

Unique Membrane Affinity of Compound **2** – A Breakdown in Log P

Time-resolved fluorescence measurements of compounds **1**, **2**, and **3** introduced to lipid bilayer vesicle solutions display unique and distinctive partitioning behavior. As shown in Figures 5.4 and 5.5, compound **1** displays two fluorescence lifetimes that closely match the lifetimes found for **1** in bulk carbonate buffer. This result strongly suggests that **1** does not partition into the bilayer despite its log *P* value of 4.0 and instead remains in aqueous solution (Figures 5.5-5.7 and Table 5.3). From these results, we conclude that if compound **1** associates with the DPPC lipid bilayer, it does so at concentrations below the detection limits of our instrumentation.

Compound **2** displays four unique fluorescence lifetimes all with significant amplitudes (Figures 5.6-5.7 and Table 5.3). The first and second lifetime match that of **2** in a bulk carbonate buffer and retain the 65/35% amplitude ratio. The third and fourth lifetimes, 3.89 ns (4%) and 0.06 ns (39%), respectively, do not match any lifetimes found in any bulk solvent tested. Given that these lifetimes are present in the DPPC-vesicle containing solutions but not in the simple buffer itself, we attribute these two new lifetimes to compound **2** associating with the lipid bilayer. Compound **2** has a calculated log *P* value of 4.5, meaning that the solute is expected to have a strong tendency to partition into biological membranes. Despite the fact that compound **1** with its log *P* of 4.0 does not appear to associate with DPPC vesicles, the behavior of compound **2** is consistent with membrane affinity.

For Compound **3**, the shortest lifetime found in DPPC vesicles, τ_1: 0.19 ns (93%), matches that in bulk carbonate buffer. Compound **3** in DPPC vesicle containing solutions

also shows an intermediate lifetime at τ_2: 0.84 ns (5%) that is similar to the 0.6 ns lifetime observed from compound **3** emission in the frozen carbonate buffer. Finally, compound **3**, like compound **2**, shows a third, longer fluorescence lifetime, 3.60 ns, albeit with very low amplitude (2%). The intermediate lifetime may be consistent with **3** associating with the bilayer in a way that restricts conformational freedom (as is the case in frozen carbonate buffer), but the amplitude of this contribution to the decay trace does not scale with anticipated behavior based on log *P*.

Origin of Short Lifetime in DPPC-Compound **2** System

Perhaps the most dramatic change for any of the compounds studied in carbonate buffer and carbonate buffer with DPPC vesicles was the emergence of a very short decay ($\leq$ 0.1 ns) component for compound **2** that accounted for ~33% of the decay trace total amplitude. Typically, a lifetime this short points to very efficient non-radiative decay. Subsequent experiments carried out with compound **2** in a frozen carbonate buffer (with no vesicles) also showed an extremely short fluorescence lifetime, 0.10 ns (88%), and a third long fluorescence lifetime (2.23 ns). Based on this frozen-buffer result, we propose that *if* compound **2** is integrating into the bilayer, the extremely short lifetime (τ_4: 0.06 ns) reflects a geometrically restricted local solvation environment. Similar effects have been reported for solutes adsorbed to strongly associating solid-liquid interfaces where close registry between an aqueous solvent and a hydrophilic silica substrate creates a cage-like structure around adsorbates. This cage-like structure restricts isomerization after photoexcitation and markedly shortens the adsorbate's fluorescence lifetime relative to bulk solution limits.[55, 186] Drawing on the findings from these earlier studies, we propose

that the sub 0.2 ns lifetime observed for compound **2** in the DPPC solutions results from the solute associating with the membrane in such a way so as to restrict its conformational mobility following photoexcitation. While the excited state photophysical behavior of compounds **1**–**3** remains unknown, the behavior exhibited by compound **2** is consistent with a photoexcited solute that is unable to be stabilized by its surrounding solvation environment and therefore relaxes back to the ground state through a non-radiative decay pathway.

Origin of Long Lifetime in DPPC-Compound **2** and **3** Systems

A lifetime common to the emission decay from both compounds **2** and **3** in DPPC solutions is longer than all other observed lifetimes. Although this lifetime always shows a small amplitude, the effects of this ≥3 ns lifetime are readily evident in the decay traces of DPPC containing solutions (Figure 5.5) and is completely absent in simple carbonate buffer solutions. A longer lifetime implies greater stabilization of a solute's excited state electronic structure.[187-189] Given that this long lifetime appears only in vesicle containing solutions, we assign this radiative decay pathway to a small population of compounds **2** and **3** that interact with a part of the lipid membrane in a way that still allows either the solute or the membrane to reorganize itself following photoexcitation.

We explored the possibility that this new lifetime resulted from a small population of compounds **2** and **3** having a different conformation within or near the DPPC bilayer by measuring the NOE spectra of these species in different solvents. However, these experiments showed no obvious intramolecular conformational signatures denoting a folded or otherwise contorted structure (NOE spectra are presented in Supporting

Information of the manuscript)[185]. We also considered that the long lifetime may result from excited state isomerization as related families of solutes are known to incorporate multiple rotamer and twisted conformations of the aromatic rings.[190-191] Furthermore, thienopyrimidines are known to aggregate in solution leading to a phenomenon described as aggregate induced emission.[192]

While our results cannot identify specific conformations, and the corresponding amplitudes associated with this long lifetime are very small, the observed behavior *is* consistent with compounds **2** and **3** aggregating through some sort of lipid-membrane assisted mechanism. Evidence supporting this hypothesis comes in part from thienopyrimidines known tendency to aggregate in solution,[192] *and* in part from our observation that this long lifetime (that would coincide with significant enhancement in emission intensity from solute aggregate formation) becomes statistically insignificant at higher temperatures where thermal energy would be expected to keep aggregates from forming.

Overall, the fluorescence lifetimes obtained from the TCSPC studies reported herein indicate that none of the studied thienopyrimidines **1**–**3** were found to accumulate in measurable amounts in the DPPC vesicles. These results suggest that membrane partitioning is not the most important factor in determining the activity of the thienopyrimidines against Mtb. This insight suggests that the IC_{50} values of compounds **1**–**3** likely correlate to specific binding mechanisms of cyt-*bd* rather than to differences in concentrations in biological membranes due to differences in bioaccumulation.

Conclusion

Time-resolved fluorescence spectroscopy was employed to study the membrane affinity of three thieno[3,2-*d*]pyrimidin-4-amines compounds all having a phenethylamine substituent attached to the same heterocyclic core. Compounds **1**–**3** differ only in the substituent at the para-position on their phenethyl group. It was hypothesized that the compounds' membrane affinities would correlate with their activity as measured by their IC_{50} values. Therefore, if a compound displays significant IC_{50} values for intended target proteins, those same compounds are expected to display appreciable partitioning behavior into DPPC lipid membranes. All three thienopyrimidine compounds displayed log *P* values indicating a strong membrane preference, with log *P* values of 4.0, 4.5, and 5.9 for **1**, **2**, and **3**, respectively. Compound **3** displayed the most promising IC_{50}, has the highest log *P* value, and was hypothesized to show largest partitioning behavior.

Results showed that Compound **1**, when introduced into a lipid bilayer vesicle, did not show indication of partitioning behavior; the measured lifetimes corresponded to those of **1** in bulk carbonate buffer. On the other hand, upon integration into a lipid bilayer vesicle solution, compound **2** displayed four unique lifetimes. The first two lifetimes were that of **2** in bulk carbonate buffer. The third lifetime is suggestive of an alternate non-radiative decay pathway induced and stabilized by lipid bilayer vesicles. The fourth lifetime of **2** in lipid vesicles was predicted to be that of **2** in a conformationally restricted environment, enhancing its non-radiative decay pathway and resulting in an extremely short radiative decay. Compound **3** displayed three lifetimes

when integrated into a lipid vesicle solution. The first two lifetimes are suggestive of **3** that remains in bulk carbonate buffer. The third lifetime has a very small contribution to the time resolved emission and is not considered to be significant. Overall, the results presented here argue against a hypothesis that correlates membrane affinity with a solute's toxicological efficacy, and instead indicate that differences in activity for the studied thienopyrimidines should be attributed to differences in direct association with their target membrane proteins rather than to changes in membrane uptake and transport. Moreover, the studies reported here describe methodology that should prove useful for predicting the activity of compounds in cases where membrane uptake (rather than receptor binding) is the limiting factor for activity.

CHAPTER SIX

QUANTITATIVE MEMBRANE PARTITIONING STUDIES OF DICAMBA

Katelyn M. Duncan, Elise Conter, Robert A. Walker

Introduction

An organism's uptake of synthetic organic solutes from the environment can be quantified by the bioaccumulation, bioconcentration, and biomagnification factors. Each factor compares the concentration of the solute within the organism to the concentration of the solute at the source of exposure.[7] The bioaccumulation factor (BAF) compares the concentration of the solute within the organism to any environmental source; including dietary uptake, inhalation, metabolic transformation, growth dilution, and excretion.[7] The bioconcentration factor (BCF) only compares the concentration of the solute within the organism to the concentration of the solute in the water alone and is absorbed through respiratory and dermal surfaces of aquatic species excluding the organism's diet.[7, 10] The last factor, biomagnification (BMF), is a food chain description that only analyzes the concentration of the solute within the organism with respect to its food source. BAF and BCF are more commonly used in literature to describe solute absorption by an organism from the environment. The water-octanol partitioning coefficient (log P) is the primary property used to model and predict BCF and BAF values.[6, 193] As a result, a solute's log P value assumes great importance when developing and determining exposure estimates and making risk assessments for potentially harmful agents.

The Environmental Protection Agency (EPA) is the leading regulatory body for evaluating the environmental fate of pesticides and herbicides.[98, 194-195] A solute's environmental fate is predicted based on solute properties including aqueous solubility, vapor pressure, partitioning coefficients, and half-lives.[196] While prediction techniques are useful, they fail to describe the specific chemical interactions that occur when a solute bioconcentrates within a biological membrane. Work described in this chapter used fluorescence spectroscopy and differential scanning calorimetry to study Dicamba, an herbicide commonly found in Montana ground waters. Experiments sought to quantify the specific chemical interactions that occur when Dicamba was introduced to a model biological membrane. In selecting Dicamba, we ensured that this herbicide met the search criteria that included water solubility as well as an appropriate log P value ($0 < \log P < 5$) indicating membrane affinity. Dicamba is also naturally fluorescent so that sensitive time-resolved emission spectroscopy can characterize changes in the solute's local solvation environment.

Dicamba is an auxinic herbicide, or a growth regulator, that increases the growth of the plant until it outgrows its nutrients and dies.[197-198] Dicamba is commonly used to control annual and perennial broadleaf weeds, crops, and grass lands.[197-198] In ambient conditions, Dicamba is volatile on plant surfaces and will be transported by wind to other farm fields where the herbicide is not intended for use.[197] This high volatility of Dicamba has resulted in the creation of Dicamba-resistant plants as well as millions of dollars in lawsuits.[199-200] The EPA and world health organization have classified Dicamba as noncarcinogenic to humans and set regulatory daily intake for drinking water.[197, 201] The solubility of Dicamba in water is very high at 720 g/L, and Dicamba has been found to remain in waterways rather than interact with the soil.[198] A recent study found that in Billings, Montana, 3% of surface

waters have measurable amounts of Dicamba, presumably from application of this herbicide on corn crops.[202] Dicamba has also been found in 0.9% of well waters sampled across Montana.[203]

Dicamba is naturally fluorescent with excitation and emission wavelengths in pH 7 buffer of 270 nm and 415 nm, respectively. Dicamba has a strong electron withdrawing group as well as a strong electron donating group, in the 1 and 2 positions of the ring, respectively, allowing for stabilization upon excitation in polar solvents. With a pKa of 1.97, Dicamba is deprotonated in most environmental waters and commonly used in the salt form (Figure 6.1).[204] Dicamba has a Log P value of 2.6 (ChemDraw Prime 19.0) indicating that it should partition into biological membranes.

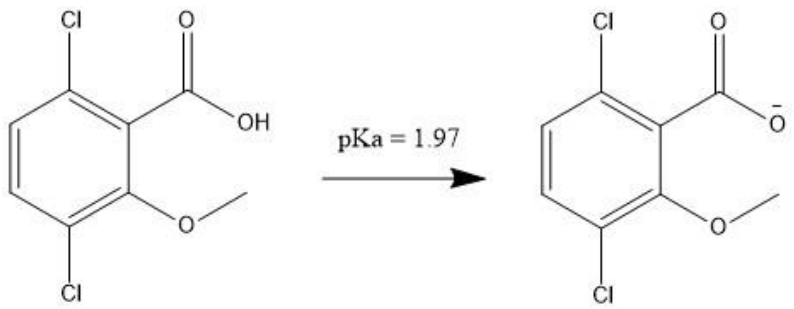

Figure 6.1. Chemical structure of Dicamba when protonated (left) and deprotonated (right). The pKa of Dicamba is 1.97.[204]

Based on studies described in Chapters 2-4 of Coumarin 15X and L-Phenylalanine, Dicamba displays all the necessary properties that predict a strong membrane affinity. Additionally, when the membrane is in the liquid-crystalline phase and water is integrated within the membrane, the partitioning behavior of Dicamba is predicted to increase due to the large solubility of Dicamba in water.

Results and Discussion

The same experimental methodologies described in Chapters 2-5 were used for the analysis of Dicamba in bulk solvents and in DPPC lipid vesicles. However, a more extensive examination into the steady-state photophysical behavior was carried out prior to time-resolved fluorescence analysis of Dicamba in bulk solvents. Then, time-resolved fluorescence analyzed Dicamba introduced to a DPPC lipid vesicle solution at two different Dicamba concentrations. Finally, differential scanning calorimetry (DSC) was used to understand the effect of Dicamba on the lipid bilayer. This work is preliminary in its findings; however, the results indicate unique photophysical behaviors that depend on the local solvation environment. Furthermore, the unexpected changes in data are suspected to be due to Dicamba degradation in an aqueous solution.

In the sections below, the fluorescence behavior of Dicamba was investigated in in each of the four main bulk solvents (carbonate buffer, methanol, acetonitrile, and cyclohexane) with the addition of Millipore (unbuffered) and a pH 1.5 Millipore solution (adjusted with HCl). Millipore was added to the list of bulk solvents for comparison to the buffer fluorescence behavior. The addition of pH 1.5 Millipore was done to understand the effect of protonating the carboxylic acid (pKa = 1.97) on Dicamba's fluorescence behavior. The steady-state fluorescence behavior of Dicamba can be seen in Figure 6.2 and summarized in Table 6.1.

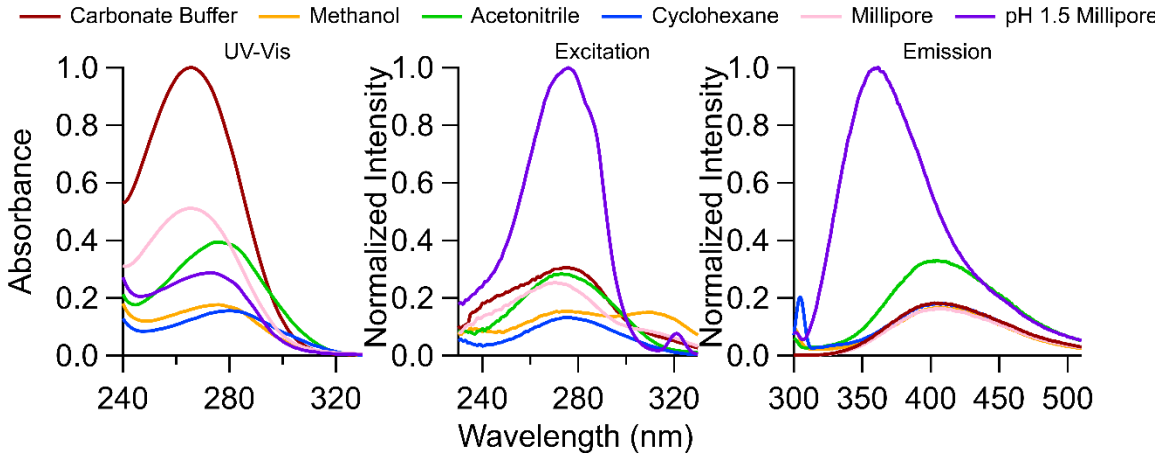

Figure 6.2. Normalized fluorescence behavior of 1-day old 100 µM Dicamba in each of the bulk solvents. UV-Vis absorbance (left), excitation spectra (middle), and the emission spectra (right). Excitation spectrum was measured by collecting emission at 405 nm. Emission spectrum was measured by exciting at 275 nm.

Table 6.1. Fluorescence properties of Dicamba in each of the bulk solvents at 20 °C.

solvent	λ_{abs} (nm)	λ_{ex} (nm)	λ_{em} (nm)
Carbonate Buffer	266	279/315	405
Methanol	269	277/309	406
Acetonitrile	267	273	402
Cyclohexane	277	276	405
Millipore	264	270/310	406
pH 1.5 Millipore	264	276	362

Excitation Behaviors

The absorbance and excitation behaviors of Dicamba in polar protic solvents differ the behavior seen in the other solvents (Figure 6.2). The UV-Vis absorbance displays a single absorbance peak at ~275 nm. The excitation spectra, however, displays two excitation peaks, one at 275 nm and one at 310 nm that changes depending on the concentration and local solvation environment of Dicamba. This dual excitation peak can be seen more clearly in Figure 6.3 with the separation of solvents by number of peaks.

Interestingly, the second emission peak at 310 nm only occurs in polar protic solvents. In a nonpolar solvent, polar aprotic solvent, and when fully protonated, only a single excitation peak occurs.

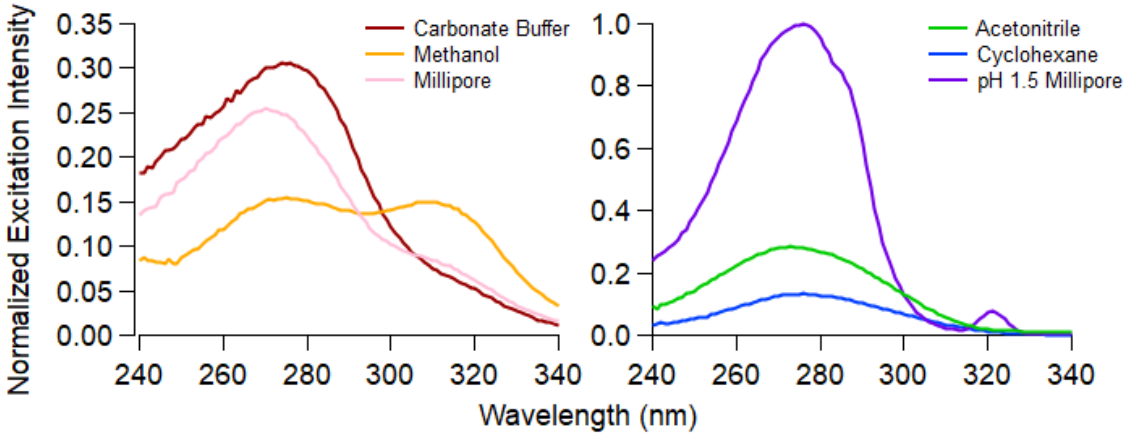

Figure 6.3. Excitation spectra of 1-day old 100 µM Dicamba in all bulk solvents. Solvents displaying dual excitation peaks (left) and solvents displaying a single excitation peak (right).

The appearance of dual excitation peaks is evident in solutions of Dicamba in carbonate buffer and Millipore and more prominent in methanol. To evaluate if the appearance of a 310 nm peak was concentration dependent, an excitation spectrum was taken for a series of dilutions of Dicamba in bulk carbonate buffer from 10 mM to 1 µM (Figure 6.4).

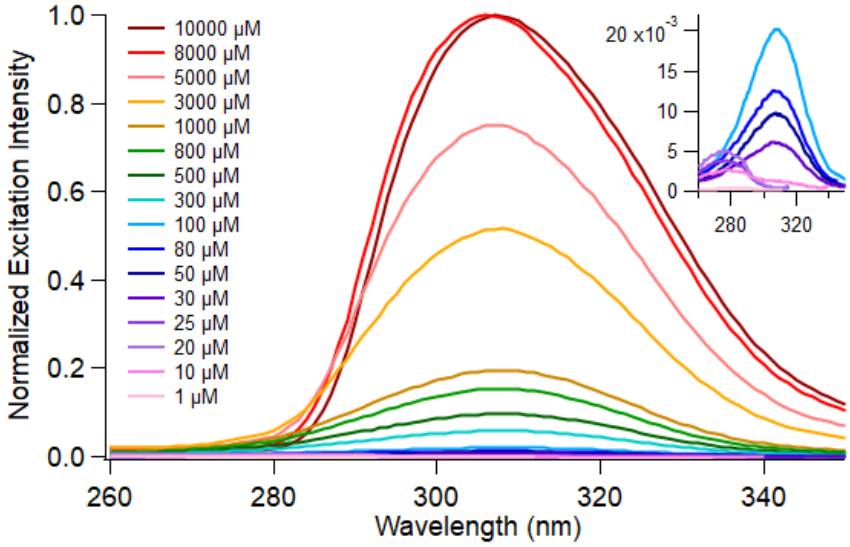

Figure 6.4. Excitation spectrum of 2-day old Dicamba in carbonate buffer from 10 mM to 1 µM. Concentrations of 100 µM to 1 µM are enlarged in top right corner for ease of viewing. Excitation spectra were measured by collecting emission at 400 nm.

At high Dicamba concentrations the major excitation peak is at 310 nm (Figure 6.4) and as concentrations decreases, the excitation peak shifts to a lower wavelength of ~280 nm. Interestingly, a single excitation peak was measured throughout the entire experimental procedure differing from what was seen in the initial bulk solvent excitation spectrum (Figure 6.3). The 275 nm peak is predicted to be the main excitation wavelength due to its consistency between the absorbance and excitation spectra. The 310 nm excitation peak is hypothesized to be the result of either a dimerization or degradation product that is influenced by the polar protic local solvation environment.

Emission Behaviors

In organic solvents, the emission peak was centered at 405 nm for all solvents and changed very little with regards to solvent polarity or hydrogen bonding availability (Figure 6.3). However, given Dicamba's unusual concentration dependence seen in the

excitation spectrum, the emission behavior of Dicamba in carbonate buffer solutions were also measured as a function of concentration (Figure 6.5).

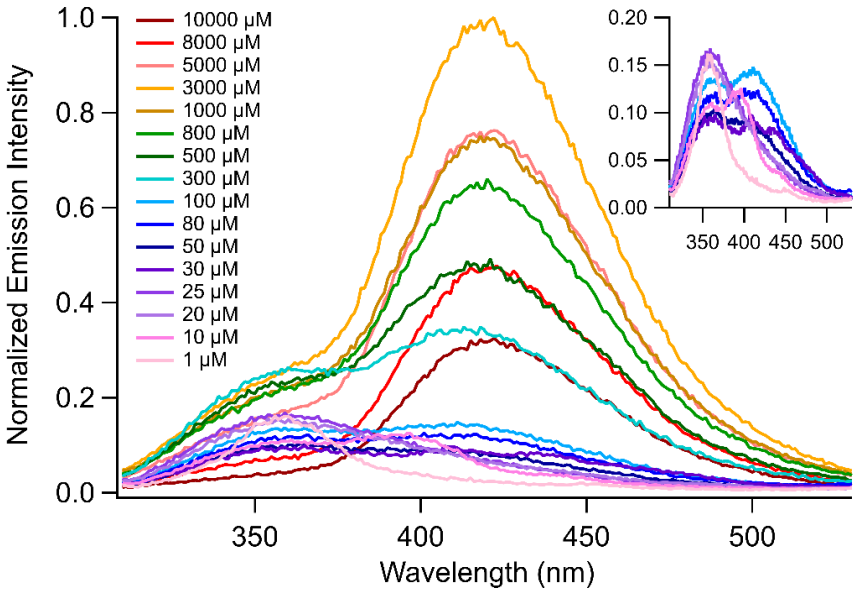

Figure 6.5. Emission spectrum of 2-day old Dicamba in carbonate buffer from 10 mM to 1 µM. Emission behavior was measured by exciting the solution at 270 nm. Concentrations of 100 µM to 1 µM are enlarged in the top right corner for ease of viewing.

The emission behavior of Dicamba in carbonate buffer displays two emission peaks (Figure 6.5). At high concentrations (10 mM), the major emission peak is centered at 420 nm and a minor peak at 340 nm. As concentration decreases, the 420 nm peak decreases significantly in intensity and the major emission peak switches to 340 nm. The appearance of a second peak at 340 nm is inconsistent with the fluorescence behavior reported in Figure 6.2. After further investigation, the appearance of the 340 nm peak was discovered to occur 2-days after the solution was made. The change in emission behavior between Figures 6.2 and 6.5 were attributed to either the dimerization or degradation of Dicamba in a carbonate buffer solution. To determine if the change in emission behavior

was due to degradation or dimerization, an emission spectrum was taken of 100, 10, and 1 µM Dicamba in carbonate buffer over 30 hours to quantify the time at which the second emission peak developed (Figure 6.6).

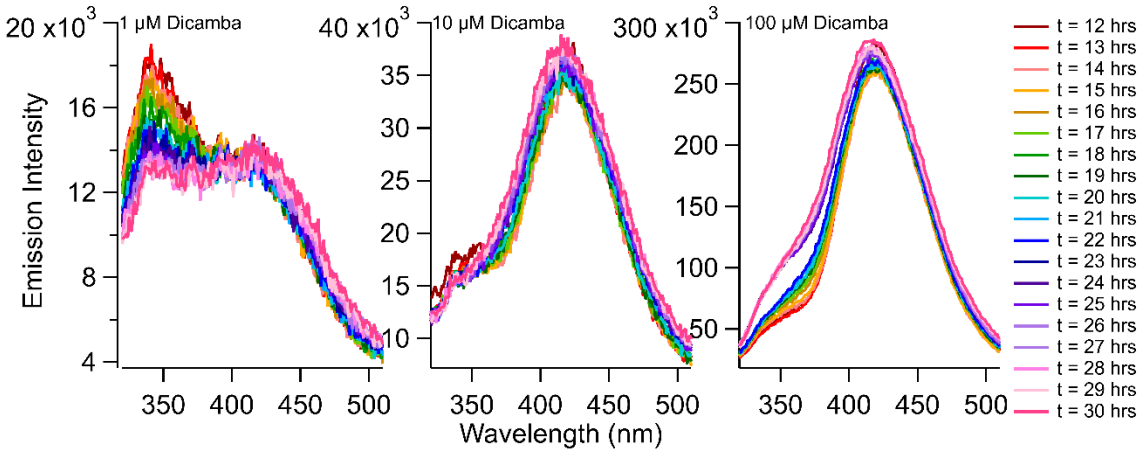

Figure 6.6. Emission spectra of 1 µM (left), 10 µM (middle), and 100 µM (right) Dicamba in carbonate buffer over 30 hours.

The emission behavior of 1 µM Dicamba in bulk carbonate buffer displayed the largest change over 30 hours (Figure 6.6). Specifically, the 340 nm emission peak intensity decreased over 30 hours while the 420 nm emission peak intensity remained the same. The 10 µM Dicamba displayed no real change in peak intensity over 30 hours for either the 340 nm or the 420 nm peak. The emission behavior of 100 µM Dicamba displayed a large drop in the 340 nm peak intensity at 22 hours with no real change in peak intensity at 420 nm.

Originally, the goal of the time study was to quantify when the 340 nm emission peak first became visible to assess if the 340 nm and 420 nm emission intensities were anticorrelated. However, the results displayed in Figure 6.6 showed only a decrease in peak intensity at 340 nm over time. Due to an observed decrease in peak intensity,

photodegradation is predicted to be responsible for the change in emission behavior of Dicamba and not dimerization. Current work in collaboration with Dr. Sharon Neufeldt and graduate student Grace Ibsen is attempting to identify degradation products of Dicamba.

Time-Resolved Fluorescence Spectroscopy

The same bulk solvents used in the steady-state fluorescence measurements were also used in time-resolved fluorescence measurements. The TCSPC fluorescence decay and corresponding calculated lifetimes of Dicamba in each of the bulk solvents can be found in Figure 6.7 and Table 6.2, respectively.

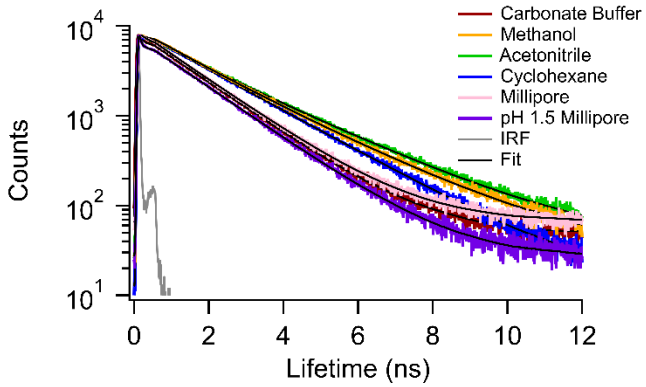

Figure 6.7. TCSPC spectra of 100 µM Dicamba in each of the bulk solvents at 20 °C. The results from fitting these emission traces to Equation 1.5 are reported in Table 6.2. The gray trace is the instrument response function (IRF).

Table 6.2. Fluorescence lifetimes (in ns) of 100 µM Dicamba in each of the bulk solvents measured at 20 °C. Uncertainties in fluorescence lifetimes are ± 0.2 ns.

solvent	τ_f
Carbonate Buffer	1.49
Methanol	1.90
Acetonitrile	1.98
Cyclohexane	1.86
Millipore	1.49
pH 1.5 Millipore	1.35

A single fluorescence lifetime was measured for Dicamba in each of the bulk solvents. All organic solvents (methanol, acetonitrile, and cyclohexane) display an indistinguishable fluorescence lifetime of ~1.9 ns. However, a distinguishable lifetime of 1.5 ns was measured for Dicamba in aqueous solutions (carbonate buffer and Millipore). The measurable differences in the fluorescence lifetimes between Dicamba in organic solvents and aqueous solvents allow time-resolved fluorescence to be used to assess if the solute will enter the membrane or remain in aqueous solution. However, the uniform lifetimes of Dicamba in all organic bulk solvents display a limitation of this technique in quantifying solvation specific details about a solute's partitioning behavior.

Concentration played a significant role in steady-state fluorescence behavior; therefore, a similar approach was taken with time-resolved fluorescence. The partitioning behavior of both 100 µM and 24 µM Dicamba in DPPC lipid vesicle solutions was studied. The time-resolved fluorescence behavior of 100 µM Dicamba in a DPPC lipid vesicle solution can be seen in Figure 6.8 with the corresponding calculated fluorescence lifetimes and amplitudes reported in Table 6.3.

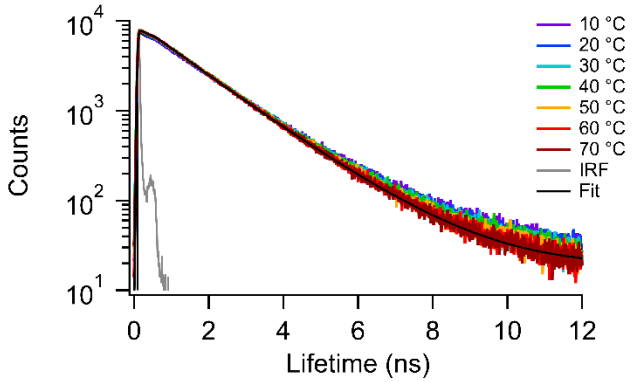

Figure 6.8. TCSPC spectra of 100 µM Dicamba in DPPC vesicles as a function of temperature. Results from fitting these emission traces to Equation are 1.5 are reported in Table 6.3. the gray trace is the instrument response function (IRF).

Table 6.3. Fluorescence lifetimes (in ns) and amplitudes (in parentheses) of Dicamba in DPPC vesicles from 10 to 70 °C and back down to 10 °C. Uncertainties in lifetimes are ± 0.2 ns; uncertainties in amplitudes are ± 0.04.

temp. (°C)	**100 µM Dicamba in DPPC** τ_1 (A_1)	τ_2 (A_2)
10	1.03 (0.48)	2.07 (0.52)
20	1.04 (0.48)	2.07 (0.52)
30	1.07 (0.52)	2.17 (0.48)
40	1.06 (0.50)	2.01 (0.50)
50	1.07 (0.49)	1.96 (0.51)
60	1.14 (0.58)	1.96 (0.42)
70	1.22 (0.57)	1.73 (0.43)
60	1.15 (0.58)	1.96 (0.42)
50	1.16 (0.61)	2.02 (0.39)
40	1.16 (0.62)	2.02 (0.38)
30	1.00 (0.43)	1.95 (0.57)
20	1.05 (0.52)	2.00 (0.48)
10	0.90 (0.40)	1.95 (0.60)

The integration of 100 µM Dicamba into a DPPC lipid vesicle solution resulted in two fluorescence lifetimes having equivalent amplitude. The first lifetime (1.1 ns) is measurably shorter than that of Dicamba in bulk carbonate buffer (1.5 ns) and the second lifetime matches that of Dicamba in an organic solvent (~2 ns). In effort to achieve a lifetime of Dicamba in bulk carbonate buffer, the parameters were restricted to a single lifetime of 1.5 ns (that of Dicamba in bulk carbonate buffer and halfway between the two reported lifetimes); however, doing so led to unacceptably poor fits. A visual representation of 100 µM Dicamba in DPPC vesicles as a function of temperature can be seen in Figure 6.9.

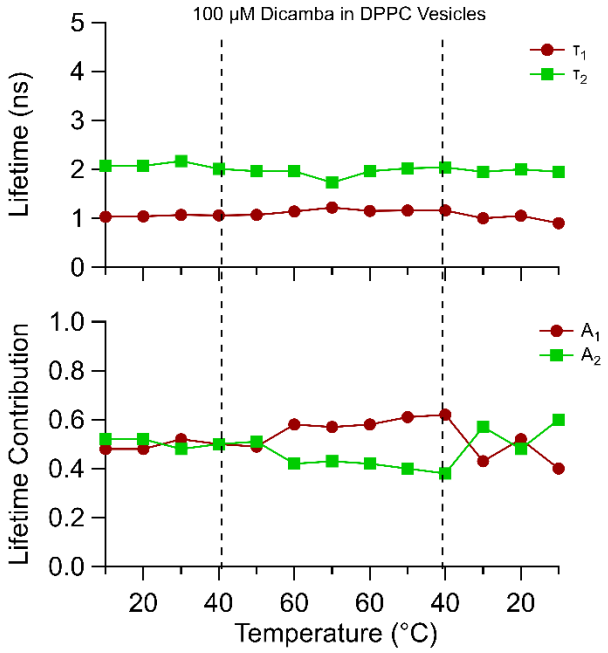

Figure 6.9. Fluorescence lifetimes (top) and corresponding amplitudes (bottom) of 100 µM Dicamba in DPPC lipid vesicles. The dashed vertical line is the $T_{gel\text{-}lc}$ of the DPPC bilayer at 40.4 °C.

There are two observations to note in Figure 6.9: (1) neither lifetime reported in DPPC vesicle solutions matches the 1.5 ns lifetime found in bulk carbonate buffer, and (2) the fluorescence behavior did not change as a function of temperature. The absence of a bulk carbonate buffer lifetime with the integration of Dicamba into DPPC vesicles is unusual as the DPPC vesicles are prepared in a carbonate buffer solution. The first lifetime of 1 ns determined in DPPC vesicles is measurably different (lifetime uncertainty is ± 0.2 ns) than that of 1.5 ns in bulk carbonate buffer. A bulk carbonate buffer fluorescence lifetime in DPPC vesicles is always expected when assigning local solvation environments. Importantly, all fluorescence lifetimes and corresponding amplitudes are unrestricted and independently calculated to achieve a χ^2 between 0.9-1.1. The discrepancy between the first lifetime reported and that of bulk carbonate buffer is

suspected to be a result of the degradation of Dicamba; however, further investigation is required.

The second observation from 100 µM Dicamba in a DPPC vesicle solution is the lack of temperature dependence of the fluorescence lifetimes. The fluorescence lifetimes should change as a function of temperature due to fluorescence quenching.[205-206] Uniquely, the steady-state emission behavior of 100 µM Dicamba in DPPC vesicles displays a strong temperature dependence under the same experimental procedures (Figure 6.10). The recovery of the emission peak throughout the temperature cycle implies Dicamba does not experience thermal degradation within the 3-hour timescale of the experiment.

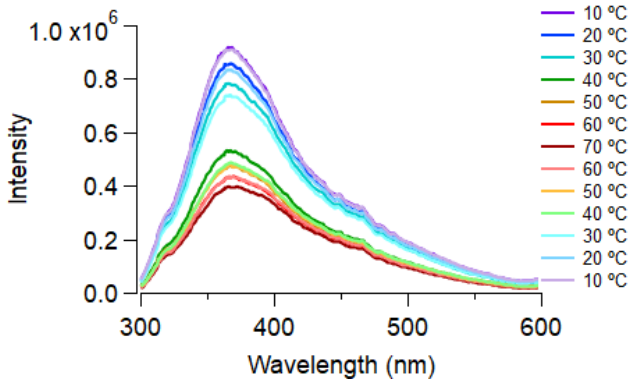

Figure 6.10. Steady-state fluorescence emission spectrum of 100 µM Dicamba in a DPPC vesicle solution measured as a function of temperature. The emission behavior was measured by exciting the solution at 270 nm.

As meantioned previously, Dicamba in a DPPC vesicle solution displayes a 1.1 ns lifetime that is measuably different from the fluorescence lifeitme of Dicamba in a bulk carbonte buffer solution. The discrepency between the liftimes are speculated to be a result of Dicamba degredation. Interestingly, the second lifetime (2 ns) of Dicamba in DPPC vesicle solutions closely matches the lifetime of Dicamba in organic solvents. The

second lifetime is evidence of Dicamba association with the DPPC bilayer vesicle measurable concentrations. However, the polar and nonpolar local solvation environments are indistingishable from one another due to identical lifetimes of Dicamba in all bulk organic solvents.

The steady-state fluroescence behavior of Dicamba displayed a strong dependence on concentration. Therefore, the concentration of Dicamba was decreased to 24 μM and was introduced into DPPC lipid vesicle solutions. The TCSPC fluorescence decay can be found in Figure 6.11 with the corresponding calculated lifetimes found in Table 6.4.

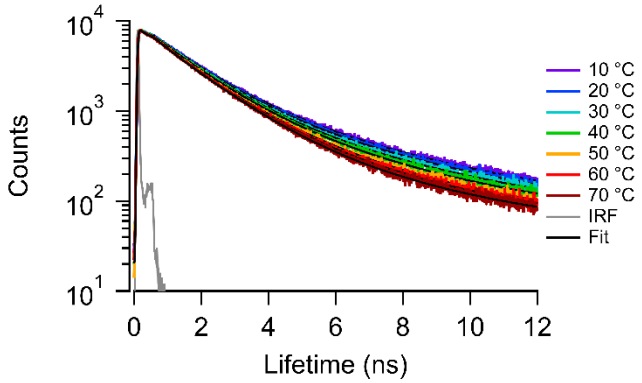

Figure 6.11. TCSPC spectra of 24 μM Dicamba in DPPC as a function of temperature. Results from fitting these emission traces to Equation 1.5 are reported in Table 6.4. The gray trace is the instrument response function (IRF).

Table 6.4. Fluorescence lifetimes (in ns) and amplitudes (in parentheses) of 24 μM Dicamba in DPPC vesicles from 10 to 70 °C and back down to 10 °C. Uncertainties in lifetimes are ± 0.2 ns; uncertainties in amplitudes are ± 0.04.

temp. (°C)	**24 μM Dicamba in DPPC**		
	τ_1 (A_1)	τ_2 (A_2)	τ_3 (A_3)
10	0.54 (0.11)	1.43 (0.74)	4.29 (0.14)
20	0.56 (0.12)	1.42 (0.75)	4.28 (0.13)
30	0.56 (0.13)	1.46 (0.75)	4.17 (0.12)
40	0.53 (0.16)	1.45 (0.73)	4.10 (0.11)
50	0.49 (0.18)	1.45 (0.72)	3.95 (0.10)
60	0.40 (0.15)	1.44 (0.77)	4.09 (0.08)
70	0.31 (0.12)	1.41 (0.81)	4.11 (0.08)
60	0.33 (0.12)	1.42 (0.79)	4.03 (0.09)
50	0.35 (0.12)	1.41 (0.79)	4.07 (0.09)
40	0.32 (0.11)	1.42 (0.79)	3.97 (4.10)
30	0.41 (0.11)	1.43 (0.78)	3.95 (0.11)
20	0.38 (0.11)	1.42 (0.77)	3.95 (0.13)
10	0.41 (0.12)	1.43 (0.75)	3.88 (0.14)

The first observation to note from Table 6.4 is the presence of 3 fluorescence lifetimes with 24 μM Dicamba in DPPC vesicles in comparison to the two lifetimes calculated with 100 μM Dicamba in DPPC vesicles. The only difference between the two systems is a 4-fold decrease in the concentration of Dicamba. As seen in Table 6.4, the first lifetime (~0.5 ns) and third lifetime (~4 ns) do not match anything found in bulk solvents. However, the second lifetime (1.5 ns) does match that of Dicamba in bulk carbonate buffer. A visual representation of the fluorescence lifeitmes and corresponding lifetime contributions are shown in Figure 6.12.

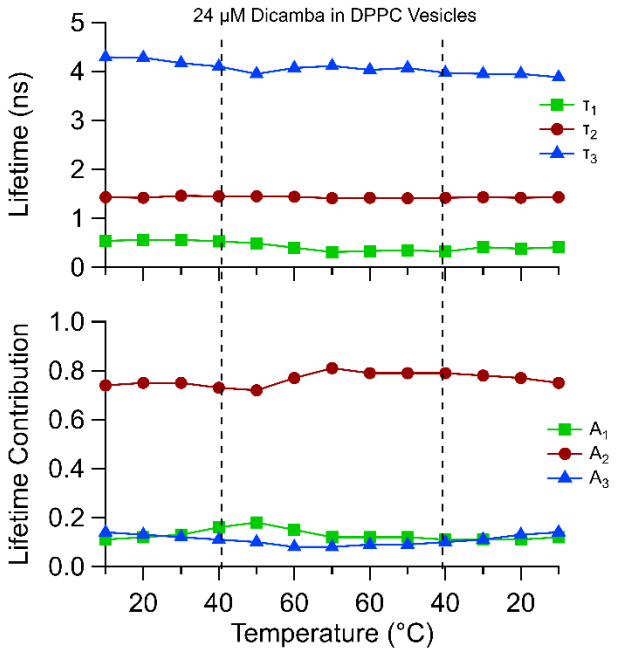

Figure 6.12. Fluorescence lifetimes (top) and corresponding amplitudes (bottom) of 24 µM Dicamba in DPPC lipid vesicles. The dashed vertical line is the $T_{gel\text{-}lc}$ of the DPPC bilayer at 40.4 °C.

Similar to the behavior found in 100 µM Dicamba in DPPC vesicles, 24 µM Dicamba in DPPC vesicles does not display the expected decrease in fluorescence lifetime as a function of temperature. The second lifetime, assigned to Dicamba in bulk carbonate buffer, accounts for ~75% of the overall fluorescence behavior at all temperatures sampled. Both the short (~0.5 ns) lifetime and long (~4 ns) lifetime each account for ~12% of the overall emission intensity. Further investigation is required to assign a local solvation environment to the first and third lifetime of Dicamba in DPPC vesicles. The appearance of three lifetimes when 24 µM Dicamba was a part of the vesicle containing solution suggests Dicamba association with the lipid bilayer. If there were no association, the fluorescence behavior would resemble that of Dicamba in bulk carbonate buffer. Additionally, the fluorescence behavior determined with 24 µM

Dicamba in DPPC vesicles differs from that of 100 μM Dicamba further displaying the strong concentration dependence of Dicamba on fluorescence behavior.

The fluorescence behavior of Dicamba in DPPC vesicles does not readily lend itself to a simple explanation. Previous studies using this technique have highlighted the possibilities that fluorescence behavior may not be quantifiable by bulk solvent behavior. The C15X study described in Chapter 2 highlighted the strengths of using TCSPC to measure partitioning behaviors of solutes with well-defined solvatochromic fluorescence behavior. The fluorescence lifetimes of C151.5 and C152 in a vesicle containing solution directly corresponded to bulk solvent behavior. However, the same approach was taken with the L-Phe study (Chapter 4) and thienopyrimidine study (Chapter 5).

Each study showed that the partitioning behavior of a solute cannot always be predicted by matching the results from lipid vesicle solutions to properties found in bulk solvents. For example, L-Phe displayed a conformationally restricted rotamer lifetime that was only optically visible when water was introduced to the polar headgroup. Additionally, the methyl-substituted thienopyrimidine compound displayed evidence of geometrically restricted local solvation environment that was only assigned after constraining the compound's conformational freedom in a frozen solvent cage. Therefore, we assume the unassigned lifetimes of both 100 μM and 24 μM Dicamba in DPPC lipid vesicles are evidence of membrane association, but further experiments are required to identify the specific membrane interactions.

Differential Scanning Calorimetry (DSC)

To understand the effect of Dicamba association with DPPC vesicles has on the lipid bilayer itself, specifically, the $T_{gel\text{-}lc}$ of DPPC, Differential Scanning Calorimetry (DSC) was employed. The same concentrations of Dicamba used in the fluorescence time-study (100, 10, and 1 µM) were included in a 20 mM DPPC lipid vesicle solution and the resulting peak transitions are shown in Figure 6.13.

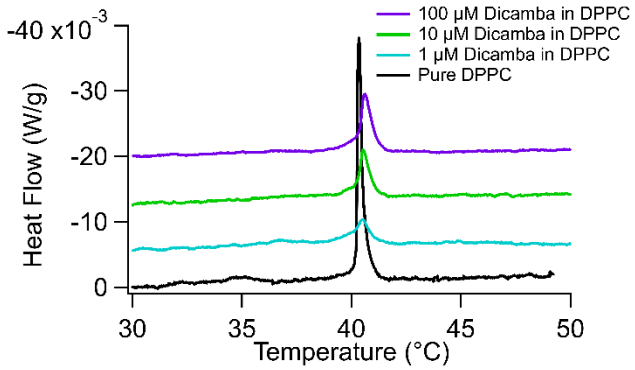

Figure 6.13. DSC spectra of pure DPPC vesicle solutions and DPPC vesicle solutions containing 100, 10, and 1 µM Dicamba. All transitions are endothermic and offset for ease of viewing.

The $T_{gel\text{-}lc}$ of pure DPPC is 40.4 °C and the $T_{gel\text{-}lc}$ of DPPC with the addition of 100 µM, 10 µM, and 1 µM Dicamba are 40.63 °C, 40.54 °C, and 40.50 °C, respectively (Figure 6.13). The slight increase in the DPPC $T_{gel\text{-}lc}$ implies that Dicamba is in the bilayer, increasing the heat required to induce the transition.[97] The higher concentrations of Dicamba led to a larger stabilization effect. Additionally, the integration of Dicamba to the lipid vesicle displayed a decrease in peak intensity and broadening of the peak indicating a decrease in the amount of lipid molecules participating cooperatively in the transition.[94] Together, the peak shift to higher temperatures, broadening of the peak, and decrease in intensity further indicates Dicamba association with the DPPC lipid bilayer.

However, the association of Dicamba with the DPPC lipid membrane is predicted to be weak as these effects are small and the cohesive forces of the lipid bilayer remain.

Conclusion

The goal of this work was to identify *if* the herbicide Dicamba associates with a model biological membrane. The steady-state and time-resolved fluorescence behavior in combination with the DSC results displayed evidence of Dicamba association with the DPPC lipid bilayer. Steady-state fluorescence spectroscopy highlighted the unique fluorescence behavior of Dicamba with a strong dependence on concentration and age of solution. The time-resolved fluorescence behavior of 100 μM Dicamba in DPPC lipid vesicle solutions exhibited a fluorescence lifetime that corresponds to Dicamba in organic solvents. Decreasing the concentration of Dicamba in a DPPC vesicle solution to 24 μM resulted in three fluorescence lifetimes further indicating a strong concentration dependence. The DSC results of Dicamba in a DPPC vesicle solution showed an increase in the $T_{gel\text{-}lc}$ indicating a stabilization effect of Dicamba on the membrane.

While there are still many questions left unanswered, Dicamba was does appear to associate with the DPPC lipid bilayer vesicles. Degradation is currently hypothesized to be the cause for the varying fluorescence behavior in bulk solvents and in vesicle containing solutions. Currently, the experimental focus is on identifying the specific degradation products of Dicamba with exposure to light. Once known, further experimental procedures can be identified leading to a full understanding of the partitioning behavior of Dicamba into model biological membranes.

CHAPTER SEVEN

CONCLUSIONS AND FUTURE DIRECTIONS

Summary

The experiments described in this dissertation analyzed the specific chemical interactions that occur when a solute is introduced to a model biological membrane. Time-resolved and steady-state fluorescence spectroscopy in combination with differential scanning calorimetry was employed to answer the specific chemical questions that arise when a solute is introduced to a biological membrane:

1) Does the solute partition into the membrane?
2) *Where* does the solute partition *within* the membrane?
3) *How much* of the solute concentrates within that local solvation environment?
4) Does solute integration alter membrane properties?

The partitioning behavior of model solutes, amino acids, potential pharmaceutical candidates, and herbicides were quantitatively characterized to understand the specific chemical interactions that are involved in solute partitioning into phosphocholine lipid bilayers. The photophysical behaviors of each of these compounds were characterized in a variety of bulk solvents that were chosen to mimic the various local solvation environments within a lipid vesicle bilayer. Additionally, solute's effect on the lipid membrane transition temperatures were measured using differential scanning calorimetry. Each chapter in this dissertation analyzed either a different class of solutes or increased the chemical complexity in the membrane.

Research presented in Chapter 2 analyzed three model solutes differing only by a methyl-group on the 7-amine. These small structural changes resulted in dramatically different partitioning behaviors. Despite a log P value indicating organic phase solubility, C151 did not partition into the membrane regardless of temperature or bilayer phase. The moderately hydrophobic solute, C151.5, only partitioned into the polar headgroup with small dependences on bilayer phase and temperature. C152, the most hydrophobic of the three, fully partitioned into the membrane with a pronounced dependence on bilayer phase and temperature. Concluding that small structural changes in the solute significantly change the solutes membrane affinity in a way not predicted by the log P value.

Chapter 3 describes work done in effort to create a more complex, and representative, description of biological membranes with the addition of two amino acids to the lipid bilayer. L-Phenylalanine (L-Phe) and N-Acetyl-Tryptophan (NAT) were integrated, separately, into the lipid bilayer and the change in partitioning behavior of C151 and C152 was studied. Literature has reported L-Phe increased membrane permeability making it an optimal candidate for this study.[91] The partitioning behavior of C151 did not change with the addition of L-Phe. C151 remained in buffer solution indicating L-Phe only increases membrane permeability if the solute has an initial propensity to partition. The addition of L-Phe to the bilayer inhibited C152 from accumulating in the polar headgroup and drove C152 further into the nonpolar tails when the membrane was in the gel-phase. However, L-Phe did not have a large impact on the partitioning behavior of C152 once the membrane transitioned into the liquid-crystalline

phase. The other amino acid, NAT, was predicted to create a NAT/DPPC complex with the bilayer creating an alternate binding site for C151 and C152 to interact with. This alternate binding site was speculated to be the cause of a second lifetime found in C151 and NAT in DPPC vesicle solution. The NAT/DPPC complex was predicted to occur with C152 as well; however, was less evident due to the large membrane affinity of C152.

Chapter 4 followed up Chapter 3 to confirm the hypotheses formed and quantify the partitioning behavior of L-Phe alone. Results showed that in the presence of a lipid vesicle system, 70% of L-Phenylalanine remained in bulk buffer and 30% displayed a 1.8 ns lifetime that does not match any behavior observed in bulk solvents. This second lifetime was assigned to L-Phe integration into the membrane inducing a restriction of any rotational isomerization. Literature reported an identical fluorescence lifetime attributed to the restriction of a specific rotamer conformation in a peptide containing L-Phenylalanine.[127] The appearance of the second lifetime occurs near the $T_{gel\text{-}lc}$ of the DPPC bilayer and is attributed to bilayer hydration. The polar headgroup is intrinsically polar aprotic and the integration of water into the bilayer creates a polar protic environment. This switch in the local solation environment of the polar headgroup allows L-Phenylalanine to become optically observable due to a 5.5-fold increase in quantum yield between a polar aprotic and polar protic environment. To test generalizability of this finding, the appearance of the rotamer lifetime at/around the $T_{gel\text{-}lc}$ was measured with three other lipid vesicle systems. This behavior was general. The appearance of the rotamer lifetime occurred at or around the lipid $T_{gel\text{-}lc}$ in DSPC and DMPC lipid vesicles.

There was no detectable affinity of L-Phe with DLPC vesicles which could be due to a switch in non-radiative decay pathways at low temperatures.[29] Supporting our hypothesis from Chapter 3, L-Phenylalanine does integrate into the polar headgroup of the lipid bilayer.

Chapter 5 described work done in collaboration with Dr. Mary Cloninger and Sarah Hopfner. This study analyzed the partitioning tendencies, or lack thereof, of three potential tuberculosis drug candidates into a DPPC lipid bilayer. Compound **1**, despite a log P value of 4.0 showed no affinity for the lipid bilayer and was predicted to remain in bulk buffer. Compound **2** (log P = 4.5) showed the largest membrane interactions with 4 lifetimes in the presence of lipid bilayer vesicles. The first two lifetimes matched compound **2** in bulk carbonate buffer and the third lifetime was predicted to be an alternate non-radiative decay pathway induced and stabilized by the lipid bilayer vesicle. The fourth lifetime is predicted to be **2** in a conformationally restricted local solvation environment that enhances its non-radiative decay pathway resulting in an extremely short fluorescence lifetime. Compound **3** was expected to have the greatest membrane affinity (log P = 5.9), but instead displayed two lifetimes that are congruent with **3** remaining in bulk buffer and a third lifetime (with a very small amplitude) that is predicted to be a similar alternate non-radiative decay pathway as found in **2**. Compound **3** displayed the highest activity levels in comparison to **1** and **2**, which is contrary to the time-resolved results indicating **2** having the larger membrane affinity. Originally, our hypothesis predicted drug activity correlates with membrane bioaccumulation. However,

our hypothesis was disproved. These results imply that compounds **1**, **2**, and **3** interact through direct protein-target specificity rather than a general membrane affinity.

Chapter 6 describes the ongoing work to quantify membrane partitioning behaviors of the herbicide Dicamba in DPPC lipid bilayers. The steady-state and time-resolved fluorescence displayed a strong dependence on concentration and local solvation environment. Two excitation peaks were measured in polar protic solvents and only a single excitation peak in nonpolar and polar aprotic solvents, as well as when Dicamba is protonated in pH 1.5 Millipore water. Steady-state emission measurements displayed a shift in the main emission peak from 420 nm at high concentrations (10 mM) to 340 nm at low concentrations (1 μM). Dimerization was initially hypothesized to be the result of the switch in emission peaks with a change in concentration. However, emission behavior characterized over 30 hours pointed towards degradation rather than dimerization. Time-resolved fluorescence measurements displayed a change in fluorescence behavior of Dicamba from bulk buffer solution to a vesicle containing solution indicating membrane association. Additionally, a change in the time-resolved fluorescence behavior with a 4-fold decrease in concentration was measured. The initial findings in this work propose that Dicamba begins degrading as soon as it is in solution and current work is being done to quantify the degradation products. While preliminary in its findings, Dicamba shows a strong concentration dependence and membrane affinity due to a change in fluorescence behavior when in a vesicle containing solution.

The work presented here studied diverse classes of solutes and identified specific properties involved in solute-membrane interactions. Intramolecular interactions and

local solvation environments were found to play a large role in solute partitioning into biological membranes. Using the techniques described herein, quantifying *where* the solute partitioned, *how much* of the solute resided within that local solvation environment, and solutes effect on the membrane itself was done with a variety of solutes. These studies were carried out in effort to identify how and under what circumstances the log P scale failed to predict membrane affinity *and* to begin creating the data necessary for the development of more refined descriptions of solute partitioning into biological membranes.

Future Directions

The work presented in chapters 2-6 show that membrane partitioning depends sensitively on nuanced solute structure. Each specific chapter characterized a different chemical interaction that controls solute partitioning behavior. Specifically, local solvation environment, conformational confinement, hydrophobicity, hydrogen bonding capabilities (between the solute-solute and solute-lipid), as well as local charge characteristics on the compound itself all dictated the solute propensity to partition. This research brought to light the unique partitioning behavior of each solute measured that was unable to be predicted by traditional tools, like log P.

The work described in Chapters 3 and 4, studied the effect of amino acids on partitioning and the partitioning behavior of the amino acid itself, revealed interesting research opportunities. The first study would be to analyze and quantify the difference in partitioning behavior between all three aromatic amino acids. Tyrosine (Tyr) and Tryptophan (Trp) alone have been more widely studied in literature; however, their

specific partitioning behavior has not been quantified as was done with Phenylalanine (Phe) in this work. As seen in Figure 7.1, the fluorescence properties of Tyr and Trp are much higher in intensity than those of Phe.

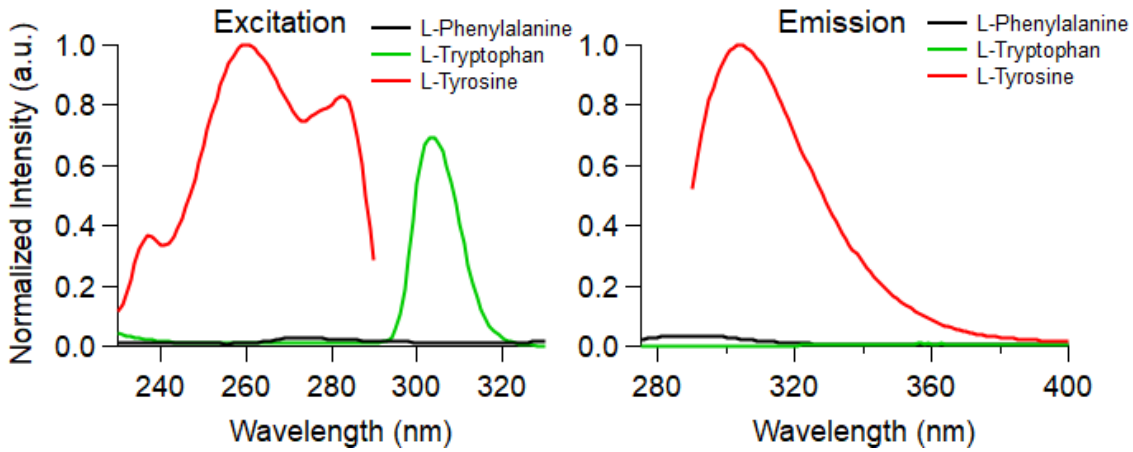

Figure 7.2. Steady-State excitation (left) and emission (right) of Phenylalanine, Tyrosine, and Tryptophan in carbonate buffer.

Literature has shown that the Tyr and Trp have a strong dependence on temperature, but emission peak wavelengths remain unaltered with only a decrease in intensity with temperature.[113] Studies have reported Trp also has a tendency to partition into the organic phase making Trp a good candidate for further analysis.[32] Computational studies have calculated the energy cost for Trp partitioning to be much higher than Phe at the membrane surface but decreases in energy as the solute partitions further into the membrane.[33] Other computational studies have shown Tyr partitioning into the nonpolar region of the membrane unfavorable due to the phenol.[34] Ample amount of literature is available that predict how these amino acids might integrate into lipid membranes;[32-34, 207-208] however, most of these studies use fluorescence probes or study the impact

indirectly. One large benefit to the experimental capabilities described here is the ability to directly analyze the compound as long as they are naturally fluorescent.

Additional experiments would include short chain peptides, either dipeptides or tripeptides. The expansion could begin by altering the aromatic amino acid in question or linking the aromatic amino acids to attempt to quantify the energy transfer to Trp that occurs in proteins. Alternatively, linking a single fluorescent peptide to other (non-fluorescent) peptides having different hydrophobicities might change peptide distribution within a membrane bilayer. This work would deepen our understanding of how peptides and small protein integrate into lipid bilayers and in doing so, create a more quantitative understanding of real biological membranes.

Other Lipid Bilayer Systems

Other prominent lipids in eukaryotic membranes are phosphatidylethanolamines' (PE) and phosphatidylserines (PS). PE lipids are identical to PC lipids with the exception of a primary ammonium functional group. PE lipids have a higher affinity for hydrogen-bonding dramatically changing partitioning behavior of solutes.[33] PS lipids are negatively charged and studies have shown that PS lipids display a strong interaction with positively charged drugs.[209] Additionally, a change in PS lipid chain length is proposed to alter its interactions with cholesterol and proteins.[210] Other experimental avenues to pursue include natural lipids such as egg-PC lipids and other lipid bilayers consisting of other biologically derived content. Egg-PC lipids contain a mixture of PC and PE lipids creating a realistic description of membranes with which synthetic organic solutes can interact with in actual biological lipid bilayers.[33, 211]

Further Analysis of Dicamba and Other Herbicides

The Montana Department of Agriculture (MDA) reports concentrations of herbicides found in groundwaters and surface-waters across the state of Montana.[202-203, 212] For Dicamba, the human health standard reported by the MDA is 200 ppb (~900 nM) in groundwater, 14,000 ppb (63 μM) in fish, and 17,300 ppb (78 μM) in invertebrates. The MDA reports a 3% detection frequency of Dicamba near Billings at a concentration of 2.7 ppb (12.2 nM) in groundwater and only 0.9% detection frequency of 2.7 ppb (12.2 nM) in surface-waters.[202] In the Fairfield bench, Dicamba was detected in 0.44% of all groundwaters sampled at a concentration of 0.2305 ppb (1 nM).[212] In the Milk Watershed, Dicamba was detected in 6.7% of groundwaters sampled at 0.078 ppb (0.35 nM) and in Phillips County in all groundwaters sampled at 0.078 ppb (0.35 nM) concentrations. In well-waters sampled across Montana, Dicamba was detected with 0.9% frequency at concentrations of 0.078 ppb (0.35 nM).[203]

The MDA reports mentioned above display low concentrations and a small number of detections of Dicamba in Montana waterways. The studies reported in this work measured Dicamba in aqueous solution and found a unique fluorescence behavior that is speculated to be due to Dicamba degradation once in solution. The low concentration of Dicamba detected in Montana waterways and the speculated degradation of Dicamba could indicate that either the herbicide degrading once used or Dicamba is degrading once in solution. If Dicamba is operating as intended, the compound degrades quickly and is not in the original form that is looked for when groundwaters are being sampled. However, the herbicide could be degrading once in solution based on the studies reported here. Due to the low concentration of Dicamba reported by the MDA,

further studies of Dicamba partitioning should seek to identify the degradation products analyze the partitioning behavior of the degradation products. Additional studies should include the behavior of Dicamba at concentrations that correspond to those found in agriculture. Namely, the concentration of the detection standard of 200 ppb (~900 nM) as well as the 1 nM and 10 nM concentrations of Dicamba commonly found in Montana waterways. In identifying the behavior of Dicamba at relevant concentrations, a more biologically relevant prediction can be made on the impact Dicamba has on biological membranes.

Further studies analyzing the partitioning behavior of herbicides should focus on other herbicides that are more commonly found in Montana waterways at higher concentrations. Such herbicides are 2,4-D and Bentazon which are found in 100% and 55%, respectively, of groundwaters sampled. Other herbicides would include Glyphosate and Chlorsulfuron which do not have significant detection in Montana waterways; however, display measurable fluorescence properties with excitation wavelengths within the limits of our instrumentation. The steady-state fluorescence behavior of Bentazon was characterized in depth by Rhys Trousdale, a second-year graduate student in the Walker Research Group. The steady-state and time-resolved fluorescence properties of Bentazon in bulk solvents can be seen in Figure 7.2 and the excitation and emission peaks found in Table 7.1.

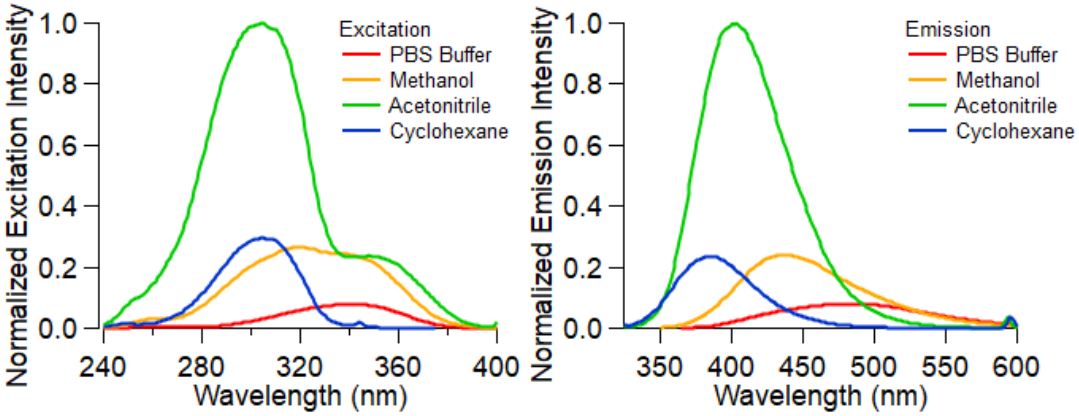

Figure 7.*2*. Excitation spectra (left) and emission spectra (right) of Bentazon in bulk solvents.

Table 7.4. Fluorescence properties of Bentazon in each of the bulk solvents at 20 °C.

solvent	λ_{ex} (nm)	λ_{em} (nm)
PBS Buffer	344	493
Methanol	320/340	436
Acetonitrile	305	401
Cyclohexane	305	387

Figure 7.2 shows that Bentazon has promising solvatochromic behavior in different solvation environments. Bentazon, with a log P value of 2.3, is also commonly found in all ground waters across Montana making it a good candidate for this study.

REFERENCES CITED

1. Chiou, C. T.; Freed, V. H.; Schmedding, D. W.; Kohnert, R. L., Partition-Coefficient and bioaccumulation of Selected Organic Chemicals. *Environ. Sci. Technol.* **1977,** *11* (5), 475-478.

2. Alengebawy, A.; Abdelkhalek, S. T.; Qureshi, S. R.; Wang, M. Q., Heavy Metals and Pesticides Toxicity in Agricultural Soil and Plants: Ecological Risks and Human Health Implications. *Toxics* **2021,** *9* (3).

3. Gupta, N.; Yadav, K. K.; Kumar, V.; Kumar, S.; Chadd, R. P.; Kumar, A., Trace elements in soil-vegetables interface: Translocation, bioaccumulation, toxicity and amelioration - A review. *Sci Total Environ* **2019,** *651* (Pt 2), 2927-2942.

4. Mojiri, A.; Zhou, J. L.; Robinson, B.; Ohashi, A.; Ozaki, N.; Kindaichi, T.; Farraji, H.; Vakili, M., Pesticides in aquatic environments and their removal by adsorption methods. *Chemosphere* **2020,** *253*, 126646.

5. Mrema, E. J.; Rubino, F. M.; Brambilla, G.; Moretto, A.; Tsatsakis, A. M.; Colosio, C., Persistent organochlorinated pesticides and mechanisms of their toxicity. *Toxicology* **2013,** *307*, 74-88.

6. Endo, S.; Escher, B. I.; Goss, K. U., Capacities of membrane lipids to accumulate neutral organic chemicals. *Environ Sci Technol* **2011,** *45* (14), 5912-21.

7. Arnot, J. A.; Gobas, F. A. P. C., A review of bioconcentration factor (BCF) and bioaccumulation factor (BAF) assessments for organic chemicals in aquatic organisms. *Environ. Rev.* **2006,** *14* (4), 257-297.

8. Baur, J. R. B., R.W., Ultraviolet and volatility loss of herbicides. *Arch. Eniron. Contam.* **1974**, 275-288.

9. Cox, C., Dicamba. *Journal of Pesticide Reform* **1994,** *14*, 30-36.

10. Hoffman, D. J. R., Barnett A.; Burton Jr., G. Allen; Cairns Jr., John;, *Handbook of Ecotoxicology*. 2nd Edtion ed.; Lewis Publishers: Boca Raton, 2003.

11. Chiou, C. T. F., Virgil H.; Schmedding, David, W.; Kohnert, Rodger L., Partition Coeffcient and Bioaccumulation of Selected Organic Chemicals. *J. Environ. Sci. Technol.* **1977,** *11*, 475-478.

12. Chamberlain, K. E., Avis A.; Bromilow, Richard H., 1-Octanol/Water Partition Coefficient (K_{ow}) and pK_a for Ionisable Pesticides Measured by a pH-Metric Method. *Pestic. Sci* **1996,** *47*, 265-271.

13. Czub, G. M., Bioaccumulation Potential of Persistent Organic Chemicals in Humans. *Environ. Sci. Technol.* **2004,** *38*, 2406-2412.

14. Leo, A.; Hansch, C.; Elkins, D., Partition coefficients and their uses. *Chem. Rev.* **1971,** *71* (6), 525-616.

15. Pollastri, M. P., Overview on the Rule of Five. *Curr. Protoc. Pharmacol.* **2010,** *Chapter 9*, Unit 9 12.

16. Neely, W. B. B., Gary E., *Environmental Exposure From Chemicals*. CRC PRess: Boca Raton, FL, 2018; Vol. Volume 1, p 254.

17. Lipinski, C. A., Drug-like properties and the causes of poor solubility and poor permeability. *J. Pharmacol. Tox. Met.* **2000,** *44* (1), 235-49.

18. Lipinski, C. A.; Lombardo, F.; Dominy, B. W.; Feeney, P. J., Experimental and computational approaches to estimate solubility and permeability in drug discovery and development settings. *Adv. Drug Deliv. Rev.* **2001,** *46* (1-3), 3-26.

19. Steel, W. H.; Foresman, J. B.; Burden, D. K.; Lau, Y. Y.; Walker, R. A., Solvation of nitrophenol isomers: consequences for solute electronic structure and alkane/water partitioning. *J. Phys. Chem. B* **2009,** *113* (3), 759-66.

20. Verber, D., F.; Johnson, Stephen R.; Cheng, Hung-Yuan; Smith, Brian R.; Ward, Keith W.; Kopple, Kenneth D., Molecular Porperties tha tINfluence the Oral Bioavailability of Drug Candidates. *J. Med. Chem.* **2002,** *45*, 2615-2623.

21. Steel, W. H.; Walker, R. A., Measuring dipolar width across liquid-liquid interfaces with 'molecular rulers'. *Nature* **2003,** *424* (6946), 296-9.

22. Valko, K., Application of high-performance liquid chromatography based measurements of lipophilicity to model biological distribution. *J. Chromatogr. A* **2004,** *1037* (1-2), 299-310.

23. Hughes, L. D. P., David S.; Nigsch, Florian; Mitchell, John B.O., Why Are Some Properites More Difficult to Predict than Others? A Study of QSPR Models of Solublility, Melting Point, and Log P. *J. Chem. Inf. Model* **2008,** *48*, 220-232.

24. Nicolson, G. L., The Fluid-Mosaic Model of Membrane Structure: Still relevant to understanding the structure, function and dynamics of biological membranes after more than 40 years. *Biochim. Biophys. Acta* **2014,** *1838* (6), 1451-1466.

25. Nickels, J. D.; Smith, M. D.; Alsop, R. J.; Himbert, S.; Yahya, A.; Cordner, D.; Zolnierczuk, P.; Stanley, C. B.; Katsaras, J.; Cheng, X.; Rheinstadter, M. C., Lipid Rafts: Buffers of Cell Membrane Physical Properties. *J Phys Chem B* **2019,** *123* (9), 2050-2056.

26. Bent, D. V. H., E., Excited State Chemistry of Aromatic Amino Acids and Related Peptides. II. Phenylanine. *J. Am. Chem. Soc.* **1974,** *97(10)*, 2606-2612.

27. Teale, F. W. J. W., G., Ultraviolet Fluorescence of the Aromatic Amino Acids. *Biochem. J.* **1957,** *65*, 476-482.

28. Chen, R. F., Fluorescence Quantum Yields of Tryptophan and Tyrosine. *Anal. Lett.* **1967,** *1* (1), 35-42.

29. Leroy, E.; Lami, H.; Laustria.G, Fluorescence Lifetime and Quantum Yield of Phenylalanine Aqueous Solutions. Temperature and Concentration Effects. *Photochem Photobiol* **1971,** *13* (5), 411-421.

30. Omidyan, R.; Ataelahi, M.; Azimi, G., Excited-state deactivation mechanisms of protonated and neutral phenylalanine: a theoretical study. *RSC Adv.* **2015,** *5* (37), 29032-29039.

31. Rzeska, A. S., K.; Malicka, J.; Lankiwicz, L.; Wiczk, W., Phophysics of phenylalanine analogues Part 1. Constrained analogues of phenylalanine modified at phenyl ring. *Photochem. Photobiol.* **2000,** *133*, 33-38.

32. Chakrabarti, A. C., Permeability of membranes to amino acids and modified amino acids: Mechanisms involved in translocation. *Amino Acids* **1994,** *6*, 213-229.

33. Johansson, A. C.; Lindahl, E., The role of lipid composition for insertion and stabilization of amino acids in membranes. *J. Chem. Phys.* **2009,** *130* (18), 185101.

34. MacCallum, J. L.; Bennett, W. F.; Tieleman, D. P., Distribution of amino acids in a lipid bilayer from computer simulations. *Biophys. J.* **2008,** *94* (9), 3393-404.

35. White, S. H.; Wimley, W. C., Hydrophobic interactions of peptides with membrane interfaces. *Biochim. Biophys. Acta* **1998,** *1376* (3), 339-52.

36. Rosa, A. S.; Cutro, A. C.; Frias, M. A.; Disalvo, E. A., Interaction of Phenylalanine with DPPC Model Membranes: More Than a Hydrophobic Interaction. *J Phys Chem B* **2015,** *119* (52), 15844-7.

37. Linde, C. D. *Physico-Chemical Properties and Environmental Fate of Pesticides*; State of California Environmental Protection Agency: Sacramento, California, 1994; pp 1-53.

38. Neely, W. B. B., Gary E., *Environmental Exposure from Chemicals*. CRC PRess: Boca Raton, FL, 2018; Vol. Volume 2, p 159.

39. Calamari, D., Assessment of persistent and bioaccumulating chemicals in the aquatic environment. *Toxicology* **2002,** *181-182*, 183-6.

40. Rodrigues, E. T.; Alpendurada, M. F.; Ramos, F.; Pardal, M. A., Environmental and human health risk indicators for agricultural pesticides in estuaries. *Ecotoxicol. Environ. Saf.* **2018,** *150*, 224-231.

41. Sim, M., Case studies in the use of toxicological measures in epidemiological studies. *Toxicology* **2002,** *181-182*, 405-409.

42. Nichols, J. W. B., Mark; Dimitrov, Sabcho D.; Escher, Beate, I.; Han, Xing; Kamert, Nynke, Bioaccumulation Assesment Using Predictive Approaches. *Integ. Enviorn. Assess. Maneg.* **2009,** *5*, 20.

43. Gobrogge, C. A.; Blanchard, H. S.; Walker, R. A., Temperature-Dependent Partitioning of Coumarin 152 in Phosphatidylcholine Lipid Bilayers. *J. Phys. Chem. B* **2017,** *121* (16), 4061-4070.

44. Gobrogge, C. A.; Kong, V. A.; Walker, R. A., Temperature Dependent Solvation and Partitioning of Coumarin 152 in Phospholipid Membranes. *J. Phys. Chem. B* **2016,** *120* (8), 1805-12.

45. Gobrogge, C. A.; Kong, V. A.; Walker, R. A., Temperature-Dependent Partitioning of C152 in Binary Phosphatidylcholine Membranes and Mixed Phosphatidylcholine/Phosphatidylethanolamine Membranes. *J. Phys. Chem. B* **2017,** *121* (33), 7889-7898.

46. Gobrogge, C. A.; Walker, R. A., Quantifying Solute Partitioning in Phosphatidylcholine Membranes. *Anal. Chem.* **2017,** *89* (22), 12587-12595.

47. Moriguchi, I. H., S.; Nakagome, I.; Hirano, H., Compairson of Reliablitiy of log P Values for Drugs Calculated by Several Methods. *Chem. Pharm. Bull* **1994,** *42* (4), 974-978.

48. Xing, L. G., Robert C., Novel Methods for the Prediction of logP, pK_a, and logD. *J. Chem. Inf. Comput. Sci* **2002,** *42*, 796-805.

49. Li, J.; Zhang, C.-F.; Ming, Z.-Z.; Hao, G.-F.; Yang, W.-C.; Yang, G.-F., Coumarin-based novel fluorescent zinc ion probe in aqueous solution. *Tetrahedron* **2013,** *69* (23), 4743-4748.

50. Purnell, G. E.; McNally, M. T.; Callis, P. R.; Walker, R. A., Buried Liquid Interfaces as a Form of Chemistry in Confinement: The Case of 4-Dimethylaminobenzonitrile at the Silica-Aqueous Interface. *J. Am. Chem. Soc.* **2020,** *142* (5), 2375-2385.

51. Roy, D.; Liu, S.; Woods, B. L.; Siler, A. R.; Fourkas, J. T.; Weeks, J. D.; Walker, R. A., Nonpolar Adsorption at the Silica/Methanol Interface: Surface Mediated Polarity

and Solvent Density across a Strongly Associating Solid/Liquid Boundary. *J. Phys. Chem. C* **2013,** *117* (51), 27052-27061.

52. Becker, W., *Advanced Time-Correlated Single Photon Counting Techniques*. Springer: Berlin Heidelberg, Germeny, 2005; p 415.

53. Nad, S. K., Manoj; and Pal, H., Photophysical Properties of Coumarin-152 and Coumarin-481 Dyes: Unusual Behavior in Nonpolar nad Higher Polarity Solvents. *J. Phys. Chem. A* **2003,** *107*, 4808-4816.

54. Nad, S.; Pal, H., Unusual Photophysical Properties of Coumarin-151. *J. Phys. Chem. A* **2001,** *105* (7), 1097-1106.

55. Purnell, G. E.; Walker, R. A., Hindered Isomerization at the Silica/Aqueous Interface: Surface Polarity or Restricted Solvation? *Langmuir* **2018,** *34* (34), 9946-9949.

56. Brem, R.; Chan, H. S.; Dill, K. A., Extracting microscopic energies from oil-phase solvation experiments. *J. Phys. Chem. B* **2000,** *104* (31), 7471-7482.

57. Kumar, S. K. S., Igal; Sharp, Kim; Rossky, Peter J.; Friedman, Richard; Honig, Barry, Size Dependence of Transfer Energies. 1. A Flory-Huggins Approach. *J. Phys. Chem.* **1995,** *99*, 8382-8391.

58. De Vries, A. H. Y., Serge; Mark, Alan E.; Marrink, Siewert J., Molecuclar structure of the lecithin ripple phase. *PNAS 102*, 5392-5396.

59. Hirst, L. S.; Ossowski, A.; Fraser, M.; Geng, J.; Selinger, J. V.; Selinger, R. L., Morphology transition in lipid vesicles due to in-plane order and topological defects. *Proc. Natl. Acad. Sci. U.S.A.* **2013,** *110* (9), 3242-7.

60. Jorgensen, K. I., J.H.; Mouritsen, O.G.; Bennett, D.; Zuckermann, M.J., The effects of density fluctuations on the parititoning of foreign molecules into lipid bilayers: Application to anaesthetics and insecticides. *Biochim. Biophys. Acta* **1991,** *1067*, 241-253.

61. Mouritsen, O. G.; Zuckermann, M. J., Model of interfacial melting. *Phys. Rev. Lett.* **1987,** *58* (4), 389-392.

62. Alarcon, L. M.; de Los Angeles Frias, M.; Morini, M. A.; Belen Sierra, M.; Appignanesi, G. A.; Anibal Disalvo, E., Water populations in restricted environments of lipid membrane interphases. *Eur. Phys. J. E* **2016,** *39* (10), 94.

63. Foglia, F.; Lawrence, M. J.; Lorenz, C. D.; McLain, S. E., On the hydration of the phosphocholine headgroup in aqueous solution. *J. Chem. Phys.* **2010,** *133* (14), 145103.

64. Pinto, O. A.; Disalvo, E. A., A new model for lipid monolayer and bilayers based on thermodynamics of irreversible processes. *PLOS One* **2019,** *14* (4), 1-19.

65. Watanabe, N.; Suga, K.; Slotte, J. P.; Nyholm, T. K. M.; Umakoshi, H., Lipid-Surrounding Water Molecules Probed by Time-Resolved Emission Spectra of Laurdan. *Langmuir* **2019,** *35* (20), 6762-6770.

66. Eze, M. O., Phase Tranistions in Phosopholipid Bilayers: Lateral Phase Separations Play Vital Roles in Biomembranes. *Biochem. Educ.* **1991,** *19*, 204-208.

67. Leekumjorn, S.; Sum, A. K., Molecular studies of the gel to liquid-crystalline phase transition for fully hydrated DPPC and DPPE bilayers. *Biochim. Biophys. Acta* **2007,** *1768* (2), 354-65.

68. van Meer, G.; Voelker, D. R.; Feigenson, G. W., Membrane lipids: where they are and how they behave. *Nat. Rev. Mol. Cell Biol.* **2008,** *9* (2), 112-24.

69. Pandey, P. R.; Roy, S., Headgroup mediated water insertion into the DPPC bilayer: a molecular dynamics study. *J. Phys. Chem. B* **2011,** *115* (12), 3155-63.

70. Kwon, J. H.; Liljestrand, H. M.; Katz, L. E., Partitioning of moderately hydrophobic endocrine disruptors between water and synthetic membrane vesicles. *Environ. Toxicol. Chem.* **2006,** *25* (8), 1984-92.

71. Kwon, J. H. L., H.M.; Katz, L.E; Yamaoto, H., Partitioning Thermodynamics of Selected Endocrine Disrupotrs between Water and Synthetic Membrane Vesicles: Effects of Membraen Compositions. *Environ. Sci. Technol.* **2007,** *41*, 4011-4018.

72. Oliver, M.; Adrover, M.; Frontera, A.; Ortega-Castro, J.; Miró, M., In-vitro prediction of the membranotropic action of emerging organic contaminants using a liposome-based multidisciplinary approach. *Sci. Tot. Environ.* **2020,** *738*.

73. van Wezel, A. P. C., G.; van Miltenburg, J.K.; Opperhuizen, A., Membrane burdens of chlorinated benzenes lower the main phase transtion temperature in dipalmitoyl-phosphatidylcholine vesicles: implications for toxicity by narcotic chemicals. *Environ. Toxicol. Chem.* **1996,** *15*, 203-212.

74. Meyer, H., On the theory of alcohol narcosis: first communication. Which property of anesthetic determines its narcotic effect? *Arch. Exp. Pathol. Pharmakol.* **1899,** *425*.

75. Overton, C. E., *Studies of Narcosis*. Verlag Gustav Fischer: Jena, Germany, 1901.

76. Kah, M.; Brown, C. D., LogD: lipophilicity for ionisable compounds. *Chemosphere* **2008,** *72* (10), 1401-1408.

77. Bahl, S. K. K., K.; Peirson, I.G.; Pearl, G.M., The Rule of Five Revisited: Applying Log D in Place of Log P in Drug-Likeness Filters. *Mol. Pharm.* **2007,** *4*, 556-560.

78. Gobas, F. A.; Lahittete, J. M.; Garofalo, G.; Shiu, W. Y.; Mackay, D., A novel method for measuring membrane-water partition coefficients of hydrophobic organic chemicals: comparison with 1-octanol-water partitioning. *J. Pharm. Sci.* **1988,** *77* (3), 265-72.

79. van der Heijden, S. A.; Jonker, M. T., Evaluation of liposome-water partitioning for predicting bioaccumulation potential of hydrophobic organic chemicals. *Environ. Sci. Technol.* **2009,** *43* (23), 8854-8859.

80. Endo, S.; Escher, B. I.; Goss, K. U., Capacities of membrane lipids to accumulate neutral organic chemicals. *Environ. Sci. Technol.* **2011,** *45* (14), 5912-21.

81. Takegami, S. K., K.; Funakoshi, T.; Kitade, T. , Partitioning of Anti-inflammatory Steroid Drugs into Phosphatidylcholine and Phosphatidylcholine-Cholesterol Small Unilamellar Vesicles as Studied by Second-Derivative Spectrophotometry. *Chem. Pharm. Bull.* **2007,** *56*, 663-667.

82. Rai, V.; Tan, H. S.; Michniak-Kohn, B., Effect of surfactants and pH on naltrexone (NTX) permeation across buccal mucosa. *Int. J. Pharm.* **2011,** *411* (1-2), 92-7.

83. Maherani, B.; Arab-Tehrany, E.; Kheirolomoom, A.; Geny, D.; Linder, M., Calcein release behavior from liposomal bilayer; influence of physicochemical/mechanical/structural properties of lipids. *Biochimie* **2013,** *95* (11), 2018-33.

84. Duncan, K. M.; Casey, A.; Gobrogge, C. A.; Trousdale, R. C.; Piontek, S. M.; Cook, M. J.; Steel, W. H.; Walker, R. A., Coumarin Partitioning in Model Biological Membranes: Limitations of logP as a Predictor. *J Phys Chem B* **2020,** *124* (38), 8299-8308.

85. Arias, J. M.; Cobos Picot, R. A.; Tuttolomondo, M. E.; Ben Altabef, A.; Díaz, S. B., Interaction of N-acetylcysteine with DPPC liposomes at different pH: a physicochemical study. *New J. Chem.* **2020,** *44* (35), 14837-14848.

86. Arias, J. M.; Tuttolomondo, M. E.; Díaz, S. B.; Altabef, A. B., Molecular view of the structural reorganization of water in DPPC multilamellar membranes induced by l -cysteine methyl ester. *J. Molec. Struct.* **2018,** *1156*, 360-368.

87. Cutro, A. C.; Disalvo, E. A., Phenylalanine Blocks Defects Induced in Gel Lipid Membranes by Osmotic Stress. *J. Phys. Chem. B* **2015,** *119* (31), 10060-5.

88. Cutro, A. C.; Disalvo, E. A.; Frias, M. A., Effects of Phenylalanine on the Liquid-Expanded and Liquid-Condensed States of Phosphatidylcholine Monolayers. *Lipid Insights* **2019,** *12*, 1-9.

89. Rosa, A. S.; Cutro, A. C.; Frias, M. A.; Disalvo, E. A., Interaction of Phenylalanine with DPPC Model Membranes: More Than a Hydrophobic Interaction. *J. Phys. Chem. B* **2015,** *119* (52), 15844-7.

90. Khandelia, H.; Ipsen, J. H.; Mouritsen, O. G., The impact of peptides on lipid membranes. *Biochim. Biophys. Acta* **2008,** *1778* (7-8), 1528-36.

91. Perkins, R.; Vaida, V., Phenylalanine Increases Membrane Permeability. *J. Am. Chem. Soc.* **2017,** *139* (41), 14388-14391.

92. Nandi, S.; Pyne, A.; Ghosh, M.; Banerjee, P.; Ghosh, B.; Sarkar, N., Antagonist Effects of l-Phenylalanine and the Enantiomeric Mixture Containing d-Phenylalanine on Phospholipid Vesicle Membrane. *Langmuir* **2020,** *36* (9), 2459-2473.

93. Kanwa, N.; De, S. K.; Maity, A.; Chakraborty, A., Interaction of aliphatic amino acids with zwitterionic and charged lipid membranes: hydration and dehydration phenomena. *Phys. Chem. Chem. Phys.* **2020,** *22* (6), 3234-3244.

94. Alanso, A. G., Felix M., Effect of Detergents and Fusogenic Lipids on Phospholipid Phase Transitions. *J. Membr. Biol.* **1983,** *71*, 183-187.

95. Kodama, M.; Kuwabara, M.; Seki, S., Successive Phase-Transition Phenomena and Phase-Diagram of the Phosphatidylcholine-Water System as Revealed by Differential Scanning Calorimetry. *Biochim. Biophys. Acta* **1982,** *689* (3), 567-570.

96. Link, K. A.; Spurzem, G. N.; Tuladhar, A.; Chase, Z.; Wang, Z.; Wang, H.; Walker, R. A., Organic Enrichment at Aqueous Interfaces: Cooperative Adsorption of Glucuronic Acid to DPPC Monolayers Studied with Vibrational Sum Frequency Generation. *J. Phys. Chem. A* **2019,** *123* (26), 5621-5632.

97. Jain, M. K. W., Nora Min, Effect of Small Molecules on the Dipalmitoyl Lecthin Liposomal Bilayer: III. Phase Transition in Lipid Bilayer. *J. Membrane Biol.* **1977,** *34*, 157-201.

98. Barcclo, D., Environmental Protection Agency and other methods for the determination of priority pesticides and their transformation products in water. *J. Chromatogr.* **1993,** *643*, 117-143.

99. Guidence for Industry. Environmenal Assesment of Human Drug and Biologies Applications. Administration, U. S. D. o. H. a. H. S. F. a. D., Ed. Rockville, MD, 1998.

100. Lipinski, C. A., Drug-like properties and the causes of poor solubility and poor permeability. *J Pharmacol Toxicol Methods* **2000,** *44* (1), 235-49.

101. Nicolson, G. L., The Fluid-Mosaic Model of Membrane Structure: still relevant to understanding the structure, function and dynamics of biological membranes after more than 40 years. *Biochim. Biophys. Acta* **2014,** *1838* (6), 1451-66.

102. Singer, S. J. N., G.L., The Fluid Mosaid Model of the Structure of Cell Membranes. *Science* **1972,** *175*, 720-731.

103. Duncan, K. M.; Steel, W. H.; Walker, R. A., Amino acids change solute affinity for lipid bilayers. *Biophys. J.* **2021,** *120* (17), 3676-3687.

104. Chakrabarti, A. C., Permeability of membranes to amino acids and modified amino acids: Mechanisms involved in translocation. *J. Amino Acids* **1994,** *6*, 213-229.

105. Chakrabarti, A. C. D., D.W., Permeability of lipid bilayers to amino acids and phosphate. *Biochim. Biophys. Acta* **1992,** *1111*, 171-177.

106. Griffith, E. C.; Perkins, R. J.; Telesford, D. M.; Adams, E. M.; Cwiklik, L.; Allen, H. C.; Roeselova, M.; Vaida, V., Interaction of L-Phenylalanine with a Phospholipid Monolayer at the Water-Air Interface. *J. Phys. Chem. B* **2015,** *119* (29), 9038-48.

107. White, S. H. W., W, C., Hydrophobic interactions of peptides with membarne interfaces. *Biochim. Biophys. Acta* **1998,** *1376*, 339-352.

108. Williams, R. A. M., C.DS.; Burnett, J.R., Phenylketonuria: An Inborn Error of Phenylalanine Metabolism. *Clin. Biochem. Rev.* **2008,** *29*, 31-41.

109. Nandi, S.; Ghosh, B.; Ghosh, M.; Layek, S.; Nandi, P. K.; Sarkar, N., Phenylalanine Interacts with Oleic Acid-Based Vesicle Membrane. Understanding the Molecular Role of Fibril-Vesicle Interaction under the Context of Phenylketonuria. *J. Phys. Chem. B* **2021,** *125* (34), 9776-9793.

110. Mittal, L. J.; Mittal, J. P.; Hayon, E., Primary processes in the photochemistry of phenylalanine and derivatives in aqueous solution. Biphotonic photoionization and photodissociation reactions. *J. Am. Chem. Soc.* **2002,** *95* (19), 6203-6210.

111. Mittal, L. J. M., J.P.; Hayon, E., Biphotonic photodissociation of phenylalanine in aqueous solutions at 20 °C. *Chem. Phys. Lett.* **1973,** *18*, 319-322.

112. Chin, K. K. T.-S., C.C.; McCallum, J.; Jockusch, S.; Turro, N.J.; Scaiano, J.C.; Foote, C.S.; Garcia-Garibay, M.A., Quantitative Determination of Singlet Oxygen Generate4d by Excited State Aromatic Amino Acids, Proteins, and Immunoglobulins. *J. Am. Chem. Soc.* **2008,** *130*, 6912-6913.

113. Gally, J. A. E., G.M., The Effect of Temperature on the Fluorescence of Some Aromatic Amino Acids and Proteins. *Biochim. Biophys. Acta* **1962,** *60*, 499-509.

114. Lorenz, U. J.; Rizzo, T. R., Structural melting of an amino acid dimer upon intersystem crossing. *J. Am. Chem. Soc.* **2014,** *136* (42), 14974-80.

115. Tournon, J. E.-B. A., Intramolecular Charge-Transfer Interactions in Benzyl Derivatives. *J. Chem. Phys.* **2015,** *56*, 5128-5134.

116. Andersen, J. U.; Cederquist, H.; Forster, J. S.; Huber, B. A.; Hvelplund, P.; Jensen, J.; Liu, B.; Manil, B.; Maunoury, L.; Brøndsted Nielsen, S.; Pedersen, U. V.; Rangama, J.; Schmidt, H. T.; Tomita, S.; Zettergren, H., Photodissociation of protonated amino acids and peptides in an ion storage ring. Determination of Arrhenius parameters in the high-temperature limit. *Phys. Chem. Chem. Phys.* **2004,** *6* (10), 2676-2681.

117. Nikogosyan, D. N. G., H., Laser-Induced Photodecomposition of Amino Acids and Peptdies: Extrapolation to Corneal Collagen. *IEEE J. Sel.* **1999,** *5*, 1107-1115.

118. Rzeska, A.; Stachowiak, K.; Malicka, J.; Lankiewicz, L.; Wiczk, W., Photophysics of phenylalanine analogues - Part 1. Constrained analogues of phenylalanine modified at phenyl ring. *J. Photochem. Photobiol. A. Chem.* **2000,** *133* (1-2), 33-38.

119. Rzeska, A. M., J.; Stachowiak, K; ; Szymariska, A.; Lankiewicz, L.; Wiczk, W., Photophysics of phenylalanine analogues Part 2. Linear analogues of phenylalanine. *J. Photochem. Photobiol. A. Chem.* **2001,** *140* (1), 21-26.

120. Chapman, D. U., J.; Keough, K.M., Biomembrane Phase Transitions. *J. Biol. Chem.* **1974,** *249*, 2512-2521.

121. Link, K. A.; Spurzem, G. N.; Tuladhar, A.; Chase, Z.; Wang, Z.; Wang, H.; Walker, R. A., Cooperative Adsorption of Trehalose to DPPC Monolayers at the Water-Air Interface Studied with Vibrational Sum Frequency Generation. *J Phys Chem B* **2019,** *123* (42), 8931-8938.

122. Duncan, K. M.; Casey, A.; Gobrogge, C. A.; Trousdale, R. C.; Piontek, S. M.; Cook, M. J.; Steel, W. H.; Walker, R. A., Coumarin Partitioning in Model Biological Membranes: Limitations of logP as a Predictor. *J. Phys. Chem. B* **2020,** *124* (38), 8299-8308.

123. de Vries, A. H.; Yefimov, S.; Mark, A. E.; Marrink, S. J., Molecular structure of the lecithin ripple phase. *Proc. Natl. Acad. Sci. U.S.A.* **2005,** *102* (15), 5392-5396.

124. Chen, W.; Dusa, F.; Witos, J.; Ruokonen, S. K.; Wiedmer, S. K., Determination of the Main Phase Transition Temperature of Phospholipids by Nanoplasmonic Sensing. *Sci. Rep.* **2018,** *8* (1), 14815.

125. Lentz, B. R.; Freire, E.; Biltonen, R. L., Fluorescence and calorimetric studies of phase transitions in phosphatidylcholine multilayers: kinetics of the pretransition. *Biochem.* **1978,** *17* (21), 4475-80.

126. Leroy, E. L., H.; Laustrait, G., Fluorescence lifetime and quantum yield of phenylalanine aqueous solutions. Temperature and concentration effects. *J. Photochem. Photobiol.* **1971,** *13*, 411-421.

127. Duneau, J. P. G., N.; Cremel, G.; Nullans, G.; Hubert, P.; Genest, D.; Vincent, M.; Gallay, J.; Genest, M., Time resolved fluorescence properties of phenylalanine in different environments. Comparison with molecular dynamics simulation. *Biophys. Chem.* **1993,** *73*, 109-119.

128. Demetzos, C., Differential Scanning Calorimetry (DSC): a tool to study the thermal behavior of lipid bilayers and liposomal stability. *J. Liposome Res.* **2008,** *18* (3), 159-73.

129. Majhi, P. R. B., A., Temperature-Induced Micelle-Vesicle Transitions in DMPC-SDS and DMPC-DTAB Mixtures Studied by Calorimetry and Dynamic Light Scattering. *J. Phys. Chem. B* **2002,** *106*, 10753-10763.

130. Ogata, K.; Uchida, W.; Nakamura, S., Understanding thermal phases in atomic detail by all-atom molecular-dynamics simulation of a phospholipid bilayer. *J. Phys. Chem. B* **2014,** *118* (49), 14353-65.

131. Olsztynska, S. K., M.; Dupuy, N., Influence of Near-Infrared Radiation on the pK_a values of L-Phenylalanine *J. Appl. Spectrosc.* **2006,** *60*, 648-652.

132. Cavanaugh, J. R., The rotational isomerism of phenylalanine by nuclear magnetic resonance. *J. Am. Chem. Soc.* **1967,** *89* (7), 1558-64.

133. Stephinewski, M. B., A.; Pasenkiewicz-Gierula, M.; Karttunen, M.; Rog, T., Effects of the Lipid Bilayer Phase State on the Water Membrane Interface. *J. Phys. Chem. B* **2010,** *114*, 11784-11792.

134. Pasenkiewicz-Gierula, M.; Baczynski, K.; Markiewicz, M.; Murzyn, K., Computer modelling studies of the bilayer/water interface. *Biochim. Biophys. Acta* **2016,** *1858* (10), 2305-2321.

135. Shinoda, W., Permeability across lipid membranes. *Biochem. Biophys. Acta* **2016,** *1858* (10), 2254-2265.

136. Kucerka, N.; Nieh, M. P.; Katsaras, J., Fluid phase lipid areas and bilayer thicknesses of commonly used phosphatidylcholines as a function of temperature. *Biochim Biophys Acta* **2011,** *1808* (11), 2761-71.

137. Bunally, S. B.; Luscombe, C. N.; Young, R. J., Using Physicochemical Measurements to Influence Better Compound Design. *SLAS Discov.* **2019,** *24* (8), 791-801.

138. Peetla, C.; Stine, A.; Labhasetwar, V., Biophysical Interactions with Model Lipid Membranes: Applications in Drug Discovery and Drug Delivery. *Mol. Pharm.* **2009,** *6* (5), 1264-1276.

139. Perlovich, G. L., Thermodynamic Approaches to the Challenges of Solubility in Drug Discovery and Development. *Mol. Pharm.* **2014,** *11* (1), 1-11.

140. Cao, Y. C.; Xiang, T. X.; Anderson, B. D., Development of structure-lipid bilayer permeability relationships for peptide-like small organic molecules. *Mol. Pharm.* **2008,** *5* (3), 371-388.

141. Chamberlain, K.; Evans, A. A.; Bromilow, R. H., 1-octanol/water partition coefficient (K-ow) and pK(a) for ionisable pesticides measured by a pH-metric method. *Pestic. Sci.* **1996,** *47* (3), 265-271.

142. Leo, A.; Hansch, C.; Elkins, D., Partition Coefficients and Their Uses. *Chem. Rev.* **1971,** *71* (6), 525-+.

143. Keseru, G. M.; Makara, G. M., The influence of lead discovery strategies on the properties of drug candidates. *Nat. Rev. Drug Discov.* **2009,** *8* (3), 203-212.

144. Meanwell, N. A., Improving Drug Candidates by Design: A Focus on Physicochemical Properties As a Means of Improving Compound Disposition and Safety. *Chem. Res. Toxicol.* **2011,** *24* (9), 1420-1456.

145. Hughes, J. D.; Blagg, J.; Price, D. A.; Bailey, S.; DeCrescenzo, G. A.; Devraj, R. V.; Ellsworth, E.; Fobian, Y. M.; Gibbs, M. E.; Gilles, R. W.; Greene, N.; Huang, E.; Krieger-Burke, T.; Loesel, J.; Wager, T.; Whiteley, L.; Zhang, Y., Physiochemical drug properties associated with in vivo toxicological outcomes. *Bioorg. Med. Chem. Lett.* **2008,** *18* (17), 4872-4875.

146. Goude, R.; Amin, A. G.; Chatterjee, D.; Parish, T., The Arabinosyltransferase EmbC Is Inhibited by Ethambutol in Mycobacterium tuberculosis. *Antimicrob. Agents Chemo.* **2009,** *53* (10), 4138-4146.

147. Aubry, A.; Fisher, L. M.; Jarlier, V.; Cambau, E., First functional characterization of a singly expressed bacterial type II topoisomerase: The enzyme from Mycohacterium wherculosis. *Biochem. Biophys. Res. Comm.* **2006,** *348* (1), 158-165.

148. Bald, D.; Villellas, C.; Lu, P.; Koul, A., Targeting Energy Metabolism in Mycobacterium tuberculosis, a New Paradigm in Antimycobacterial Drug Discovery. *mBio* **2017,** *8* (2), 11.

149. Aung, H. L.; Berney, M.; Cook, G. M., Hypoxia-Activated Cytochrome bd Expression in Mycobacterium smegmatis Is Cyclic AMP Receptor Protein Dependent. *J. Bacteriol.* **2014,** *196* (17), 3091-3097.

150. Shi, L. B.; Sohaskey, C. D.; Kana, B. D.; Dawes, S.; North, R. J.; Mizrahi, V.; Gennaro, M. L., Changes in energy metabolism of Mycobacterium tuberculosis in mouse lung and under in vitro conditions affecting aerobic respiration. *Proc. Nat. Acad. Sci. U.S.A.* **2005,** *102* (43), 15629-15634.

151. Wayne, L. G.; Sohaskey, C. D., Nonreplicating persistence of Mycobacterium tuberculosis. *Annu. Rev. Microbiol.* **2001,** *55*, 139-163.

152. Matsoso, L. G.; Kana, B. D.; Crellin, P. K.; Lea-Smith, D. J.; Pelosi, A.; Powell, D.; Dawes, S. S.; Rubin, H.; Coppel, R. L.; Mizrahi, V., Function of the cytochrome bc(1)-aa(3) branch of the respiratory network in mycobacteria and network adaptation occurring in response to its disruption. *J. Bacteriol.* **2005,** *187* (18), 6300-6308.

153. Mascolo, L.; Bald, D., Cytochrome bd in Mycobacterium tuberculosis: A respiratory chain protein involved in the defense against antibacterials. *Prog. Biophys. Molec. Biol.* **2020,** *152*, 55-63.

154. Malasala, S.; Polomoni, A.; Ahmad, M. N.; Shukla, M.; Kaul, G.; Dasgupta, A.; Chopra, S.; Nanduri, S., Structure based design, synthesis and evaluation of new thienopyrimidine derivatives as anti-bacterial agents. *J. Molec. Struct.* **2021,** *1234*, 13.

155. Harrison, G. A.; Bridwell, A. E. M.; Singh, M.; Jayaraman, K.; Weiss, L. A.; Kinsella, R. L.; Aneke, J. S.; Flentie, K.; Schene, M. E.; Gaggioli, M.; Solomon, S. D.; Wildman, S. A.; Meyers, M. J.; Stallings, C. L., Identification of 4-Amino-Thieno 2,3-d Pyrimidines as QcrB Inhibitors in Mycobacterium tuberculosis. *mSphere* **2019,** *4* (5), 14.

156. S. Arnett, M. M., M. Singh, C. Stallings, L. Weiss, S. Wildman Thieno[2,3-d]pyrimidines and benzofuro[3,2-d]pyrimidines as Antimicrobial Agents. WO2019018359A1, 2019.

157. Hopfner, S. M.; Lee, B. S.; Kalia, N. P.; Miller, M. J.; Pethe, K.; Moraski, G. C., Structure guided generation of thieno [3,2-*d*] pyrimidin-4-amine *Mycobacterium tuberculosis bd* oxidase inhibitors. *RSC Med. Chem.* **2021,** *12* (1), 73-77.

158. Baskaran, S., Lew, W., Oslob, J. D., Yoburn, J. C., Zhong, M. Thienopyrimidines useful as Aurora kinase inhibitors and their preparation, pharmaceutical compositions, and their use for treatment of Aurora kinase-mediated diseases. 0216, 2006.

159. Zhan, M.; Deng, Y. F.; Zhao, L. F.; Yan, G. Y.; Wang, F. Y.; Tian, Y.; Zhang, L. X.; Jiang, H. X.; Chen, Y. W., Design, Synthesis, and Biological Evaluation of Dimorpholine Substituted Thienopyrimidines as Potential Class I PI3K/mTOR Dual Inhibitors. *J. Med. Chem.* **2017,** *60* (9), 4023-4035.

160. Zhang, Y. M.; Chen, Y. D.; Zhang, D. F.; Wang, L.; Lu, T.; Jiao, Y., Discovery of Novel Potent VEGFR-2 Inhibitors Exerting Significant Antiproliferative Activity against Cancer Cell Lines. *J. Med. Chem.* **2018,** *61* (1), 140-157.

161. Ghith, A.; Ismail, N. S. M.; Youssef, K.; Abouzid, K. A. M., Medicinal Attributes of Thienopyrimidine Based Scaffold Targeting Tyrosine Kinases and Their Potential Anticancer Activities. *Arch. Pharm.* **2017,** *350* (11), 24.

162. C. Beauregard, A. J. B., R. L. Davis, D. A. Gamache, J. M. Yanni Aminopyrimidine Inhibitors of Histamine Receptors for the Treatment of Disease. 2010.

163. Pal, K.; Raza, M. K.; Legac, J.; Rahman, M. A.; Manzoor, S.; Rosenthal, P. J.; Hoda, N., Design, synthesis, crystal structure and anti-plasmodial evaluation of tetrahydrobenzo 4,5 thieno 2,3-d pyrimidine derivatives. *RSC Med. Chem.* **2021,** *12* (6), 970-981.

164. Pethe, K.; Bifani, P.; Jang, J. C.; Kang, S.; Park, S.; Ahn, S.; Jiricek, J.; Jung, J. Y.; Jeon, H. K.; Cechetto, J.; Christophe, T.; Lee, H.; Kempf, M.; Jackson, M.; Lenaerts, A. J.; Pham, H.; Jones, V.; Seo, M. J.; Kim, Y. M.; Seo, M.; Seo, J. J.; Park, D.; Ko, Y.; Choi, I.; Kim, R.; Kim, S. Y.; Lim, S.; Yim, S. A.; Nam, J.; Kang, H.; Kwon, H.; Oh, C. T.; Cho, Y.; Jang, Y.; Kim, J.; Chua, A.; Tan, B. H.; Nanjundappa, M. B.; Rao, S. P. S.; Barnes, W. S.; Wintjens, R.; Walker, J. R.; Alonso, S.; Lee, S.; Oh, S.; Oh, T.; Nehrbass, U.; Han, S. J.; No, Z.; Lee, J.; Brodin, P.; Cho, S. N.; Nam, K., Discovery of Q203, a potent clinical candidate for the treatment of tuberculosis. *Nat. Med.* **2013,** *19* (9), 1157-1160.

165. Lee, B. S.; Hards, K.; Engelhart, C. A.; Hasenoehrl, E. J.; Kalia, N. P.; Mackenzie, J. S.; Sviriaeva, E.; Chong, S. M. S.; Manimekalai, M. S. S.; Koh, V. H.; Chan, J.; Xu, J. Y.; Alonso, S.; Miller, M. J.; Steyn, A. J. C.; Gruber, G.; Schnappinger, D.; Berney, M.; Cook, G. M.; Moraski, G. C.; Pethe, K., Dual inhibition of the terminal oxidases eradicates antibiotic-tolerant Mycobacterium tuberculosis. *EMBO Mol. Med.* **2021,** *13* (1), 16.

166. Thesseling, A.; Rasmussen, T.; Burschel, S.; Wohlwend, D.; Kagi, J.; Muller, R.; Bottcher, B.; Friedrich, T., Homologous bd oxidases share the same architecture but differ in mechanism. *Nat. Comm.* **2019,** *10*, 7.

167. Safarian, S.; Hahn, A.; Mills, D. J.; Radloff, M.; Eisinger, M. L.; Nikolaev, A.; Meier-Credo, J.; Melin, F.; Miyoshi, H.; Gennis, R. B.; Sakamoto, J.; Langer, J. D.; Hellwig, P.; Kuhlbrandt, W.; Michel, H., Active site rearrangement and structural divergence in prokaryotic respiratory oxidases. *Science* **2019,** *366* (6461), 100-+.

168. Safarian, S.; Rajendran, C.; Muller, H.; Preu, J.; Langer, J. D.; Ovchinnikov, S.; Hirose, T.; Kusumoto, T.; Sakamoto, J.; Michel, H., Structure of a bd oxidase indicates similar mechanisms for membrane-integrated oxygen reductases. *Science* **2016,** *352* (6285), 583-586.

169. Wang, W. W.; Gao, Y.; Tang, Y. T.; Zhou, X. T.; Lai, Y. Z.; Zhou, S.; Zhang, Y. Y.; Yang, X. N.; Liu, F. J.; Guddat, L. W.; Wang, Q.; Rao, Z. H.; Gong, H. R., Cryo-EM structure of mycobacterial cytochrome bd reveals two oxygen access channels. *Nat. Comm.* **2021,** *12* (1), 8.

170. Safarian, S.; Opel-Reading, H. K.; Wu, D.; Mehdipour, A. R.; Hards, K.; Harold, L. K.; Radloff, M.; Stewart, I.; Welsch, S.; Hummer, G.; Cook, G. M.; Krause, K. L.; Michel, H., The cryo-EM structure of the bd oxidase from M. tuberculosis reveals a unique structural framework and enables rational drug design to combat TB. *Nat. Comm.* **2021,** *12* (1), 10.

171. Singer, S. J.; Nicolson, G. L., The Fluid Mosaic Model of the Structure of Cell Membranes. *Science* **1972,** *175* (4023), 720-+.

172. Panicker, L.; Sharma, V. K.; Datta, G.; Deniz, K. U.; Parvathanathan, P. S.; Ramanathan, K. V.; Khetrapal, C. L., Interaction of aspirin with DPPC in the lyotropic, dppc-aspirin-H2O/D2O membrane. *Mol. Cryst. Liq. Cryst. Mol.* **1995,** *260*, 611-621.

173. Puglisi, G.; Fresta, M.; Ventura, C.; Mazzone, G.; Vandelli, M. A., Methotrexate Interaction with a Lipid-Membrane Model of DPPC. *J.Therm. Anal.* **1995,** *44* (6), 1287-1299.

174. Mady, M. M.; Shafaa, M. W.; Abbase, E. R.; Fahium, A. H., Interaction of Doxorubicin and Dipalmitoylphosphatidylcholine Liposomes. *Cell Biochem. Biophys.* **2012,** *62* (3), 481-486.

175. Lipinski, C. A., Drug-like properties and the causes of poor solubility and poor permeability. *J. Pharmacol. Toxicol. Methods* **2000,** *44* (1), 235-249.

176. Lipinski, C. A.; Lombardo, F.; Dominy, B. W.; Feeney, P. J., Experimental and computational approaches to estimate solubility and permeability in drug discovery and development settings (Reprinted from Advanced Drug Delivery Reviews, vol 23, pg 3-25, 1997). *Adv. Drug Deliv. Rev.* **2001,** *46* (1-3), 3-26.

177. Duncan, K. M.; Steel, W. H.; Walker, R. A., Amino acids change solute affinity for lipid bilayers. *Biophys. J.* **2021,** *120* (17), 3676-3687.

178. Alifrangis, L. H.; Christensen, I. T.; Berglund, A.; Sandberg, M.; Hovgaard, L.; Frokjaer, S., Structure-property model for membrane partitioning of oligopeptides. *J. Med. Chem.* **2000,** *43* (1), 103-113.

179. Ma, B.; Zha, H. Y.; Li, N.; Yang, D.; Lin, G., Effect of Structural Modification of alpha-Aminoxy Peptides on Their Intestinal Absorption and Transport Mechanism. *Mol. Pharm.* **2011,** *8* (4), 1073-1082.

180. Sharifian, G. M., Recent Experimental Developments in Studying Passive Membrane Transport of Drug Molecules. *Mol. Pharm.* **2021,** *18* (6), 2122-2141.

181. Chen, I. J.; Taneja, R.; Yin, D. X.; Seo, P. R.; Young, D.; MacKerell, A. D.; Polli, J. E., Chemical substituent effect on pyridine permeability and mechanistic insight from computational molecular descriptors. *Mol. Pharm.* **2006,** *3* (6), 745-755.

182. Duncan, K. M.; Casey, A.; Gobrogge, C. A.; Trousdale, R. C.; Piontek, S. M.; Cook, M. J.; Steel, W. H.; Walker, R. A., Coumarin Partitioning in Model Biological Membranes: Limitations of log P as a Predictor. *J. Phys. Chem. B* **2020,** *124* (38), 8299-8308.

183. Gobrogge, C. A.; Kong, V. A.; Walker, R. A., Temperature-Dependent Partitioning of C152 in Binary Phosphatidylcholine Membranes and Mixed Phosphatidylcholine/Phosphatidylethanolamine Membranes. *J. Phys. Chem. B* **2017,** *121* (33), 7889-7898.

184. Gomez, J. E.; McKinney, J. D., M-tuberculosis persistence, latency, and drug tolerance. *Tuberculosis* **2004,** *84* (1-2), 29-44.

185. Hopfner, S. M. D., K.M.; Trousdale, R.C.; Cloninger, M.J.; Walker, R.A., Testing membrane affinity of thienopyrimidine drug candidates with time-resolved fluorescence emission. *Mol. Pharm. (In Preperation).* **2022**.

186. Purnell, G. E.; McNally, M. T.; Callis, P. R.; Walker, R. A., Buried Liquid Interfaces as a Form of Chemistry in Confinement: The Case of 4-Dimethylaminobenzonitrile at the Silica-Aqueous Interface. *J. Am. Chem. Soc.* **2020,** *142* (5), 2375-2385.

187. Nad, S.; Pal, H., Unusual photophysical properties of coumarin-151. *J. Phys. Chem. A* **2001,** *105* (7), 1097-1106.

188. Nad, S.; Kumbhakar, M.; Pal, H., Photophysical properties of coumarin-152 and coumarin-481 dyes: Unusual behavior in nonpolar and in higher polarity solvents. *J. Phys. Chem. A* **2003,** *107* (24), 4808-4816.

189. Roy, D.; Liu, S. L.; Woods, B. L.; Siler, A. R.; Fourkas, J. T.; Weeks, J. D.; Walker, R. A., Nonpolar Adsorption at the Silica/Methanol Interface: Surface Mediated Polarity and Solvent Density across a Strongly Associating Solid/Liquid Boundary. *J. Phys. Chem. C* **2013,** *117* (51), 27052-27061.

190. Ahmed, M.; Younis, O.; Orabi, E. A.; Sayed, A. M.; El-Dean, A. M. K.; Hassanien, R.; Davis, R. L.; Tsutsumi, O.; Tolba, M. S., Synthesis of Novel Biocompatible Thienopyrimidine Chromophores with Aggregation-Induced Emission Sensitive to Molecular Aggregation. *ACS Omega* **2020,** *5* (46), 29988-30000.

191. Sayed, M.; Younis, O.; Hassanien, R.; Ahmed, M.; Mohammed, A. A. K.; Kamal, A. M.; Tsutsumi, O., Design and synthesis of novel indole derivatives with aggregation-induced emission and antimicrobial activity. *J. Photochem. Photobiol. A: Chem.* **2019,** *383*, 11.

192. Hu, R.; Leung, N. L. C.; Tang, B. Z., AIE macromolecules: syntheses, structures and functionalities. *Chem. Soc. Rev.* **2014,** *43* (13), 4494-4562.

193. Neely, W. B. B., Dean R.; Blau, Gary E., Partition Coefficient to Measure Bioconcentrartion Potential of Organic Chemicals in Fish. *Environ. Sci. Technol.* **1974,** *8*, 1113-1115.

194. Andreu, V.; Picó, Y., Determination of pesticides and their degradation products in soil: critical review and comparison of methods. *TrAC Trends in Analytical Chemistry* **2004,** *23* (10-11), 772-789.

195. Howard, P. H. M., D.C.G., Identifying New Persistant and Bioaccumulative Organics Among Chemicals in Commerce. *Environ. Sci. Technol.* **2010,** *44*, 2277-2285.

196. Jones, K. C. d. V., P., Persistant organic pollutants (POPs): state of the science. *Environ. Polllut.* **1999,** *100*, 209-221.

197. Reregistration Eligibility Decision for Dicamba and Associated Salts Agency, U. S. E. P., Ed. Washington D.C., 2006; pp 1-32.

198. Bunch, T. R. G., J.A.; Buhl, K Stone, D. Dicamba Technical Fact Sheet. http://npic.orst.edu/factsheets/archive/Dicamba_tech.html.

199. Zimmerman/Reed. Breaking news: Bayer ag, formerly monsanto company, agrees to $400 million settlement of Dicamba drift litigation alleging damage to soybean crops from off-target movement of Dicamba herbicides. 2021.

200. Hettinger, J. Dicamba on Trial 2021. https://investigatemidwest.org/2021/09/10/epa-asks-bayer-basf-for-more-information-on-2021-Dicamba-damage/ (accessed April 16, 2022).

201. 2011 Edition of the Drinking Water Standards and Health Advisories. Agency, U. S. E. P., Ed. Washington, D.C., 2011.

202. Mulder, R. S., C., Groundwater, Surface Water, and Sediment monitoring for Pesticides and Nitrate in Billings, Montana. Agriculture, M. D. o., Ed. Helena, Montana, 2011.

203. Schmidt, C. G., Permanent Montitoring Well Network Summary Report. In *Montana Department of Agriculture*, 2008.

204. Lewis, K. A.; Tzilivakis, J.; Warner, D. J.; Green, A., An international database for pesticide risk assessments and management. *HERA* **2016,** *22* (4), 1050-1064.

205. Deepa, H. R., Effect of temperautre on fluorescence quenching and emission characteristics of laser dyes. *J. Phys.: Conf. Ser* **2020,** *1473*.

206. Dobek, K.; Karolczak, J., The influence of temperature on C153 steady-state absorption and fluorescence kinetics in hydrogen bonding solvents. *J. Fluoresc.* **2012,** *22* (6), 1647-57.

207. Sengupta, D.; Smith, J. C.; Ullmann, G. M., Partitioning of amino-acid analogues in a five-slab membrane model. *Biochim. Biophys. Acta* **2008,** *1778* (10), 2234-43.

208. Bishai, F. K., E.; Augenstein, L., Intra- and intermolecular factors affecting the excited states of aromatic amino acids. *Biochim. Biophys. Acta* **1967,** *140*, 381-394.

209. Carrozzino, J. M. K., M.G., Intereaction of Basic Drugs with Lipid Bilayers Using Liposome Electrokinetic Chromatography. *Pharm. Res.* **2004,** *21*, 2327-2335.

210. Harayama, T.; Riezman, H., Understanding the diversity of membrane lipid composition. *Nat. Rev. Molec. Cell Biol.* **2018,** *19* (5), 281-296.

211. Lipids, A. P., Phase Transition Temperatures for Glycerophospholipids. pp 1-2.

212. Groundwater Monitoring for Pesticides and Nitrate in Greenfield Bench, Montana; Summary of Findings. Agriculture, M. D. o., Ed. Helena, Montana, 1992-2015.

213. Lakowicz, J. R., *Principles of Fluorescence Spectroscopy*. Springer: New York, NY, 2006.

214. Wurth, C.; Grabolle, M.; Pauli, J.; Spieles, M.; Resch-Genger, U., Relative and absolute determination of fluorescence quantum yields of transparent samples. *Nat Protoc* **2013,** *8* (8), 1535-50.

215. Brouwer, A. M., Standards for photoluminescence quantum yield measurements in solution (IUPAC Technical Report). *Pure Appl. Chem.* **2011,** *83* (12), 2213-2228.

APPENDICES

APPENDIX A

COUMARIN PARTITIONING IN MODEL BIOLOGICAL MEMBRANES: LIMITATIONS OF LOG P AS A PREDICTOR

Synthesis of C151.5

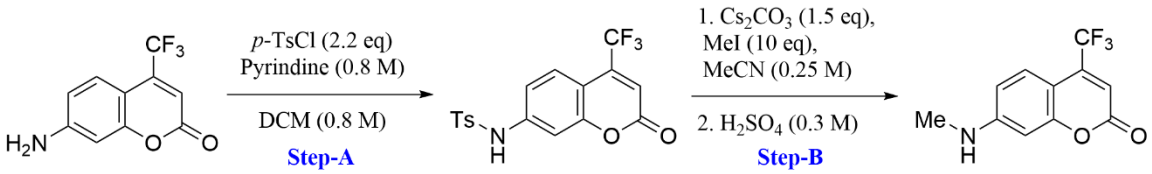

Figure A-2.1. Synthesis of C151.5. Synthesis procedure was done by modifying the procedure found in Reference. [49]

Part A

In an oven dried round bottomed flask equipped with a magnetic stirrer bar, under nitrogen, 7-amino-4-trifluromethylcoumarin (1 eq) was dissolved in dry dichloromethane (0.8M). Pyridine (0.8M) was added dropwise followed by the addition of *p*-toluenesulfonyl chloride (2.2 eq) in one portion. The reaction was stirred at room temperature for 4 hours. Once the reaction was completed by TLC, the reaction was diluted with ethyl acetate, washed with citric acid x 3, brine x 1, dried over sodium sulfate. Solvent was removed *in vacuo*, then washed with a small amount of cooled dichloromethane and filtered to yield **4-methyl-N-(2-oxo-4-(trifluoromethyl)-2H-chromen-7-yl)benzenesulfonamide** as a white solid (40% yield)

^{1}H NMR: (500 MHz, $CDCl_3$, *J* = Hz) 7.82 (d, 2H, *J* = 8.5), 7.61 (dq, 1H, , *J* = 1.8, 5.2, 8.8), 7.33 (d, 2H, , *J* = 8.0),

Part B

In a nitrogen filled glovebox, cesium carbonate (1.5 eq) was added to an oven dried round bottomed flask equipped with a reflux condenser and magnetic stirrer bar. In the fumehood under nitrogen, **4-methyl-N-(2-oxo-4-(trifluoromethyl)-2H-chromen-7-**

yl)benzenesulfonamide was added followed by acetonitrile. Iodomethane was added dropwise and the reaction was heated to 80°C and stirred at this temperature overnight. Once the reaction as completed by TLC, solvent was removed *in vacuo*, and conc. sulfuric acid (0.3 M) was added dropwise. The reaction was heated to 90°C and stirred at the temperature for 30 minutes, the reaction was then allowed to cool to room temperature and stirred at room temperature for 10 hours. The reaction was quenched with cold deionized water, extracted with dichloromethane, dried over sodium sulfate and solvent was removed *in vacuo* and purified by column chromatography (1:1 Hexane: Ethyl Acetate) to yield **7-(methylamino)-4-(trifluoromethyl)-coumarin** as a yellow solid (42% yield).

^{1}H NMR (500 MHz, $CDCl_3$) δ : 7.47 (dq, 1H , *J* = 1.9, 3.7, 8.9), 6.57 (dd, 1H, , *J* = 2.2, 8.9), 6.50 (d, 1H, , *J* = 2.5), 6.43 (s, 1H), 2.93 (s, 3H). **^{13}C NMR** (126 MHz, $CDCl_3$) δ : 160.5, 157.4, 153.2, 142.3, 126.3, 121.0, 111.4, 108.9, 104.1, 98.1, 30.4 **HRMS** (ES+) Calcd. for $C_{11}H_8F_3NO_2$ [M+H+]+. 243.0507 Found 244.0570

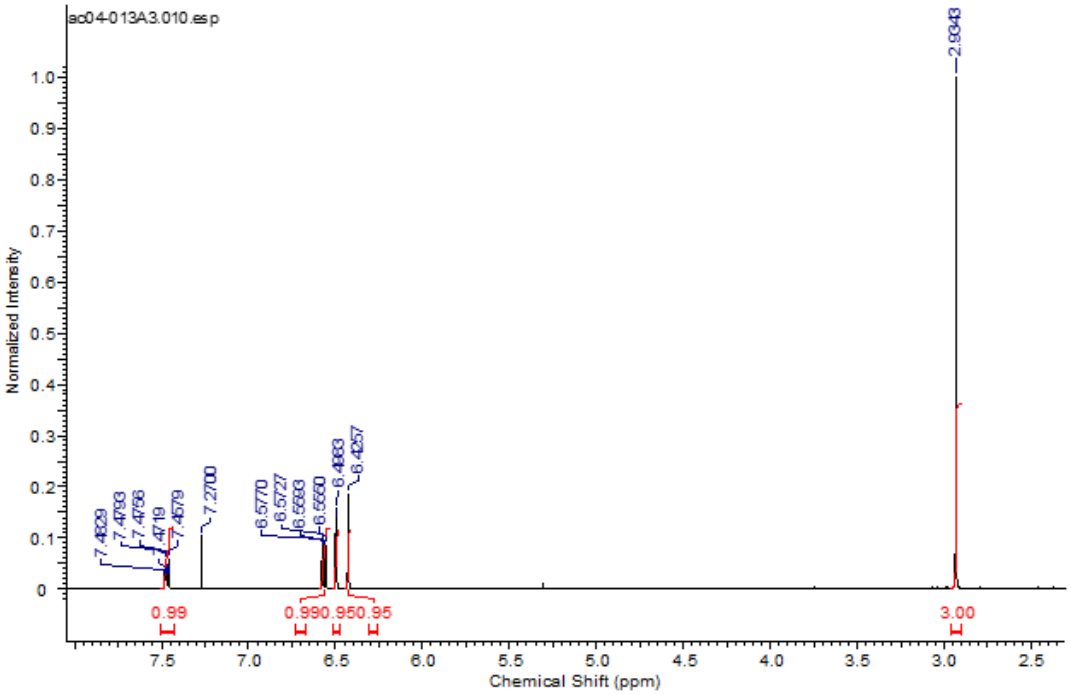

Figure A-2.2. Final H-NMR of C151.5

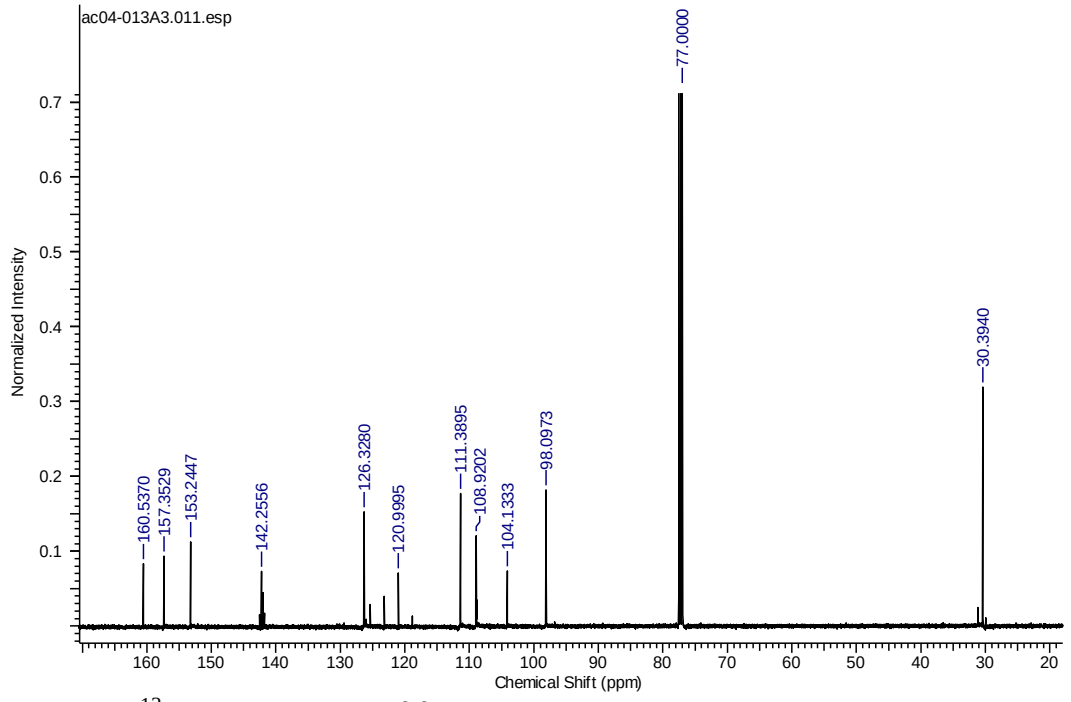

Figure A-2.3. ^{13}C- NMR spectra of final C151.5 product.

Quantum Yield and Radiative Rate Calculations

A brief explanation of the data analysis used here is described below and is further described in reference 2. The quantum yields for C151.5 in PBS buffer, methanol, and acetonitrile as well as C151 in PBS buffer were determined by using C152 in acetonitrile as a relative fluorescence standard. While C152 in cyclohexane was used as a reference for calculating the quantum yield of C151.5 in cyclohexane. Equation A-2.1 was used for calculating the quantum yield for the standard where n_x and n_s are the refractive indices of the sample and the standard, respectively, and m_x and m_s are the slopes of linear fits of the standard and the sample at various dilutions.

$$\phi_{f(x)} = \left(\frac{m_x}{m_s}\right)\left(\frac{n_x}{n_s}\right)^2 \phi_{f(s)} \quad \text{(A-2.1)}$$

The integrated fluorescence intensity was graphed as a function of absorbance for a series of 5 dilutions to create the slope of linear fits for the standard and the sample. To correct the amplitudes for only the radiative emission, the combination of radiative and nonradiative rates must first be calculated using Equation A-2.2 and the experimental lifetime of the solute in the respective environment.

$$\frac{1}{\tau} = k_{rad} + k_{nr} \quad \text{(A-2.2)}$$

Then using the quantum yield calculated from Equation A-2.1 and the spontaneous emission rates from Equation A-2.2, the k_{rad} can be calculated using Equation A-2.3.

$$\phi_{f(x)} = \frac{k_{rad}}{k_{rad}+k_{nr}} \quad \text{(A-2.3)}$$

The amplitudes of that environment (A_i) are divided by the respective radiative of that rates ($k_{r,i}$) for the given environment and normalized against all other radiative rate corrected amplitudes of the system:

$$X_i = \frac{\frac{A_i}{k_{r,i}}}{\left(\frac{A_i}{k_{r,a}}+\frac{A_i}{k_{r,b}}+\frac{A_i}{k_{r,c}}\right)} \quad \text{(A-2.4)}$$

Where A_i is the given amplitude that is produced using the FluoFit system software and X_i is the respective radiative rate corrected amplitude.

Steady-State Spectra of C15X

Steady-state measurements were collected using a Horiba Fluorolog-3 spectrofluorometer at concentrations of 6 µM C15X in bulk solvents. Excitation and emission spectra were taken at the solute's respective excitation and emission wavelengths in individual bulk solvents. Each spectrum was normalized to the maximum intensity between the bulk solvents of each individual solute.

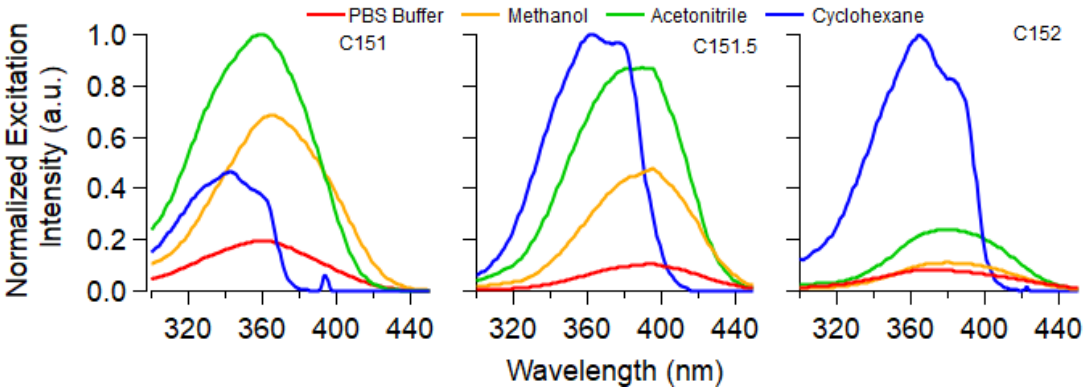

Figure A-2.4. Steady-state excitation spectra of C15X in each of the bulk solvents.

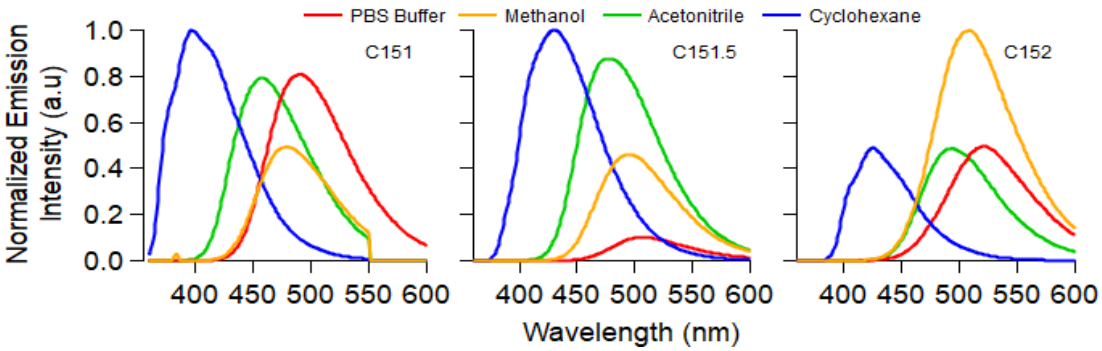

Figure A-2.5. Steady-state emission spectra of C15X in each of the bulk solvents.

C151 in its excited state creates an intramolecular charge transfer (ICT) state in polar solvents. This ICT state causes the two protons on the 7-amine to go from both being in or out of the plane of the rings. This ICT state creates strong solvatochromic response and a stabilization effect resulting in a longer fluorescence emission lifetime in polar solvents.[51, 53-54] In contrast to C151, C152 is believed to form a nonradiative, twisted intramolecular charge transfer (TICT) state in polar, protic environments.[53-54] In the TICT state, the methyl groups of C152 are perpendicular to the plane of the rings. C152 non-radiatively decays to the ground state resulting in a lifetime that is quite short.[53, 55] The ICT and TICT states of C151 and C152 have a solvatochromic effect and can be seen in the ~100 nm shift in emission wavelength (Figure A-2.6). While the photophysical properties of C151.5 are not as well characterized as well as they are for C151 and C152, C151.5 also has a ~100 nm shift in emission wavelength and is assumed

to have a charge transfer state; however, the details of the charge transfer state are not yet known. The emission spectra of each of the coumarin solutes can be seen in Figure A-2.5.

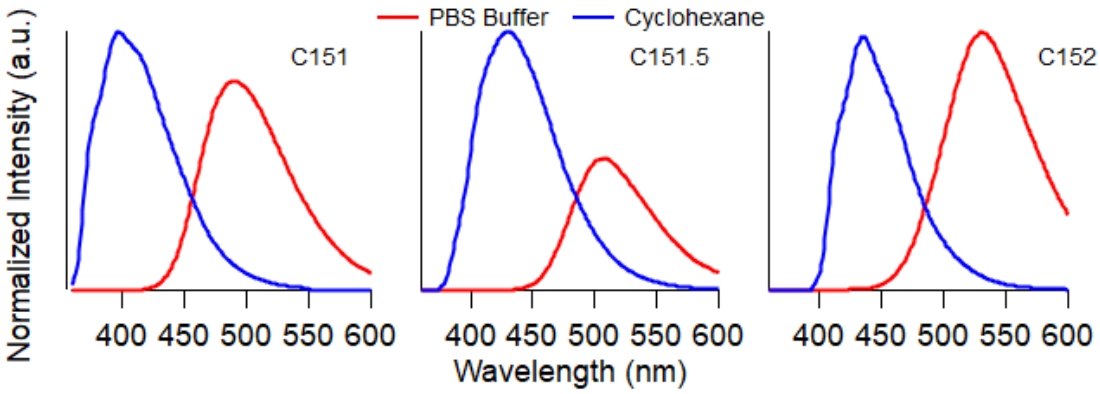

Figure A-2.6. C15X solvatochromic shift seen in nonpolar solvent (cyclohexane) and polar solvent (PBS Buffer).

Full Collection of Lifetimes and Amplitudes

Table A-2.5. Lifetimes (ns) and amplitudes (in parenthesis) of C15X in DPPC as temperature is increased from 10 °C to 70 °C and subsequently decreased to 10 °C. All lifetimes are an average of 4-6 individual trials and all amplitudes are corrected for radiative rate. Uncertainties in lifetimes and amplitudes are ±0.2 ns and ± 0.04, respectively.

temp. (°C)	**C151**	**C151.5**		**C152**		
	buffer τ_1	buffer τ_1 (A_1)	polar τ_2 (A_2)	buffer τ_1 (A_1)	polar τ_2 (A_2)	nonpolar τ_3 (A_3)
10	4.62	3.37 (0.34)	5.73 (0.66)	0.62 (0.43)	2.30 (0.39)	4.55 (0.18)
20	4.57	3.23 (0.41)	5.88 (0.59)	0.54 (0.47)	2.20 (0.45)	4.32 (0.08)
30	4.52	3.22 (0.48)	6.09 (0.52)	0.45 (0.47)	1.99 (0.49)	4.56 (0.04)
40	4.65	3.21 (0.34)	5.73 (0.66)	0.45 (0.34)	1.51 (0.63)	4.34 (0.03)
50	4.81	3.48 (0.29)	5.59 (0.71)	0.35 (0.10)	1.03 (0.88)	4.61 (0.02)
60	4.65	3.23 (0.42)	5.91 (0.58)	0.37 (0.14)	0.78 (0.84)	4.39 (0.02)
70	4.52	3.19 (0.54)	6.03 (0.46)	0.32 (0.20)	0.65 (0.78)	4.25 (0.02)
60	4.65	3.18 (0.41)	5.98 (0.59)	0.39 (0.15)	0.80 (0.83)	4.46 (0.02)
50	4.69	3.36 (0.29)	5.74 (0.71)	0.39 (0.11)	1.03 (0.87)	4.73 (0.02)
40	4.65	3.21 (0.37)	6.00 (0.63)	0.43 (0.32)	1.51 (0.64)	4.47 (0.03)
30	4.57	3.18 (0.39)	6.16 (0.61)	0.43 (0.42)	1.88 (0.53)	4.41 (0.05)
20	4.6	3.14 (0.36)	6.10 (0.64)	0.53 (0.43)	2.20 (0.47)	4.37 (0.10)
10	4.70	3.09 (0.30)	6.15 (0.70)	0.65 (0.43)	2.34 (0.38)	4.56 (0.19)

C151 and C151.5 in DPPC vesicles.

The time-resolved emission decay of C151 and C151.5 in a vesicle solution is zoomed in on the long lifetime tail of the spectra. The C151 in DPPC solution the red 70 °C trace is almost superimposable onto the purple 10 °C trace. The C151.5 in DPPC zoomed in spectra the red 70 °C is the lowest on the spectra and the purple 10 °C trace is at the top of the grouping. The difference seen with C151.5 is a measurable difference within the capabilities of the instrument.

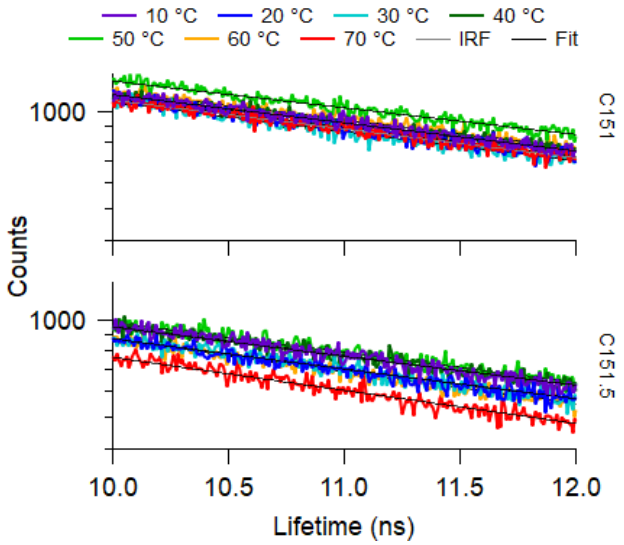

Figure A-2.7. A zoomed in look at the time-resolved emission decay of C151 and C151.5 in a DPPC vesicle solution.

Van't Hoff Analysis of C15X

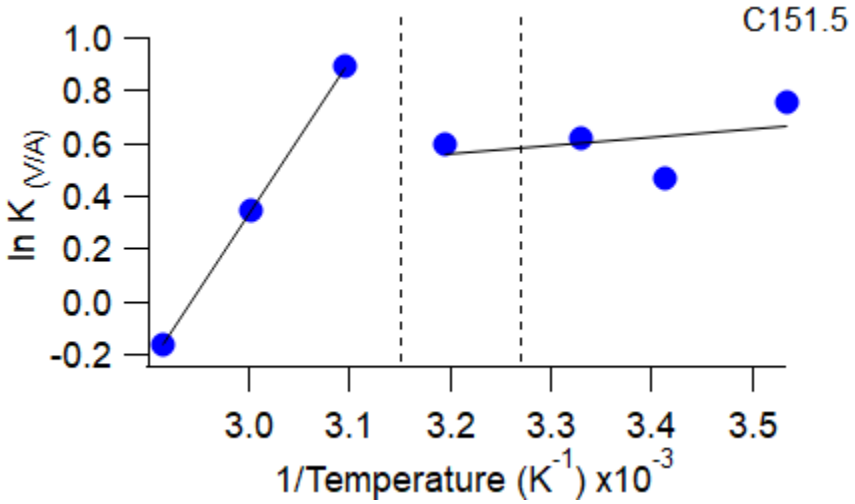

Figure A-2.8. Van't Hoff plots for C151.5 in DPPC vesicle solutions. The natural log of the C151.5 population associated with the vesicle to the C151.5 population in the aqueous surroundings ($K_{V/A}$) is plotted as a function of temperature. The transition and pretransition temperatures of DPPC vesicles are marked with dashed lines. Solid black lines are linear flits whose slope and intercept were used to find ΔH and ΔS, respectively.

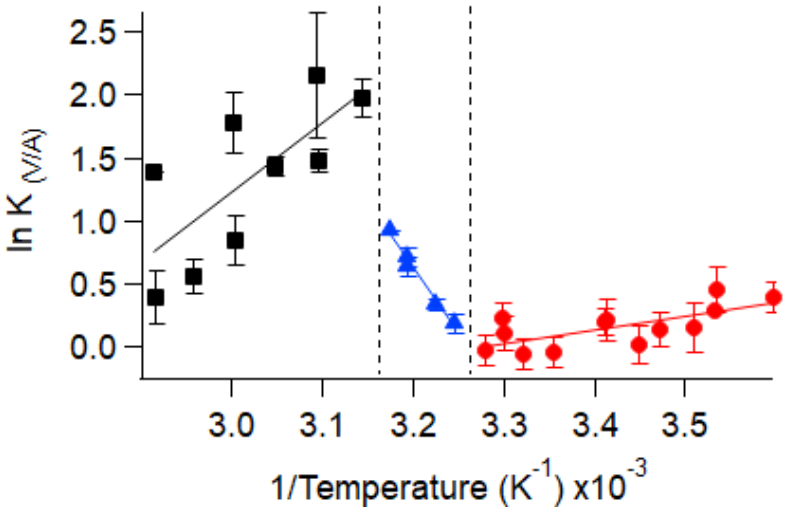

Figure A-2.9. Van't Hoff analysis of C152 in DPPC vesicle solutions. Data include results from this work and previous studies performed in our laboratory.[43] The natrual log of C152 population associated with the vesicle to the C152 population of the aqueous surroundings ($K_{V/A}$) is plotted as a function of temperature. The tranistion and pretransition temperatures are marked with dashed lines. Solid slines are linear fits whose slope and intercept was used to find ΔH and ΔS, respectively. Red, blue, and black markers indicate the ratio of population below the tansition temperautre, between the pretransition temeprature and transition temperautre, and above the transition temperautre, respectively.

APPENDIX B

AMINO ACIDS CHANGE SOLUTE AFFINITY FOR LIPID BILAYERS

DSC spectra of DPPC with L-PA in PBS Buffer

The effect of the concentration of L-PA on the DPPC vesicles was analyzed by DSC and can be found in Figure B-3.1. The spectra show that there is no further effect on the $T_{gel\text{-}lc}$ of DPPC in pure PBS buffer as the concentration of L-PA increases.

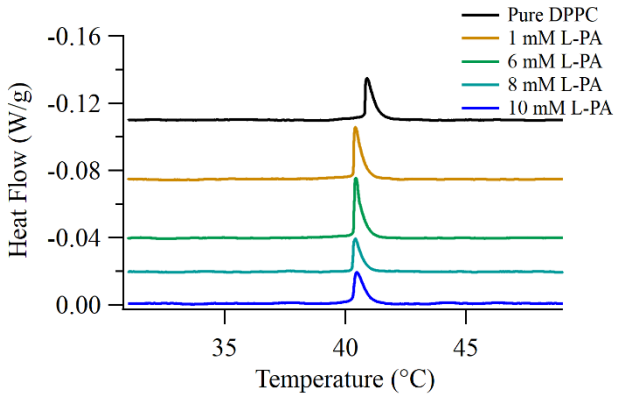

Figure B-3.3**.** DSC spectra of 20 mM DPPC vesicles rehydrated with pure PBS buffer as well as 1, 6, 8, and 10 mM L-PA in PBS buffer. Each trace is endothermic and offset for the ease of viewing.

Bulk Solvent Fluorescence Decay of C151 and C152 with L-PA

Solutions were made using 6 μM C151 and C152 with 10 mM L-Phenylalanine (L-PA) and N-acetyl-DL-tryptophan (NAT), separately, in each of the bulk solvents (PBS buffer, methanol, acetonitrile, and cyclohexane). Bulk solvents were chosen to mimic the local solvation environments found in a lipid bilayer. Methanol and acetonitrile for the polar protic and polar aprotic environments of the lipid headgroup, respectively. And cyclohexane for the nonpolar tails. Fluorescence traces shown in Figure B-3.2 and B-3.3 were taken at 10 °C and were fit using Equation B-3.1. Temperature dependent data shown in Table B-3.1 – B3.4 were taken from 10 °C to 60 °C in 10 °C increments while equilibrating at each temperature for 5 minutes.

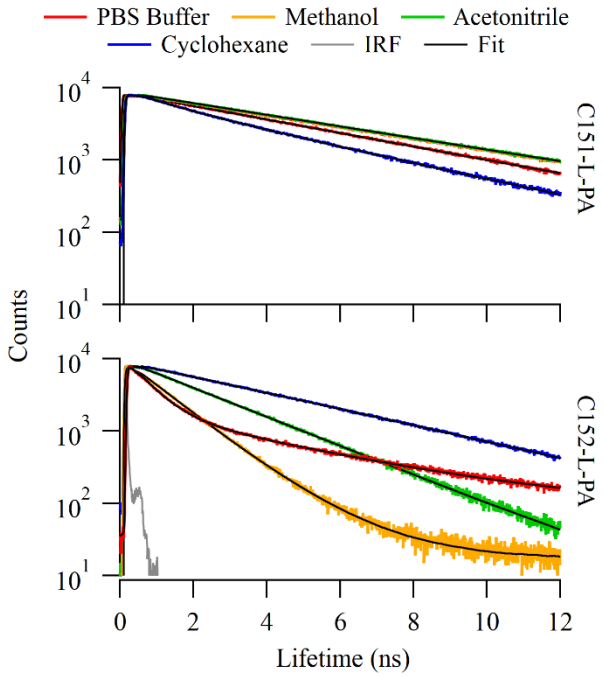

Figure B-3.2. TCSPC spectra of 6 µM coumarins with 10 mM L-PA taken at 10 °C. The top panel shows results for C151-L-PA and bottom panel shows results for C152-L-PA. The results from fitting emission traces with Equation 3.1 are reported in Table 3.1. The grey trace is the instrument response function (IRF).

Table B-3.1. Fluorescence lifetimes and amplitudes of C151 with L-PA as a function of temperature as well as the χ^2 for each lifetime. Numbers in parenthesis are amplitude of the respective lifetime.

Temp.	**PBS Buffer**		**Methanol**		**Acetonitrile**		**Cyclohexane**		
(°C)	χ^2	τ_1	χ^2	τ_1	χ^2	τ_1	χ^2	τ_1 (A_1)	τ_2 (A_2)
10	1.17	4.58	1.22	5.24	1.06	5.37	0.96	1.12 (0.24)	3.80 (0.76)
20	1.11	4.53	1.21	5.24	1.05	5.33	1.01	0.98 (0.34)	3.66 (0.66)
30	1.08	4.51	1.15	5.23	1.01	5.36	1.06	0.79 (0.43)	3.42 (0.57)
40	1.11	4.48	1.09	5.23	1.02	5.38	0.98	0.65 (0.52)	3.19 (0.48)
50	1.07	4.46	1.07	5.19	1.02	5.43	0.99	0.49 (0.58)	2.87 (0.42)
60	1.12	4.40	1.09	5.18	1.06	5.52	1.06	0.39 (0.65)	2.65 (0.35)

Table B-3.2. Fluorescence lifetimes and amplitudes of C152 with L-PA as a function of temperature as well as the χ^2 for each lifetime. Numbers in parenthesis are amplitude of the respective lifetime.

Temp.	PBS Buffer			Methanol		Acetonitrile		Cyclohexane	
(°C)	χ^2	τ_1 (A_1)	τ_2 (A_2)	χ^2	τ_1	χ^2	τ_1	χ^2	τ_1
10	1.10	0.60 (0.81)	3.77 (0.19)	1.32	1.04	1.02	2.16	1.03	3.98
20	1.07	0.50 (0.81)	3.80 (0.19)	1.27	0.95	1.00	1.94	1.03	3.82
30	1.01	0.41 (0.82)	3.75 (0.18)	0.92	0.84	1.04	1.76	1.09	3.87
40	1.06	0.33 (0.82)	3.69 (0.18)	1.03	0.74	1.00	1.62	1.07	3.85
50	1.12	0.28 (0.82)	3.60 (0.18)	0.97	0.66	1.03	1.51	0.98	3.85
60	1.11	0.23 (0.81)	3.51 (0.19)	0.95	0.59	0.99	1.41	1.00	3.89

<u>Bulk Solvent Fluorescence Decay of C151 and C152 with NAT</u>

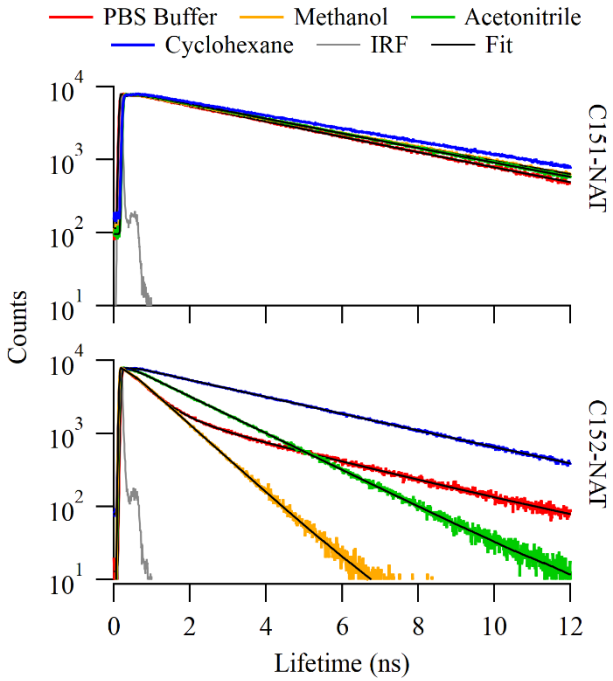

Figure B-3.3. Time-resolved emission of 6 µM coumarins with 10 mM NAT in DPPC vesicle solution taken at 10 °C. The top panel shows results for C151-NAT and bottom panel shows results for C152-NAT. The results from fitting emission traces with Equation 3.1 are reported in Table 5.3. The grey trace is the instrument response function (IRF).

Table B-3.3. Fluorescence lifetimes and amplitudes of C151 with NAT as a function of temperature.

Temp. (°C)	PBS Buffer		Methanol		Acetonitrile		Cyclohexane		
	χ^2	τ_1	χ^2	τ_1	χ^2	τ_1	χ^2	τ_1 (A_1)	τ_2 (A_2)
10	1.13	4.04	1.63	4.36	1.01	4.24	1.19	4.20 (0.79)	0.78 (0.21)
20	1.13	3.88	1.53	4.28	1.04	4.11	1.14	4.14 (0.82)	0.68 (0.18)
30	1.12	3.71	1.47	4.13	1.03	3.98	1.04	4.36 (0.83)	0.90 (0.17)
40	1.12	3.51	1.36	4.02	1.04	3.83	1.03	4.92 (0.80)	1.45 (0.20)
50	1.13	3.32	1.24	3.88	0.97	3.69	1.14	4.93 (0.87)	1.52 (0.13)
60	1.16	3.15	1.29	3.74	1.01	3.56	1.35	4.84 (1.00)	

Table B-3.4. Fluorescence lifetimes and amplitudes of C152 with NAT as a function of temperature.

Temp. (°C)	PBS Buffer			Methanol		Acetonitrile		Cyclohexane	
	χ^2	τ_1 (A_1)	τ_2 (A_2)	χ^2	τ_1	χ^2	τ_1	χ^2	τ_1
10	1.15	0.58 (0.77)	3.36 (0.23)	1.05	1.08	0.96	1.98	1.10	3.70
20	1.10	0.48 (0.77)	3.22 (0.23)	0.96	0.93	1.05	1.78	1.14	3.68
30	1.12	0.39 (0.77)	3.09 (0.23)	0.97	0.81	1.13	1.62	1.06	3.68
40	1.14	0.30 (0.78)	2.92 (0.22)	0.98	0.71	0.98	1.49	1.02	3.69
50	1.06	0.26 (0.78)	2.79 (0.22)	0.96	0.63	1.02	1.39	1.09	3.72
60	1.02	0.22 (0.79)	2.63 (0.21)	1.02	0.56	1.01	1.30	1.05	3.81

APPENDIX C

QUANTITATIVE MEMBRANE PARTITIONING STUDIES OF L-PHENYLALANINE

Structures of L-Phe and Lipid Vesicles Used in This Work

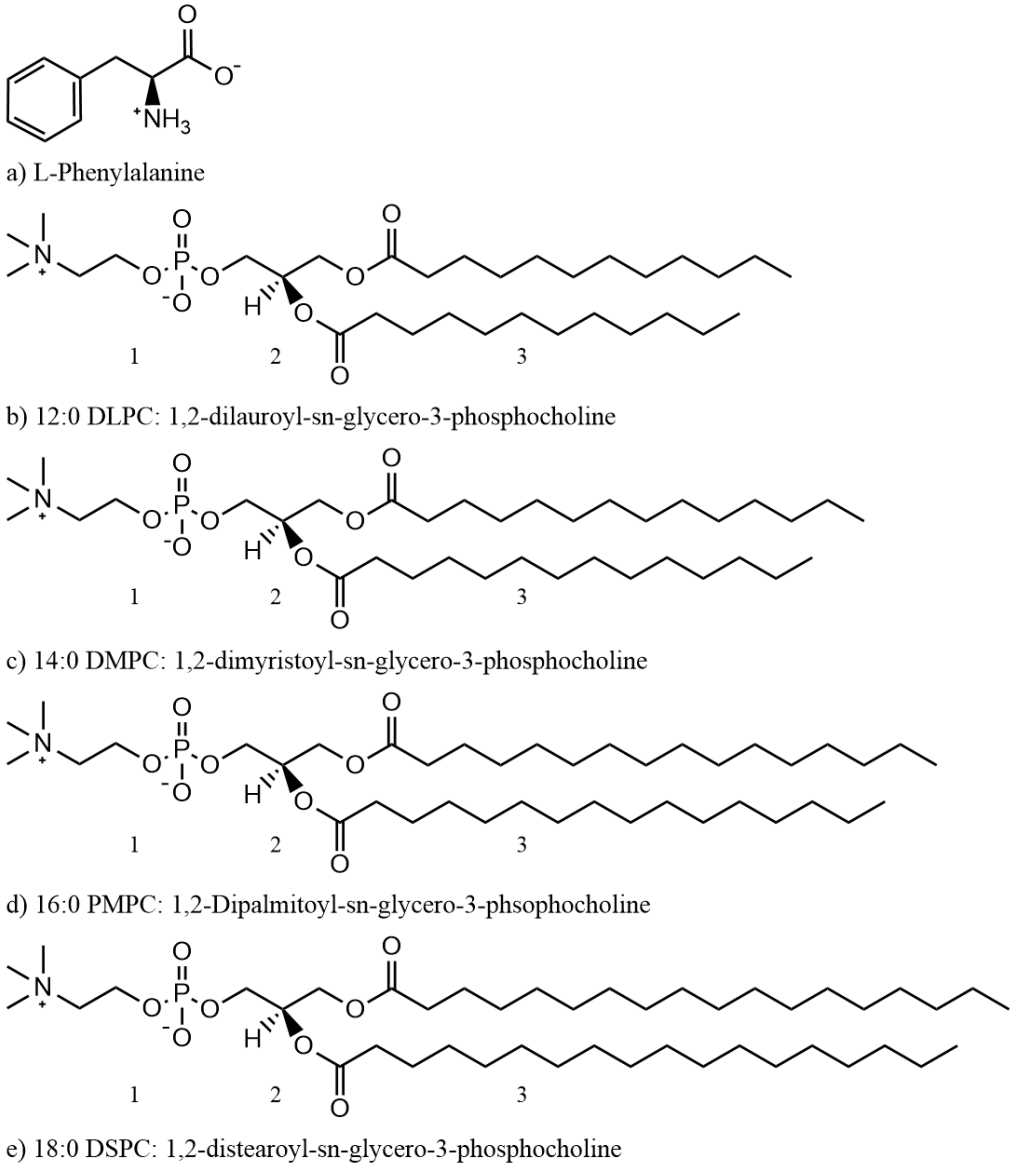

Figure C-4.1. Chemical structures of (a) L-Phenylalanine, (b) 1,2-dilauroyl-sn-glycero-3-phosphocholine (12:0 DLPC) lipid, (c) 1,2-dimyristoyl-sn-glycero-3-phosphocholine (14:0 DMPC) lipid, (d) 1,2-Dipalmitoyl-*sn*-glycero-3-phsophocholine (16:0 DPPC) lipid, and (e) 1,2-distearoyl-sn-glycero-3-phosphocholine (18:0 DSPC) lipid. Number assignments refer to various environments created by the lipid with 1) polar zwitterionic headgroup, 2) the polar glycerol-backbone and ester groups, and 3) nonpolar, hydrophobic hydrocarbon tails. The COOH pKa-value for L-Phe is 2.2 and amino pKa-value is 9.9 giving L-Phe local charges on structure at pH 7 used for these experiments.

Steady-State Spectra of L-Phe in Bulk Solvents

Steady state measurements were collected using a Horiba Fluorolog-3 spectrofluorometer at concentrations of 10 mM for carbonate buffer and methanol, 1.4 mM in acetonitrile, and 0.1 mM for cyclohexane. The range in concentration is due to poor solubility of L-Phe in acetonitrile and cyclohexane. Excitation and emission spectra were taken at the solute's respective excitation and emission wavelengths in individual bulk solvents. Each spectrum was normalized to the maximum intensity between bulk solvents for each individual absorbance, excitation, and emission spectra.

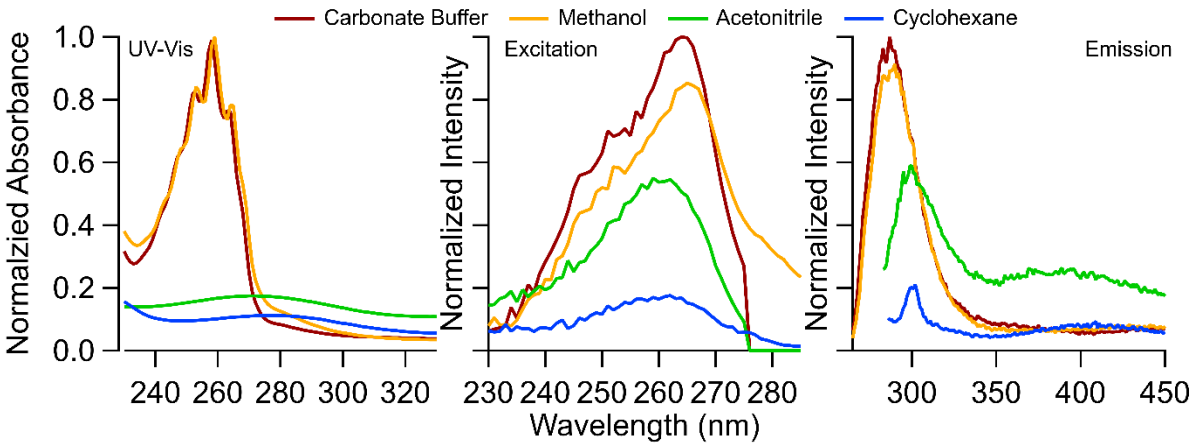

Figure C-4.2. Absorbance (left), excitation (middle), and emission (right) spectra for L-Phe in each of the bulk solvents.

Fluorescence Lifetimes, Quantum Yield Calculations, and Radiative Rate Calculations of L-Phe in Bulk Carbonate Buffer and Methanol as a Function of Temperature

Time-resolved emission of L-Phe in bulk carbonate buffer and methanol as a function of temperature can be seen in Figure C-4.3 – C-4.4, respectively. Each reported lifetime is a fit of each fluorescence decay using Equation 4.1. At each temperature, the solution was equilibrated for five minutes before data was accumulated. The resulting

fluorescent lifetimes of L-Phe in bulk carbonate buffer and methanol can found in Table C-4.1.

A brief explanation of how the quantum yields and radiative rates were collected will be described here with a further explanation of technique found in the references.[45, 213-214] The quantum yields of L-Phe in bulk carbonate buffer and methanol were measured as a function of temperature from -5 °C to 80 °C. The quantum yield for L-Phe in acetonitrile was only measured at 20 °C. Calculations were not successfully measured for L-Phe in cyclohexane due to the low solubility as well as the extremely poor absorbance. Equation C-4.1 was used for calculating the reference quantum yield ($\varphi_{f(x)}$) using Tyrosine in Millipore water as a reference ($\varphi_{f(s)}$).[215] The refractive indices for the sample and standard are n_x and n_s, respectively. The integrated fluorescence intensity was plotted as a function of absorbance for a sequence of four serial dilutions to create a slope of linear fits for the standard and sample, m_x and m_s, respectively. Each dilution was repeated at each reported temperature with an equilibration time of five minutes before data accumulation.

$$\phi_{f(x)} = \left(\frac{m_x}{m_s}\right)\left(\frac{n_x}{n_s}\right)^2 \phi_{f(s)} \qquad \text{(C-4.1)}$$

To correct the amplitudes for only the radiative emission, the combination of the radiative (k_{rad}) and nonradiative (k_{nr}) rates must first be calculated using Equation C-4.2. The experimental lifetime (τ) of the solute in the respective environment at each respective temperature is used to calculate corresponding k_{rad} and k_{nr}.

$$\frac{1}{\tau} = k_{rad} + k_{nr} \qquad \text{(C-4.2)}$$

Using the quantum yield found in Equation C-4.1 and the spontaneous emission rates from Equation C-4.2, the k_{rad} can be calculated using Equation C-4.3.

$$\phi_{f(x)} = \frac{k_{rad}}{k_{rad}+k_{nr}} \quad \text{(C-4.3)}$$

A given amplitude at a specific temperature divided by the respective radiative rate at the same temperature is normalized against all other radiative rate corrected amplitudes of that system only at the corresponding temperature (Equation C-4.4). Where A_i is the given amplitude that is produced using the FluoFit system software, $k_{r,i}$ is the corresponding radiative rate at the same temperature, and X_i is the resulting radiative rate corrected amplitude at the defined temperature.

$$X_i = \frac{\frac{A_i}{k_{r,i}}}{\left(\frac{A_i}{k_{r,a}}+\frac{A_i}{k_{r,b}}\right)} \quad \text{(C-4.4)}$$

The radiative rate of L-Phe in carbonate buffer was used to correct the amplitude of L-Phe that remains in carbonate buffer when in the presence of a lipid vesicle system. The amplitude of L-Phe associated with the membrane and proposed to be a conformationally restricted rotamer (k_{rot}) was corrected using the radiative rate of L-Phe in bulk methanol. Methanol was chosen because it is the closest model available to mimic the polar protic environment of water permeating into the polar headgroup of the lipid bilayer. Temperatures reported in Table C-4.1 are the same temperatures used throughout all experimental procedures for all lipid vesicles used in this study.

Table C-4.1. Fluorescence properties of L-Phe in bulk carbonate buffer and methanol from -5 °C to 80 °C. Lifetimes are ± 0.2 ns. Numbers in parenthesis next to lifetime are amplitudes of that lifetime. Quantum yields (φ_f) and radiative rates (k_f) were measured in this work.

temp. (°C)	Carbonate Buffer			Methanol		
	τ_f (ns)	φ_f	k_f (10^6 s^{-1})	τ_f (ns)	φ_f	k_f (10^6 s^{-1})
-5	11.03	0.036	3.29	8.68	0.047	5.38
0	10.81	0.036	3.37	8.34	0.042	5.01
5	9.13	0.039	4.24	7.93	0.039	4.93
10	8.31	0.027	3.23	7.56	0.033	4.40
15	7.33	0.026	3.49	7.17	0.033	4.67
20	6.42	0.023	3.52	6.74	0.033	4.89
25	5.56	0.021	3.70	6.27	0.031	5.01
30	4.81	0.018	3.66	5.78	0.033	5.77
35	4.17	0.016	3.85	5.40	0.028	5.15
40	3.59	0.014	4.01	4.91	0.033	6.69
50	2.71	0.012	4.42	4.09	0.031	9.24
60	2.13 (0.89), 0.74 (0.11)	0.010	4.64	3.35	0.029	10.8
70	1.66 (0.84), 0.66 (0.16)	0.009	5.13	2.73	0.027	12.4
80	1.30 (0.80), 0.52 (0.20)	0.005	4.06	2.21	0.026	9.50

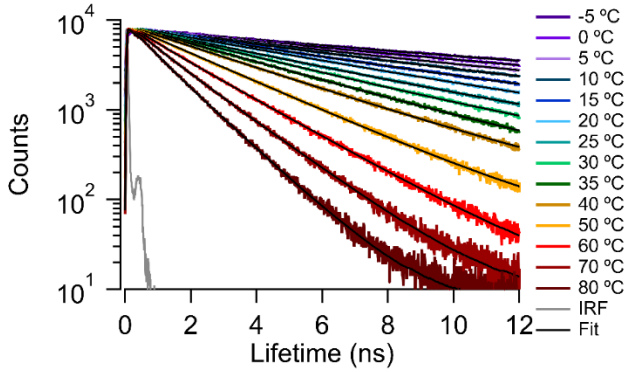

Figure C-4.3. TCSPC spectra of L-Phe in bulk carbonate buffer as a function of temperature. Results from fitting these emission traces to Eq 4.1 are reported in Table C-4.1.

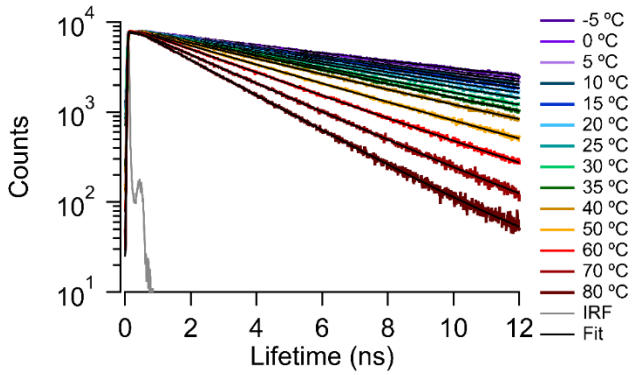

Figure C-4.4. TCSPC spectra of L-Phe in bulk methanol as a function of temperature. Results from fitting these emission traces to Eq. 4.1 are reported in Table C-4.1.

Fluorescence Behavior of 2.5 mM L-Phe in DPPC Lipid Vesicles

The fluorescence behavior of 2.5 mM L-Phe in DPPC lipid vesicles was measured at selected temperatures can be found below. This was done to test aggregation effects of L-Phe at a 4-fold smaller concentration than what was used in this study. Results show that there was no significant change to the lifetimes and amplitudes of 10 mM L-Phe in DPPC lipid vesicles.

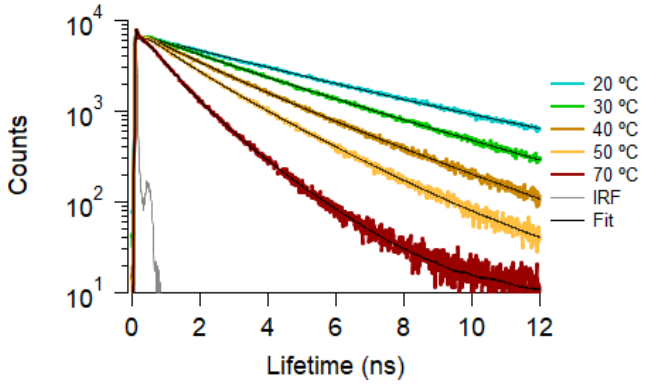

Figure C-4.5. TCSPC spectra of 2.5 mM L-Phe in DPPC lipid vesicles as a function of temperature. Results from fitting these emission traces to Equation 4.1 are reported in Table C-4.2.

Table C-4.2. Fluorescence lifetimes (in ns) and amplitudes (in parentheses) of 2.5 mM L-Phe in DPPC vesicles at selected temperature ramp from 20 to 70 °C in and back down to 10 °C. Amplitudes have been corrected for their respective radiative rates. Uncertainties in lifetimes are ± 0.2 ns; uncertainties in amplitudes are ± 0.04.

temp. (°C)	buffer τ_1 (A_1)	K_{rot} τ_2 (A_2)
20	4.63	
30	3.75 (0.91)	1.49 (0.09)
40	3.12 (0.74)	1.66 (0.26)
50	2.39 (0.73)	1.24 (0.27)
70	1.59 (0.58)	0.74 (0.42)
50	2.44 (0.68)	1.27 (0.32)
40	2.93 (0.80)	1.47 (0.20)
30	3.86 (0.86)	1.73 (0.14)
20	4.57	

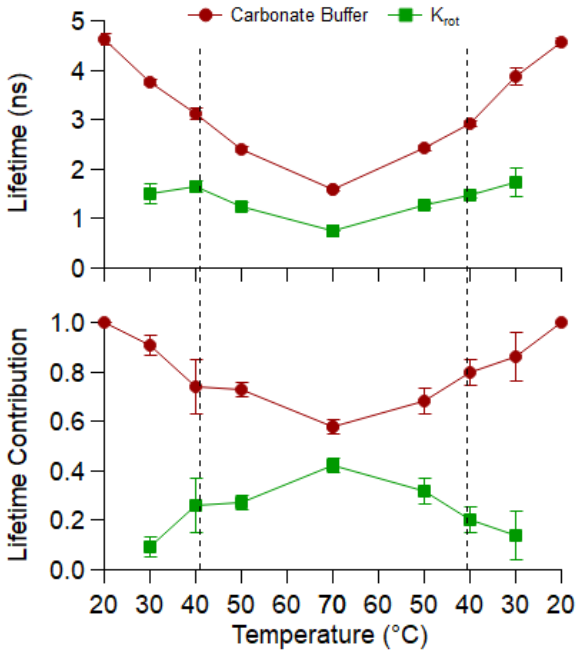

Figure C-4.6. Fluorescence lifetimes (top) and respective radiative rate corrected lifetime contribution (bottom) of 2.5 mM L-Phe in DPPC lipid vesicles. The major lifetime is assigned to a L-Phe in carbonate buffer (τ_1, burgundy circles), and a rotamer confinement lifetime (k_{rot}) of L-Phe in the DPPC polar headgroup region (τ_2, green squares). The dashed lines indicate the $T_{gel\text{-}lc}$ of the DPPC lipid bilayer at ~41.5 °C. Each point is an average of 2 independent trials and the respective error bars are one standard deviation based on the results of those 2 trials. In some instances, the uncertainty is smaller than the marker used to represent that data point.

Comparing the Fluorescence Behavior of
D_2O Carbonate Buffer to H_2O Carbonate Buffer

The fluorescence lifetimes of 10 mM L-Phe in H_2O carbonate buffer and D_2O carbonate buffer were measured as a function of temperature. This was done to measure the effect of H-bonding on the thermal stabilization of the rotamer lifetime. While the lifetimes between the two buffer solutions are different, the appearance of the second lifetime occurs at 60 °C for both solutions. However, the amplitude of the second lifetime in D_2O carbonate is significantly higher than that of H_2O carbonate buffer. There discrepancy between the two amplitudes is predicted to be due to the stronger H-Bonding capabilities of D_2O in comparison to H_2O allowing for more stabilization of the rotamer conformation.

Table C-4.3. Fluorescence lifetimes (in ns) and amplitudes (in parentheses) of 10 mM L-Phe in H_2O carbonate buffer and D_2O carbonate buffer at temperature ramp from 0 °C to 80 °C. Amplitudes have been corrected for their respective radiative rates. Uncertainties in lifetimes are ± 0.2 ns; uncertainties in amplitudes are ± 0.04.

temp. (°C)	H_2O Carbonate Buffer τ_f (ns)	D_2O Carbonate Buffer τ_f (ns)
0	10.81	8.00
10	8.31	6.43
20	6.42	5.01
30	4.81	3.86
40	3.59	2.98
50	2.71	2.30
60	2.13 (0.89), 0.74 (0.11)	1.87 (0.88), 0.88 (0.12)
70	1.66 (0.84), 0.74 (0.16)	1.57 (0.69), 0.91 (0.31)
80	1.30 (0.80), 0.52 (0.20)	1.41 (0.43), 0.84 (0.57)